**Terms and Conditions of Use of Digitised Theses from Trinity College Library Dublin**

**Copyright statement**

All material supplied by Trinity College Library is protected by copyright (under the Copyright and Related Rights Act, 2000 as amended) and other relevant Intellectual Property Rights. By accessing and using a Digitised Thesis from Trinity College Library you acknowledge that all Intellectual Property Rights in any Works supplied are the sole and exclusive property of the copyright and/or other IPR holder. Specific copyright holders may not be explicitly identified. Use of materials from other sources within a thesis should not be construed as a claim over them.

A non-exclusive, non-transferable licence is hereby granted to those using or reproducing, in whole or in part, the material for valid purposes, providing the copyright owners are acknowledged using the normal conventions. Where specific permission to use material is required, this is identified and such permission must be sought from the copyright holder or agency cited.

**Liability statement**

By using a Digitised Thesis, I accept that Trinity College Dublin bears no legal responsibility for the accuracy, legality or comprehensiveness of materials contained within the thesis, and that Trinity College Dublin accepts no liability for indirect, consequential, or incidental, damages or losses arising from use of the thesis for whatever reason. Information located in a thesis may be subject to specific use constraints, details of which may not be explicitly described. It is the responsibility of potential and actual users to be aware of such constraints and to abide by them. By making use of material from a digitised thesis, you accept these copyright and disclaimer provisions. Where it is brought to the attention of Trinity College Library that there may be a breach of copyright or other restraint, it is the policy to withdraw or take down access to a thesis while the issue is being resolved.

**Access Agreement**

By using a Digitised Thesis from Trinity College Library you are bound by the following Terms & Conditions. Please read them carefully.

I have read and I understand the following statement: All material supplied via a Digitised Thesis from Trinity College Library is protected by copyright and other intellectual property rights, and duplication or sale of all or part of any of a thesis is not permitted, except that material may be duplicated by you for your research use or for educational purposes in electronic or print form providing the copyright owners are acknowledged using the normal conventions. You must obtain permission for any other use. Electronic or print copies may not be offered, whether for sale or otherwise to anyone. This copy has been supplied on the understanding that it is copyright material and that no quotation from the thesis may be published without proper acknowledgement.

# Identification and Evolutionary Response Analysis of Continuous and Discrete Structural Systems Using Wavelet Transform

by

Arunasis Chakraborty

Thesis submitted to the

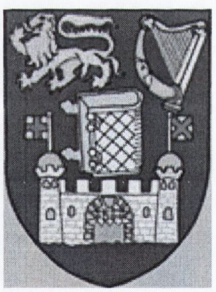

University of Dublin, Trinity College

for the Degree of

**Doctor of Philosophy**

# DECLARATION

The author hereby declares that this thesis, in whole or part, has not been submitted to any other University as an exercise for a degree. Except where reference is made in the text, it is essentially the author's own work.

The author confirms that the library may lend or copy this thesis, upon request, for academic purposes.

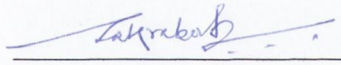

ARUNASIS CHAKRABORTY

April 2006

# ACKNOWLEDGEMENTS

I would like to express my deep sense of gratitude to my supervisor Dr. Biswajit Basu for his valuable suggestions, guidance and encouragements throughout the period of my research work.

I am also very grateful to Dr. Roger West and Dr. Margaret O'Mahony for providing me an excellent working environment and for the facilities in the Department of Civil, Structural and Environmental Engineering. I would like to thank Dr. Brian Broderick and Mr. Dermot Geraghty for the financial support during my study.

I feel privileged to receive the postgraduate fellowship from RPS-MCOS Consulting Engineers and would like to thank Mr. P. J. Rudden for awarding me the scholarship during the second year of my study.

I am indebted to Chris O'Donovan, George Jones and Dave McAuley for their valuable help and suggestions during my laboratory work.

I really feel fortunate to stay with Gujju_bhai (Patel) and Madrassi (Bharath) and my heartfelt thanks goes to them for their warm company, which has never let me feel homesick.

I would also like to thank my parents and brother for their constant support and encouragements during my tenure in Trinity College, Dublin.

# ABSTRACT

Performance based design of structures require stringent serviceability criteria to be satisfied based on functional requirements and economic implications. Thus, performance evaluation of structural dynamic systems not only helps to detect any deterioration, alerting the user of subsequent structural failure in advance, but also helps to estimate the remaining service life of the structure. This helps in deciding on the preventive measures those are required to maintain design serviceability criteria during operation in the remaining period of service life. The objective of this research work is, therefore, to investigate the mathematical techniques to evaluate the performance of structural systems via system identification and their behaviour, when subjected to evolutionary stochastic processes.

First of all, a wavelet-based algorithm is developed to solve the inverse problem so that the parameters of a dynamical system can be estimated from the measured time history of the response. Although conventionally this problem of system idenfication is performed either in time domain (e.g. using Kalman filter technique) or in frenquency domain (using Fourier transform), both the techniques are known to have their own limitations in the estimation of system parameters. In this context, time-frequency based approach has gained momentum in the recent past. A wavelet-based time-frequency analysis is adopted in the present thesis to estimate the natural frequencies and mode shapes of linear structural systems and their changes. The proposed wavelet-based formulation, which is applicable for both off-line and on-line identification and monitoring of dynamical systems is then validated using numerical simulations and experimental results. The proposed identification technique is further used to identify localized modes of a class of non-linear systems.

Once the parameters of the dynamical systems are identified, the estimation of performance of structures demands the study of the response behaviour of the system when subjected to design loads, which are often non-stationary in nature. The prerequisite to this study is to develop a proper model for the non-stationary input processes. The characterization of the non-stationary processes become more complex for the cases involving both amplitude and frequency non-stationary (e.g. earthquake). A wavelet-

based model is formulated to encompass non-stationary amplitude and frequency content in the input. For this purpose, a concept of frequency dependent amplitude modulation is introduced in the present study. Using this frequency dependent amplitude modulation, both single component as well as spatially varying earthquake ground motions are modelled.

Finally, an input-output relation of linear dynamical systems subjected to non-stationary processes is established using wavelet transform on continuoum models and in a finite element framework separately. The discrete model in fiinite element framework is then utilised to study the response of multi-supported dynamical systems such as multi-span bridges and systems with non-classical damping such as primary-secondary systems. The study reveals that due to frequency non-stationarity in the excitation process, higher modes are often excited in structural systems such as bridges and primary-secondary systems. Moreover, the effect of rotational inertia involved in primary-secondary systems often contribute to the frequency non-stationarity in the response significantly. Hence, the time-frequency analysis of these structures are important with serious design implications.

In the present thesis, the application of wavelet tools in system identification uses a modified form of Littlewood-Paley basis function. This basis function is completely localized in frequency and can be used in sub-band coding leading to wavelet packet transformation, which not only enables to evaluate parameters with desired level of accuracy but also can be used to evaluate the closely spaced modes of the dynamical systems. Furthermore, the frequency localization characteristic enables estimation of localized mode of a class of non-linear systems.

The representation of non-stationary stochastic processes using frequency dependent amplitude modulation as proposed in this thesis is general in the sense that it can take into account the non-stationarity in both intensity as well as frequency content. The proposed wavelet-based time-frequency model can be used for both single-variate process as well as multi-variate processes.

The wavelet-based input-output relation presented in this study for continuoum and finite element models can evaluate the behaviour of the linear dynamical systems subjected to evolutionary stochastic processes. The proposed model differs from

conventional random vibration analysis using Fourier-Stieltz integral in the estimation of frequency non-stationarity in the output and is more generalized than other wavelet-based formulation as it is valid for any wavelet basis function (without any restrictions to orthogonality).

The principal findings of this research work advocates the usages of the wavelet-based time-frequency analysis for system identification, modelling of evolutionary stochastic processes and random vibration analysis.

# TABLE OF CONTENTS

# List of Figures

# List of Tables

# Chapter 1: Introduction

## 1.1 General Introduction

Almost every structural system in the mechanical world deteriorates with time. Different causes behind the structural deterioration are aging, operational complexities, and natural and man-made hazards and/or accidents. Although performance deterioration of many structures has little impact, lifeline and other important structures possess serious threats on safety. Examples of these structures are bridges, communication towers, chemical plants, pipelines, nuclear power plants, dams etc. Further, performance based design of structures demand stringent serviceability criteria to be satisfied from the functionality point of view with serious economic implications. Thus monitoring of structural health forms the prerequisite to the safe operation of structures, which not only helps to monitor the overall performance of the dynamical systems but also help to evaluate their residual life and to adopt decision to prevent any structural as well as collateral damage. The fundamental principle behind the evaluation of structural health is the estimation of structural properties such as mass, stiffness or natural frequencies and mode shapes, and damping. The evaluation of structural parameters helps to detect change on the overall performance of the dynamical systems and forms the basis of further evaluation of their residual life. Besides identification of structural parameters, proper modeling of the dynamic response characteristics of the structural systems as well as the external forces acting on them plays a vital role in better assessment of the structural behavior for performance based design and operation.

## 1.2 System Identification

System identification of structures has emerged as an interesting and important problem in the last two decades. Identification of structural systems involves an inverse procedure to identify the structural parameters from the recorded response of structures. The goal is to estimate the dynamic properties such as natural frequencies and mode shapes of vibration, energy dissipation, permanent deformation and strength deterioration of damaged structures from the measured responses under different conditions like ambient vibrations, earthquakes, wind, impacts and several other types of excitations. System identification of structures is the preceding step for design of active and passive control of structures [Meirovitch (1993)] and structural health monitoring [Micaletti *et al* (1999), Segawa *et al* (2000), Sone *et al* (2000)]. Identified parameters provide design criterion for both linear and non-linear structures subjected to seismic and other loadings [Scneviratna and Krawinkler (1996), Chusilp (1999), Ewins (2001].

### 1.2.1 Linear Systems

The simplest way to model a structural dynamic system is to approximate it by a linear dynamical system. Modal analysis of the response of structures is an important tool for identification of linear structural systems. Natural frequencies of a structure depend on its mass and stiffness distributions. The deformation patterns at these frequencies or the mode shapes are informative of the dynamical characteristics of the structures. Analysis of response signals of structures may be performed in two different paradigms: (i) time

domain analysis and (ii) frequency domain analysis. Several approaches to time domain system identification have been developed like state estimation using Kalman filter [Hoshiya and Saito (1984)], stochastic analysis and modeling, recursive modeling and least squares method.

The classical method of frequency domain analysis is by means of Fourier transform [Newland (1993)], and its algorithmic implementation, the Discrete Fourier Transformation (DFT). Though DFT has been widely used for modal analysis and other system identification tasks, it has several limitations. Fourier analysis is inherently global in nature and fails to capture the time varying nature of a phenomenon. An approach for signal analysis, which circumvents the above problem, is the time-frequency analysis [Newland (1994a, 1994b), Prochazka *et al* (1998), Basu and Gupta (1997, 1998)]. In the framework of multi resolution time-frequency analysis, wavelet methods developed by several researchers [Mallat (1989), Daubechies (1992), Chui (1992)] have been widely popular and successful for signal analysis. Wavelets produce representation of a signal using time limited local functions having variable scales. Wavelet analysis has recently been used for a number of system identification tasks [Katida (1998)]. There have been several research works in literature on the use of wavelet to identify the modal parameters [Piombo *et al* (2000), Lardies and Gouttebroze (2002)]. In some of these studies modal frequency, mode shapes and modal damping were identified. Random decrement technique has been used in some studies, which is known to have certain drawbacks. A shifted version of wavelet transform proposed by Staszewski (1997) was used to detect frequencies. This works better for closely spaced frequencies. In Lardies and Gouttebroze (2002), modified Morlet wavelet was used which works better than the traditional Morlet

wavelet. Though some studies on use of wavelets have been carried out in system identification, yet it remains to be seen how different wavelets perform or which would be the suitable wavelet.

Significant amount of research on system identification has been carried out in relation to structural dynamic systems, which includes research by Hart and Yao (1977), Beck (1980), Kozin and Natke (1986), Lin *et al* (1990), Ghanem and Shinuzoka (1995), Shinuzoka and Ghanem (1995) amongst others. The application of the information available is useful for damage detection and health monitoring of structural systems. Recently, active and semi-active control of structures has received considerable attention [Spencer and Nagarajaiah (2003)]. Effective implementation of these control schemes requires on-line identification of structural systems.

In identifying the structural systems once the model is decided on, the relevant parameters need to be estimated. The most important parameter of the structure is its stiffness or natural frequency for a single degree of freedom (SDOF) system. Similar information may be obtained via natural frequency and mode shapes for a multi degree of freedom (MDOF) structure. The information of stiffness and the variation of stiffness with time are of importance in designing control strategies e.g. in active and semi-active tuned mass dampers (TMDs) (Soong [1990], Spencer and Nagarajaiah [2003], Yang *et al* [2004]). Estimation of parameters in the structural systems based on frequency domain methods though popular due to their simplicity in application, suffers from the drawback that they are based on average temporal information. Hence, these cannot be used for time varying systems. Most of these time domain methods are also based on identifying models with time invariant parameters. Recent research efforts have been aimed towards

identifying and tracking time varying parameters either by recursive and other modified time domain techniques or by Hilbert/Gabor transformed analysis techniques (e.g. Varadarajan and Nagarajaiah [2004], Spina *et al* [1996]). Among the time-frequency analysis tools, wavelet analysis has gained popularity in identification of systems. Being capable of retaining local frequency content information and its variation with time and having the advantage of flexible windowing over short time Fourier transform, wavelet has become a powerful technique to identify time varying and non-linear systems [Katida (1998), Lardis and Goattebroze (2002), Piombo *et al* (2000), Staszewaski (1997, 1998), Ghanem and Romeo (2000, 2001), Basu (2003, 2004)]. Wavelet analysis provides a variety of bases function to suit specific purposes. For example, Newland (1983, 1994) used Harmonic wavelet for vibration analysis; Lardies and Gouttebroze (2002) proposed a modified Morlet wavelet basis while Basu and Gupta (1998, 1999) and Chatterjee and Basu (2004) used a modified L-P basis function for reasons suitable for specific applications.

Most of the system identification strategies including those based on wavelet analysis have concentrated on the off-line identification of the time varying parameters of the systems. Smyth *et al* (1999) had obtained on-line estimation of the parameters of MDOF non-linear hysteretic systems. The algorithm is based on the measurement of restoring forces. While the wavelet analysis techniques have been successfully used mostly in off-line identification of the time varying structural dynamic parameters of a system, it has the potential of on-line identification, using time-frequency properties. The on-line identification of system parameters can be achieved in a simple and computationally straightforward way by using wavelet analysis useful for adaptive

control of linear structural dynamic systems, which has not been explored much, so far.

### 1.2.2 Non-linear System: Mode Localization

The fundamental difference between the linear and non-linear system is that the principle of superposition does not hold for non-linear systems. Thus for system whose restoring force contains non-linear terms, decoupling of the governing equations based on eigen analysis of the system matrices is not possible. However, a synchronous motion among the degrees of freedom is known to exist, which is commonly termed as 'vibration in unison'. According to Rosenburg (1966), all degrees of freedom attain extremes or pass through zero simultaneously during this synchronous periodic motion, which is analogous to the normal mode of linear system and hence is called 'non-linear normal mode' (NNM). Among the popular solution techniques for non-linear systems are normal form techniques [Jezequel and Lamarque (1991)], perturbation techniques [Neyfah (2000)], method of harmonic balance [Shaw and Pierre (1993), Peschek *et al* (2002)] and method of multiple scales [Nayfeh and Mook (1984)]. King and Vakakis (1994) proposed energy based approach and constructed NNMs using transformed linear modal coordinates. Besides these techniques, invariant manifold [Shaw and Pierre (1993a, 1993b)] based approach is known to have specific advantages for a class of problems.

Estimation of response of non-linear system under both free and forced vibrations are often performed using reduced order model [Shaw *et al* (1991, 1999), Vakakis *et al* (1996), Vakakis (1997)], which has close resemblance with modal reduction techniques that are often adopted for linear systems. Shaw and Pierre (1993a, 1993b) proposed

response evaluation of the non-linear systems using invariant manifold approach. In this approach certain degrees of freedoms are considered, as master and the rest are slaves. The master and slave degrees of freedom hold certain relations that are consistent with the system dynamics. The invariant manifolds are tangent to their respective eigen modes at the equilibrium points. The overall response of the non-linear dynamical system is evaluated based on the response at the master degrees of freedom, which are related to the slave degrees of freedom through invariant manifolds. Bovin *et al* (1995) used polynomial expression function to correlate master and slave degrees of freedom and formed NNMs for weakly non-linear systems. Neyfeh *et al* (1996) used similar technique for cubic non-linear systems. Peschek *et al* (2002) proposed numerical technique to solve invariant manifold equations for general non-linear system, where the master coordinates are transformed into polar coordinates and Galerkin approach is adopted to obtain the response. The advantage of invariant manifold based approach is in their application to tackle both conservative as well as non-conservative systems along with gyroscopic or general damping. Although, there has been research on solving the response of non-linear dynamical systems by NNMs, not much attention has been focused by the researchers on identifying the system from the vibration signals.

## 1.3 Non-stationary Excitation Model

Once the system parameters have been identified, evaluation of structural response requires modeling of input processes. Characterization of input processes is required not

only for time history simulation, but also for carrying out random vibration analysis for safe design of the structures as the input excitation processes are often stochastic in nature (e.g. earthquake).

### 1.3.1 Single Component Earthquake Ground Motion Model

Characterization of earthquake ground motions for the purpose of random vibration analysis is mostly performed using stationary or amplitude modulated stationary models. Exact time history simulation of earthquake ground motions have been studied by various researchers and physical models are developed provided detailed site-specific information is available. Earthquake ground motions are known to be non-stationary in both intensity and frequency content arising due to reflection, refraction and attenuation of different seismic waves (such as S and P waves) through different soil strata [Clough and Penzien (1993)]. Stationary or amplitude modulated stationary models are incapable of addressing issues related to temporal variations of the frequency content. Housner (1964) proposed to model earthquake as a stationary white noise whose intensity represents the energy of the recorded time history in an average sense. In separate studies, Kanai (1957) and Tajimi (1960) proposed to model earthquake as the response power spectral density function of a second order linear filter subjected to Gaussian white noise. Parameters of this linear filter represent site properties like soil damping and natural frequency. This model is widely used for random vibration analysis of linear/non-linear structures and is commonly called Kanai-Tajimi spectra. Although these stationary models can incorporate local soil parameters, they are inherently incapable of modeling

non-stationarity involved in earthquake ground motions. For this purpose, an amplitude modulated stationary process model was proposed by Amin and Ang (1968), Shinuzoka and Sato (1967) and Shinuzoka and Deodatis (1988) among the others. According to this concept, a stationary random process model is multiplied by a deterministic uniform amplitude modulation function. The parameters of this deterministic envelope function are evaluated from the recorded accelerogram. A number of envelope functions are proposed in the literature among which the model proposed by Shinuzoka and Sato (1967) is the widely used. Der Kiureghian (1989) proposed uniform amplitude modulation using exponential function, gamma function and piecewise linear function and evaluated their parameter based on recorded time history of Orion earthquake [Der Kiureghian and Crempien (1989)].

From these studies, it can be noticed that earthquake is either modeled as stationary process or amplitude modulated non-stationary process, which are incapable of modeling evolutionary nature of the frequency content of ground motions. A fully non-stationary earthquake ground motion model is proposed by Conte and Peng (1997), where the ground motion is expressed as sum of sigma oscillatory processes, each of which is amplitude modulated stationary process. The parameters of the sigma oscillatory processes are optimized so that the simulated power spectral density (PSD) function matches with the recorded PSD. This is one of the first and the only model that has been proposed so far to account for non-stationary nature earthquake ground motions. Though successful in representing the non-stationarity in frequency content, number of unknown parameters in their study was 105. Rofooei *et al* (2001) proposed a non-stationary Kanai-Tajimi model for earthquake simulation. Their model is relatively simple and is

applicable to time history simulation but cannot be used for random vibration analysis. Beside conventional techniques, contemporary signal processing tools like wavelet analysis has gained popularity in the field of random vibration in the recent past. Mukherjee and Gupta (2002a, 2002b) proposed wavelet based model for spectrum compatible earthquake simulation. In these studies, earthquake time history is simulated as a summation of time histories in a number of non-overlapping frequency bands such that overall time history matches with the design spectrum. Although these models focus on the exact simulation of earthquake records, they are too complex to use for random vibration analysis of linear or non-linear structures. Moreover unavailability of site-specific data poses serious challenges for exact modeling and simulation of ground motion time histories, especially in view of evolutionary nature of frequency content of earthquake ground motions. Very few studies, so far, have been addressed the problem of developing models to account for stochastic variation of frequency content with time, which is often noticed in the earthquake ground motions.

### 1.3.2 Spatially Varying Earthquake Ground Motion (SVEGM) Model

Besides response evaluation of structures due to a single component of earthquake ground motions, seismic response analysis of extended structures such as long span bridges, large foundations, dams, pipelines and tunnels has drawn attention of several previous researchers. Seismic waves travel through different layers of soil, where the primary waves of different frequencies travel with different speeds and are mixed with secondary waves originating from reflection and refraction through different soil layers.

These phenomena of wave passage and loss due to coherency have pronounced effects on the response of extended structures. Moreover, it has been observed by the previous researchers that the structures whose spatial extent is large i.e. extended structures like bridges; tunnels suffer spatially varying earthquake ground motion. This is due to the fact that besides phase shift effect and loss due to coherency, ground motion suffers attenuation from one support to another. All these effects along with non-uniformity in the ground motions due to local soil characteristics are commonly called spatial variability effect. Recent research works based on the recorded seismological data of SMART-1 array in Taiwan show the importance of the proper mathematical model to analyze the effects of spatial variability of seismic ground motion on the stochastic response of the structures. Harichandran and Vanmarcke (1986), Loh (1995) showed that the seismic ground motion could vary significantly over the spatial extent of the structure and proposed an exponential model for coherence between the support motions. Chen and Harichandran (2001) used linear model to predict the response over the extent of large structure like dam. In separate studies, Harichandran and Vanmarcke (1986), Hao *et al* (1989), Hindy and Novak (1980), Abrahamson (1993) and Uscinski (1977) proposed exponential models for loss due to coherency. Although, these studies were mostly preformed in the framework of stationary random vibration analysis, the problem becomes more complex if non-stationary ground motions are considered.

## 1.4 Stochastic Response Analysis of Structural Systems

Stochastic response analysis of structures under random excitations has remained an active area of research over the last few decades. For this purpose, structures can be classified into two categories; (a) single or multi supported structures whose spatial extent is small like buildings and (b) large multi supported structures like bridges, pipelines etc.

### 1.4.1 Structures with Small Spatial Extent

Although stationary analysis is relatively simple to perform, most of the vibrations due to earthquake ground motions lead to non-stationary responses. Conventional techniques to tackle these problems have been discussed in texts of random vibrations [Newland (1993), Lin and Cai (1995)]. Researches by Caughey and Stumph (1961), Barnoski and Maurer (1969) and Bornio and Paola (1988) have provided input-output relations of dynamical systems subjected to random excitations. These studies mainly address non-stationary response of a single degree of freedom (SDOF) system under amplitude-modulated white noise or other stationary processes. Gasprini (1979) and Gasprini and DebChaudhury (1980) have proposed input-output relations of multi degree of freedom (MDOF) systems, where the input is modelled as uniform amplitude modulated Gaussian white noise. They used a state space model of the MDOF system to estimate the evolutionary response at the output as well as the first passage time of failure. These

studies are incapable of addressing issues related to temporal variations of the frequency content in the input and hence the output. To account for the temporal variation in frequency content, short term Fourier transform (STFT) based approaches exist in literature. But the STFT based approaches have their own limitations as the resolution of these techniques depends upon the width of the time window used.

Conte and Peng (1997) have proposed an explicit analytical form for correlation matrix and the time varying power spectral density function of the response of a MDOF system. In this study, the input is considered to be a stationary random vector process modulated by an envelope function proposed by Saragoni and Hart (1974). Although this analytical form can model the response with non-stationary in both amplitude and frequency content, it becomes difficult to implement such algorithm for real life structures using series solution.

The conventional techniques can be used to account for amplitude non-stationarity; the techniques in dealing with frequency non-stationarity are far more complex. For this purpose, wavelet based time-frequency analysis is a promising alternative to account for both types of non-stationarity. Basu and Gupta (1997, 1998) have proposed input-output relations of dynamical system under random excitations using continuous wavelet transformation. A modified form of Littlewood-Paley (L-P) basis function, which is the real part of the harmonic wavelet basis function [Newland (1993)] was proposed to evaluate the second order moment statistics of the response. Tratskas and Spanos (2003) have recently proposed the discrete wavelet transformation technique using harmonic wavelet basis function to study the response of multi degree freedom system under random support excitations. Spanos and Failla (2004) have

proposed a generalized mathematical model for evolutionary random process. This work provides a framework for generalized definition of non-stationary random processes and is valid for any wavelet basis function (orthogonal or non-orthogonal).

### 1.4.2 Structures with Large Spatial Extent

Earlier research work by Lin and Loceff (1980) showed that the assumption of spatial uniformity in ground motions for large structures leads to erroneous results. To overcome this problem, DerKurieghan and Hofer (1992) and Loh and Ku (1995) proposed response spectrum based techniques to take into account the effects of spatial as well as temporal variation of the seismic ground motions. These studies mostly emphasized on the correlation between the support motions and the different modes in stationary random vibration framework. Berrah and Kausel (1992) proposed a correlation factor based approach that depends on the structural properties and the wave propagation phenomenon to study the effects of spatial variation. All the above-mentioned studies were performed to evaluate the effects of spatially varying earthquake ground motions (SVEGM) on extended structures. Previous researchers established the model of SVEGM during their studies on SMART-1 array data of Taiwan. Harichandran and Wang (1988), and Harichandran *et al* (1996) studied the response of structures for which the seismic ground motions could vary significantly over the spatial extent and proposed an exponential model for coherence between the support motions.

Although the above-mentioned research studies mostly use stationary random vibration theory, earthquake is known to be inherently non-stationary in both intensity

and frequency content. The effect of SVEGM on structures becomes more complex in the light of these phenomena and hence needs proper attention. To model the non-stationary amplitude of the ground motions, a uniform amplitude modulation using exponential function or gamma function or piecewise linear functions were proposed by Der Kiureghian and Crempien (1989). The parameters of these amplitude-modulating functions were evaluated based on the recorded time history of Orion earthquake.

### 1.4.3 Primary-Secondary Systems

Besides structures with either large spatial extent, a fresh kind of problem arises for structures that house other small structures. These are known as primary-secondary (P-S) systems. Several researchers have studied dynamic response analysis of P-S systems in the past [Singh (1975), Der Kiureghian *et al* (1983), Sackman *et al* (1983)]. Broadly, these systems can be classified into two major groups – non-structural secondary systems such as mechanical instruments and structural secondary systems such as piping networks, which are firmly attached to the primary structure. It is a general practice to evaluate the response of the secondary system based on the response of the primary system at the locations where the secondary system is supported. This floor response spectra based approach is widely popular among the engineers and different design codes (4, 105) have specific guidelines based on this cascading approximation. Although this approximation works better when the frequencies of the primary and secondary systems are well apart, it gives erroneous results during tuning between the primary and secondary systems [Singh (1975)]. This tuning effect along with variations in mass

imbalance between the primary-secondary systems often leads to significant dynamic interaction between the responses of the primary and the secondary systems. Moreover, the difference in material properties and damping characteristics of the P-S systems give rise to non-classical damping due to which decoupling of the dynamic equilibrium equation using modal matrix based on conventional eigen analysis is not possible. Under this condition, the response can be evaluated by direct time integration or by modal decoupling using complex modal matrix obtained from eigenanalysis considering damping as proposed by Foss (1958). Besides complex eigenanalysis, some of the earlier studies by Der Kiureghian and Hoffer (1992) proposed a perturbation approach, where the secondary structure is treated as a system with small parameters and the response is obtained using different modal combination rules.

A vast majority of these research investigations deal with the response of P-S systems in a deterministic framework. But in reality, structures are subjected to random inputs like earthquake induced ground motion or wind. Villaverde (1988) proposed a modified form of Rosenblueth's modal combination rules for P-S systems subjected to white noise. Sinha and Igusa (1995) have studied the response of P-S systems subjected to amplitude-modulated white noise. Although these studies consider the excitation to be white noise or amplitude modulated stationary signal, an input like earthquake ground motion is known to possess non-stationary intensity and frequency content. Conventional non-stationary random vibration analysis based on short time Fourier transform (STFT), whose resolution largely depends on the window width faces inherent difficulties due to constant window width. Moreover, numerical instabilities like Gibbs phenomenon are often observed in Fourier analysis, which renders further challenges to their

implementation for spectral analysis of complex structures such as P-S systems. Besides numerical instability associated with Fourier based approach for spectral analysis, simulation based approach has its own difficulties as it needs generation of an ensemble of the input processes before their algorithmic implementation for direct time integration. Exact simulation of the time history records for random process like earthquake from a single realization of recorded time history is not only computationally exhaustive but also challenging in absence of detailed site information. An alternative to this problem is the time-frequency based approach [Cohen (1989), Qian and Chen (1996)]. Due to the difficulties in non-stationary spectral analysis using conventional techniques, contemporary techniques based on wavelet transform has gained momentum in the recent past. Basu and Gupta (1997, 1998) have proposed wavelet based input-output relations of linear systems. They have used continuous wavelet transform to obtain time varying stochastic response of the dynamical systems. Failla *et al.* (2003) used discrete wavelet transform to study the non-stationary response of multi-degree of freedom non-linear system.

## 1.5 Wavelet Transform

Since wavelet transform is used as a key mathematical tool in the system identification, characterization of excitation processes and stochastic response analysis of structural dynamic system in this thesis, an overview of the technique with some details is presented. The wavelet transform has been used by researchers for several applications

such as filtering, transient analysis, time-frequency analysis, non-stationary analysis, discontinuity detection, data compression, and system identification and damage detection among many others. The capability of the wavelet for carrying out time frequency analysis has been exploited in this thesis for the identification of modal parameters, characterization of ground motions and non-stationary response of dynamical systems.

In wavelet analysis a signal $x(t)$, a function of time $t$, is expressed as a composition of several time localized shifted and scaled basis functions, $\psi\left(\frac{t-b}{a}\right)$ where '$b$' and '$a$' are the shifting and scaling parameters respectively. The shift or translational parameter centers the wavelet function so that information can be obtained about the signal around the location $t = b$. The dilation or scale parameter, '$a$' can be varied to compress or extend the basis function to control the range of frequencies about which information can be obtained in the vicinity of the location $t = b$, by wavelet transformation. Wavelet transform converts an initial data sequence representing a chosen length of input signal $x(t)$ into a new two-dimensional sequence, which consists of the coefficients $W_\psi x(a,b)$ and is defined by [Chan (1995), Rao and Bopardikar (1998)]

$$W_\psi x(a,b) = \frac{1}{\sqrt{a}} \int_{-\infty}^{+\infty} x(t)\psi\left(\frac{t-b}{a}\right)dt \tag{1.1}$$

The wavelet transform is an integral transform which convolutes the wavelet basis function $\psi(t)$, called the mother wavelet with the function $x(t)$ being analyzed to generate the wavelet coefficients. The wavelet coefficients expressed in equation 1.1 provides temporal information of the function $x(t)$ at a scale of '$a$' corresponding to the frequencies at that scale given by the Fourier transformation of $\frac{1}{\sqrt{a}}\psi\left(\frac{t-b}{a}\right)$ i.e. $\sqrt{a}\hat{\psi}(a\omega)e^{-i\omega b}$; $\hat{\psi}(\omega)$ being the Fourier transform of the mother basis $\psi(t)$. The coefficient $W_\psi x(a,b)$, at a given scale of '$a$', is a function of a shift parameter '$b$', which reflects the concentration of the frequencies corresponding to the given scale, around the time $t = b$. The admissibility criteria that is satisfied by the time function $\psi(t)$ to be a mother wavelet is given by [Rao and Bopardikar (1998)]

$$C_\psi = \int_{-\infty}^{+\infty} \frac{|\hat{\psi}(\omega)|^2}{|\omega|} d\omega < \infty \tag{1.2}$$

where, $\hat{\psi}(\omega)$ is the Fourier transform of the basis function $\psi(t)$. In the present thesis, the following continuous basis functions have been used for wavelet analysis.

### 1.5.1 Harmonic Wavelet Basis Function

Harmonic wavelet has the mother wavelet $\psi(t)$ whose spectrum is exactly like a box so that its Fourier transform $\hat{\psi}(\omega)$ is defined as

$$\hat{\psi}(\omega) = \frac{1}{\sqrt{2\pi}} \quad \text{if } 2\pi \le \omega \le 4\pi \tag{1.3}$$

$$= \quad 0 \qquad \text{elsewhere}$$

Then by calculating the inverse Fourier transform $\psi(t)$, the corresponding complex wavelet is

$$\psi(t) = \frac{\left(e^{i4\pi t} - e^{i2\pi t}\right)}{i2\pi t} \tag{1.4}$$

with real and imaginary parts. The introduction of a complex function allows two real wavelets to be represented by a single expression. The real part of $\psi(t)$ represents an even wavelet and the imaginary part represents an odd wavelet. The Fourier transform of the general baby wavelet, at level *'j'* (i.e. scaled by $a = 2^j$), and translated by *'b'*, is defined as

$$\hat{\psi}(\omega) = \left(\frac{1}{\sqrt{2\pi}}\right)\sqrt{2^{-j}}\, e^{\frac{i\omega b}{2^j}} \qquad \text{for } 2\pi \le \frac{\omega}{2^j} \le 4\pi$$

$$= \quad 0 \qquad \text{elsewhere} \tag{1.5}$$

On inverse Fourier transform, equation 1.5 gives

$$\psi\left(\frac{t-b}{2^j}\right)=\frac{\left(e^{i4\pi\left(\frac{t-b}{2^j}\right)}-e^{i2\pi\left(\frac{t-b}{2^j}\right)}\right)}{i2\pi\left(\frac{t-b}{2^j}\right)} \tag{1.6}$$

The harmonic wavelets have been found particularly suitable for vibration analysis because their harmonic structure is similar to the naturally occurring vibration signals of the structures and therefore they correlate well with experimental signals [Newland (1993)].

### 1.5.2 Modified L-P Basis Function

An equivalent of the Harmonic wavelet, when the basis function is real, is Littlewood-Paley wavelet. This wavelet basis function is defined by

$$\psi(t)=\frac{1}{2\pi}\cdot\frac{\sin(4\pi t)-\sin(2\pi t)}{t} \tag{1.7}$$

A possible variation of the wavelet is one, which retains the characteristic of the basis function (close to transient vibration signals, i.e. oscillatory and decaying) but could reduce the frequency bandwidth of the mother wavelet. Hence, the derived modified wavelet is called the modified L-P wavelet and has been proposed and used by Basu and Gupta (1997, 1998). The shifted and scaled version of this is called the baby modified

L-P wavelets. This wavelet basis has also been used by Basu (2003, 2004, 2005) for damage detection in structures.

The modified L-P basis function is defined by

$$\psi(t) = \frac{1}{\pi\sqrt{2F_1(\sigma-1)}} \cdot \frac{\sin(2\pi F_1 \sigma t) - \sin(2\pi F_1 t)}{t} \tag{1.8}$$

where $\sigma$ (is a scalar) > 1. In frequency domain the wavelet basis can be represented by

$$|\hat{\psi}(\omega)| = \frac{1}{\sqrt{4\pi F_1(\sigma-1)}}, F_1 \leq \left|\frac{\omega}{2\pi}\right| \leq \sigma F_1$$

$$= \quad 0 \quad \text{otherwise} \tag{1.9}$$

In the above equation, $\sigma = 2$ leads to conventional L-P basis function, which is the real part of the harmonic wavelet basis proposed by Newland (1993). $F_1$ is the initial cut-off frequency of the mother wavelet. By choosing appropriate values for the bandwidth, the frequency content of the mother wavelet can be adjusted. If for numerical computation the scaling parameter is discretized as, $a_j = \sigma^j$ (in an exponential scale), then the scaled version of the mother basis function has mutually non-overlapping frequency bands and are also orthogonal. This property can be conveniently utilized to detect natural frequencies and modal properties for the dynamical systems as can be seen in the following chapters in this thesis.

### 1.5.3 Morlet Basis Function

Morlet wavelet basis function also has similar characteristics of a vibrating signal (i.e. exponentially decaying sinusoids), which is given by

$$\psi(t) = e^{-t^2/2}\cos(\lambda t) \tag{1.10}$$

On taking Fourier transform, it can be shown that the frequency domain description of the above basis function with central frequency at $\lambda$ is given by

$$\hat{\psi}(\omega) = \frac{e^{\left(-\omega^2-\lambda^2\right)}}{2}\left(e^{\frac{(\omega-\lambda)^2}{2}} + e^{\frac{(\omega+\lambda)^2}{2}}\right) \tag{1.11}$$

## 1.6 Organisation of Thesis

The work reported in this thesis is mainly focused on the identification of the structural parameters from the measured time history records and estimation of their vibration characteristics when subjected to evolutionary input. A generalized time-frequency framework is proposed to model these non-stationary inputs with time varying frequency content for obtaining the non-stationary output. The thesis has been segmented into eight chapters following this chapter.

In **Chapter 2,** a methodology for identification of modal parameters of a structural systems using wavelet analysis is proposed. The proposed technique differs from the other works on using wavelet for this problem in the choice of the basis function. A modified form of Littlewood-Paley (L-P) basis function is used for the identification of the parameters. This basis has the advantage being more closely representing a vibrating signal. Further it is localized in frequency and hence can be used to detect the frequency and the associated parameters better. The current work identifies modal parameters such as natural frequencies and mode shapes of a linear multi degree of freedom (MDOF) system using the wavelet transform. Based on this wavelet-based technique for parameter estimation an online identification of variation of stiffness in structural systems has been presented. Further, an algorithm for detection of variation in modes shapes in time-varying linear multi-degree-of-freedom (MDOF) systems has been developed. Several types of changes in stiffness such as a sudden jump, a ramp change or a sudden change with subsequent restoration of stiffness have been considered as illustrative examples in case of single-degree-of-freedom (SDOF) and MDOF systems.

**Chapter 3** presents a wavelet based identification procedure for obtaining the fundamental frequency and the mode shape of dynamical systems when the recorded time history response is contaminated with measurement noise. For this purpose, a simply supported bridge is considered, which is excited by a point-load moving with constant velocity. A laboratory experiment is then performed using a reinforced concrete beam, which is vibrated by an impulsive load at the middle. The fundamental mode and mode shape is then estimated from the noise contaminated strain response time histories at key locations.

**Chapter 4** presents wavelet-based identification of localized normal modes of a non-linear system. Although conventional normal modes do not exist in non-linear systems, a synchronous motion is known to exist for a class of non-linear problems. This '*vibration in unison*' imposes a definite relation among the degrees of freedom, when the system vibrates close to their equilibrium points. A wavelet-based identification of these motion and the associated parameters have been discussed in this chapter.

In **Chapter 5**, the input excitation such as an earthquake process has been stochastically characterized to represent the non-stationary amplitude and frequency content in order to use it to analyze the response of the identified structural dynamic systems. A frequency dependent amplitude modulating function is proposed for the characterization of seismic ground motions. Using this proposed characterization, a generalized evolutionary model for earthquake ground motion is developed in the present study. The earthquake ground motion process is modeled as a summation of amplitude modulated stochastic orthogonal processes in different frequency bands. A non-linear least square technique is adopted to minimize the error between the temporal energy growth of the recorded time history and that obtained from the proposed model in each frequency bands. This gives the amplitude modulating function in different frequency bands for the purpose of minimizing the error in temporal energy, wavelet based time-frequency analysis is used to evaluate the time varying energy content in different frequency bands. Finally, the proposed wavelet-based model for single component earthquake ground motion is extended to model the spatially varying earthquake ground motions (SVEGM).

Following the wavelet-based model for identification of structural parameters of dynamical systems and modeling of non-stationary input, **Chapter 6** discusses wavelet-based non-stationary response analysis of boundary value problems. For this purpose, a short span bridge is first considered; whose governing equation of motion possesses non-homogenous boundary conditions. The supports motions for these kinds of structures do not suffer spatial variations. The proposed formulation uses the continuous parameter wavelet based random vibration theory coupled with Mindlin-Goodman transformation (1950), to estimate the evolutionary power spectral density function of the response of the bridge in closed form. For this purpose, modified L-P basis function has been used to evaluate the stochastic response of the system. The basis function used in the present study being completely localized in frequency, simplifies the numerical work considerably. The proposed mathematical formulation can evaluate time varying stochastic response with amplitude as well as frequency non-stationarity and is validated through statistical simulation.

**Chapter 7** presents a wavelet-based formulation of the input-output relation of the spatially extended structures in finite element framework. For this purpose, a bridge has been modelled as a simply supported beam with multiple spans in the finite element framework to obtain the dynamic properties. The non-stationary spatially varying support motions are characterized following the proposed generalized wavelet-based approach. An exponential coherence function is used to model the spatial variation of the ground motion. A wavelet based non-stationary response analysis of a discrete primary-secondary systems is also proposed in this chapter, where the secondary piping network is housed inside the secondary structure. The stiffness and damping characteristics of the

two sub-systems vary considerably and hence give rise to a system with non-classical damping. The primary structure is subjected to random support motion with non-stationarity in both amplitude and frequency content. Continuous wavelet transform is used to provide input-output relation between the base motion and the response of the secondary system. Numerical examples based on statistical simulation are used to illustrate the efficiency and accuracy of the proposed wavelet-based model.

In the final chapter, a summary of the work has been presented based on the analytical and experimental results presented in the previous chapters. The overall objectives of the proposed work and their advantages and disadvantages have been discussed in this chapter. Finally, a few suggestions have been proposed for the further research.

# Chapter 2: Identification of Modal Parameters of MDOF Systems

## 2.1 Introduction

In this chapter, a methodology is proposed for identification of the modal frequencies and mode shapes of a time invariant structure using a modified version of the Littlewood-Paley (L-P) wavelet for time-frequency analysis. Besides being close to the vibrating signals, this wavelet basis function can be used to develop a sub-band coding leading to the wavelet packets for better accuracy as desired. The basis is also localized in frequency and hence does not suffer from the problem of band overlapping. The technique is presented for extracting the modal parameters of a linear multi degree of freedom (MDOF) system by decomposition of the original signal into frequency bands via wavelet transform, and time dependent analysis of each band using the basic properties of eigen-values of vibration modes. Two example cases of three degrees of freedom (3DOF) and five degrees of freedom (5DOF) linear viscously damped systems have been considered here. The vibration data are generated by simulating the response of the damped MDOF systems under free vibration conditions. The response signals are used to identify the modal parameters.

Following this identification procedure, a wavelet based on-line identification of stiffness of structural system has been proposed for time varying systems. A modified L-P wavelet basis with wavelet packets has been used in the proposed algorithm. Formulations for a single degree of freedom (SDOF) system and MDOF system have been presented. Illustrations have been used to show the efficiency of the proposed tracking algorithm.

## 2.2 Wavelet Based Algorithm for System Identification

The wavelet transform has been used by researchers for several applications such as filtering, transient analysis, time-frequency analysis, non-stationary analysis, discontinuity detection, data compression, system identification and damage detection among many others. The capability of the wavelet for carrying out time frequency analysis has been exploited in this chapter for the identification of modal parameters of both time invariant as well as time varying dynamical systems.

### 2.2.1 Time Invariant Systems: Off-line Identification Strategies

A methodology to extract the natural frequencies, mode shapes and modal damping from the ambient free vibration response of a linear MDOF system is presented here. The responses $X(t)$ of a $n$-DOF classically damped linear system under free vibration condition is governed by the differential equation

$$[M]\{\ddot{X}\}+[C]\{\dot{X}\}+[K]\{X\}=0 \tag{2.1}$$

where, $[M]$, $[C]$ and $[K]$ are the mass, damping and stiffness matrices with the over-dot representing the differentiation with respect to time. To decouple equation 2.1 into $n$-SDOF equations, the following transformation is used

$$\{X(t)\} = [\Phi]\{U(t)\} \tag{2.2}$$

where, $\Phi$ is the modal matrix or the matrix of the mode shapes and $U(t)$ is the vector of modal responses. Assuming damping matrix to be proportional to the mass and stiffness matrices, the $k^{th}$ modal response can be obtained from the decoupled modal equations

$$\ddot{u}_k + 2\rho_k \omega_{n_k} \dot{u}_k + \omega_{n_k}^2 u_k = 0; \qquad k = 1,2,...,n. \tag{2.3}$$

In equation 2.3, $\rho_k$, $\omega_{n_k}$ are the $k^{th}$ damping ratio and natural frequency respectively. The $m^{th}$ degree-of-freedom or state of response can be represented by a linear combination of mode shapes and modal responses as

$$x_m = \sum_{k=1}^{n} \phi_m^k u_k; \qquad m = 1,2,...,n. \tag{2.4}$$

The solution of equation 2.3 is given by

$$u_k(t) = e^{-\rho_k \omega_{n_k} t}\left[C_{1_k} \cos(\omega_{d_k} t) + C_{2_k} \sin(\omega_{d_k} t)\right] \tag{2.5}$$

where, $C_{1_k}$ and $C_{2_k}$ are arbitrary constants to be obtained from the initial conditions [i.e. $u_k(0)$ and $\dot{u}_k(0)$] and $\omega_{d_k} = \omega_{n_k}\sqrt{1-\rho_k^2}$. Equation 2.5 can be written as

$$u_k = \alpha_k(t)\cos(\omega_{d_k} t + \theta_k) \tag{2.6}$$

where $\alpha_k(t)$ is a slowly varying function of time for lightly damped system i.e. $\rho_k \langle\langle 1.0$ and $\theta_k$ is the phase angle. The response $u_k(t)$ can be reasonably considered to be a narrow banded signal with frequencies around $\omega_{d_k}$.

The wavelet transform of the response $x_m(t)$ at $m^{th}$ degree-of-freedom can be expressed as (section 1.5)

$$W_\psi x_m(a_j, b) = \frac{1}{a_j}\int_{-\infty}^{+\infty} x_m(t)\psi\left(\frac{t-b}{a_j}\right)dt \tag{2.7}$$

where, both $x_m(t)$ and the wavelet basis function $\psi(t)$ are real. In the present chapter, the modified form of the L-P basis function (section 1.5.2) is used. The scaling parameter is discretized in an exponential scale '$a_j$' and the discretization is performed as $a_j = \sigma^j$, where $\sigma$ is a scalar and the parameter '$b$' is discretized in linear scale. On wavelet transforming both sides of equation 2.4 gives

$$W_\psi x_m(a,b) = \sum_{k=1}^{n} \phi_m^k W_\psi u_k(a,b); \qquad m = 1,2,...,n. \tag{2.8}$$

The normalized energy $E_j(x_m)$ for the response $x_m$, in the frequency band corresponding to a scaling factor $a_j = \sigma^j$ with the index '*j*', can be represented by a proportional quantity as

$$E_j(x_m) \propto \frac{1}{a_j^2} \int W_\psi^2 x_m(a_j, b)db; \qquad m = 1,2,...,n. \tag{2.9}$$

Let the natural frequencies $\omega_{n_1}, \omega_{n_2}, ..., \omega_{n_n}$ be contained in the bands with scale or dilation parameter indices, $j_1, j_2, ..., j_n$ respectively. Since, response of the $k^{th}$ mode $u_k$, is narrow banded with frequencies around $\omega_{d_k}$ (where $\omega_{n_k} \approx \omega_{d_k} \in \left[\frac{\pi}{a_{j_k}}, \frac{\sigma\pi}{a_{j_k}}\right]$, for lightly damped system) and $\hat{\psi}(a_j\omega)$ has frequencies in the $j^{th}$ band within the interval $\left[\frac{\pi}{a_j}, \frac{\sigma\pi}{a_j}\right]$

$$W_\psi u_k(a_j, b) = \int u_k(t)\psi\left(\frac{t-b}{a_j}\right)dt = \sqrt{a_j}\int \hat{u}_k(\omega)\hat{\psi}(a_j\omega)e^{-i\omega b}dw \approx 0 \text{ if } j \neq j_k \tag{2.10}$$

On using equation 2.8 and 2.10, one gets

$$\begin{aligned} W_\psi x_m(\sigma^j, b) &\approx 0 && \text{if } j \neq j_k,\ k = 1,2,...,n \\ &= \phi_m^k W_\psi u_k(a_{j_k}, b) && \text{if } j = j_k,\ k = 1,2,...,n \end{aligned} \tag{2.11}$$

Thus, equations 2.9 and 2.11 lead to

$$E_j(x_m) \neq 0 \qquad if \quad j = j_k,\ k = 1,2,...,n$$

$$\approx 0 \qquad \text{otherwise} \tag{2.12}$$

To detect the bands of frequencies in which the natural frequencies lie, the energy corresponding to each band is calculated for a particular state of response using equation 2.9. The bands, which do not contain the natural frequencies, lead to insignificant energy contribution. Hence, the first $n$ bands with significant energy content are the bands where the natural frequencies are located. These bands are in increasing order corresponding to the first '$n$' natural frequencies i.e. the lowest frequency band has the first natural frequency and so on.

However, the chosen bands may lead to bands with relatively broad interval in which the natural frequencies lie. To refine the estimates into finer intervals, so that natural frequencies could be determined to a better precision, wavelet packets are used. This is an extension of wavelet transform to provide level-by-level time-frequency description and is easily adaptable for the modified L-P basis. The wavelet packet enables extraction of information from signals with an arbitrary time-frequency resolution satisfying the product constraint in the time-frequency window. In this technique, to refine the estimation of the $k^{th}$ natural frequency, $\omega_{n_k}$, located in the $j_k^{th}$ band, i.e. with frequency band $\left[\frac{\pi}{a_{j_k}}, \frac{\sigma\pi}{a_{j_k}}\right]$, further re-division is carried out. If it is required to further subdivide the band in '$M$' parts, then again an exponential scale is used to divide the band

so that the corresponding time domain function forms a wavelet basis function. In this approach [also sometimes, termed as sub-band coding, (Chan 1995)], for the $j_k^{th}$ band, the mother basis for the packet, $\psi^s(t)$ is formed with the frequency domain description

$$\hat{\psi}^s(\omega) = \frac{1}{\sqrt{2\pi(\delta-1)}} \qquad \text{for } \pi \le |\omega| \le \delta\pi$$

$$= \quad 0 \qquad\qquad\qquad \text{elsewhere} \qquad\qquad (2.13)$$

where $\delta^M = \sigma$ [with $\delta$ (a scalar) > 1]. The corresponding time domain description is given by

$$\psi^s(t) = \frac{1}{\pi\sqrt{(\delta-1)}} \cdot \frac{\sin(\delta\pi t) - \sin(\pi t)}{t} \qquad (2.14)$$

The frequency band for the $p^{th}$ sub-band within the original $j_k^{th}$ band is the interval $\left[\frac{\delta^{p-1}\pi}{a_{j_k}}, \frac{\delta^p \pi}{a_{j_k}}\right]$. The basis function for this is denoted by $\psi^{sp}_{a_{j_k},b}(t)$. The wavelet coefficient in this sub-band is denoted by $W_{\psi_{sp}} x_m(a_{j_k}, b)$. Using the wavelet coefficients in these sub-bands and then applying similar expression as in equation 2.12, to estimate the relative energies in the sub-bands, the natural frequencies can be obtained more precisely.

Once the natural frequencies are obtained and the corresponding bands are identified, the sub-band containing the $k^{th}$ natural frequency with scale parameter $j_k$ and

the sub-band parameter '$p$' are considered to obtain the $k^{th}$ mode shape. From equation 2.8, we get

$$W_{\psi_{sp}} x_m(a_j, b) = \sum_{k=1}^{n} \phi_m^k W_{\psi_{sp}} u_k(a_{j_k}, b); \qquad \text{m=1,2,...,n} \tag{2.15}$$

Now, considering the responses of two states or degrees-of-freedom in a MDOF system, (with one arbitrarily chosen as $m=1$, without loss of generality), the ratio of wavelet coefficients of the two considered degrees of freedom at an instant of time $t = b$, corresponding to band $j_k$ with sub-band, $p$, (using equation 2.11 and 2.15) yields,

$$\prod_m^{j_k} = \frac{W_{\psi_{sp}} x_m(a_{j_k}, b)}{W_{\psi_{sp}} x_1(a_{j_k}, b)} = \frac{\phi_m^k}{\phi_1^k} \tag{2.16}$$

Thus it is seen that the computed ratio of the wavelet coefficients are invariant with '$b$'. Hence, computing these ratios for different states corresponding to different values of '$m$' and assuming $\phi_1^j = 1$ (without loss of generality), the mode shape for the $k^{th}$ mode (in $j_k$ band with further sub-band division) can be obtained as

$$\{\phi_m^k\} = \{\prod_m^{j_k}\}; \qquad m = 1,2,...,n. \tag{2.17}$$

Thus, mode shape for any other mode can be obtained in a similar manner for $k$ = $1,2,...,n$.

To estimate the modal damping of a MDOF system, let us consider equation 2.6, which gives the $k^{th}$ modal response. This response $u_k(t)$ is narrow banded around $\omega_{n_k}$, and is modulated by a slowly varying time function, $\alpha_k(t) = A_k e^{-\rho_k \omega_{n_k} t}$ where, $A_k$ is a constant. Thus, if this expression is used to evaluate the wavelet coefficient in equation 2.8, then the term $\alpha_k(t)$ can be approximated by $\alpha_k(b) = A_k e^{-\rho_k \omega_{n_k} b}$ i.e. $\alpha_k(t)$ evaluated at $t=b$, and considered as a constant over the integral. This is because, $\psi\left(\frac{t-b}{a}\right)$ is more oscillatory and faster decaying as compared to $\alpha_k(t)$ and is localized around $t=b$. Further, since both $\cos(\omega_{d_k} t + \theta_k)$ and $\psi\left(\frac{t-b}{a}\right)$ are narrow banded around $\omega_{n_k}$, evaluation of the integral for the wavelet coefficient for the original band, $j_k$ and the sub-band, $p$ containing the $k^{th}$ natural frequency leads to

$$W_{\psi_{sp}} x_m(a_{j_k}, b) = \tilde{K}_{p_k} e^{-\rho_k \omega_{n_k} b} \tag{2.18}$$

where, $\tilde{K}_{p_k}$ is a factor depending on the $p^{th}$ sub-band containing the $\omega_{n_k}$ natural frequency. On evaluating equation 2.18 at '$b$' and $\left(b + 2\pi/\omega_{n_k}\right)$ and taking logarithm of the ratio of these expressions, the modal damping is obtained as

$$\rho_k = \frac{1}{2\pi} \cdot \ln \frac{W_{\psi_{sp}} x_m(a_{j_k}, b)}{W_{\psi_{sp}} x_m\left[a_{j_k}, \left(b + 2\pi/\omega_{n_k}\right)\right]} \tag{2.19}$$

### 2.2.2 Time Varying Systems: On-line Identification Strategies

Although, off-line procedures suffice from the point of view of structural health monitoring or FE model updating, on-line identification tools are preamble for implementation of vibration control algorithms.

#### *Case I: On-line Identification of SDOF System*

The on-line identification problem for a linear SDOF system is first considered. The natural frequency of the system is tracked. Let us consider a linear SDOF system with time varying stiffness. The equation of motion of this system may be represented as

$$\ddot{x} + 2\eta\omega_n(t)\dot{x} + \omega_n^2(t)x = f(t) \tag{2.20}$$

where, $\omega_n(t)$ is the time varying natural frequency, $\eta$ is the damping ratio, $x(t)$ is the displacement response due to the excitation $f(t)$. These parameters, $\omega_n(t)$ is a time varying function with discontinuities at finite number of points. Hence, the domain in time can be segmented in several intervals with the time indices $t_0 < t_1 < t_2 < \ldots < t_n$ such that the natural frequency $\omega_{n_i}(t)$ within the interval $[t_{i-1}, t_i]$ is a continuous function. Equation 2.20, thus becomes

$$\ddot{x} + 2\eta\omega_{n_i}(t)\dot{x} + \omega_{n_i}^2(t)x = f(t); t \in [t_{i-1}, t_i]\, i = 1,2,3,\ldots,n \tag{2.21}$$

On multiplying both side of equation 2.20 by $\psi\left(\frac{t-b}{a}\right)$, integrating over $b-\varepsilon$ to $b+\varepsilon$, where $b \in [t_{i-1} - \varepsilon, t_{i+1} + \varepsilon]$ and if $\omega_{n_i}(t)$ is a relatively slowly varying function of time as compared to the fast decaying function $\psi\left(\frac{t-b}{a}\right)$ centred around '$t = b$', we have

$$\int_{b-\varepsilon}^{b+\varepsilon} \ddot{x}(t)\psi\left(\frac{t-b}{a}\right)dt + 2\eta\omega_{n_i}(b)\int_{b-\varepsilon}^{b+\varepsilon} \dot{x}(t)\psi\left(\frac{t-b}{a}\right)dt + \omega_{n_i}^2(b)\int_{b-\varepsilon}^{b+\varepsilon} x(t)\psi\left(\frac{t-b}{a}\right)dt = \int_{b-\varepsilon}^{b+\varepsilon} f(t)\psi\left(\frac{t-b}{a}\right)dt \tag{2.22}$$

In equation 2.22, it has been assumed that $\omega_{n_i}(t)$ is slowly varying and hence can be taken out of the integral as approximately a constant, evaluated around '$t = b$', where the fast decaying function $\psi\left(\frac{t-b}{a}\right)$ is centred. Since, $\psi\left(\frac{t-b}{a_j}\right)$ is a decaying function centred around '$t = b$', it has the advantage that the integral in equation 2.22 may be performed over a finite interval $[b-\varepsilon, b+\varepsilon]$ around '$t = b$' without much loss of information and hence the integral in equation 2.22 may be performed approximately. The choice of $\varepsilon$ would depend on the decay of $\psi\left(\frac{t-b}{a_j}\right)$ or the related central frequency band corresponding to the scale $a_j$. On further using the approximation as discussed in equation 2.22 and on integrating by parts [see Basu and Gupta (2000), Spanos (2004)] leads to

$$\frac{\partial^2}{\partial b^2} W_\psi x(a_j,b) + 2\eta\omega_{n_i}(b)\frac{\partial}{\partial b} W_\psi x(a_j,b) + \omega_{n_i}^2(b) W_\psi x(a_j,b) = W_\psi f(a_j,b) \qquad (2.23)$$

For a particular, band with a corresponding scale of $a_j$, the partial differential equation 2.23 converts to an ordinary differential equation as

$$W''_{\psi_j} x + 2\eta\omega_n(b) W'_{\psi_j} x + \omega_{n_i}^2(b) W_{\psi_j} x = W_{\psi_j} f \qquad (2.24)$$

where, the prime denotes differentiation with respect to $b$ and $W_{\psi_j}(.)$ for brevity represents $W_\psi(.)(a_j,b)$. In the present study, the modified L-P basis function [Basu and Gupta (1997, 1998)] is used for time-frequency analysis, which has a band-limited support in frequency domain. Thus $\hat{\psi}(a_j\omega)$ is supported over $\lfloor \sigma F_1 / a_j, F_1 / a_j \rfloor$ as described in section 1.5.2. Hence, using equation 2.7 for $m = 1$, it follows that the frequency content of the signal $\hat{W}_{\psi_j} x$, a function of $b$, will be also supported over $\lfloor \sigma F_1 / a_j, F_1 / a_j \rfloor$. Thus, $W_{\psi_j} x$ is narrow banded with the central frequency $\omega_{0_j} = \frac{(\sigma+1)}{2}.\frac{F_1}{a_j}$, which is the central frequency of the $j^{th}$ band and can be represented as

$$W_{\psi_j} x(b) = A_j(b) e^{-i(\omega_{0_j} b + \phi_j)} \qquad (2.25)$$

In equation 2.25, $A_j(b)$ is the amplitude or the modulus of the wavelet coefficient function of $x(t)$, $W_{\psi_j} x(b)$, and is given by

$$A_j(b) = \left| W_{\psi_j} x(b) \right| \tag{2.26}$$

and $\varphi_j$ is the phase. On substituting, equation 2.25 in equation 2.24 leads to

$$W_{\psi_j} x(b) = H_j(b) W_{\psi_j} f(b) \tag{2.27}$$

where,

$$H_j(b) = \frac{1}{\left[\omega_{n_i}^2(b) - \omega_{0_i}^2\right] + i\left[2\eta\omega_{n_i}(b)\omega_{0_i}\right]} \tag{2.28}$$

On squaring both sides of equation 2.24, and integrating over $b-\varepsilon$ to $b+\varepsilon$, to get the local energy content of $x(t)$ in $j^{th}$ band around *b*, denoted by $E_j x(b)$, gives

$$E_j x(b) = \frac{1}{2\pi C_\psi} \cdot \frac{1}{a_j} \int_{b-\varepsilon}^{b+\varepsilon} \left| W_{\psi_j} x(b) \right|^2 db = \frac{1}{2\pi C_\psi} \cdot \frac{1}{a_j} \int_{b-\varepsilon}^{b+\varepsilon} \left| H_j(b) \right|^2 \left| W_{\psi_j} f(b) \right|^2 db \tag{2.29}$$

if $f(t)$ is assumed to be a white noise, the local energy content of $f(t)$ in any band would be almost equal and hence the term $\left|W_{\psi_j} f(b)\right|^2$ could be assumed to be almost over the range of the integral in equation 2.29. Thus, it follows that

$$E_j x(b) \propto \frac{1}{a_j} \int_{b-\varepsilon}^{b+\varepsilon} \left|W_{\psi_j} x(b)\right|^2 db \propto \frac{1}{a_j} \int_{b-\varepsilon}^{b+\varepsilon} \left|H_j(b)\right|^2 db \propto \frac{H_j(b)}{a_j} \tag{2.30}$$

if $\omega_{n_i}(b)$ is assumed to be invariant over the window $[b-\varepsilon, b+\varepsilon]$. It can be noticed that the expression is minimum when $\omega_{n_i}(b)$ is closed to $\omega_{0_i}(b)$. Alternatively, it may be stated that $E_j x(b) \propto \int_{b-\varepsilon}^{b+\varepsilon} \left|W_{\psi_j} x(b)\right|^2 db / a_j$ is maximum when $\omega_{n_i}(b) \in \lfloor \sigma F_1 / a_j, F_1 / a_j \rfloor$ for a lightly damped system $(\eta << 1)$, which indicates that $\omega_{n_i}(b)$ is contained in the $j^{th}$ band. Hence, the energies in the different bands would satisfy the inequality $E_{j-1} x(b) < E_j x(b) > E_{j+1} x(b)$ if $\omega_{n_i}(b) \in \lfloor \sigma F_1 / a_j, F_1 / a_j \rfloor$. Thus it may be concluded that provided the bands are narrow, then $\omega_{n_i}(b) \approx \omega_{0_i}(b)$, if

$$E_j x(b) = \max\{E_q x(b)\}; \forall q = 1,\ldots, N \tag{2.31}$$

where, $\max\{\ \}$ denotes the maximum over the set and $N$ is the number of bands.

If the estimation of $\omega_{n_i}(b)$ is desired with a still further precision then the technique of wavelet packet can be used. This is an extension of the wavelet transform to

provide further level-by-level time-frequency description and can be easily applied for L-P basis. The estimation of the time varying parameter $\omega_{n_i}(b) \in \lfloor \sigma F_1 / a_j, F_1 / a_j \rfloor$ is refined by further re-dividing the band. The frequency band for the $p^{th}$ sub-band within the original $j^{th}$ band is in the interval $\left[\delta^{p-1} F_1 / a_j, \delta^p F_1 / a_j\right]$. The wavelet coefficient is denoted by $W_{\psi_{sp}} x(a_j, b)$. Using these wavelet coefficients, estimating the relative energy in the sub-bands and using equation 2.31, the parameter $\omega_{n_i}(b)$ can be obtained more precisely.

### *Case II: On-line Identification of MDOF System*

Let us consider a linear MDOF system with *m* degrees of freedom represented by

$$[M]\{\ddot{X}\} + [C(t)]\{\dot{X}\} + [K(t)]\{X\} = \{R\} f(t) \tag{2.32}$$

where, $[M]$, $[C(t)]$ and $[K(t)]$ are the mass, time varying damping and time varying stiffness matrices respectively; $\{R\}$ is the influence vector for forces at different degrees of freedom and $f(t)$ is a forcing function. The displacement response vector is denoted by $\{X(t)\}$. If the elements $K_{ij}(t); i, j = 1,..,m$ in the stiffness matrix have discontinuities at a finite number of points, then it is possible to divide the time in several segments with indices arranged as $t_o < t_1 < t_2 < ... < t_n$ such that all $K_{ij}(t); i, j = 1,..,m$ are continuous function in $[t_{i-1}, t_i]$. Further, it is assumed that the variations of all $K_{ij}(t)$ are slower than

the fundamental (lowest) frequency of the system (corresponding to the longest period). It subsequently follows that assuming a variation of $\{X(t)\}$ with slowly varying amplitude $\{\phi(t)\}_i^k$ and slowly varying frequency $\omega_{k_i}(t)$ at the $k^{th}$ mode, in the time interval $[t_{i-1}, t_i]$, the displacement vector and its derivatives can be represented by

$$\{X(t)\} = \{\phi(t)\}_i^k e^{i\omega_{k_i}(t)t} \tag{2.33a}$$

$$\{\dot{X}(t)\} \approx i\omega_{k_i}(t)\{\phi(t)\}_i^k e^{i\omega_{k_i}(t)t} \tag{2.33b}$$

$$\{\ddot{X}(t)\} \approx -\omega_{k_i}^2(t)\{\phi(t)\}_i^k e^{i\omega_{k_i}(t)t} \tag{2.33c}$$

On substitution of equations 2.33a to 2.33c in the homogenous free vibration equation corresponding to equation 2.32, leads to the time-varying eigen value problem with eigen values $\omega_{k_i}^2(t)$ and eigenvectors $\{\phi(t)\}_i^k; k = 1,2,..,m$. If the system in equation 2.32 is assumed to be proportionally damped, then substituting $\{X(t)\}$ in terms of modal responses, $z_k(t)$, using

$$\{X(t)\} = [\phi(t)]_i \{z_k(t)\}; t \in [t_{i-1}, t_i] \tag{2.34}$$

In equation 2.32 and pre-multiplying both side by $[\phi(t)]_i^T = \left[\{\phi(t)\}_i^1 \{\phi(t)\}_i^2 .....\{\phi(t)\}_i^k\right]$, leads to the following *m* modal uncoupled time varying equations

$$\ddot{z}_k(t) + 2\eta_k \omega_{k_i}(t)\dot{z}_k(t) + \omega_{k_i}^2(t) z_k(t) = f_k(t); k = 1,2,..,m; t \in [t_{i-1}, t_i] \tag{2.35}$$

In equation 2.35, $\eta_k$ is the modal damping ratio, $\omega_{k_i}^2$ is the natural frequency in the $k^{th}$ mode in the interval $[t_{i-1}, t_i]$ and $f_k(t)$ is the modal force given by

$$f_k(t) = \alpha_i f(t) \tag{2.36}$$

where, $\alpha_i$ is a scalar defined by

$$\alpha_i = \frac{\{\phi^k(t)\}_i^T \{R\}}{\{\phi^k(t)\}_i^T [M] \{\phi^k(t)\}_i^T} \tag{2.37}$$

On considering the $r^{th}$ degree of freedom with the displacement response state denoted by $X_r(t)$ and wavelet transforming equation 2.34 yields

$$W_\psi x_r(a_j, b) = \sum_{k=1}^{m} W_\psi \left[\phi_{r_i}^k(t) z_k(t)\right](a_j, b); r = 1,2,..,m \tag{2.38}$$

Since the functions, $\phi_{r_i}^k(t)$ are slowly varying compared to $z_k(t)$, hence in evaluating the integral for wavelet transformation in equation 2.38, $\phi_{r_i}^k(t)$ can be approximated by $\phi_{r_i}^k(b)$, as $\psi\left(\frac{t-b}{a_j}\right)$ is localized and hence $\phi_{r_i}^k(b)$ can be taken out of the integral. This leads to

$$W_\psi x_r(a_j,b) = \sum_{k=1}^{m} \phi_{r_i}^k(b) W_\psi z_k(a_j,b); \qquad r = 1,2,..,m \tag{2.39}$$

Following similar steps as for the SDOF system in the previous, it can be concluded that for each of the modal equation given by equation 2.39

$$E_j z_k(b) \propto \frac{1}{a_j} \int_{b-\varepsilon}^{b+\varepsilon} \left| W_{\psi_j} z_k(b) \right|^2 db \tag{2.40}$$

where, the parameter $\omega_{k_i}(b)$ is invariant over $[b-\varepsilon, b+\varepsilon]$. If the forcing function is assumed to be described by a white noise as was assumed in the case of SDOF system, then by calculating the relative energies in different bands and comparing, it might be inferred that

$$E_{j_K} z_k(b) \propto \frac{1}{a_{j_K}} \int_{b-\varepsilon}^{b+\varepsilon} \left| W_{\psi_j} z_k(b) \right|^2 db = \max\left\{ E_N z_j(b) \right\}; \forall j = 1,..., N \tag{2.41}$$

where, $N$ is the number of energy bands. It implies that $\omega_{k_i}(b)$ corresponding to the $k^{th}$ mode is in the $j_k^{th}$ band i.e. $\omega_{k_i}(b) \in \left\lfloor F_1 / a_{j_K}, \sigma F_1 / a_{j_K} \right\rfloor$ and can be approximated as

$$\omega_{k_i}(b) \approx \omega_{0_{jk}} = \frac{\sigma + 1}{2} . \frac{\pi}{a_{j_k}} \tag{2.42}$$

for a lightly damped system (with $\eta_k << 1$), where $\omega_{0_{jk}}$ is the central frequency of the $j_k^{th}$ band. Let the parameters $\omega_{1_i}(b), \omega_{2_i}(b), ..., \omega_{m_i}(b)$ be contained in the bands with scale parameters identified by indices $j_1, j_2, ..., j_m$ respectively. Since, the response in the $k^{th}$ mode, i.e. $j_k^{th}$ band is narrow banded with frequency around $\left[F_1 / a_{j_K}, \sigma F_1 / a_{j_k}\right]$, it follows that the bands not containing the natural frequency leads to insignificant energy i.e.

$$E_j z_k(b) << E_{j_k} z_k(b); \forall k = 1,2,..,m; j \neq j_k \tag{2.43}$$

It follows from equations 2.41 and 2.43,

$$\left|W_{\psi_j} z_k(a_j, b)\right| << \left|W_{\psi_{j_k}} z_k(a_j, b)\right|, j \neq j_k; k = 1,2,..., m \tag{2.44}$$

which leads to the approximation

$$\left|W_{\psi_j} z_k(a_j, b)\right| \approx 0 \text{ if } j \neq j_k;\ k = 1,2,..., m \tag{2.45}$$

On using equation 2.45 in equation 2.39 gives

$$W_\psi x_r(a_j, b) = \phi_{r_i}^k(b) W_\psi z_k(a_j, b) \text{ if } j \neq j_k;\ \text{k} = 1,2,..., \text{m} \tag{2.46}$$

$$\approx 0$$

leading to

$$E_j x_r(b) \propto \frac{1}{a_j} \int_{b-\varepsilon}^{b+\varepsilon} \left[\phi_{r_i}^k(b)\right]^2 \left|W_\psi z_k(a_{j_k}, b)\right|^2 db \text{ if } j \neq j_k \text{ ; k} = 1,2,..., \text{m} \tag{2.47}$$

Thus, the '$m$' bands with the '$m$' natural frequency parameters $\omega_{k_i}(b); k = 1,...,m$ correspond to $m$ local maxima in the variation of $E_j x_r(b)$ [or its proportional quantity $(1/a_j)\int_{b-\varepsilon}^{b+\varepsilon} \left|W_\psi x_r(b)\right|^2 db$] with different values of the band parameter '$j$'. It can be represented by the inequalities

$$E_{j-1} x_r(b) < E_j x_r(b) > E_{j+1} x_r(b); \forall \text{j} = \text{j}_\text{k}; k = 1,2,...,m \tag{2.48}$$

if the modes are not too closely spaced. Once these bands are detected, the parameters $\omega_{k_i}(b)$ can be obtained as

$$\omega_{k_i}(b) \approx \frac{\sigma + 1}{2} . \frac{F_1}{a_{j_k}}; k = 1,2,..., N \tag{2.49}$$

over the interval $[b-\varepsilon, b+\varepsilon]$. The sub-band coding with wavelet packets could be applied if the parameters $\omega_{k_i}(b)$ are desired to be obtained with better precision as has been discussed in the section for the SDOF system.

Once the bands corresponding to the '$m$' modes with the parameters $\omega_{k_i}(b)$ are obtained, the time varying mode shapes $\{\phi(t)\}_i^k$ could be found by considering the wavelet coefficients of $x_r(t)$ with the scale parameters, $j_k$ and sub-band parameter $p$. These wavelet coefficients can be written as

$$W_{\psi_{sp}} x_r(a_j, b) = \phi_{r_i}^k(b) W_{\psi_{sp}} z_k(a_{j_k}, b) \tag{2.50}$$

Now, considering two different states of response of the MDOF system with one considered as $r = 1$ (without the loss of generality), the ratio of wavelet coefficients of the considered states at the time instant $t = b$ (equation (2.47) or (2.51)), gives the $r^{th}$ component of the time varying $k^{th}$ mode as

$$\pi_r^{j_k}(b) = \frac{W_{\psi_{sp}} x_r(a_{j_k}, b)}{W_{\psi_{sp}} x_1(a_{j_k}, b)} = \frac{\phi_r^k(b)}{\phi_1^k(b)} \tag{2.51}$$

Thus, computing these ratios for different states with $r = 1,2,...,m$ and assuming $\phi_1^k(b) = 1$ (without loss of generality), the time varying $k^{th}$ mode shape is obtained as

$$\{\phi_1^k(b)\} = \{\pi_r^{j_k}(b)\}; r = 1,2,...,m \tag{2.52}$$

## 2.3 Numerical Results and Discussions

A series of numerical example is presented in this section to illustrate the efficiency and accuracy of the proposed wavelet-based identification algorithm.

### 2.3.1 Case I: Off-line Estimation of Parameters of Time Invariant Systems

A MDOF model is used to simulate the displacement response and to show the application of the proposed identification methodology. The MDOF system, as shown in figure 2.1, is considered. The displacement of the $i^{th}$ mass relative to the support is denoted by $x_i(t)$. At first, simulation is carried out for a 3DOF system (n=3). The masses are $m_1$ = *300unit*, $m_2$ = *200unit* and $m_3$ = *200unit* and the spring stiffnesses are $k_1$ = *36000unit*, $k_2$ = *24000unit* and $k_3$ = *36000unit* respectively. The damping ratio is assumed to be 5% for all modes. The system is subjected to initial displacement of $x_1(0) = x_2(0) = x_3(0) = 1$ for the three degrees of freedom. Using these, the ambient vibration response is simulated.

Modified L-P wavelet is used to decompose the signals into different frequency levels. Initially the response energy is calculated for each degree of freedom in frequency bands with $\sigma = 2^{1/4}$ to broadly identify the bands that contain the natural frequencies. These bands are further divided into sub-bands using wavelet packets. Figures 2.2(a), 2.3(a) and 2.4(a) represent the ratio of wavelet coefficients of displacements $x_2(t)$ and

$x_3(t)$ with respect to the wavelet coefficients of displacement $x_1(t)$ over time for the three frequency sub-bands containing the three natural frequencies respectively. Since the response for different degrees of freedom attain same phase during modal vibration, these ratios are practically constant over time. The natural frequencies are estimated as the central frequency of the corresponding sub-bands and the corresponding mode shapes are obtained by averaging the ratios shown in figures 2.2(a), 2.3(a) and 2.4(a) using sub-band coding as discussed in section 2.2.1. The results are summarized in table 2.1. Figures 2.2(b), 2.3(b) and 2.4(b) show the plot of the mode shapes estimated using the proposed method and compared with the actual for the first three modes respectively. From figures 2.2(b), 2.3(b) and 2.4(b) and table 2.1, it can be noticed that the first modal frequency

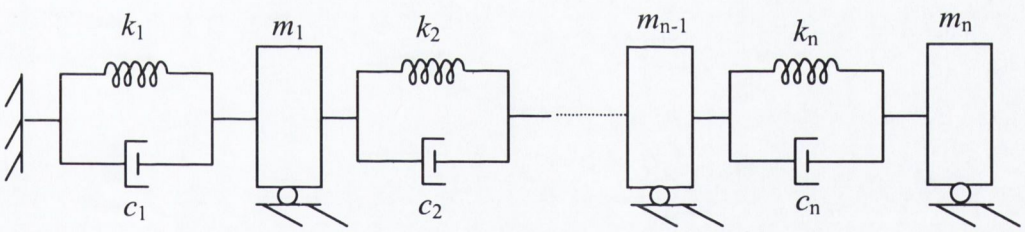


Figure 2.1: MDOF linear time invariant model

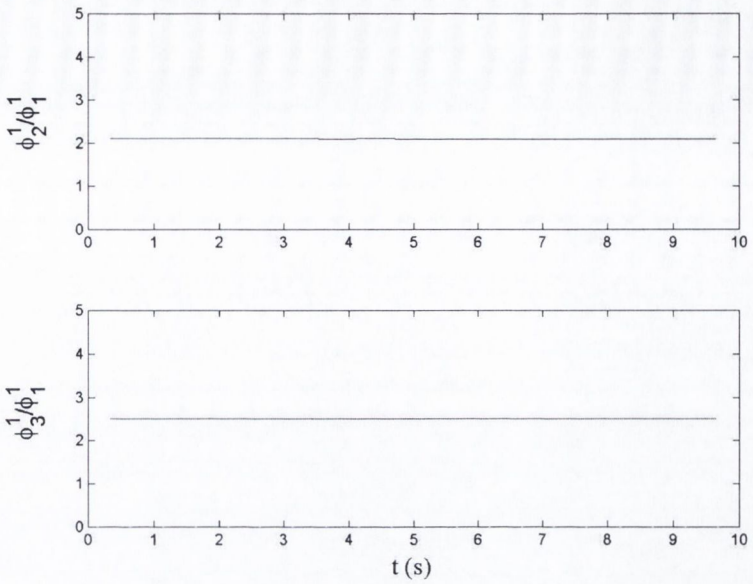


(a)

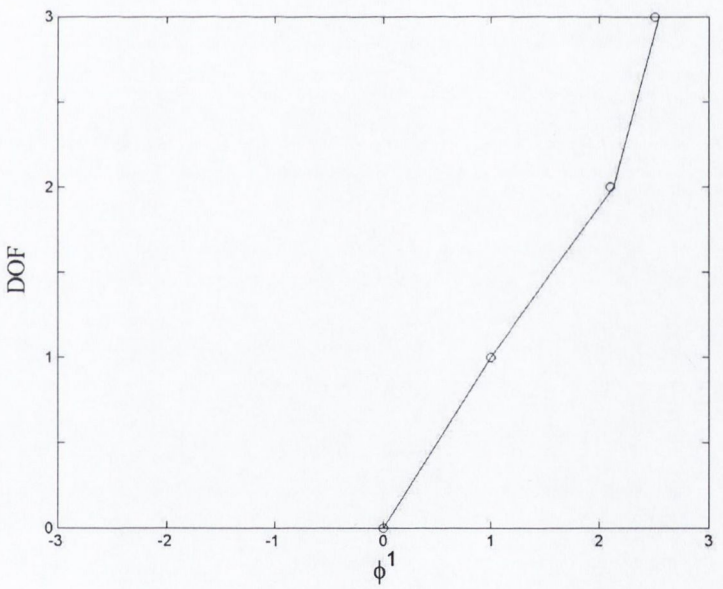


(b)

Figure 2.2: (a) Ratio of modal responses at 1st natural frequency, (b) actual and estimated 1st mode shape of the 3DOF system ('__' actual, 'o' estimated)

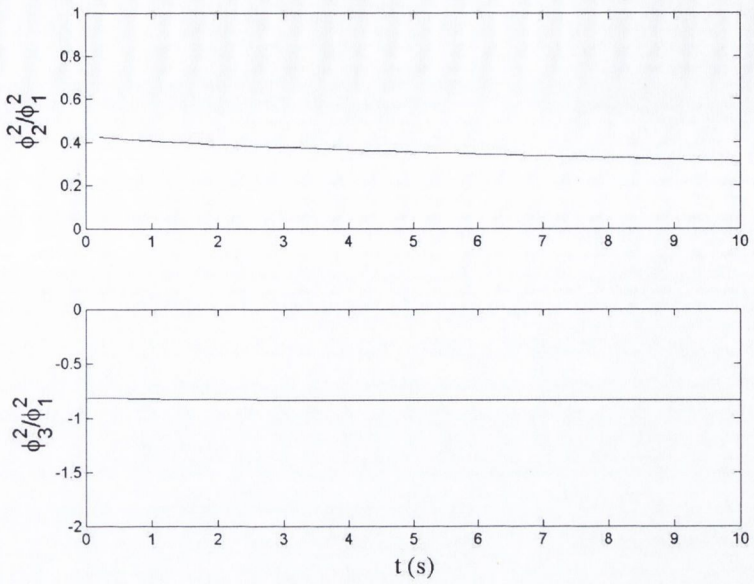


(a)

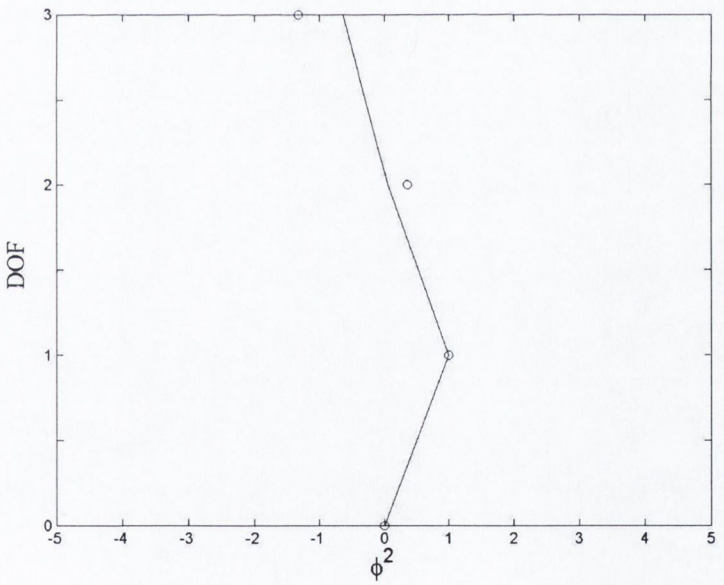


(b)

Figure 2.3: (a) Ratio of modal responses at 2nd natural frequency, (b) actual and estimated 2nd mode shape of the 3DOF system ('__' actual, 'o' estimated)

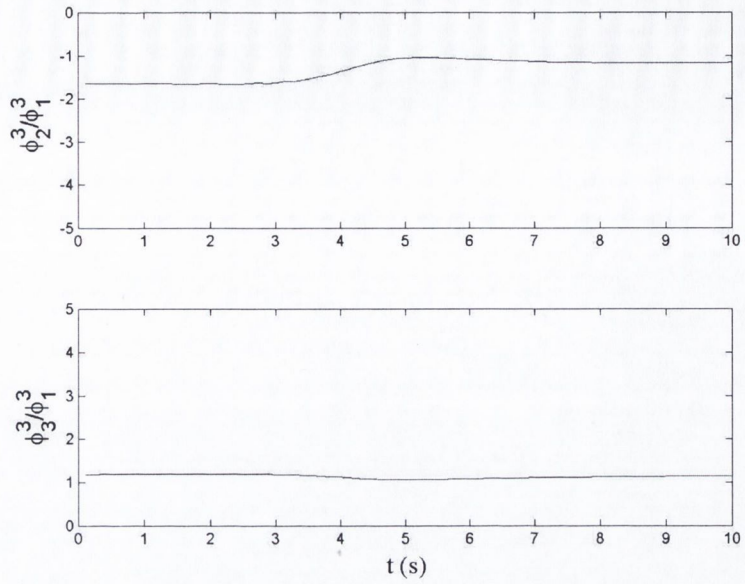


(a)

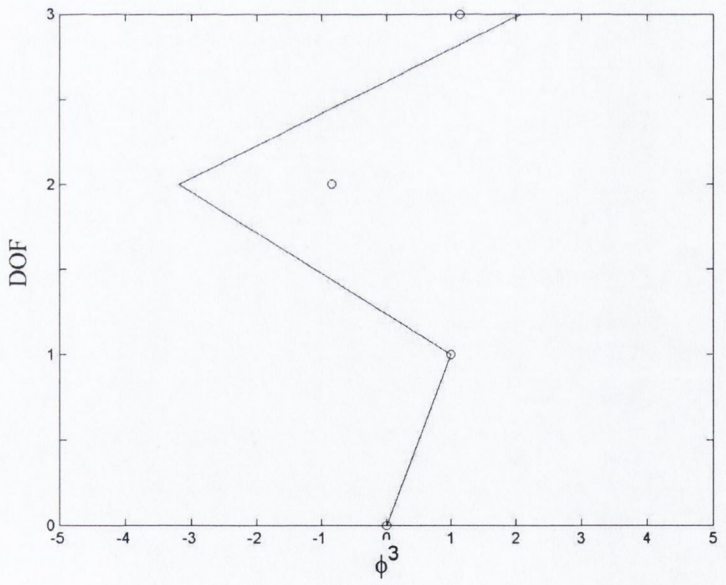


(b)

Figure 2.4: (a) Ratio of modal responses at 3rd natural frequency, (b) actual and estimated 3rd mode shape of the 3DOF system ('__' actual, 'o' estimated)

| Mode | Natural Frequency (rad/s) | | Normalized Mode Shape | | | | | Damping ratio (%) | |
|---|---|---|---|---|---|---|---|---|---|
| | | | $x_1$ | $x_2$ | $x_2$ | $x_3$ | $x_3$ | | |
| | Actual | Estimated | | Actual | Estimated | Actual | Estimated | Actual | Estimated |
| 1 | 5.39 | 5.40 | 1.00 | 2.13 | 2.10 | 2.54 | 2.51 | 0.05 | 0.04 |
| 2 | 13.99 | 13.40 | 1.00 | 0.06 | 0.36 | -0.63 | -0.83 | 0.05 | 0.02 |
| 3 | 21.34 | 20.60 | 1.00 | -3.19 | -1.32 | 2.07 | 1.14 | 0.05 | 0.01 |

Table 2.1: Actual and estimated modal parameters of 3DOF system using modified L-P wavelet

along with other modal parameters are estimated satisfactorily, which proves the effectiveness of the proposed method. It can also be observed that although the frequency ratios of wavelet coefficients for higher modes are constant over time, the accuracy in estimation reduces for the higher modes. This is due to the fact that the energy content in bands containing the higher modal frequencies reduces with increase in mode number.

To investigate the accuracy of the estimation for higher modes in further detail, a 5DOF model with two additional masses and springs ($m_4$ = 250 kg and $m_5$ = 350 kg; $k_4$ = 20000N/mm and $k_5$ = 15000N/mm) are considered while the modal damping ratio is kept as 5% for all modes. The displacement response relative to the base is simulated using initial conditions $x_4(0) = x_5(0) = 1$ along with those used in the 3DOF system. The first three modes are estimated in a similar way as in case of the 3DOF system and the results are summarized in tables 2.2(a, b). Figures 2.5(a, b) – 2.7(a, b) show the corresponding modal wavelet coefficient ratios and estimated mode shapes for the first three modes. From these results, it can be observed that the modal frequencies and mode shapes can be estimated with high level of accuracy for the first two modes as opposed to just only the first modal parameters being estimated with high level of accuracy for the 3DOF system. For the 5DOF system the estimation accuracies start deteriorating from the third mode onward and are poorer for the last two modes. The results are consistent with the results from the 3DOF system. This indicates that more number of modes and their modal properties can be identified with greater accuracy for systems with relatively greater number of degrees of freedom. Also, modal damping ratios can be estimated with reasonable accuracy with the level of accuracy deteriorating with higher modes. The higher modal damping ratios tend to be underestimated.

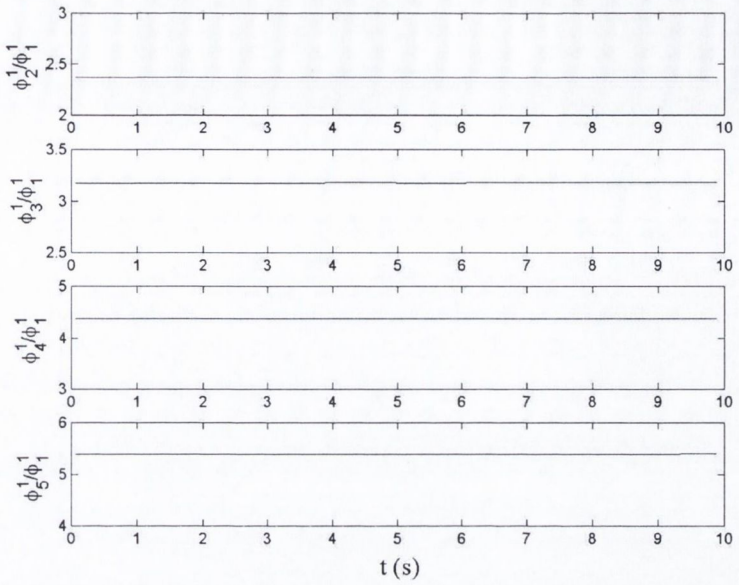


(a)

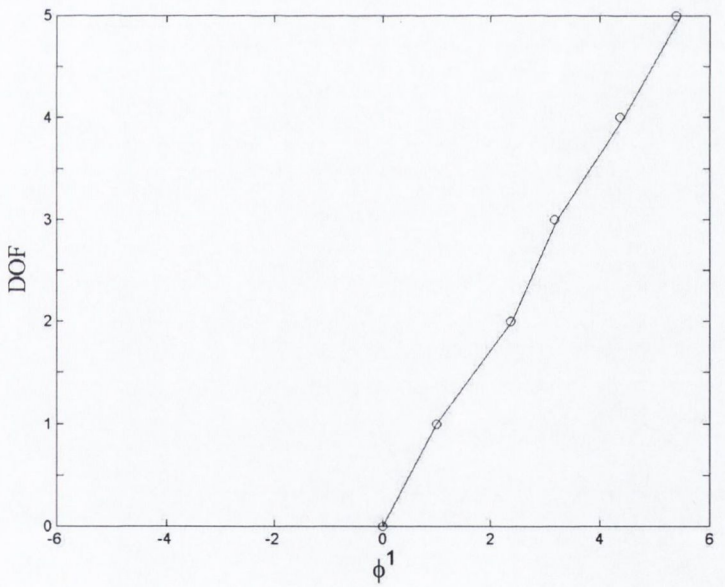


(b)

Figure 2.5: (a) Ratio of modal responses at 1st natural frequency, (b) actual and estimated 1st mode shape of the 5DOF system ('__' actual, 'o' estimated)

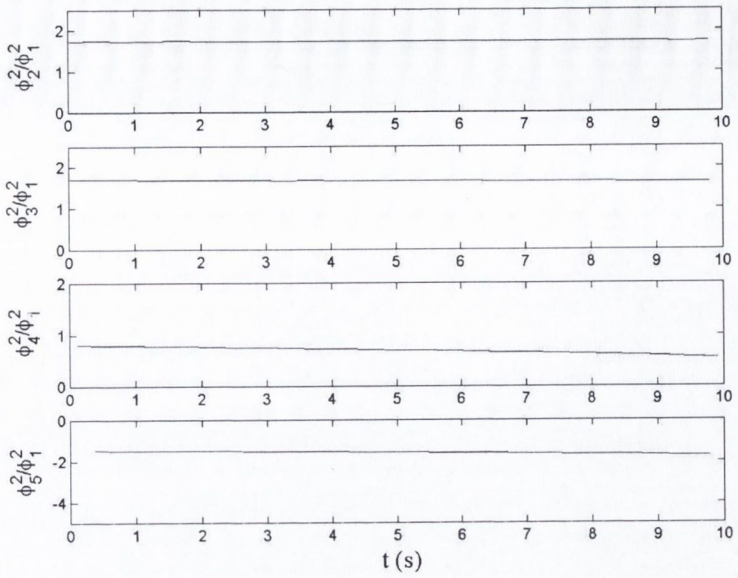


(a)

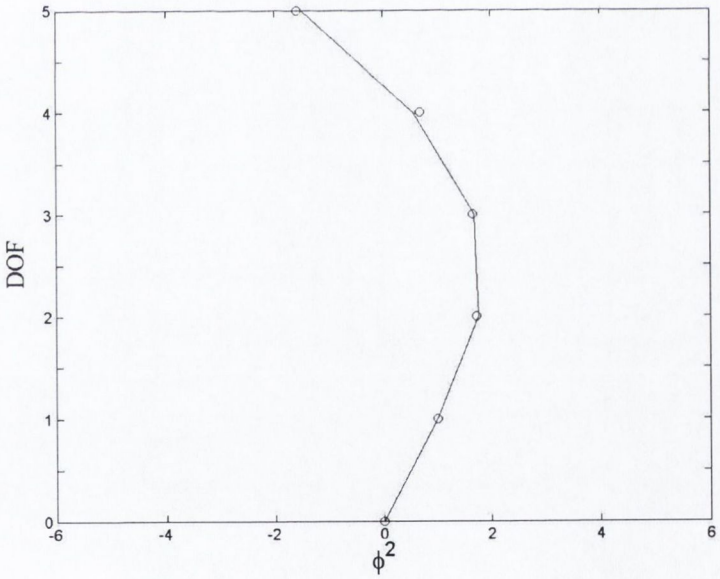


(b)

Figure 2.6: (a) Ratio of modal responses at 2nd natural frequency, (b) actual and estimated 2nd mode shape of the 5DOF system ('__' actual, 'o' estimated)

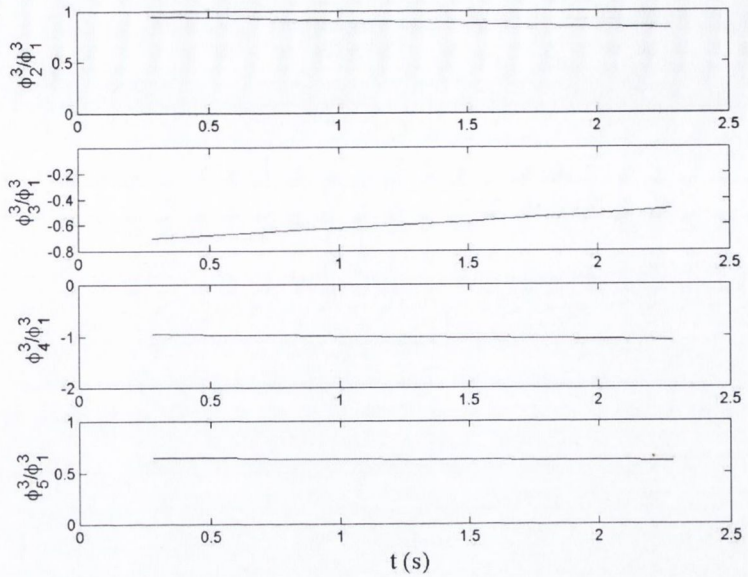


(a)

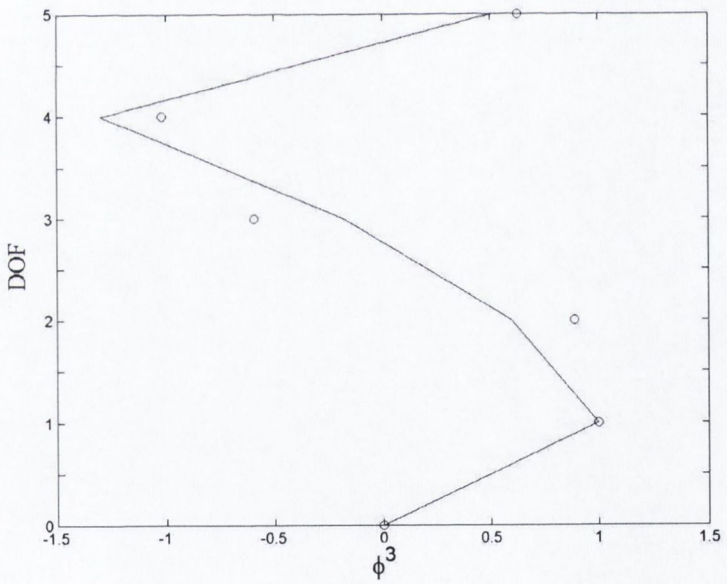


(b)

Figure 2.7: (a) Ratio of modal responses at 3rd natural frequency, (b) actual and estimated 3rd mode shape of the 5DOF system ('__' actual, 'o' estimated)

| Mode | Natural Frequency (rad/s) | | Damping ratio (%) | |
|---|---|---|---|---|
| | Actual | Estimated | Actual | Estimated |
| 1 | 2.84 | 2.88 | 0.05 | 0.04 |
| 2 | 7.69 | 7.69 | 0.05 | 0.03 |
| 3 | 12.35 | 12.59 | 0.05 | 0.02 |

(a)

| Mode | Normalized Mode Shape | | | | | | | | |
|---|---|---|---|---|---|---|---|---|---|
| | $x_1$ | $x_2$ | $x_2$ | $x_3$ | $x_3$ | $x_3$ | $x_3$ | $x_3$ | $x_3$ |
| | | Actual | Estimated | Actual | Estimated | Actual | Estimated | Actual | Estimated |
| 1 | 1.00 | 2.40 | 2.37 | 3.22 | 3.18 | 4.45 | 4.39 | 5.48 | 5.39 |
| 2 | 1.00 | 1.76 | 1.73 | 1.69 | 1.66 | 0.56 | 0.69 | -1.49 | -1.58 |
| 3 | 1.00 | 0.59 | 0.89 | -0.18 | -0.59 | -1.30 | -1.02 | 0.51 | 0.63 |
| 4 | 1.00 | -0.56 | -0.61 | -0.84 | -0.76 | 0.73 | 0.74 | -0.15 | -0.36 |
| 5 | 1.00 | -3.72 | -2.25 | 3.43 | 1.81 | -0.78 | -0.42 | 0.07 | 0.50 |

(b)

| Mode | Normalized Mode Shape | | | | | | | | |
|---|---|---|---|---|---|---|---|---|---|
| | $x_1$ | $x_2$ | $x_2$ | $x_3$ | $x_3$ | $x_3$ | $x_3$ | $x_3$ | $x_3$ |
| | | Actual | Estimated | Actual | Estimated | Actual | Estimated | Actual | Estimated |
| 1 | 1.00 | 2.40 | 2.39 | 3.22 | 3.20 | 4.45 | 4.41 | 5.48 | 5.46 |
| 2 | 1.00 | 1.76 | 1.76 | 1.69 | 1.67 | 0.56 | 0.64 | -1.49 | -1.47 |
| 3 | 1.00 | 0.59 | 0.79 | -0.18 | -0.38 | -1.30 | -1.14 | 0.51 | 0.59 |
| 4 | 1.00 | -0.56 | -0.59 | -0.84 | -0.77 | 0.73 | 0.76 | -0.15 | -0.26 |
| 5 | 1.00 | -3.72 | -2.83 | 3.43 | 2.43 | -0.78 | -0.57 | 0.07 | 0.41 |

(c)

Table 2.2: (a) Actual and estimated natural frequencies and damping ratios of 5DOF system using modified L-P wavelet with 5% damping ratios in all modes, b) Actual and estimated mode shapes of 5DOF system using modified L-P wavelet with 5% damping ratios in all modes and (c) Actual and estimated mode shapes of 5DOF system using modified L-P wavelet with 2% damping ratios in all modes

To investigate the efficiency of wavelet based system identification technique proposed, the 5DOF system is further considered with 2% damping ratios in all modes. The other parameters of the system and the initial conditions are kept unchanged. The first three mode shapes are estimated in a similar way as done earlier and the results are presented in table 2.2c. It can be seen that the mode shapes are estimated accurately for this system even with lower level of damping as compared to the earlier one. However, it has been found that the accuracy of prediction of modal damping ratios falls for system with low level of damping. This is possibly because of the fact that the response and hence the wavelet coefficients decay at a very slow rate, posing estimation problem.

### 2.3.2 Case II: On-line Estimation of Parameters of Time Varying Systems

For the purpose of illustration of the proposed algorithm for on-line identification of time varying SDOF (figure 2.8a) and MDOF (figure 2.8b) systems, a band limited white noise excitation has been simulated. The ranges of frequencies are kept wide enough to cover the frequencies of the system to be identified. To maintain stationarity, the excitation has been generated by considering a number of cycles of an arbitrary number of discrete frequencies over the range so that the temporal mean square value remains almost invariant. The excitation has been digitally simulated at a time step of $\Delta t = 0.0104s$. Figures 2.9a and 2.9b show the time history and the Fourier spectra of the excitation process. For the frequency-tracking algorithm, a moving window of 400 time steps equal to $4.16s$ has been chosen. The instantaneous frequency is identified based on the

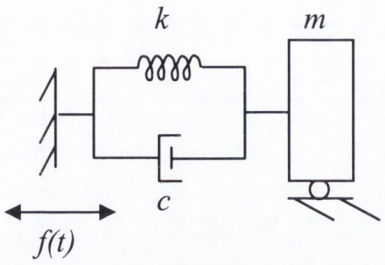


(a)

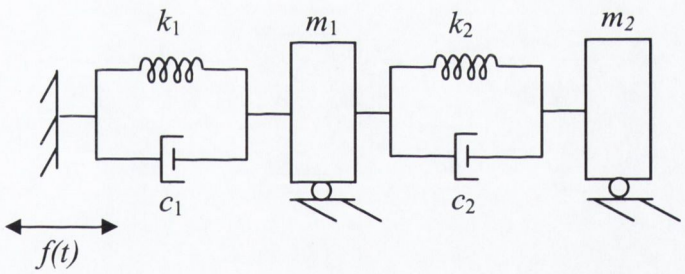


(b)

Figure 2.8: (a) SDOF linear time varying model, (b) MDOF linear time varying model

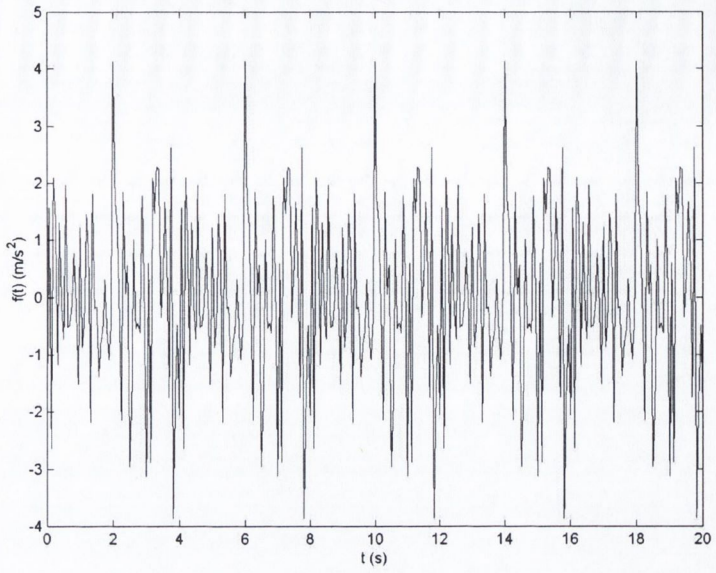


(a)

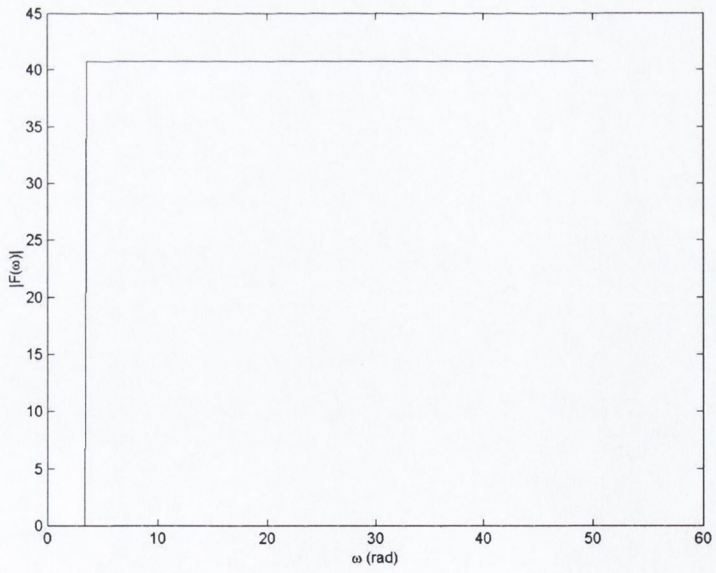


(b)

Figure 2.9: Excitation process (a) Time history, (b) Fourier Spectrum

proposed formulation using wavelet analysis on the time histories of the response states and is updated at every time step. The identified frequency is assumed to be the central frequency of the frequency band for a particular identified scale of the L-P wavelet basis function.

Figure 2.10 shows the tracked frequency of a SDOF system with time-invariant natural frequency, $\omega_n = 9 rad/s$ and damping ratio, $\eta = 5\%$. Since, a window of $4.16s$ is used, the tracking starts after an initial period of $4.16s$. The value of the initial frequency of the first band of the mother wavelet, $F_1$ is 8.25 rad/s and a value of the scaling constant, $\sigma = 1.2$ is used. Six bands are used in all and sub-band coding for packets are not used for this case. To investigate if a sudden or a sharp change in the natural frequency can be tracked, an example where the natural frequency of the SDOF system has been changed suddenly from 9rad/s to 13.25rad/s has been considered. Figure 2.11 shows how the natural frequency is tracked using the proposed method. As expected it requires certain period of lag time to follow the change until it converges to the changed frequency. It can be noticed that the system parameters change at 5.73s. But the proposed on-line wavelet based tracking algorithm requires information over finite time window, which in the present case is 4s. Thus the changed parameters are detected at 8s second with a time lag. To further observe the tracking ability of the method, a case where the change in the frequency of the SDOF system is not so sharp has been considered next. The natural frequency of the system is linearly changed in form of a ramp from 9rad/s to 13.25rad/s over a period ranging over 5s to 10s. Thus, apart from two discontinuities of slopes at 5s and 10s respectively, the variation of the frequency of the system is continuous with no discontinuity of slope. The frequency in this case can be tracked

closely as seen in figure 2.12. However, as six bands are used over the range of variation in frequency considered, the identification of the frequency occurs in five steps.

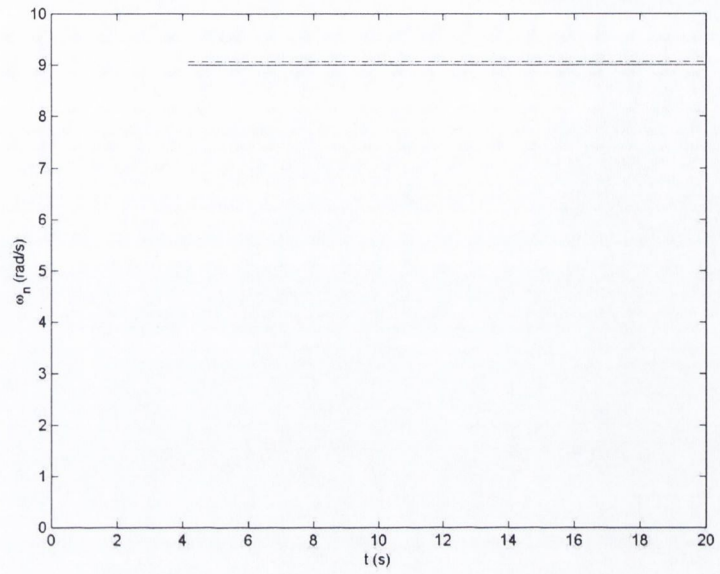


Figure 2.10: Online identification of natural frequency of a time invariant SDOF system ('__' actual, '- - -' estimated)

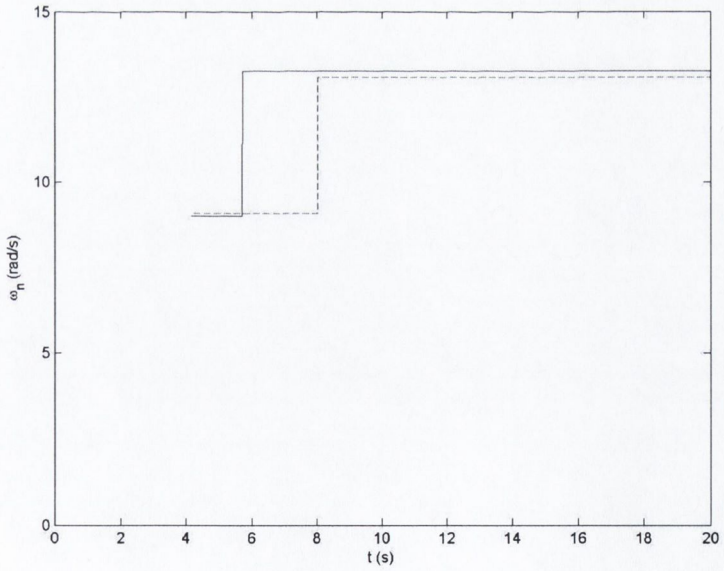


Figure 2.11: Tracking of sudden change in natural frequency of a SDOF system ('__' actual, '- - -' estimated)

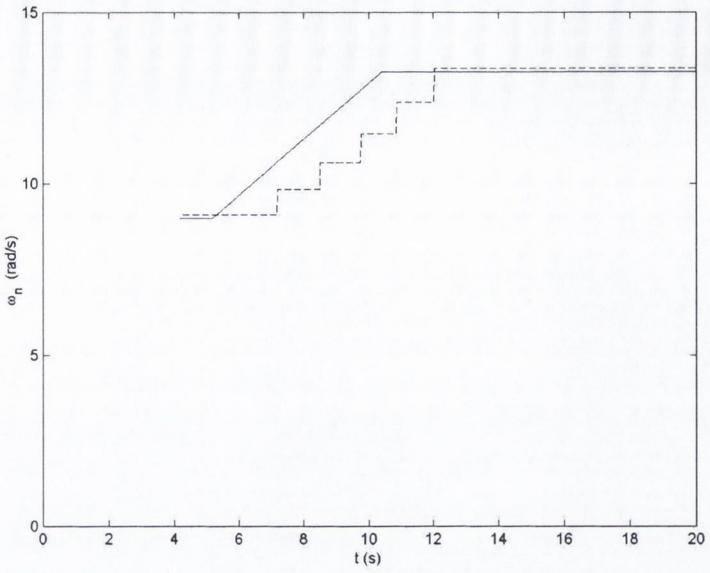


Figure 2.12: Tracking of change (ramp) in natural frequency of a SDOF system ('__' actual, '- - -' estimated)

The tracking can be more continuous by increasing the number of bands of frequencies considered for computation.

Next, to illustrate the application of the tracking methodology for MDOF systems an example of a 2DOF system has been considered. The system considered is a shear-building model with two degrees of freedom. The masses are lumped at the two nodes with the masses at first and second floors as $m_1 = 10\,unit$ and $m_2 = 15\,unit$ respectively. The floor stiffness for the first and second floor are $k_1 = 2500\,unit$ and $k_2 = 4500\,unit$ respectively. These parameters lead to the first and second natural frequencies, $\omega_1 = 9.04 rad/s$ and $\omega_2 = 30.30 rad/s$ respectively. The first and the second mode shapes are $\{\phi_{11} \quad \phi_{21}\} = \{1 \quad 1.37\}$ and $\{\phi_{12} \quad \phi_{22}\} = \{1 \quad -0.49\}$ respectively. For the identification of the 2DOF system, the parameters $F_1$ and $\sigma$ are taken as $8.25 rad/s$ and

1.2 respectively. Figures 2.13a and 2.13b show the tracking of the first natural frequency and the ratio $\phi_{21}/\phi_{11}$ corresponding to the first mode shape (assuming $\phi_{11}=1$ without loss of generality). Similarly, figures 2.14a and 2.14b show the tracking of the second natural frequency and the ratio $\phi_{22}/\phi_{12}$ corresponding to the second mode shape (assuming $\phi_{12}=1$ without loss of generality). It can be observed that for the second mode shape, there is some fluctuation primarily in identifying the mode shape parameters. It is known that the identification problem becomes difficult for the last few modes of an MDOF system. Hence, the second mode cannot be identified so accurately as the first mode for a 2DOF system. To further observe if the proposed method can track a sudden change in the system parameters of the MDOF system and follow the recovery to the original value(s), the natural frequencies and the mode shapes are changed at 5.73s to $\omega_1 = 11.57 rad/s$; $\omega_2 = 35.11 rad/s$; and $\{\phi_{11} \quad \phi_{21}\}^t = \{1 \quad 1.58\}$; $\{\phi_{12} \quad \phi_{22}\}^t = \{1 \quad -0.42\}$. Subsequently the system parameters are restored to the original value at 12.48s. Figure 2.15a and 2.15b show the tracked first natural frequency and the ratio of $\phi_{21}/\phi_{11}$. As observed earlier, there is a time lag in tracking the frequency and mode shape. The change in the frequency is tracked in (three) steps corresponding to the bands of frequencies considered. The second modal estimate is poor as was observed in case of time invariant systems and is not unexpected as discussed in the previous sub-section.

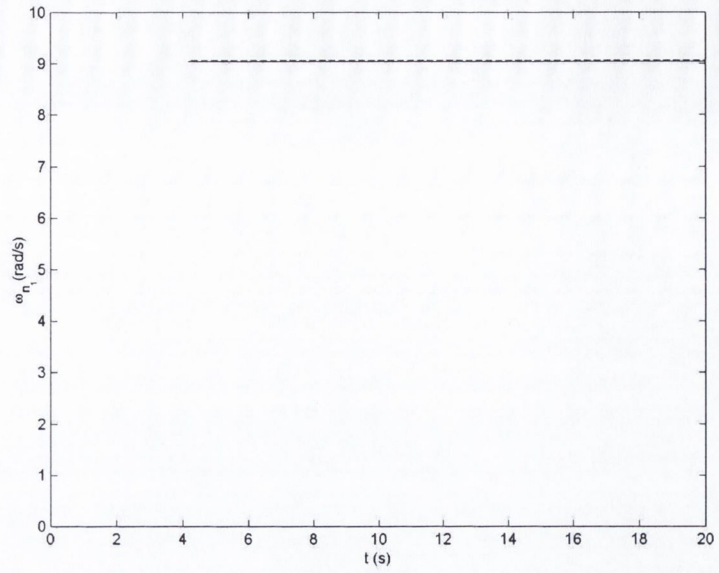


(a)

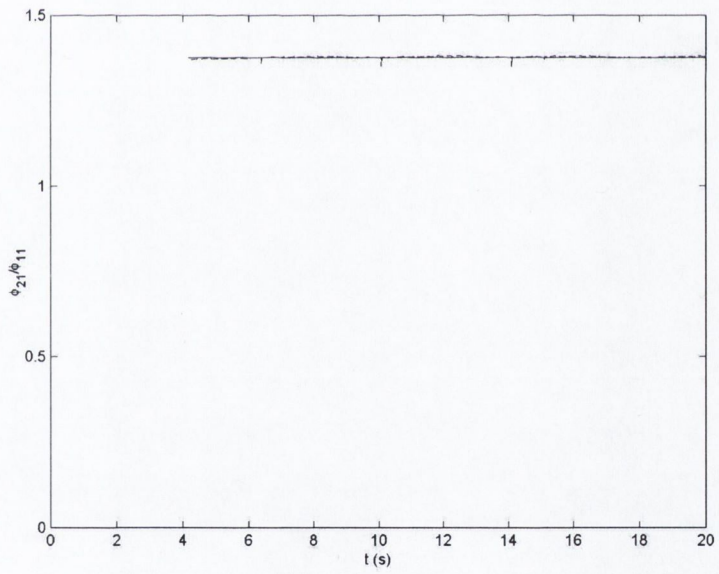


(b)

Figure 2.13: Online tracking of parameters of a 2 DOF (a) fundamental frequency and (b) fundamental mode shape ('__' actual, '- - -' estimated)

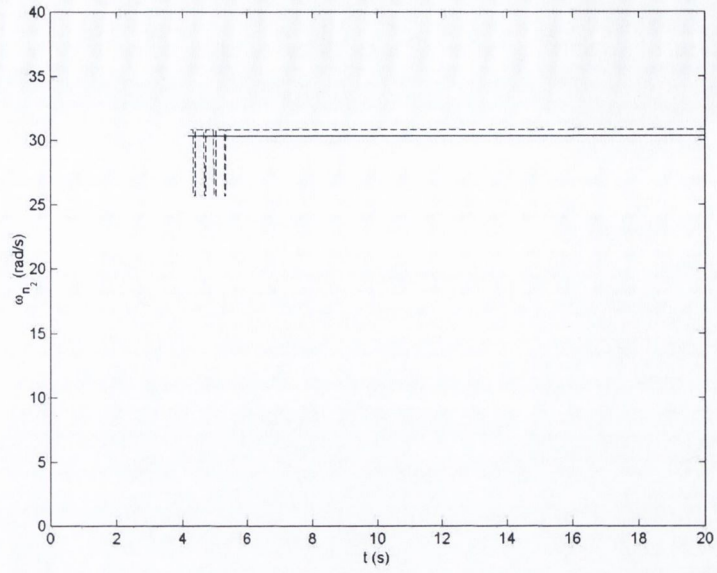


(a)

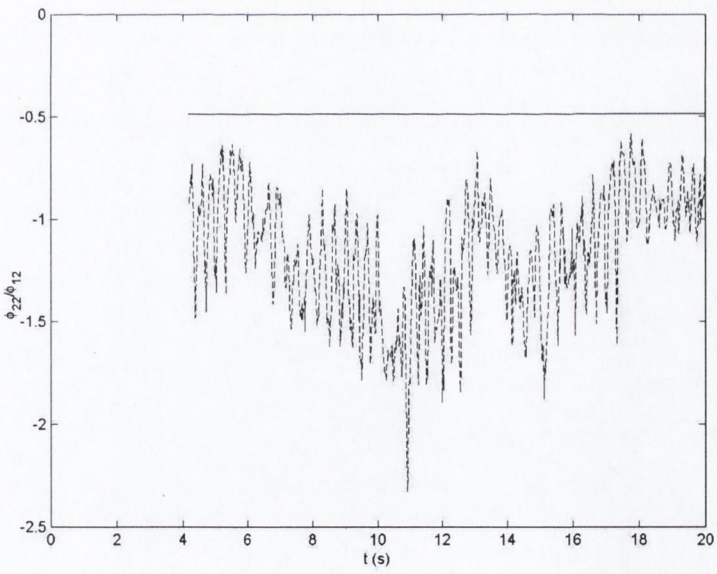


(b)

Figure 2.14: Online tracking of parameters of a 2 DOF (a) second natural frequency and (b) second mode shape ('__' actual, '- - -' estimated)

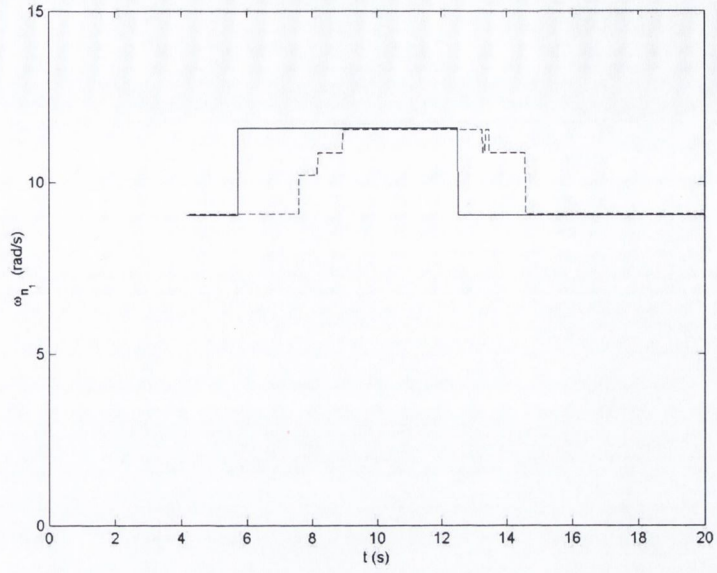


(a)

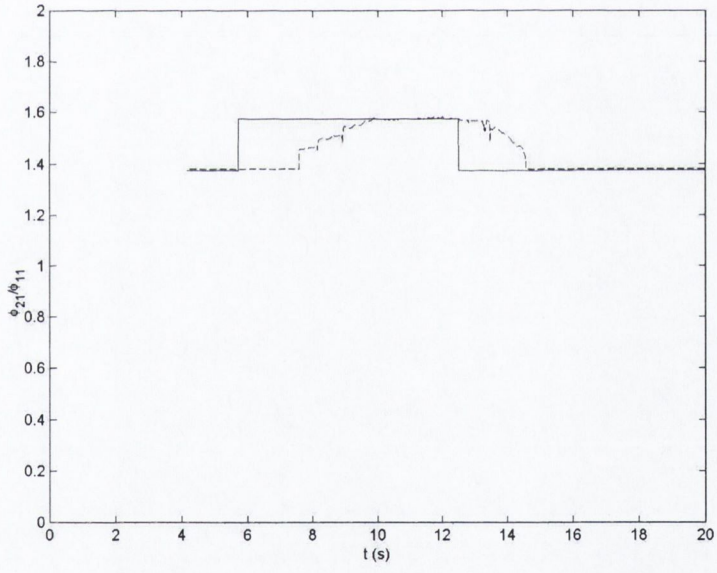


(b)

Figure 2.15: Online tracking of parameters of a 2 DOF system with sudden change in stiffness (a) fundamental frequency and (b) fundamental mode shape ('__' actual, '- - -' estimated)

## 2.4 Conclusions

In this chapter, a wavelet based methodology for identification of the modal parameters of a linear MDOF system from ambient vibration records has been proposed. The key feature of this study is to present a technique for identifying the natural frequencies, mode shapes and associated modal damping ratios of a time invariant MDOF system using the concept of wavelet packets, where the wavelet basis function used is a modified form of L-P function. An efficient wavelet based algorithm using modified L-P basis has been used in the identification methodology, which is computationally simple as well. The example cases shown that the methodology can estimate the parameters accurately. The proposed method can be extended to identify system parameters under various kinds of excitations, particularly when the input is unknown.

The proposed wavelet based structural dynamic parameter identification method has been extended for on-line identification of parameters of time varying systems. The developed theory can identify on-line variation in natural frequency of a SDOF system and the natural frequencies and mode shapes of a MDOF system arising out of change in stiffness (es). The modified L-P wavelet basis function has been used and has the advantage of adapting for wavelet packets for desired accuracy in estimation. The analytical results confirm the ability of the technique to track in several cases of stiffness variation considered here. The proposed method is simple and easy to implement for on-line identification and vibration control of stiffness varying structural systems.

# Chapter 3: Estimation of Parameters of Structural Systems with Randomness in Output Signals

## 3.1 Introduction

Following the wavelet based estimation technique of the structural parameters from the measured response as described in Chapter 2, the present chapter investigates the efficiency and accuracy of the proposed algorithm in the light of simulated and experimented noise contaminated response of the three different structures subjected to non-stationary input.

First of all, a bridge modelled as a simply supported beam, which is excited due to a moving load with constant velocity has been considered. The response is simulated using a distributed parameter model of the beam and a broad banded white noise is then simulated and added to the bridge response as measurement noise. Using this simulated noise contaminated displacements at specific locations; a wavelet-based algorithm is proposed to estimate the fundamental natural frequency and the mode shape. The proposed model for estimation of structural parameters from the noise-contaminated data is then validated using experimental observations on a simply supported reinforced concrete beam, which is excited by an impulse at the middle. A MDOF system, which is excited by a random support motion, is considered next. The support motion is simulated as amplitude modulated stationary process to represent earthquake ground motion. A broad banded white noise is then added with the simulated response of the MDOF system as measurement noise. The proposed wavelet based algorithm is then used to evaluate the system parameters from the random response of the structure. The accuracy of the proposed algorithm is discussed in the light of noise-contaminated measurement, which

proves it to be efficient to implement as a simple but robust non-destructive tool to monitor structural health.

## 3.2 Estimation of System Parameters from Noise Contaminated Response

A wavelet-based algorithm for parameter estimation from the noise-contaminated measurement is discussed in the present section for a bridge-vehicle problem, with the vehicle assumed to move with a constant velocity and a MDOF system subjected to random support excitation, like earthquake loads in the following section.

### 3.2.1 Continuous System: Bridge-Vehicle Problem

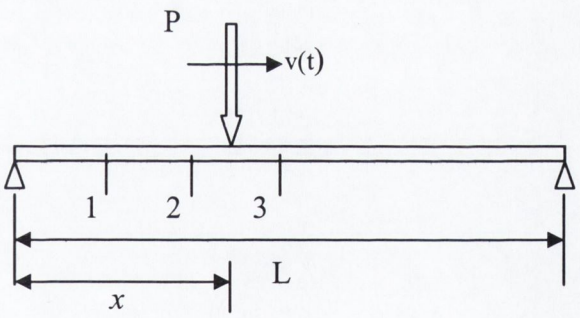


Figure 3.1: Bridge-vehicle model

A bridge is modeled as simply supported beam and the vehicle is represented by a load '$P$', which is assumed to move with a constant velocity of '$v$' as shown in figure 3.1. The governing equation of motion of the bridge can be expressed as

$$EI\frac{\partial^4 y}{\partial x^4}+m\frac{\partial^2 y}{\partial t^2}+c\frac{\partial y}{\partial t}=P\delta(x-vt) \tag{3.1}$$

where, $y(x,t)$ is the displacement of the bridge at a point '$x$' at an instant of time '$t$'. In the above equation *EI, m, c* and *P* represent the flexural rigidity, mass per unit length, coefficient of damping and weight of vehicle respectively. The boundary conditions associated with the above differential equation are given by - $y(0,t)=0$ and $y'(0,t)=0$ while the initial conditions are given by $y(x,0)=0$ and $\dot{y}(x,0)=0$ respectively, where prime and over dot denote derivative with respect to space and time respectively. The solution of equation 3.1 can be expressed as

$$y(x,t)=\sum\phi_k(x)u_k(t)+\varepsilon(t) \tag{3.2}$$

where, $\phi_k(x)$ is the mode shape function while $u_k(t)$ is the generalized response in the $k^{th}$ mode. In equation 3.2, $\varepsilon(t)$ represents Gausian white noise with zero mean that represents the measurement error. It can be shown that the mode shape of a simply supported beam is [Paz (1987)]

$$\phi_k(x) = \sin\left(\frac{k\pi x}{L}\right); k = 1,2,3.....\infty \tag{3.3}$$

Using the relation given in equation 3.2 into 3.3, the $k^{th}$ modal response can be obtained from the modal equation

$$\ddot{u}_k + 2\rho_k \omega_{n_k} \dot{u}_k + \omega_{n_k}^2 u_k = \tilde{f}_k(t) \tag{3.4}$$

where, $\rho_k$, $\omega_{nk}$ and $\tilde{f}_k(t)$ are the $k^{th}$ modal damping ratio, the $k^{th}$ modal frequency and the $k^{th}$ modal load vector respectively. It can be shown that the natural frequency of the bridge is given by [Paz (1987)]

$$\omega_{n_k} = k^2\pi^2\sqrt{\frac{EI}{m_p L^4}} \quad k = 1,2,...n \tag{3.5}$$

Taking wavelet transform on both sides of equations 3.2, yields

$$W_\psi y(a,b) = \sum \phi_k W_\psi u_k(a,b) + W_\psi \varepsilon(a_j,b) \tag{3.6}$$

The normalized energy $E_j(y)$ for the response $y$, in the frequency band corresponding to a scaling factor $a_j = \sigma^j$ with the index '$j$', can be represented by

$$E_j(y) \propto \frac{1}{a_j^2} \int W_\psi^2 u_k(a_j,b)db + \frac{1}{a_j^2} \int E\left[W_\psi^2 \varepsilon(a_j,b)\right]db = I_j(y) + \tilde{I}_j(y) \tag{3.7}$$

It can be noticed that $E\left[W_\psi u_k(a_j,b) W_\psi \varepsilon(a_j,b)\right] = 0$, where $E[.]$ represents the expected value. In general, the frequency content of a response quantity can be sub-divided into *'m'* bands with the indices for each band denoted by $j_1, j_2, ..., j_m$. Let the first natural frequency $\omega_{n_1}$ be contained in the $r^{th}$ band i.e. with index $j_r$. Thus, the component of the $1^{st}$ modal response $u_1$, in the $r^{th}$ band i.e. $u_{1_r}$, is narrow banded with frequencies around $\omega_{d_1}$ (with $\omega_{n_1} \approx \omega_{d_1} \in (\pi / a_{j_r}, \sigma\pi / a_{j_r})$, for lightly damped systems) leading to

$$W_\psi u_1(a_{j_i},b) \approx 0, \; if \; j_i \neq j_r \tag{3.8}$$

where, $i = 1,2,....m$. For the noise part, $W_\psi \varepsilon(a_j,b) \approx \delta$, $j = j_1, j_2, ..., j_m$ [where, $\delta << \left|W_\psi u_1(a_{j_p},b)\right|$]. Using equation 3.7 and 3.8, it can be shown that the energy in different frequency bands

$$E_{j_i}(y) \neq 0, \; if \; j_i = j_r$$
$$<< E_{j_r}(y) \tag{3.9}$$

To detect the frequency band in which the fundamental frequency lies, the energy corresponding to each band is calculated for a particular state of response using equation

3.7. The band that contains the maximum energy corresponds to the first natural frequency.

Once the fundamental frequency is obtained and the corresponding band is identified, the band containing the $1^{st}$ natural frequency with scale parameter $j_r$ is considered to obtain the $1^{st}$ mode shape. From equations 3.2, 3.8 and 3.9, it can be shown that

$$W_\psi y(a_{j_r}, b) = \sum \phi_k W_\psi u_k(a_{j_r}, b) + \delta \tag{3.10}$$

In the present study, mode shape is estimated based on the response at a few key locations. Since the mode shape is defined as the state when all the degrees of freedom attain same phase, the mode shape is represented as the ratio of the responses at those degrees of freedom during modal vibration. To identify the mode shape, the response at three key locations at $x = L/6$, $x = L/3$ and $x = L/2$ from the left end of the beam are considered in the present study. The responses at these three key locations are denoted by $y_1 = y(L/6, t)$, $y_2 = y(L/3, t)$ and $y_3 = y(L/2, t)$ respectively. The ratio of wavelet coefficients of $y_1$ and $y_2$ with respect to $y_3$ in both cases at every instant of time corresponding to band $j_r$ (using equations 3.6 and 3.8) yields,

$$\prod_{j_r}^{1} = \frac{W_\psi y_p(a_{j_r}, b)}{W_\psi y_3(a_{j_r}, b)} = \frac{\phi_p^1 + \delta}{\phi_3^1 + \delta}; p = 1,2,... \tag{3.11}$$

Since, $\delta << \left|W_\psi y(a_j, b)\right|$ it follows that the ratio of the wavelet coefficients are constant for every $b$ and can be expressed as

$$\prod_{j_r}^{1} = \frac{W_\psi y_p(a_{j_r}, b)}{W_\psi y_3(a_{j_r}, b)} \approx \frac{\phi_p^1}{\phi_3^1}; p = 1,2,... \tag{3.12}$$

Hence, computing these ratios corresponding to different values of '$p$' and assuming $\phi_3^1 = 1$ (without loss of generality), the mode shapes for the $1^{st}$ mode (in $j_r$ band) can be obtained as

$$[\phi^1] = [\prod_{j_r}^{1}] \tag{3.13}$$

Using the above mathematical formulation, the estimation of fundamental frequency and the corresponding mode shape of a simply supported bridge subjected to vehicular load is possible.

## 3.2.2 Discrete System with Random Input

In the present sub-section, the accuracy and efficiency of the proposed wavelet based method for parameter estimation from the measured random response of discrete systems subjected to random input has been demonstrated.

## *Problem Formulation*

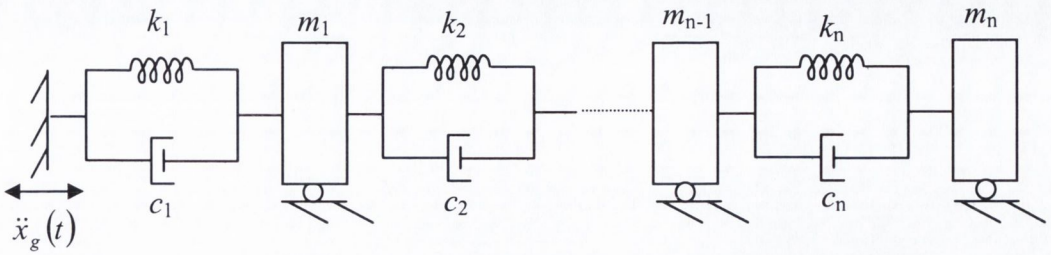


Figure 3.2: MDOF system with random input

Figure 3.2 shows an MDOF system subjected to a random support motion of $\ddot{x}_g(t)$. The governing equation of motion this $n$-DOF classically damped linear system is given by

$$[M]\{\ddot{X}\}+[C]\{\dot{X}\}+[K]\{X\}=[M]\{I\}\{\ddot{x}_g(t)\} \tag{3.14}$$

where, $[M]$, $[C]$, $[K]$ and $\{I\}$ are the mass, damping, stiffness matrices and influence vector respectively with the over-dot representing the differentiation with respect to time. Equation 3.13 can be decoupled using the transformation given by the expression in equation 2.2, which transforms it into a set $n$ first order differential equation. Using this transformation, $k^{th}$ modal response can be expressed as

$$\ddot{u}_k + 2\rho_k\omega_{n_k}\dot{u}_k + \omega_{n_k}^2 u_k = f_k(t);\ k = 1,2,...,n. \tag{3.15}$$

In the above equation, $\rho_k$, $\omega_{n_k}$ and $f_k(t)$ are the damping ratio, natural frequency and forcing function in the $k^{th}$ mode respectively and $u_k(t)$ is the $k^{th}$ modal response. Using the transformation between natural and modal coordinates, response in the $m^{th}$ degree-of-freedom or state can be represented by a linear combination of mode shapes and modal responses as

$$x_m = \sum_{k=1}^{n} \phi_m^k u_k; \qquad m = 1,2,...,n. \tag{3.16}$$

On taking wavelet transform of both side of equation 3.15, it can be shown that

$$W_\psi x_m(a,b) = \sum_{k=1}^{n} \phi_m^k W_\psi u_k(a,b); \qquad m = 1,2,...,n. \tag{3.17}$$

In the present study, a zero initial condition is assumed. Using zero initial conditions, the $k^{th}$ modal response $z_k(t)$ can be evaluated using Duhamel's integral, which is given by

$$W_\psi u_k(a_j,b) = \int_0^b h_k(b-\tau) W_\psi f_k(a_j,\tau) d\tau \tag{3.18}$$

In the above equation, $h_k(b)$ is the impulse response function of a linear single degree of freedom system Paz (1987). Therefore, the normalized energy $E_j(x_m)$ for the response

$x_m$, in the $j^{th}$ frequency band corresponding to the scaling factor $a_j = \sigma^j$, can be represented by a proportional quantity as

$$E_j(x_m) \propto \frac{1}{a_j^2} \int W_\psi^2 x_m(a_j, b) db; \qquad m = 1,2,...,n. \tag{3.19}$$

Following the mathematical formulation presented in section 2.2.1, it can be concluded that the natural frequencies $\omega_{n_1}, \omega_{n_2}, ..., \omega_{n_n}$ are contained in the bands with scale or dilation parameter indices, $j_1, j_2, ..., j_n$ respectively. Thus following the same analogy, it can be shown that estimation of equation 3.18 in bands other than $j_1, j_2, ..., j_n$ leads to insignificant energy contribution such that

$$\begin{aligned} E_j(x_m) &\neq 0 \qquad \text{if } j = j_k,\ k = 1,2,...,n \\ &\approx 0 \qquad \text{otherwise} \end{aligned} \tag{3.20}$$

Thus the first $n$ bands with significant energy content represent first '$n$' natural frequencies of the MDOF system. The natural frequencies are estimated as the mean values of the limits of the corresponding bands. A further refinement of the estimation natural frequencies is possible by introducing the concept wavelet packet as discussed in section 2.2.1. Following this approach, the $j_k^{th}$ band is further sub-divided into $p$ parts. Using this sub-division, equation can be recast in to the form

$$W_{\psi_{sp}} x_m(a_j, b) = \sum_{k=1}^{n} \phi_m^k W_{\psi_{sp}} u_k(a_{j_k}, b); \qquad \text{m=1,2,...,n} \tag{3.21}$$

The mode shape can be evaluated by taking the ratios of the wavelet coefficients of the two different degrees of freedom at an instant of time $t = b$, corresponding to band $j_k$ with sub-band, $p$, which is given by

$$\prod_m^{j_k} = \frac{W_{\psi_{sp}} x_m(a_{j_k}, b)}{W_{\psi_{sp}} x_1(a_{j_k}, b)} = \frac{\phi_m^k}{\phi_1^k} \tag{3.22}$$

The above wavelet-based algorithm can be re-modeled with random measurement noise as discussed in section 3.2.1. Finally, without loss of generality, it can be assumed that $\phi_1^j = 1$ and $k^{th}$ mode shape (in $j_k$ band with further sub-division) can be obtained as

$$\{\phi_m^k\} = \{\prod_m^{j_k}\}; \qquad m = 1,2,...,n. \tag{3.23}$$

Thus, mode shape for any other mode can be obtained in a similar manner for $k$ = $1,2,...,n$.

## 3.3 Support Motion Model

In the present study, supports motion $\ddot{x}_g(t)$ is modelled as a vector of non-stationary Gaussian random process. In this approach, the non-stationary random process is represented as

$$\ddot{x}_g(t) = e(t)\ddot{w}_g(t) \tag{3.24}$$

In the above equation, $e(t)$ is a deterministic uniform amplitude modulating function and $\ddot{w}_g(t)$ is a Gaussian random process with zero mean and a specified power spectral density function $S_{ww}(\omega)$. An exponential form of the amplitude modulation as proposed by Shinuzok and Sato (1967) is considered in the present study, which is given by

$$e(t) = \alpha(\exp(-t/\beta) - \exp(-t/\gamma)) \tag{3.25}$$

$S_{ww}(\omega)$ is modelled as Kanai-Tajimi spectra, which is the output power spectral density of a second order linear filter subjected to Gaussian white noise. $S_{ww}(\omega)$ is given by

$$S_{ww}(\omega) = \frac{1 + 4\eta_g^2(\omega/\omega_g)^2}{\left[1 - (\omega/\omega_g)^2\right]^2 + 4\eta_g^2(\omega/\omega_g)^2} \tag{3.26}$$

In equation 3.25, $\eta_g$ and $\omega_g$ are the parameters of the second order filter. To simulate the time history of $\ddot{x}_g(t)$, first $\ddot{w}_g(t)$ is simulated from the above power spectrum, which is given by the equation

$$\ddot{w}_g(t) = \sum_{n=1}^{N} A_n \cos(\lambda_n t) + B_n \sin(\lambda_n t) \tag{3.27}$$

In the above equation, $A_n$ and $B_n$ are zero mean independent Gaussian random variables with standard deviation $\sigma_n$ is given by

$$\sigma_n^2 = \int_{\omega_n}^{\omega_{n+1}} S_{ww}(\omega) d\omega \quad \ldots \quad n = 1,2,3...N \tag{3.28}$$

In equation 3.27, $N$ is the total number frequencies considered in the time history simulation of $\ddot{w}_g(t)$.

## 3.4 Numerical Results and Discussions

Using the noise contaminated response of the structures obtained from simulation; the proposed wavelet based system identification technique is used to estimate the structural parameters.

### 3.4.1 Vehicle-Bridge Problem

A simply supported beam as shown in figure 3.1 is considered to demonstrate the use of the proposed algorithm to estimate the fundamental natural frequency and the associated mode shape. The length of the beam is taken to be 45m. The mass per unit length, flexural rigidity and damping coefficient of the bridge are assumed to be 4625 kg/m, 1.62E11 N-mm$^2$ and 1850 N-s/mm respectively. Using these values in equation 3.5, the fundamental frequency of the bridge is evaluated as 28.85 rad/s. A vehicle of weight 10kN is assumed to travel at a constant velocity of 15 m/s over the bridge deck. The displacement response is simulated at three key locations L/6, L/3 and L/2 from left support respectively. Let these locations be marked as 1,2 and 3. The displacement response time histories at these locations are simulated based on the first three modal responses only. To simulate the response, a direct numerical integration scheme is followed using *Wilson-$\theta$* [Bathe (1997)] technique with $\theta=1.4$ as shown in figure 3.3. A white noise with the magnitude as 1/10$^{th}$ of the peak bridge displacement response is simulated and added to the simulated time history response of the bridge as measurement noise.

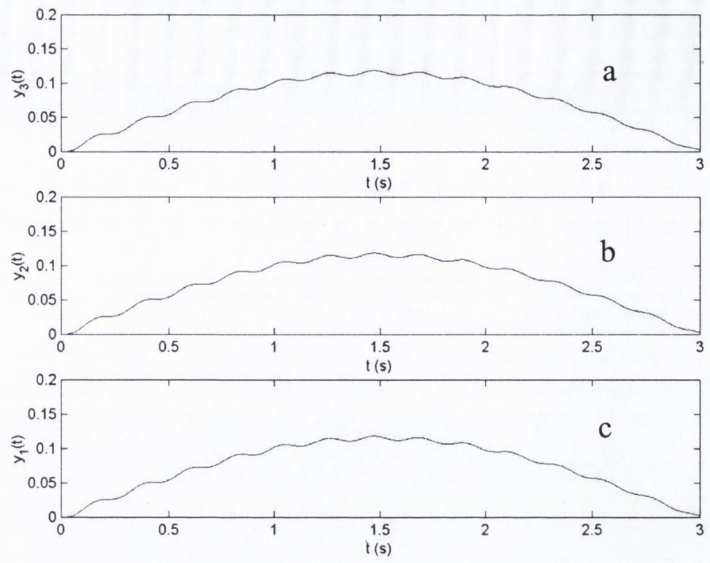


Figure 3.3: Simulated responses of the beam at locations 1, 2 and 3 due to a vehicle moving at a constant speed; (a) location 1, (b) location 2 and (c) location 3

Figure 3.4 and 3.5 show the power spectral density (PSD) obtained from fast Fourier transformation (FFT) of the simulated samples of white noise and probability distribution function (PDF) of the ensemble at $t = 5s$ respectively. It can be noticed that both PSD and PDF match closely with their respective targets. Figure 3.6 shows the time histories of the simulated measurement-noise and figure 3.7 shows the noise-contaminated responses at locations 1, 2 and 3.

Using these simulated bridge data, the inverse problem is solved to estimate the first natural frequency and the first mode shape of the bridge. For this purpose, the modified form of L-P basis function is used to calculate the energy content of the responses at different frequency bands using equation 3.7. Values of $F_1$ and $\sigma$ are assumed to be 4 Hz and 1.25. Figure 3.8 shows the plot of integral quantity in equation 3.7, which is

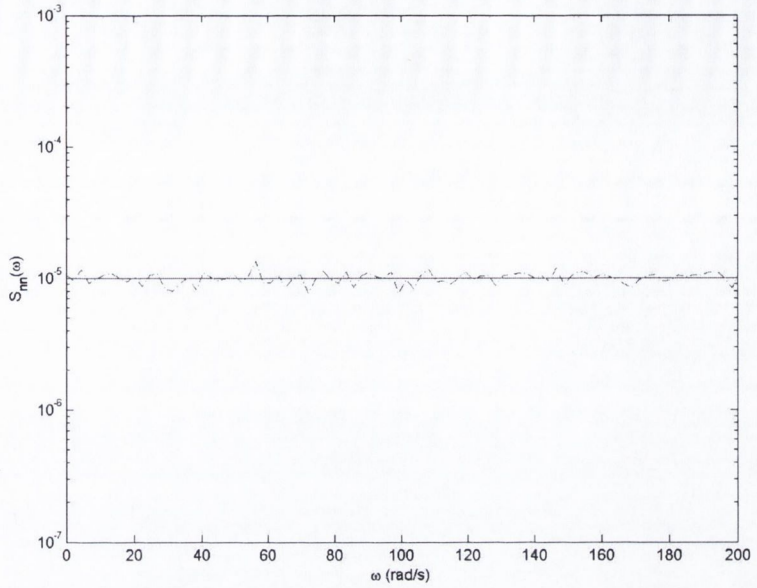


Figure 3.4: Power Spectral Density function of the broad banded white noise; ___ exact, - --- simulated

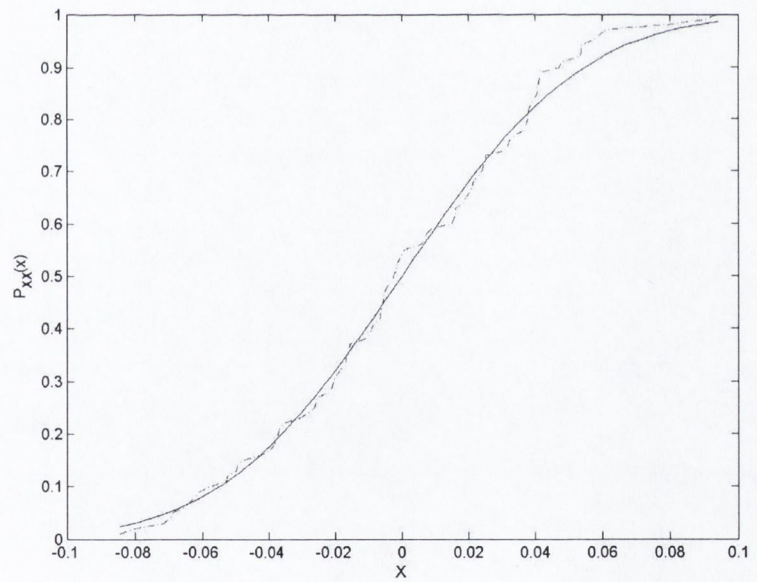


Figure 3.5: Probability Distribution Function (PDF) of the simulated samples of the stationary process the support motion at $t = 5s$ ; ___ exact, ---- simulated

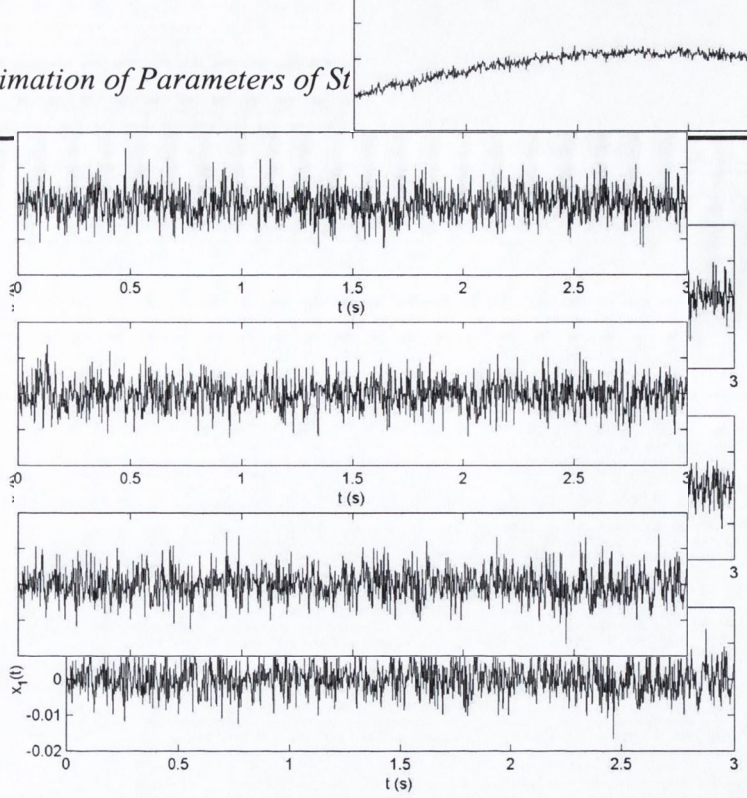


Figure 3.6: Broad banded white noise time history

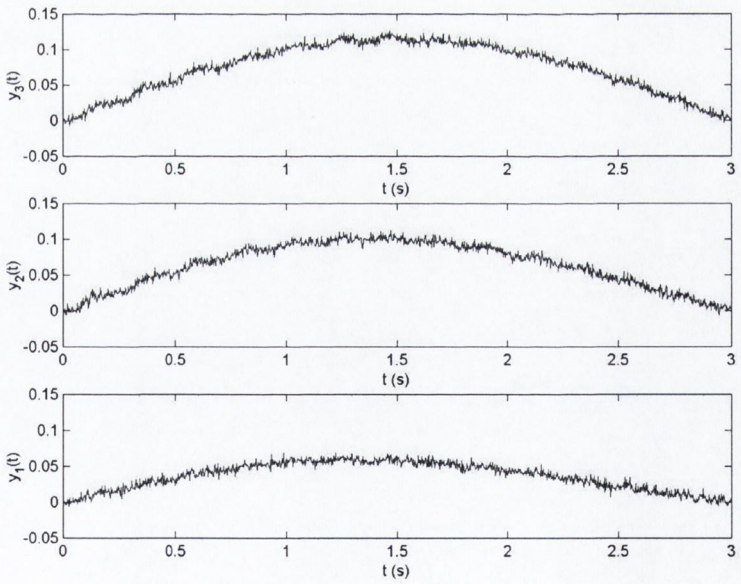


Figure 3.7: Noise contaminated displacement response of the beam at locations 1, 2 and 3

proportional to the energy content of the displacement responses measured at key locations in different bands. It can be observed that energy content are maximum in band 2 while these are insignificant in other bands as described in equation 3.9 and the frequency limits corresponding to band 2 are 25.13-31.42 rad/s. The central frequency of this band (i.e. 28.27 rad/s) is estimated as the first natural frequency of the bridge structure. This band can be further sub-divided into smaller bands to achieve desired level of accuracy.

To estimate the first mode shape, the wavelet coefficients of the response at key locations in band 2 are considered. Using equation 3.10, mode shape is estimated by taking the ratio of wavelet coefficients of the response at L/6 and L/3 with respect to the wavelet coefficients of the response at L/2 in both cases. Figure 3.9 shows these ratios over time. The wavelet coefficients at L/2 are taken to be 1 while the ratios are taken at the peak values of the wavelet coefficients only to avoid numerical instability near zero crossings. It can be observed that the ratios of wavelet coefficients are almost constant over time, which is expected as seen from equation 3.11. The little variation in the ratio of wavelet coefficients over time may be due to the numerical instability. The mode shape is estimated by taking the mean of these wavelet coefficient ratios over time, which is shown in figure 3.10. Without loss of generality, the value of the mode shape at L/2 is taken to be 1. From these results, it is observed that using the wavelet based algorithm presented here, the fundamental modal frequency and the corresponding mode shape can be estimated with a high level of accuracy.

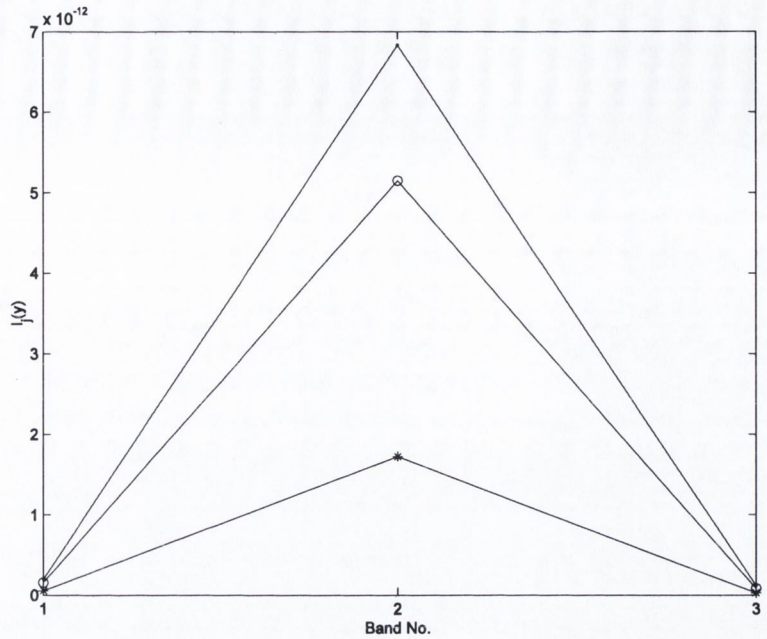


Figure 3.8: Energy in different frequency bands; -*- at 1, -o- at 2 & -.- at 3 on the beam

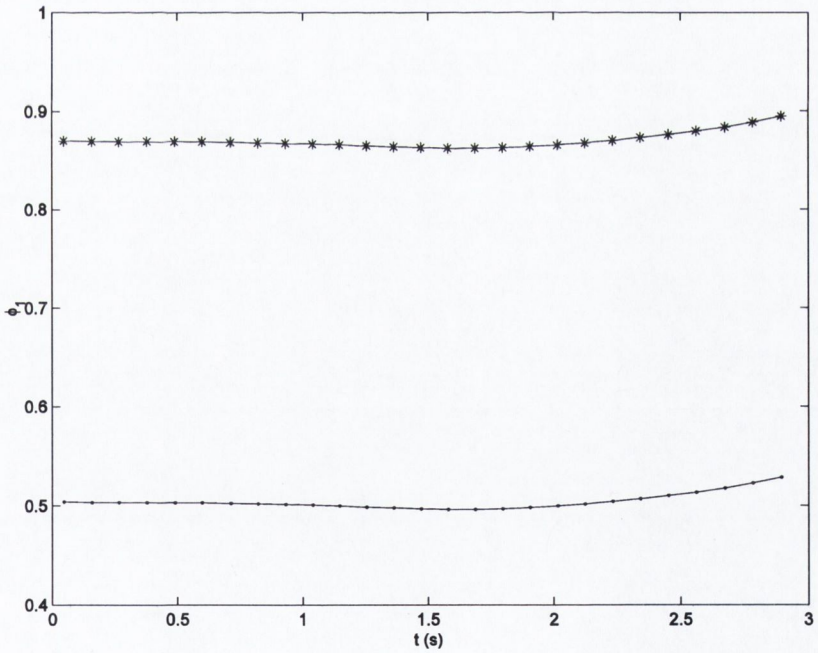


Figure 3.9: Ratios of wavelet coefficients of the responses in the band 2; -*- $\phi_{21}^1/\phi_{31}^1$ , -.- $\phi_{11}^1/\phi_{31}^1$

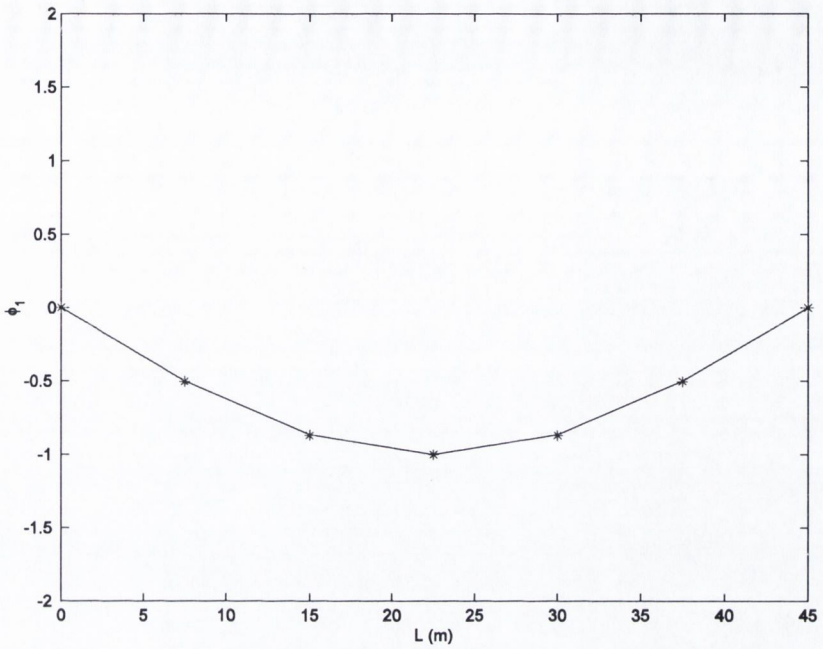


Figure 3.10: Fundamental mode shape of the bridge; - actual, * estimated

### 3.4.2 MDOF System with Random Input

The 5DOF system considered in this section has the same structural parameters as the system that has been considered in Chapter 2. An ensemble of 100 support motions is simulated following the model given in section 3.3.2. For this purpose, $\eta_g$ and $\omega_g$ are considered to as 40% and 20rad/s respectively and the envelope function parameters are $\alpha = 4.0$, $\beta = 6.22$ and $\gamma = 3.11$ respectively. Based on equation 3.27, time histories for $\ddot{w}_g(t)$ are simulated with $N = 2^{10}$. Figure 3.11 shows the original Kanai-Tajimi spectra and that obtained from simulated samples using FFT. It can be observed that simulated time history record for $\ddot{w}_g(t)$ closely matches with the target PSD.

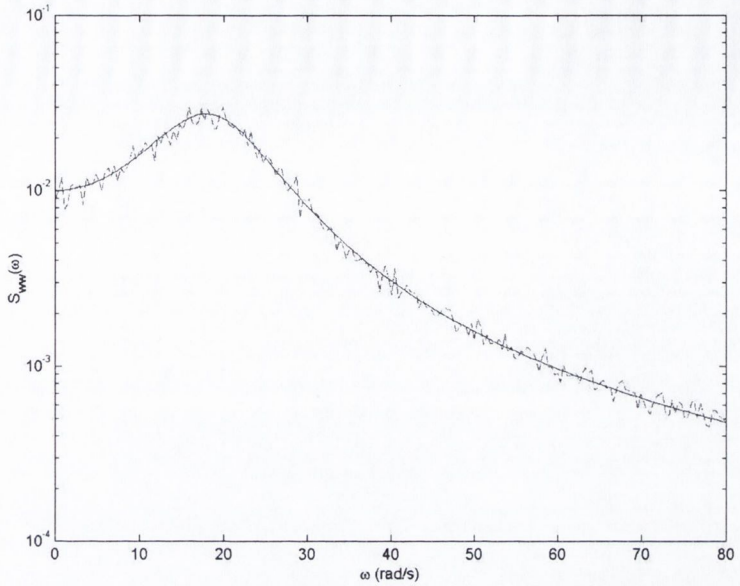


Figure 3.11: Kanai-Tajimi PSD; ___ exact, ---- simulated

Since a Gaussian model is assumed to simulate the stationary process; a statistical data analysis is performed randomly across the ensemble. Figure 3.12 shows the probability distribution function (PDF) of the random noise based on the simulated time history record at $t = 5s$. A close match has been observed between the theoretical PDF and the simulated PDF. Figure 3.13 shows the uniform amplitude modulation used to generate non-stationary time history record for $\ddot{x}_g(t)$, which has a maximum at $t = 4.78s$. Figure 3.14 shows a sample of the non-stationary time history records for $\ddot{x}_g(t)$ as given in equation 3.24. It can be noticed that the simulated support motion has an initial build up phase, which is followed by a strong motion phase when the support motion reaches its maximum and finally a decaying phase. These are general features observed in any strong motion earthquake. Using a sample realization from the simulated time histories, the

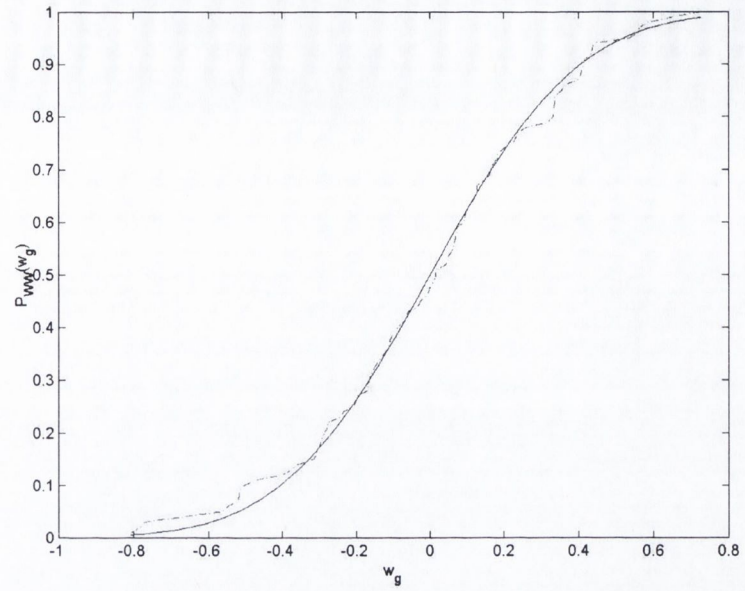


Figure 3.12: Probability Distribution Function (PDF) of the simulated samples of the stationary process the support motion at $t = 5s$ ; ___ exact, ---- simulated

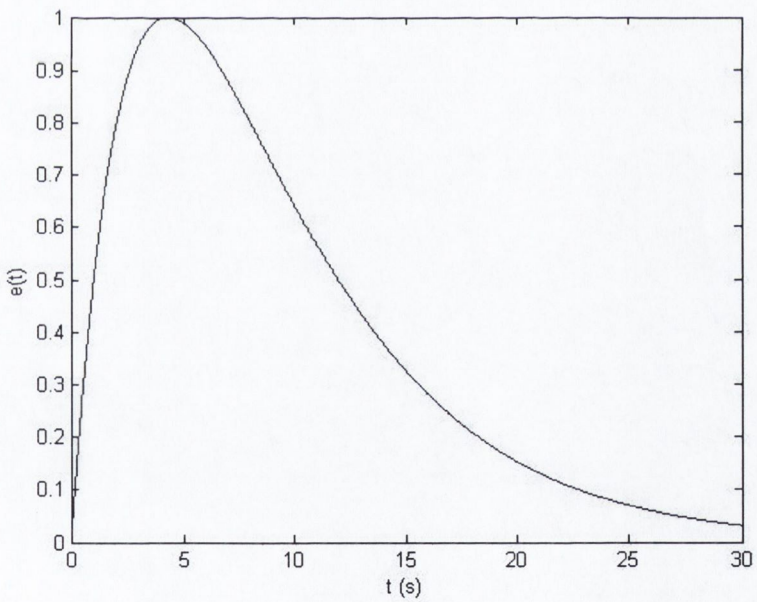


Figure 3.13: Envelope function used for amplitude modulation

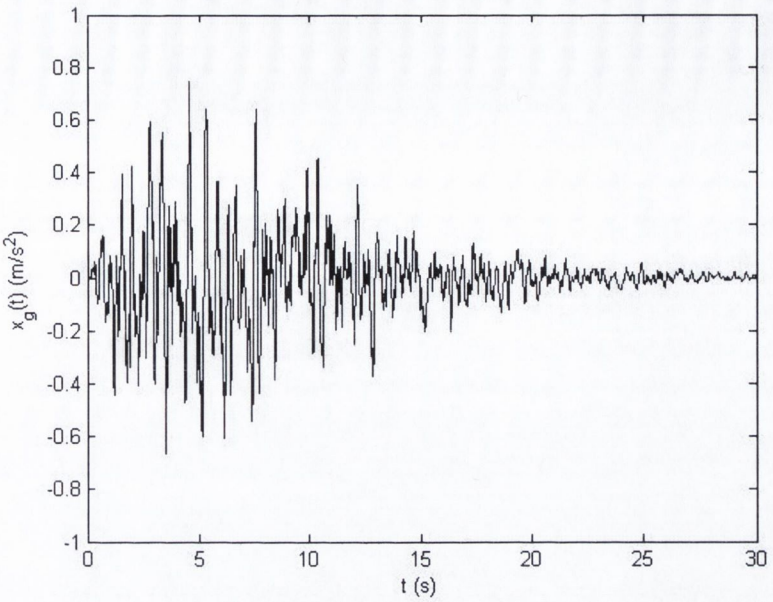


Figure 3.14: Simulated time history of random support motion

response of the 5DOF system is simulated using *Wilson-θ* technique with zero initial conditions and a simulated broad banded white noise is added as measurement noise.

Using the response time history records at different degrees of freedom, a wavelet analysis is performed to estimate the system parameters. For this purpose, ML-P basis function is used to evaluate the energy content of the displacement response in different frequency bands as shown in figure 3.15 and 3.16. Based on the energy spectrum obtained from wavelet analysis, bands 2.6-3.09rad/s and 7.0-8.32rad/s are obtained as the band containing first two natural frequencies. The natural frequencies are estimated as 2.85rad/s and 7.66rad/s respectively. Figures 3.17 to 3.18 show the wavelet coefficients in these bands. It can be observed that wavelet coefficients are in phase except at the beginning and end in figure 3.18, which may be due to the edge effect in wavelet analysis. Figure 3.19 to 3.20 show the ratio wavelet coefficients in these frequency bands.

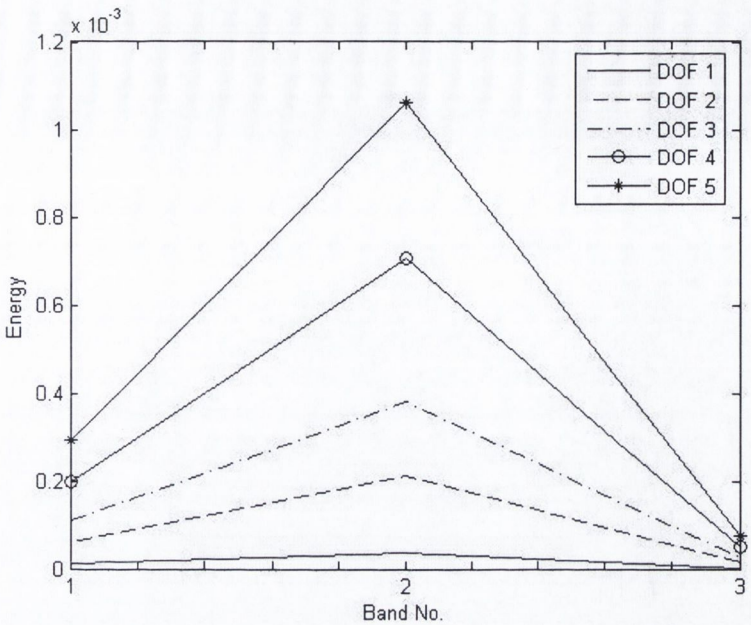


Figure 3.15: Energy in different frequency bands surrounding 1st natural frequency

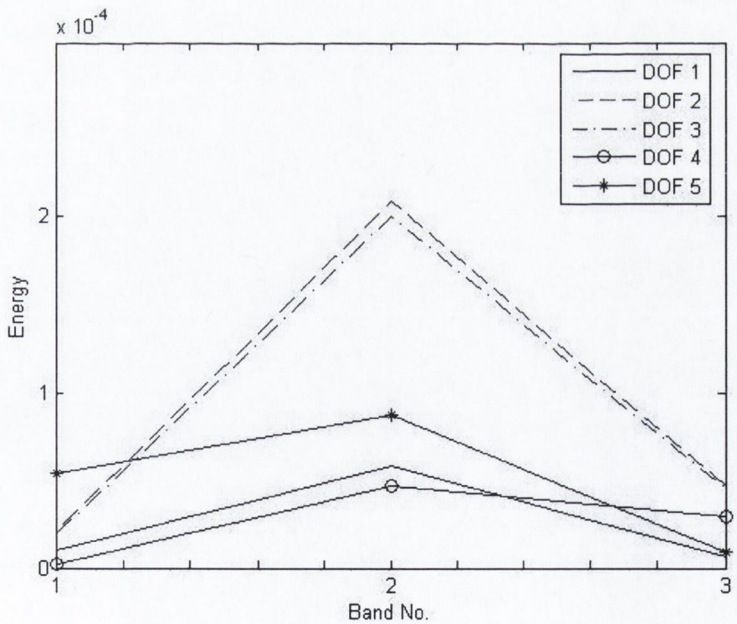


Figure 3.16: Energy in different frequency bands surrounding 2nd natural frequency

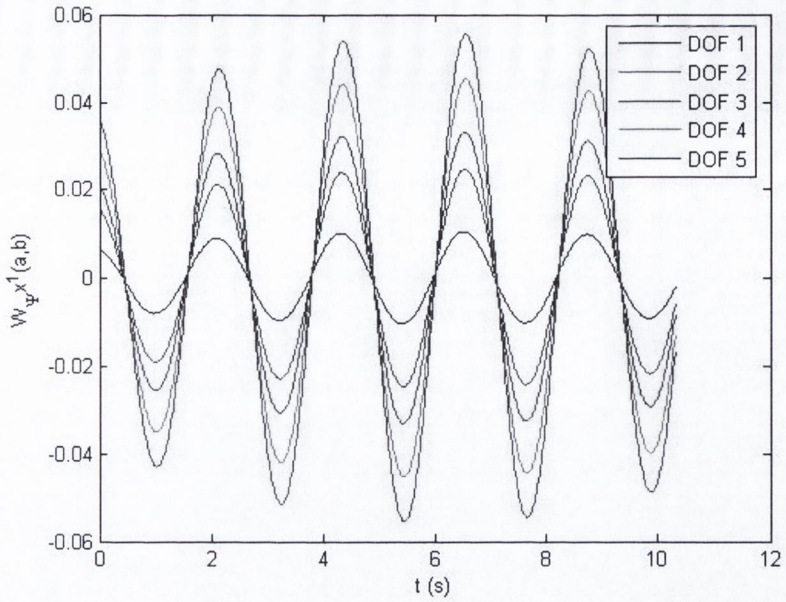


Figure 3.17: Wavelet coefficients of the response in 1st mode (frequency band 2.6-3.09 rad/s)

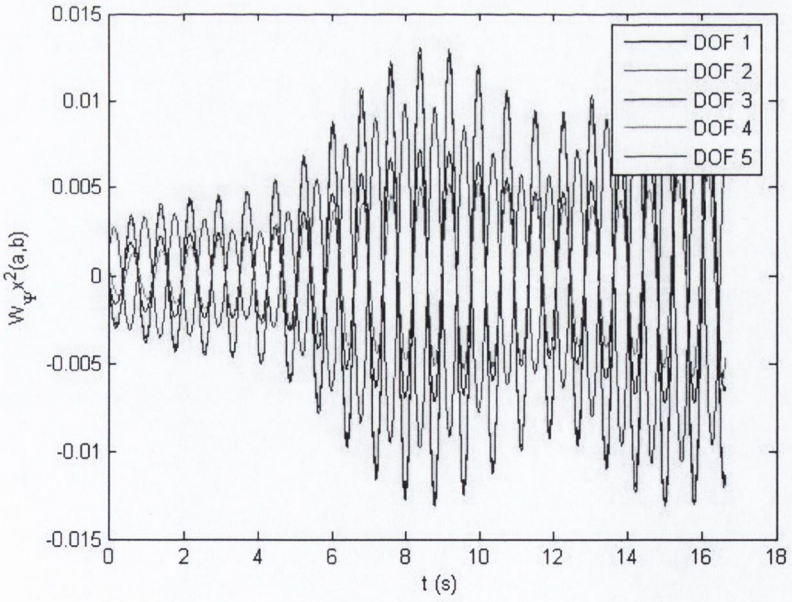


Figure 3.18: Wavelet coefficients of the response in 2nd mode (frequency band 7.0-8.32 rad/s)

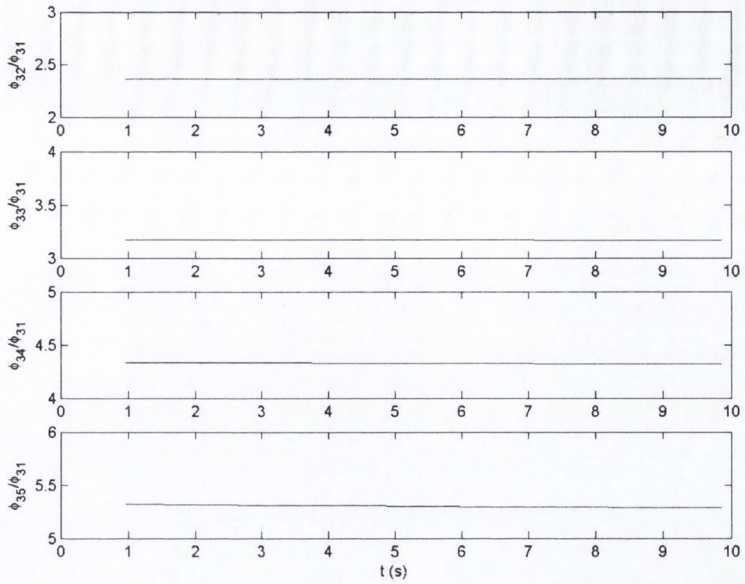


Figure 3.19: Ratio of wavelet coefficients of the modal responses at 1st natural frequency

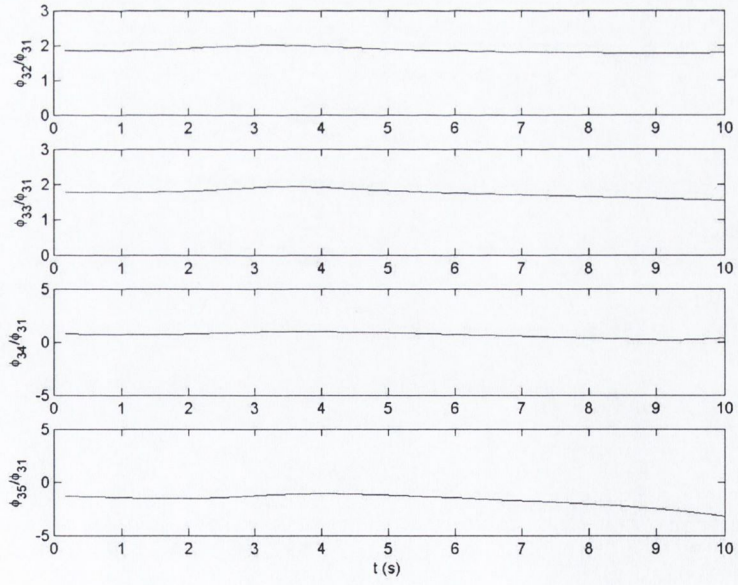


Figure 3.20: Ratio of wavelet coefficients of the modal responses at 2nd natural frequency

It can be observed that the ratio of the wavelet coefficients is fairly constant over the time as expected. Figures 3.21 to 3.23 show the estimated mode shapes corresponding to 1st, 2nd and 3rd modes respectively. An effort has been made to estimate the third natural frequency and mode shape in a similar manner. The third natural frequency is estimated as 12.59rad/s, which is fairly close to the original value and the respective mode shape is shown in figure 3.23. From this figure, it can be noticed that although the proposed wavelet based algorithm can track overall shape of the mode shape accuracy reduces in higher modes. Hence, it can be concluded that modal frequencies along with mode shapes can be estimated with the proposed wavelet based algorithm from the noise contaminated measurement with desired level of accuracy and the accuracy reduces in third mode as has been observed in chapter 2.

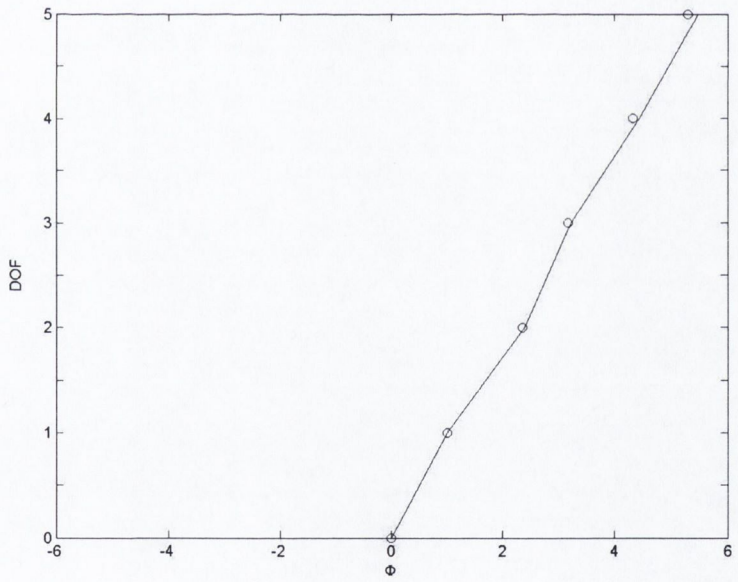


Figure 3.21: Actual and estimated 1st mode shape of the MDOF system ('__' actual, 'o' estimated)

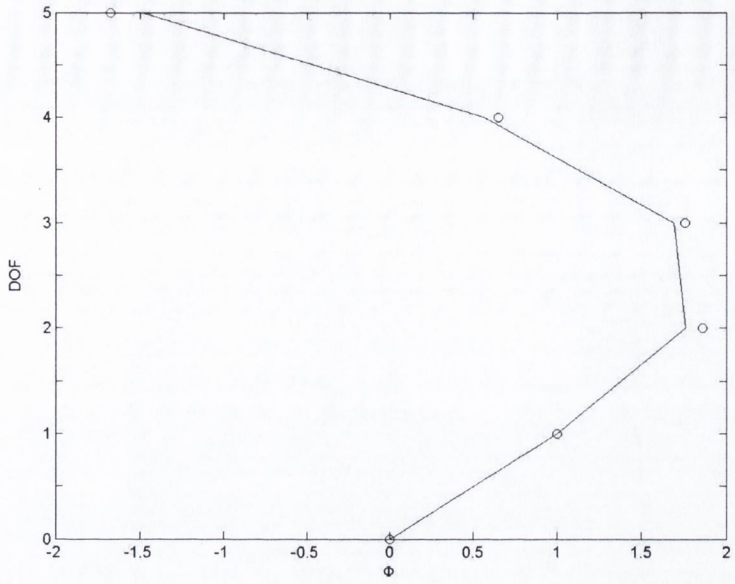


Figure 3.22: Actual and estimated 2nd mode shape of the MDOF system ('__' actual, 'o' estimated)

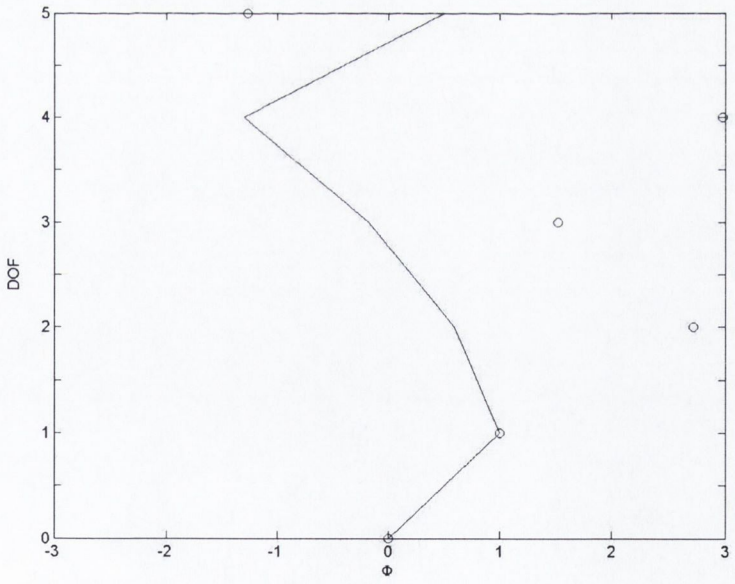


Figure 3.23: Actual and estimated 3rd mode shape of the MDOF system ('__' actual, 'o' estimated)

## 3.5 Experimental Validation of Proposed Wavelet Based Identification Technique

The proposed wavelet-based model for system identification is validated using the experimental results. For this purpose, a reinforced concrete beam is tested and the fundamental frequency and mode shape are estimated from the noise-contaminated measurement of strain time history records. Figures 3.24 and 3.25 show the schematic RC beam, which is 3.6m long and the cross section of the beam respectively. The beam is 250mm wide and 300mm deep. It is made of M40 concrete with 2-T20 bars at bottom as tension reinforcement and 2-T12 bars at the top. Figures 3.26 and 3.27 show the experimental setup and the details of the supports used for the RC beam. The beam is excited as by an impulsive load at the middle as shown in the figure 3.24 and the axial strains are measured at the location

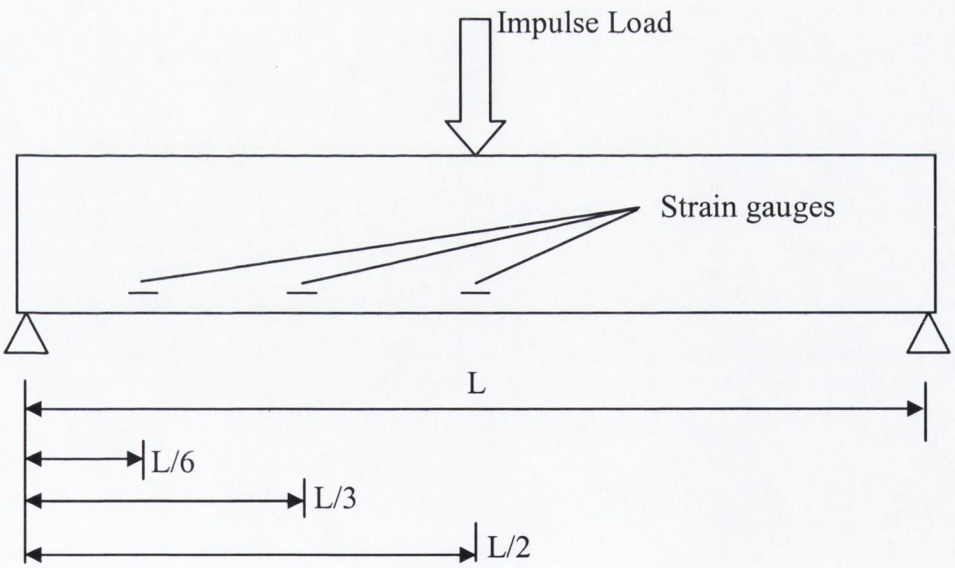


Figure 3.24: Schematic diagram of the simply supported beam

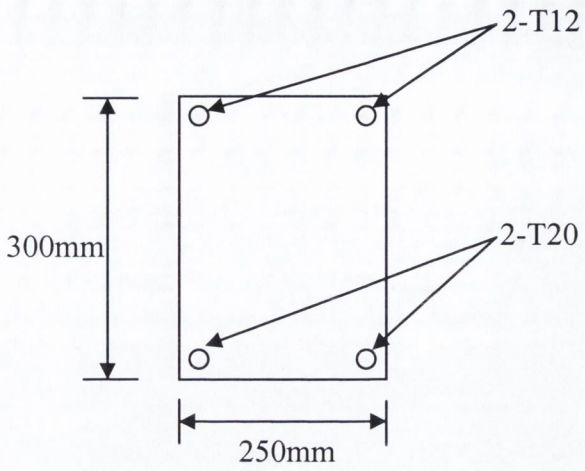


Figure 3.25: Cross section of the beam

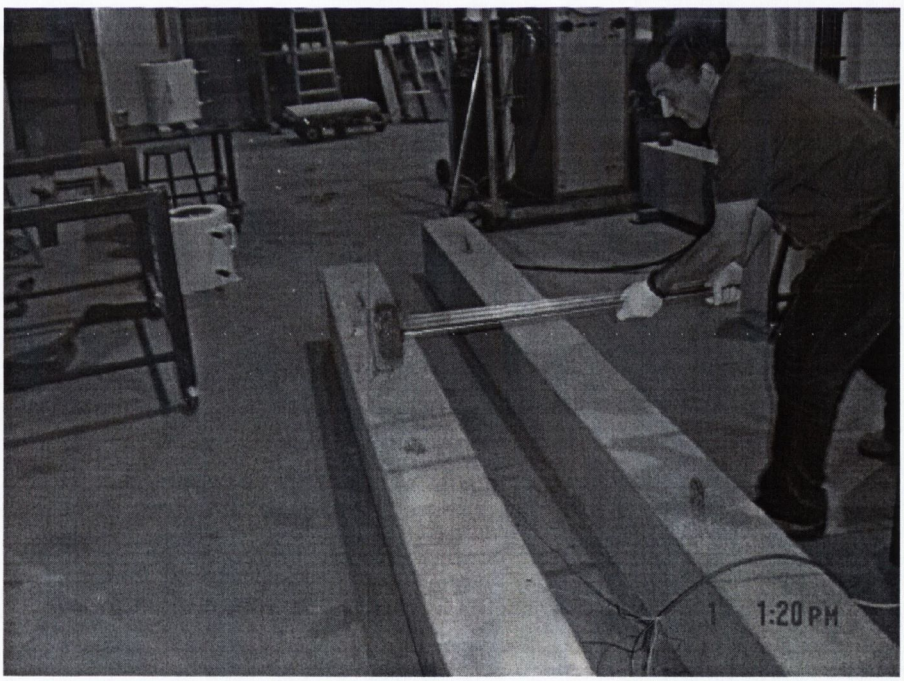


Figure 3.26: Experimental setup: RC beam with impulse load at the middle

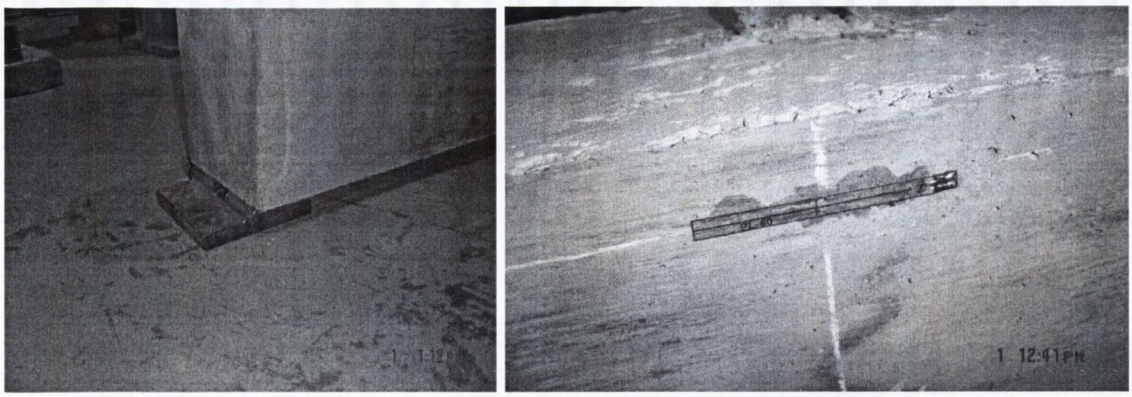

(a) (b)

Figure 3.27: Details of RC beam; (a) Roller supports at the end of the beam, (b) PL-60 strain gauge

marked as 1, 2 and 3 in the figure 3.11, which are at a distance of L/6, L/3 and L/2 from the left end respectively.

In the present study, the same experiment is performed repeatedly and the results for two separate tests of the same experiment are presented here. Figures 3.28a, 3.29a, 3.30a, 3.31a, 3.32a and 3.33a show the measured strain time histories at these key locations. Figures 3.28b, 3.29b, 3.30b, 3.31b, 3.32b and 3.33b show the Fourier energy spectra of the measured strain records. It can be observed that the energy attains the peak value at 206.9423rad/s, which corresponds to the first natural frequency of the beam.

Using these strain time history records, the proposed wavelet packet based algorithm for parameter estimation is adopted to evaluate the fundamental frequency and mode shape of the RC beam. For this purpose, the modified form of LP basis function is used, which is enables to adopt sub-band coding. The response energy in different frequency bands for different degrees of freedom are calculated based on the wavelet

model as described in equation 3.9. Figure 3.34 shows the response energy in different frequency bands. It can be noticed that the energy is maximum at second band, which corresponds to frequency range 188.4956rad/s to 224.1603rad/s. The mean value of this frequency range is estimated as the first natural frequency, which is 206.3280rad/s. Figures 3.35a and 3.35b show the wavelet coefficients for different degrees of freedom in second band for test 1 and test 2 respectively. The wavelet coefficients are in phase as the system vibrates in its mode. To evaluate the mode shape, ratio of the wavelet coefficients are taken at peaks only. Figures 3.36a and 3.36b show the ratio of the wavelet coefficients in test 1 and test 2 respectively, which can be considered constant over time. Without loss of generality, the wavelet coefficients of the response at location 3 are considered as 1 in the present calculation. It can be noticed that the ratio of the wavelet coefficients are constant over time. The mean value of these ratios over time is estimated as the fundamental mode shape of the RC beam.

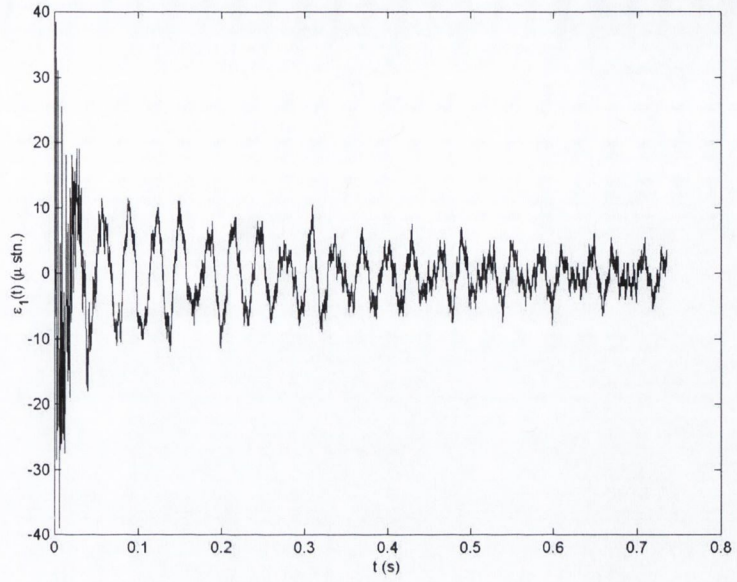


(a)

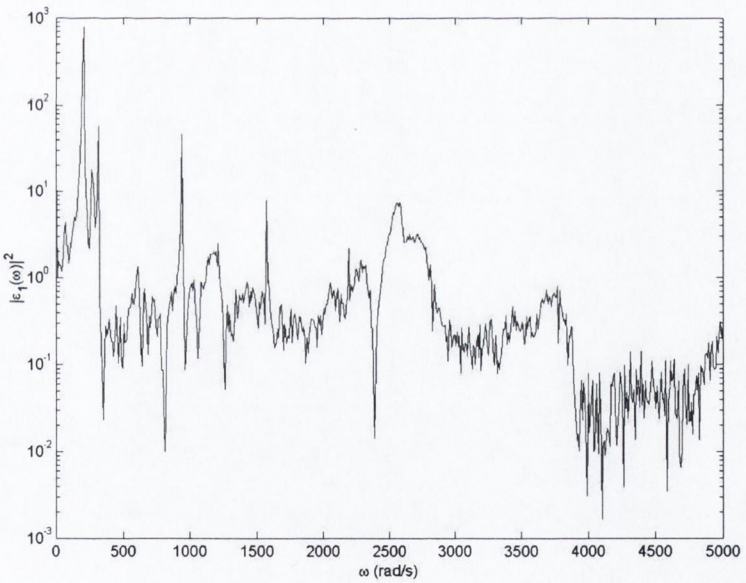


(b)

Figure 3.28: Measured strain records at locations 1 in Test 1; (a) strain time history, (b) Fourier amplitude spectra

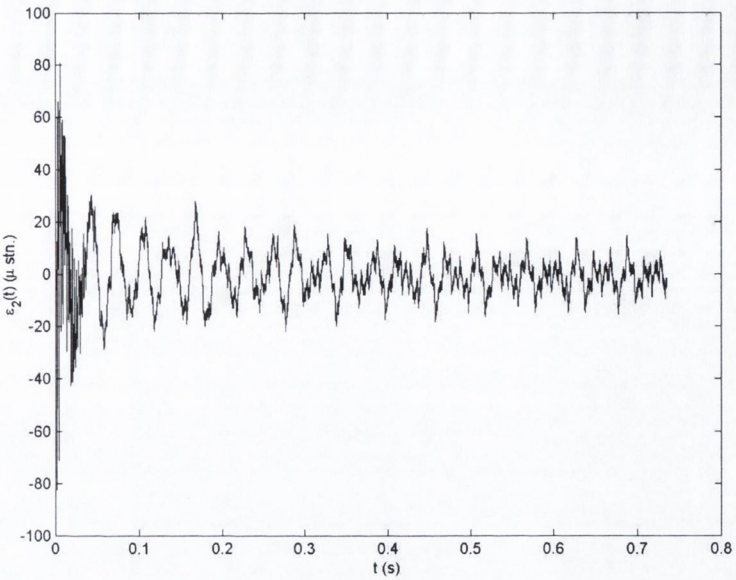


(a)

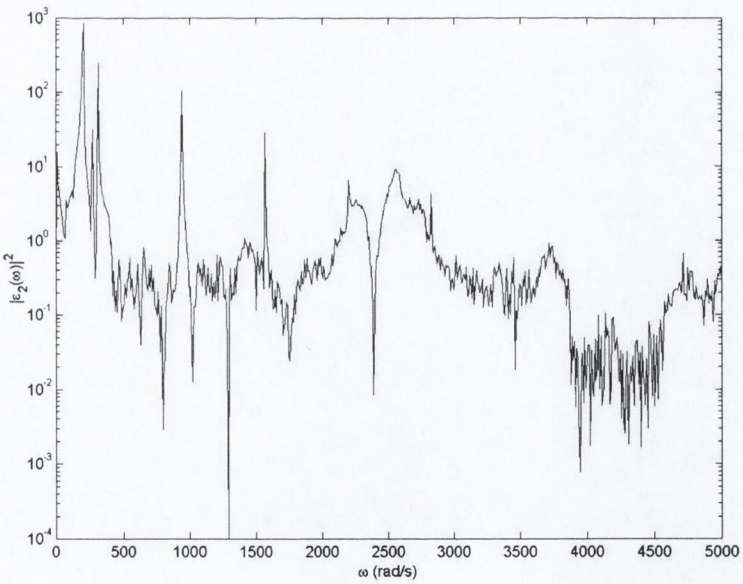


(b)

Figure 3.29: Measured strain records at locations 2 in Test 1; (a) strain time history, (b) Fourier amplitude spectra

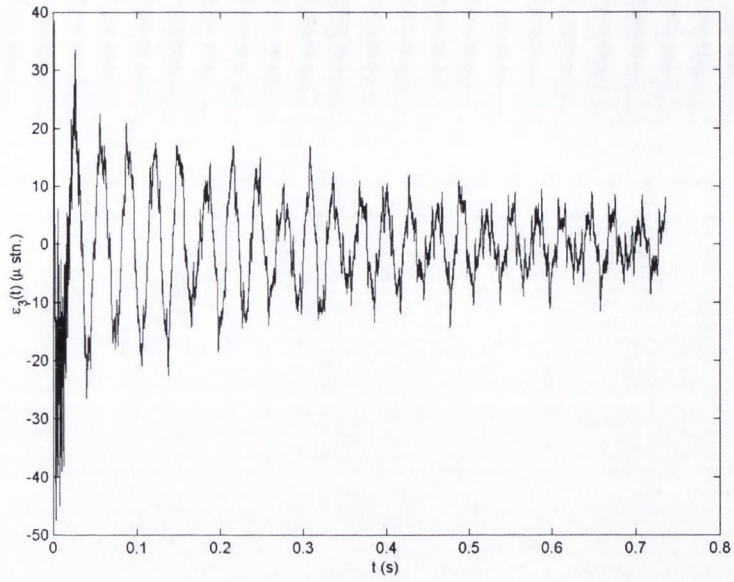


(a)

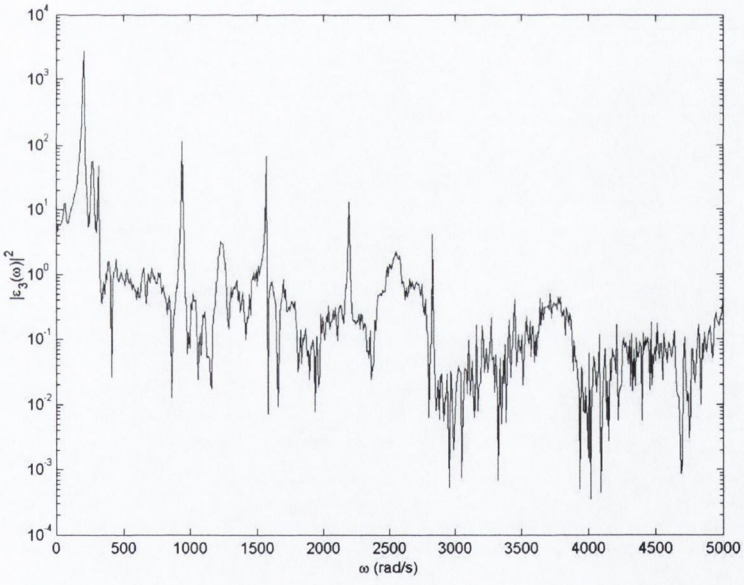


(b)

Figure 3.30: Measured strain records at locations 3 in Test 1; (a) strain time history, (b) Fourier amplitude spectra

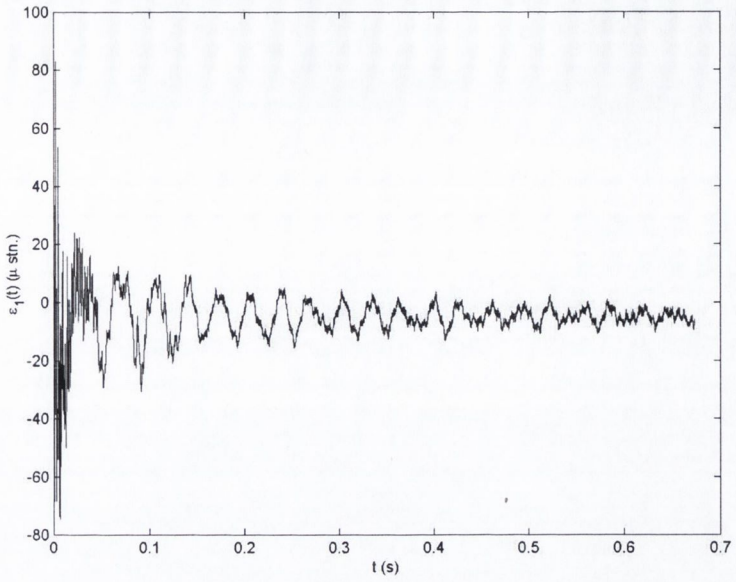


(a)

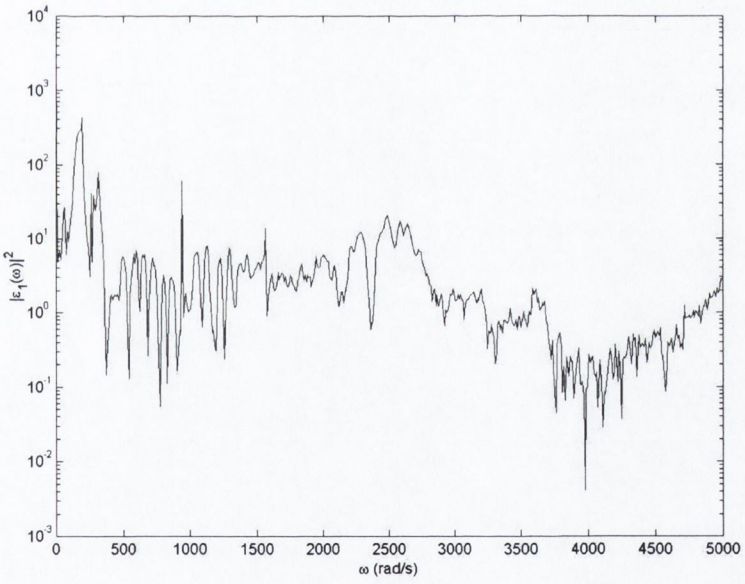


(b)

Figure 3.31: Measured strain records at locations 1 in Test 2; (a) strain time history, (b) Fourier amplitude spectra

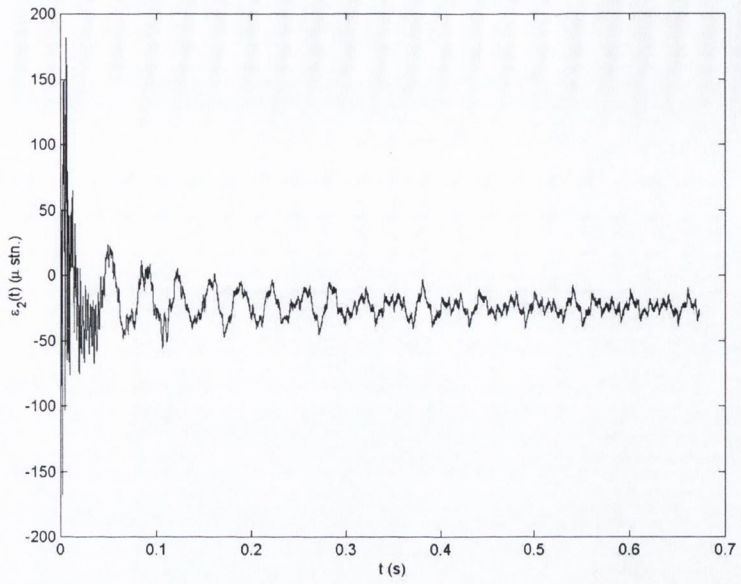


(a)

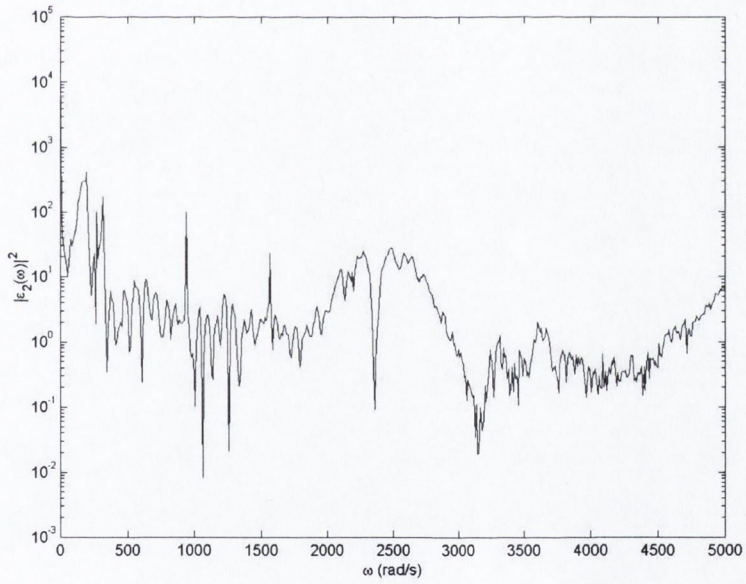


(b)

Figure 3.32: Measured strain records at locations 2 in Test 2; (a) strain time history, (b) Fourier amplitude spectra

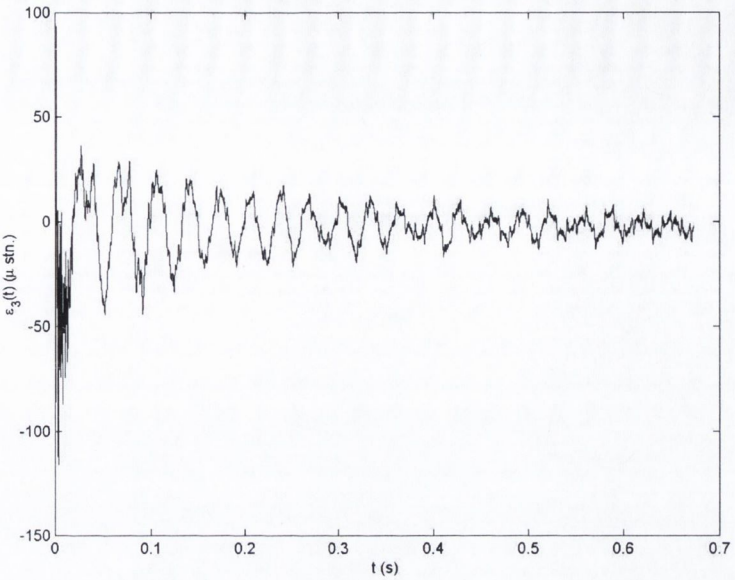


(a)

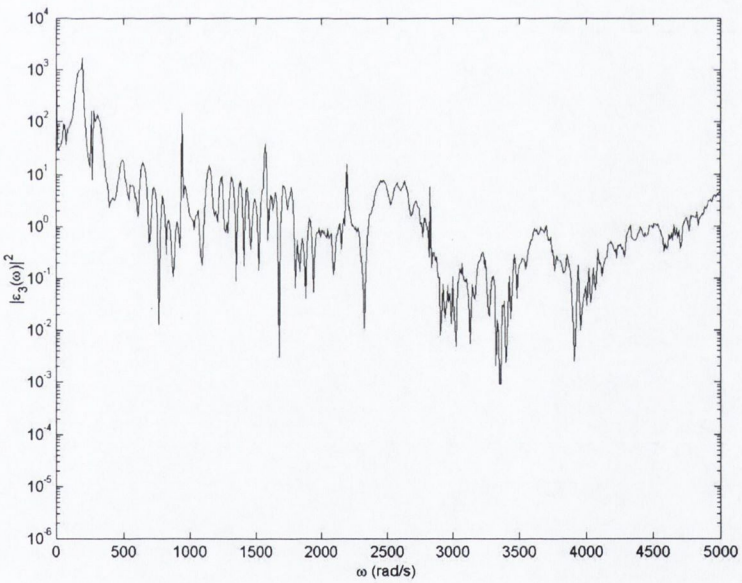


(b)

Figure 3.33: Measured strain records at locations 3 in Test 2; (a) strain time history, (b) Fourier amplitude spectra

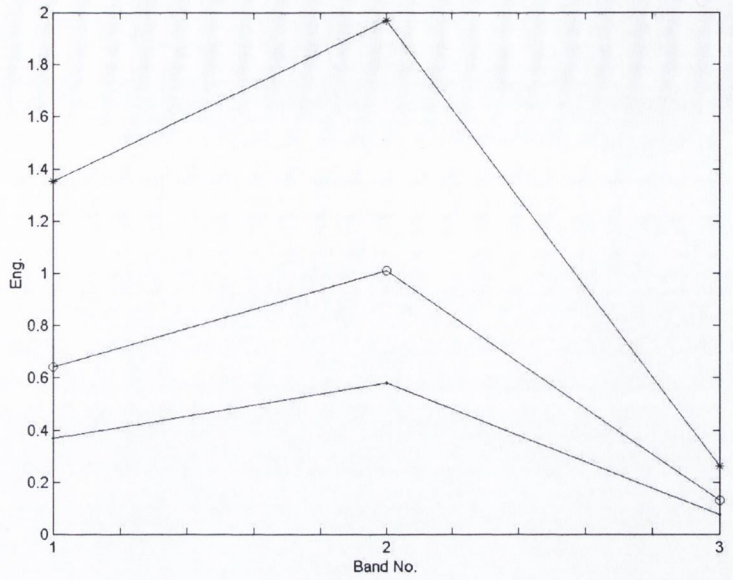


(a)

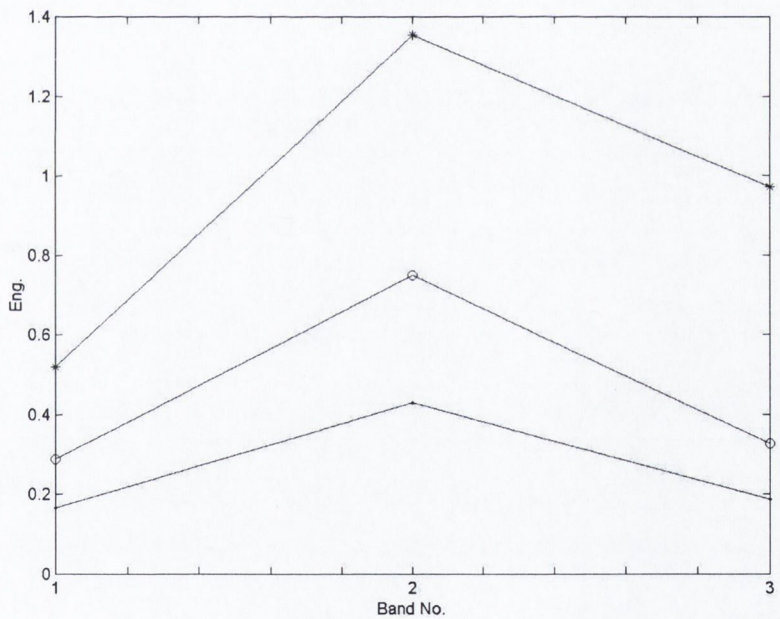


(b)

Figure 3.34: Energy in different frequency bands; (a) Test 1, (b) Test 2; '_*' location 1, '_o' location 2 and '_.' location 3

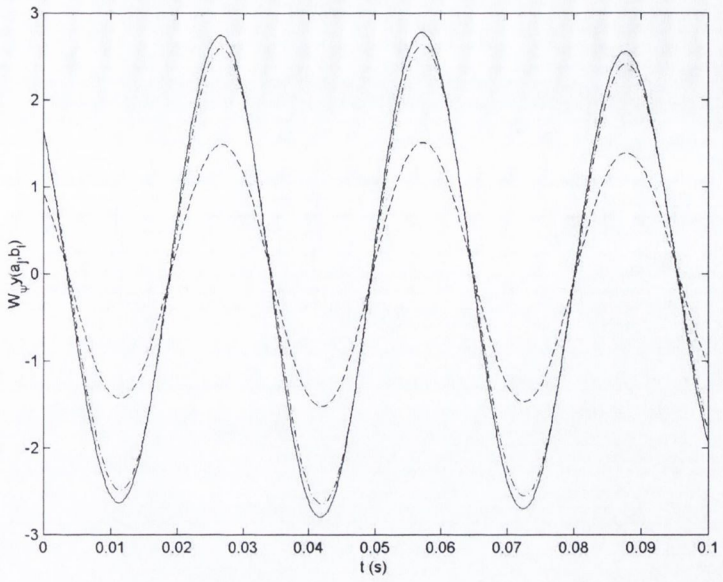


(a)

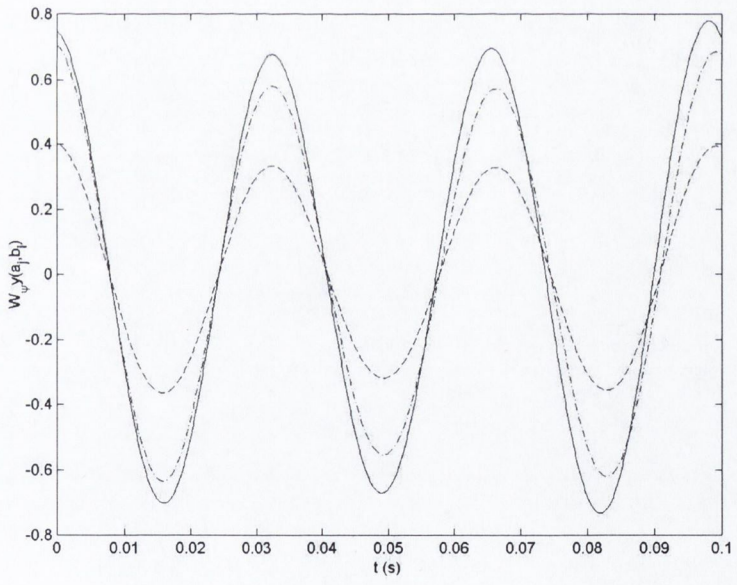


(b)

Figure 3.35: Wavelet coefficients in different frequency bands; (a) Test 1, (b) Test 2; '_.' location 1, '_ _' location 2 and '__' location 3

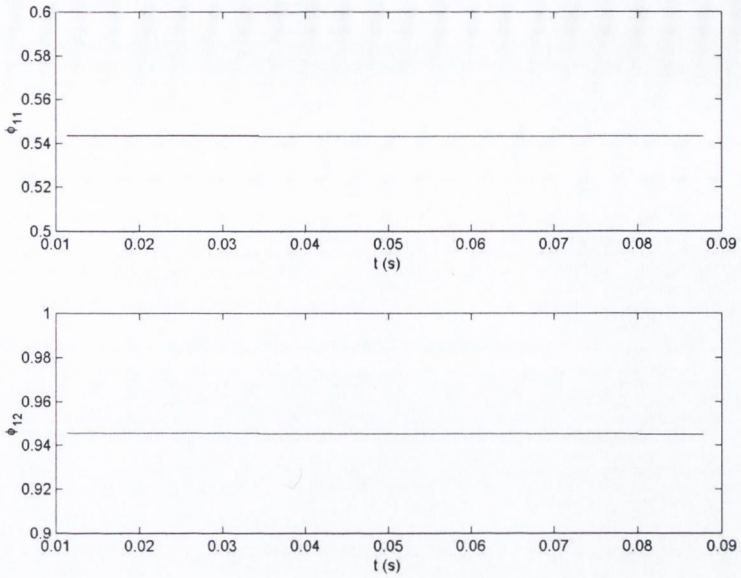


(a)

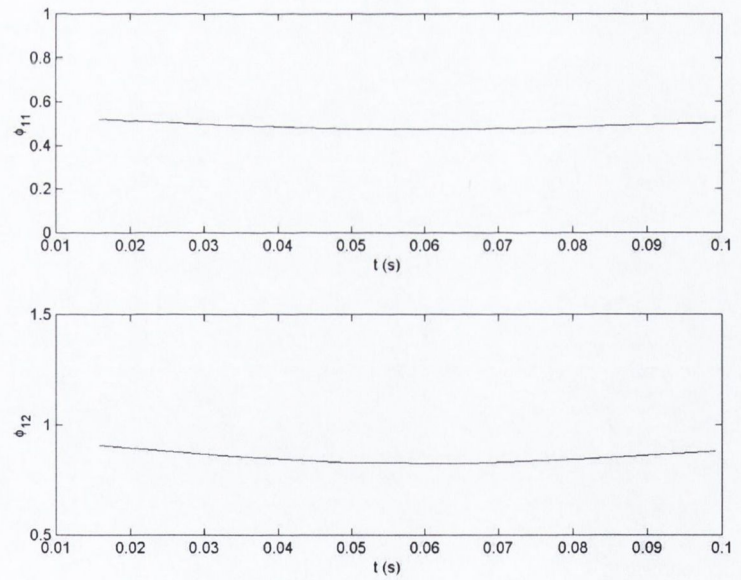


(b)

Figure 3.36: Ratio of wavelet coefficients; (a) Test 1, (b) Test 2

Figure 3.22a and 3.22b show the estimated fundamental mode shape from test 1 and test 2 respectively. It can be observed that the proposed wavelet packet based algorithm for system identification estimates natural frequency and mode shape accurately even when the response time history is contaminated with measurement noise. Hence the proposed wavelet-based time-frequency analysis for system identification an be adopted for parameter estimation for dynamical systems.

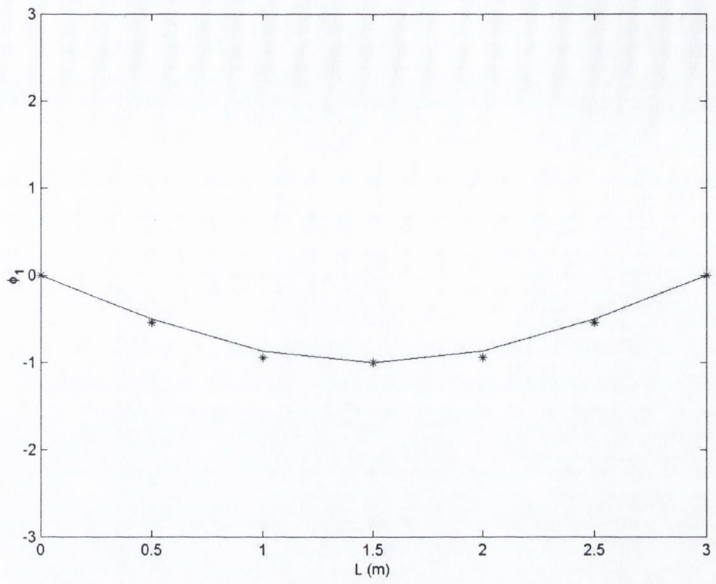


(a)

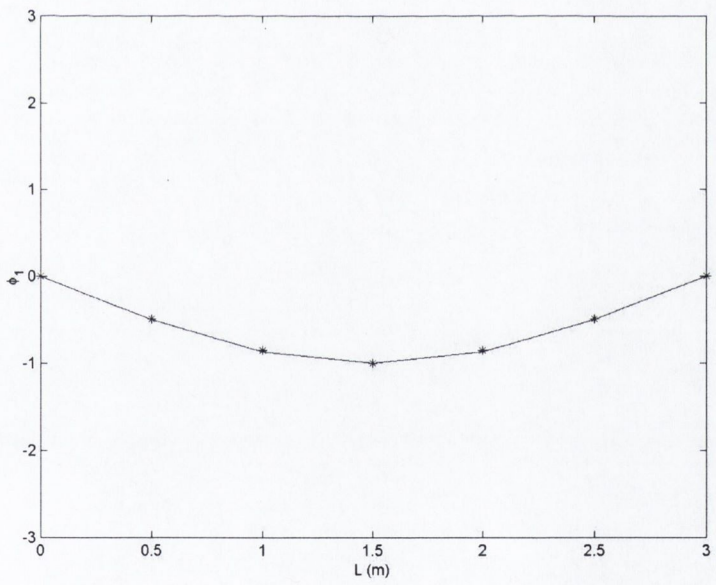


(b)

Figure 3.37: Estimated 1st mode shape of the RC beam; (a) Test 1, (b) Test 2, '__' actual, '*' estimated

## 3.6 Conclusions

The present chapter has focused on wavelet-based identification of fundamental modal frequency and the associated mode shape of a linear simply supported bridge subjected to a moving vehicular load. For this purpose, a modified form of L-P basis function is used to locate the frequency band that contains the fundamental modal frequency. The numerical results presented in this paper shows that the proposed methodology can be used to estimate the modal frequency and the mode shape of structures with desired level of accuracy, especially when the input is unknown and the data is contaminated with measurement noise. This technique can be used to estimate the natural frequencies and mode shapes of MDOF structures subjected to non-stationary input like earthquake. The modified form of L-P basis function used in the present study has the advantage that it could be used to further sub-divide the band that has maximum energy content to achieve desired level of accuracy in the estimation of modal parameters.

# Chapter 4: Wavelet Based Identification of Non-linear Normal Modes

## 4.1 Introduction

In Chapters 2 and 3, a wavelet-based methodology is proposed to identify the natural frequencies and mode shapes of linear structures. The proposed wavelet based system identification tool is used in the present chapter to estimate the localized normal modes of a non-linear system. Although orthogonal decomposition based on eigen analysis of the system properties are not possible in non-linear system, a synchronous periodic particular solution of the governing non-linear equations are possible. Moreover this synchronous periodic solution exists in the neighborhood of stable equilibrium points of Hamiltonian systems. Using this property of the non-linear dynamical systems, the study in the present chapter proposes to estimate the parameters of the non-linear systems associated with these 'vibrations in unison'. For this purpose, a two-degrees of freedom system with non-linear springs is considered. A wavelet-based time-frequency analysis is adopted here. A modified form of the real part of the Harmonic wavelet basis function (i.e. modified LP basis) is used.

## 4.2 Response of a Non-linear System using Invariant Manifolds

Many techniques exist in the literature for determining the response of nonlinear systems. In addition to brute-force simulations, there are a variety of approximate analytical methods, such as the method of multiple scales, harmonic balance, and averaging. When the system is responding in a periodic manner, it is behaving like a low order system, and

the question arises as to whether or not a reduced order model can be found that captures the system response. In fact, the analytical techniques just mentioned do precisely this, by imposing various types of approximations. For free vibration problems one uses system modes to construct reduced order models, and these techniques have been well developed for both linear and nonlinear systems. One such technique, defines the normal mode of a nonlinear oscillatory system in terms of invariant manifolds in the phase space that are tangent to the linear (eigen) modes at the equilibrium point. In such a formulation, a master mode is selected (the mode of interest), and the normal mode is constructed by a formulation in which the remaining linear modes of the system, i.e., the slave modes, depend on the master mode in a manner consistent with the system dynamics. This dependence defines the invariant manifold for the nonlinear normal mode (NNM). The construction of the NNM invariant manifold is equivalent to the determination of the constraint relationships for all of the slave coordinates

While it is possible to obtain the non-linear normal modes for a non-linear system if the system parameters are known, the inverse problem of identifying the modal parameters for the system from the response is still a challenge.

## 4.3 Wavelet Based Identification of NNM

In this section, a wavelet-based methodology has been proposed to solve the inverse system identification problem by estimating the localized normal modes of a class of non-linear system from the simulated time history records of the ambient vibration

response. Figure 4.1 shows a 2 DOF dynamical system connected to each other by non-linear spring of power '*m*' with the stiffness coefficient '*K*'. The springs at the fixed ends are combinations of linear springs of coefficients *1* and non-linear springs (of power *m*) with coefficients *1*. The governing equation of motion of this non-linear system are given by

$$\ddot{x}_1 + x_1 + x_1^m + K(x_1 - x_2)^m = 0 \tag{4.1a}$$

$$\ddot{x}_2 + x_2 + x_2^m - K(x_1 - x_2)^m = 0 \tag{4.2a}$$

In this study, the system is assumed to be excited by initial conditions only. The non-linear system is known to possess synchronous motions similar to linear system in the vicinity of the stable equilibrium points, if any synchronous motions of the masses in the system exist. The linear relation among the dependent variables corresponding to similar normal modes is given by

$$x_2(t) = cx_1(t) \tag{4.2}$$

where $c$ is a constant. The constant $c$ for a linear system (called the mode shape) represents modal ratio. Besides the values of $c$ corresponding to linear normal mode, possible additional modes are known to exist for the non-linear system corresponding to other values of $c$ for which the above synchronous relation is still valid. Although these values of $c$ do not help to decouple the governing equations of motion, the response attains maxima and minima simultaneously. This synchronous periodic nature of the non-

linear system is analogous to normal mode of linear system and is commonly called 'vibrations in unison'. The response of the system can be represented in terms of these non-linear normal modes.

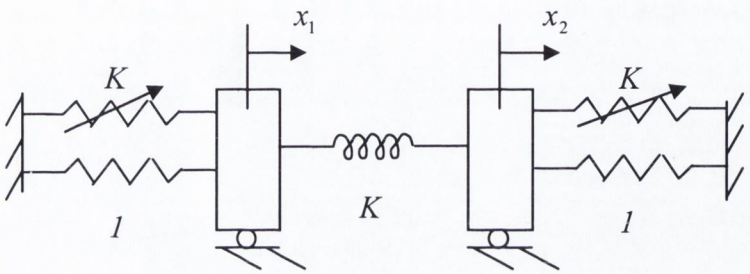


Figure 4.1: 2-DOF non-linear system

On taking wavelet transform of both sides of equation 4.1a and 4.1b as proposed by Basu and Gupta [2000], the governing equations of motion in $j^{th}$ frequency scale or band in wavelet domain can be expressed as

$$\frac{\partial^2}{\partial b^2} W_\psi x_1(a_j,b) + W_\psi x_1(a_j,b) + W_\psi \{x_1^m\}(a_j,b) + KW_\psi \{(x_1 - x_2)^m\}(a_j,b) = 0 \quad (4,3a)$$

$$\frac{\partial^2}{\partial b^2} W_\psi x_2(a_j,b) + W_\psi x_2(a_j,b) + W_\psi \{x_2^m\}(a_j,b) - KW_\psi \{(x_1 - x_2)^m\}(a_j,b) = 0 \quad (4.3b)$$

The synchronous periodic particular solution of the non-linear system in the neighborhood of equilibrium points as given by equation 4.2 can also be represented in wavelet domain as

$$W_\psi x_2(a_j,b) = cW_\psi x_1(a_j,b) \tag{4.4}$$

Using equation 4.4 into equation 4.3, the governing equation in the $j^{th}$ frequency band is given by

$$\frac{\partial^2}{\partial b^2} W_\psi x_1(a_j,b) + W_\psi x_1(a_j,b) + \left[1 + K(1-c)^m\right] W_\psi \{x_1^m\}(a_j,b) = 0 \tag{4.5a}$$

$$\frac{\partial^2}{\partial b^2} W_\psi x_1(a_j,b) + W_\psi x_1(a_j,b) - (1/c)\left[K(1-c)^m + c^m\right] W_\psi \{x_1^m\}(a_j,b) = 0 \tag{4.5b}$$

Besides similar linear normal modes, the proposed non-linear system is known to have additional normal modes, which can be evaluated by solving the non-linear relation obtained from coefficient of the similar terms and is given by [for details see Vakakis *et al* (1996)]

$$K(1+c)(c-1)^m = c\left(1-c^{m-1}\right) \qquad c \neq 0 \tag{4.6}$$

From the above equation, it can be concluded that the above relation is in parity with that obtained from research work done by Lyapunov and $c = \pm 1$ corresponds to linear normal

modes. Moreover, according to Lyapunov's theorem, the synchronous periodic solution of the non-linear equation is possible in the vicinity of the stable equilibrium points, which correspond to the normal modes of the respective linear system i.e. $c = \pm 1$. Since the solution to the governing equation of motion as given by equation 4.1 exists near the equilibrium points, the energy must be concentrated in the frequency band that contains the natural frequency of the corresponding linear system. The normalized energy $E_j(x_r)$ for the response $x_r(t)$, in the frequency band corresponding to a scaling factor $a_j$ with the index *'j'*, can be represented by a proportional quantity as

$$E_j(x_r) \propto \frac{1}{a_j^2} \int W_\psi^2 x_r(a_j, b) db \tag{4.7}$$

Let the frequency band $j_k$ contains the fundamental frequency of the respective linear system, which is obtained by removing the non-linear terms in the governing equations of motion. Then it can be concluded that according to Lyapunov's theorem

$$\begin{aligned} E_j(x_r) &\neq 0 \qquad \text{if } j = j_k,\ k = 1,2,\ldots,n \\ &\approx 0 \qquad \text{otherwise} \end{aligned} \tag{4.8}$$

Thus to detect the localized normal mode of the linear system, the response energy is evaluated in different frequency bands. The band that contains maximum energy corresponds to fundamental frequency of the corresponding linear system. Thus if a normal mode exists, this ratio of the wavelet coefficients in the band that possesses

maximum energy will be constant. This constant is evaluated as the parameter corresponding to the localized normal mode of the non-linear system, which from equation 4.4 is given by

$$c = \frac{W_\psi x_2(a_j, b)}{W_\psi x_1(a_j, b)} \tag{4.9}$$

For numerical ease and to avoid the cases with zero values of wavelet coefficients, the parameters of the non-linear normal mode is evaluated as the mean of the ratio of the wavelet coefficients at the peaks corresponding to $W_\psi x_1(a_j, b)$ and $W_\psi x_2(a_j, b)$ (as they are in phase).

## 4.4 Numerical Results and Discussions

In the numerical example, the 2-DOF model discussed in section 4.3 is used to simulate the displacement responses of the non-linear system and to show the application of the proposed methodology for the identification of non-linear normal mode. At first, the time history simulations using Wilson-$\theta$ are carried out for the 2-DOF system for two different springs with $m = 3$ and $m = 5$ respectively with non-zero initial condition for the velocities corresponding to the two degrees of freedom such that the mode is excited. Using these simulated ambient vibration records; the inverse problem is solved in each case as proposed, to evaluate the localized normal modes of the non-linear system.

For the wavelet-based identification, a modified form of the L-P basis function is used to decompose the signals into different frequency levels with $\sigma = 2^{1/4}$ to broadly identify the bands that contain the maximum energy. Figure 4.3 shows the energy content of the displacement response for different degrees of freedom in different frequency band for the case with $m = 3$. The wavelet coefficients are evaluated based on the mother wavelet whose initial cut-off frequency is given by $F_1 = 1.15 rad/s$ as described in equation 1.7. It can be noticed that the energy is maximum corresponding to band 2 while the other band contains insignificant amount of energy. The frequency limit corresponding to band 2 is 1.15-1.73rad/s, which contains the fundamental natural frequency of the linear system (1.44rad/s) obtained by removing non-linear element. Figure 4.4 shows the wavelet coefficients in different degrees of freedom, which are in phase as expected. The ratio of the wavelet coefficients in band 2 as discussed in the previous section is evaluated as the corresponding value of the normal mode of the non-linear system. For this purpose, the ratio is taken at the peak values of the wavelet coefficients to avoid numerical instability near zero crossing. Figure 4.5 shows the ratio of wavelet coefficients, which is constant over time. The mean value of the ratio of the wavelet coefficient is evaluated as the value corresponding to the localized normal mode of the non-linear system. It is estimated as -1.47, which is very close to the original value of -1.5.

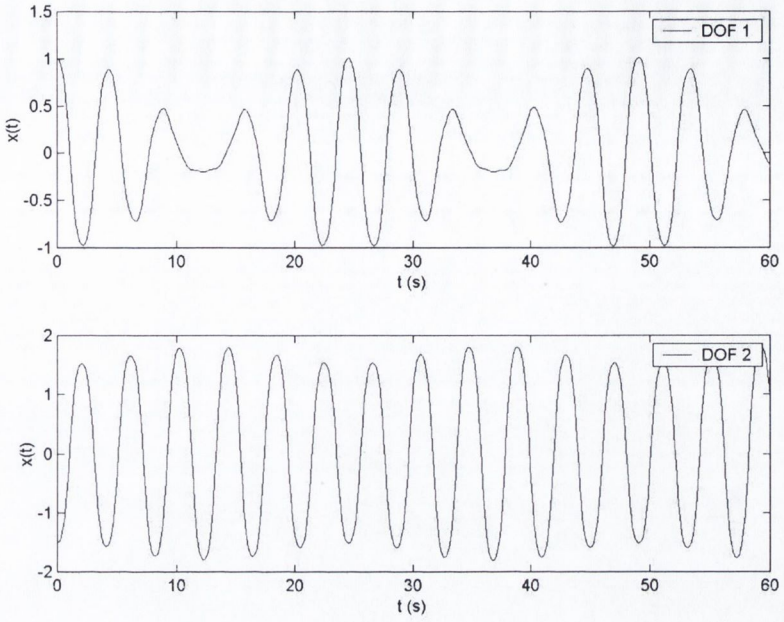


Figure 4.2: Displacement time history of the 2-DOF non-linear system for $m = 3$

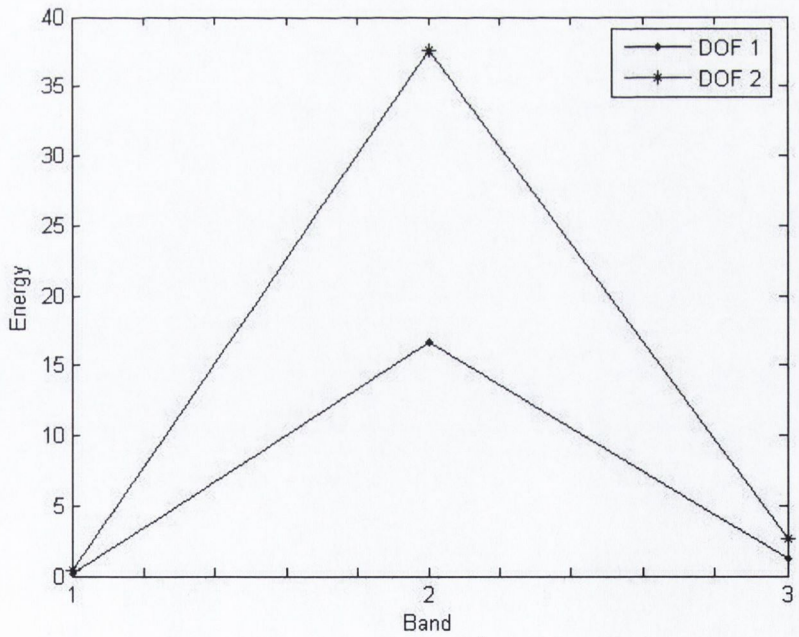


Figure 4.3: Energy of the displacement response in different frequency bands for $m = 3$

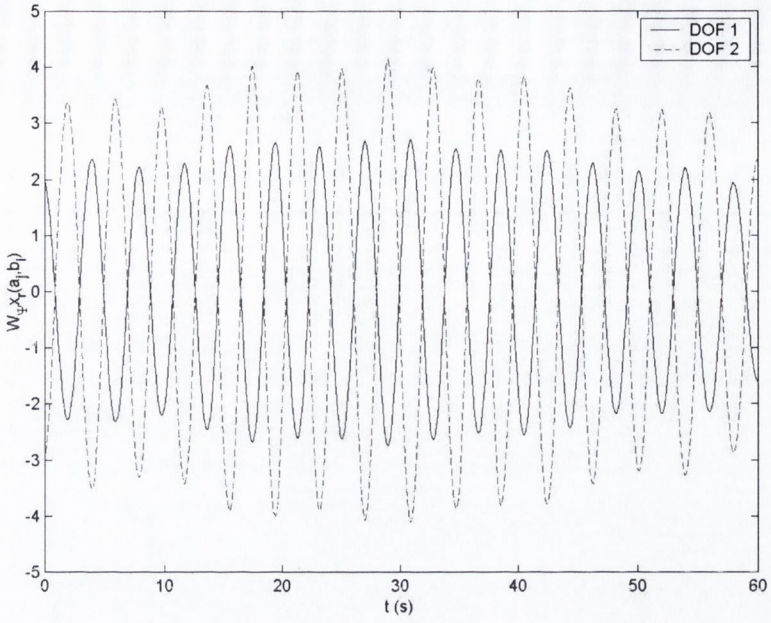


Figure 4.4: Wavelet coefficients of the response in 2nd frequency band for $m = 3$

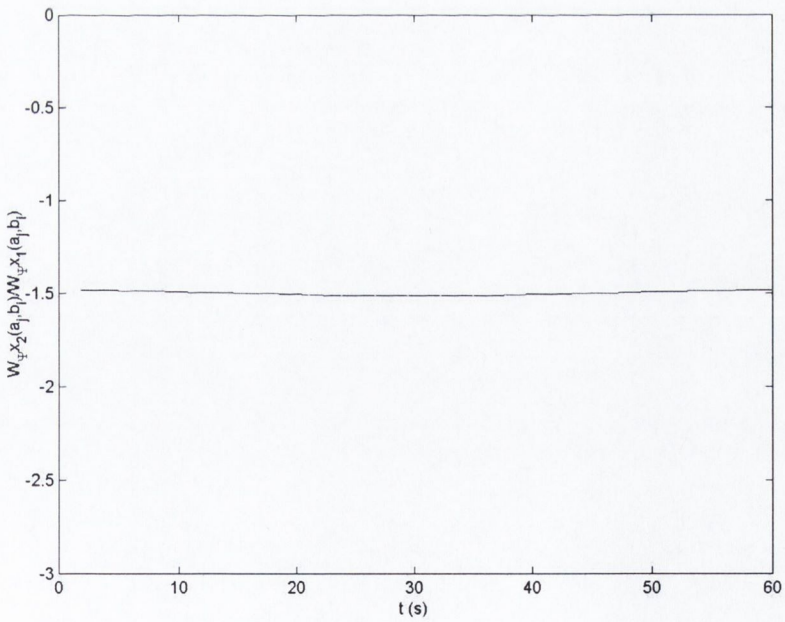


Figure 4.5: Ratio of the wavelet coefficients in the 2nd frequency band for $m = 3$

To investigate the accuracy of the proposed model further, the 2-DOF system is considered with $m = 5$. Figure 4.6 shows the simulated displacement response time histories. Using these response time histories, energies are again evaluated in different frequency bands as has been done for $m = 3$. Figures 4.7 and 4.8 show the energy content for the displacement response and the wavelet coefficients in the band that contains maximum energy respectively. The wavelet coefficients in different degrees of freedom are noticed to be in unison. Figure 4.9 shows the ratio of the wavelet coefficients at different time instants (corresponding to the peaks of the wavelet coefficients), which can be considered constant over time. The little variations may be due to the numerical error and edge effects in wavelet analysis. The localized normal mode is estimated as –1.48 against the original value –1.5.

Figures 4.10 and 4.11 show the estimated non-linear normal mode for $m = 3$ and $m = 5$ for different values of '$K$' respectively. It can be noticed that the proposed wavelet-based methodology can effectively and accurately estimate the localized normal mode of a non-linear system. In this context, the proposed wavelet-based algorithm has limitations that the corresponding localized normal mode of the non-linear system must be excited in the response time history. It is imperative that the estimation of system parameters of a linear system is often executed by exciting the system by either an impulse or a broad banded input to excite the fundamental frequencies and should not pose any major limitation to the proposed method and its accuracy. From figures 4.10 and 4.11, it can be noticed that at $c = -1$, the nonlinear system bifurcates at $K = 0.25$ and $K = 0.125$ for $m = 3$ and $m = 5$ respectively. It may be noted that the proposed wavelet-based method can estimate the localized multiple modes, when the system bifurcates.

Table 4.1a and 4.1b show the values of 'K' estimated from the identified values of localized mode (i.e. c) in equation 4.6. It requires a prior knowledge of the type of system non-linearity (i.e. m), but the estimated values of 'K' matches closely with the actual values, which proves the efficiency of the proposed wavelet-based algorithm for parameter estimation. Further, the system response can be simulated by using the estimated value of '*c*' of the NNMs.

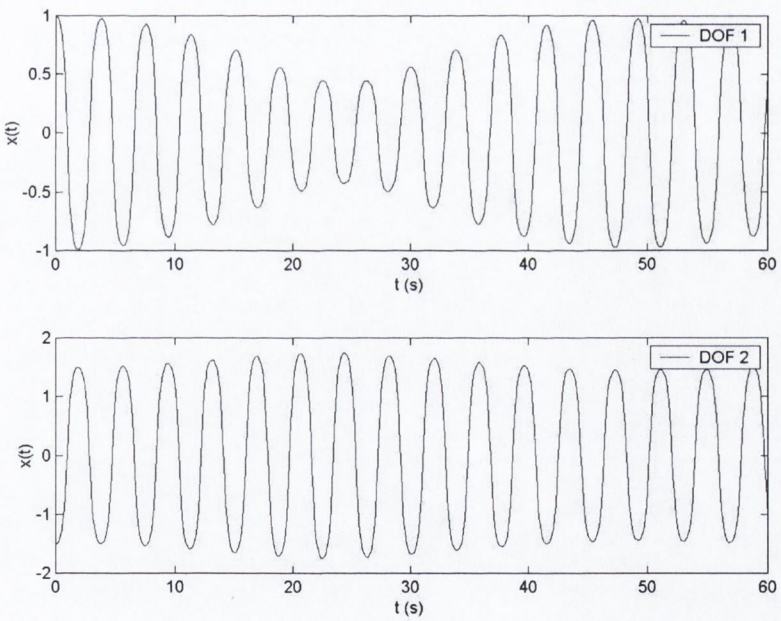


Figure 4.6: Displacement time history of the 2-DOF non-linear system for $m = 5$

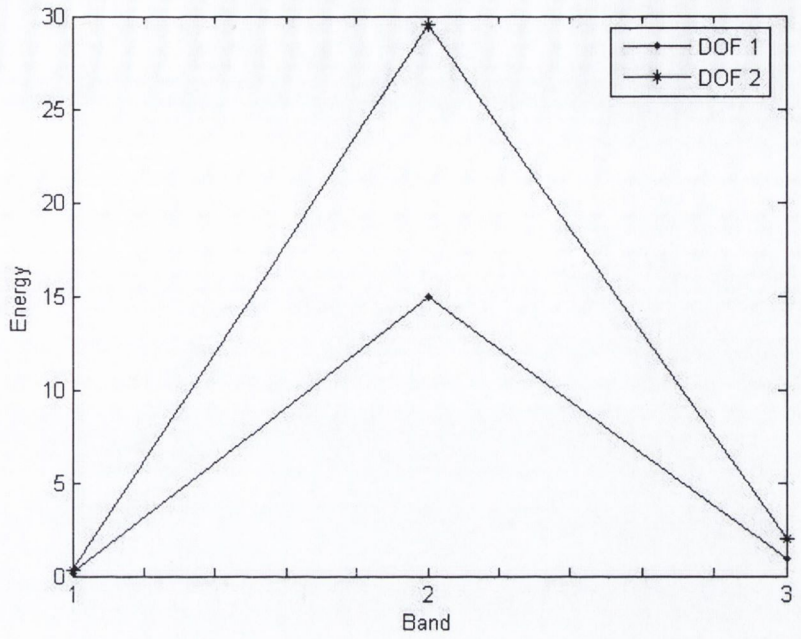


Figure 4.7: Energy of the displacement response in different frequency bands for $m = 5$

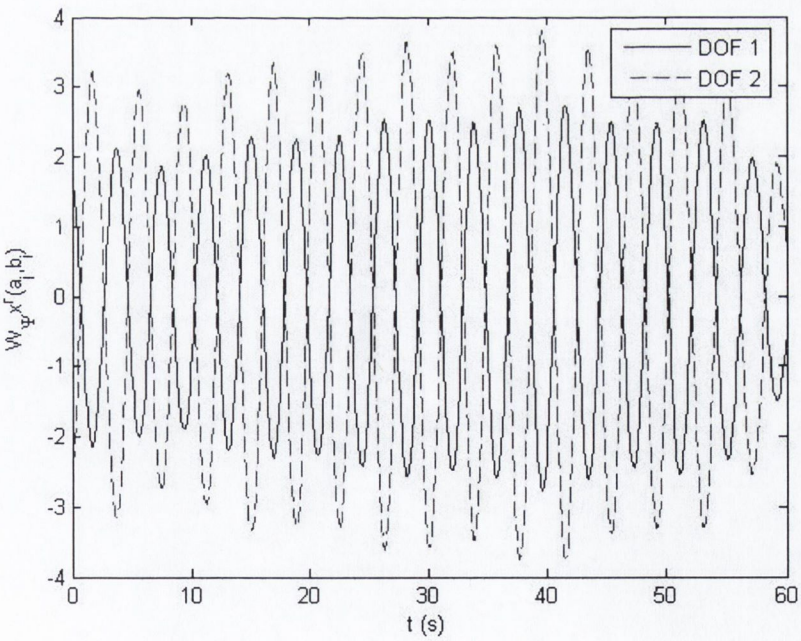


Figure 4.8: Wavelet coefficients of the response in 2nd frequency band for $m = 5$

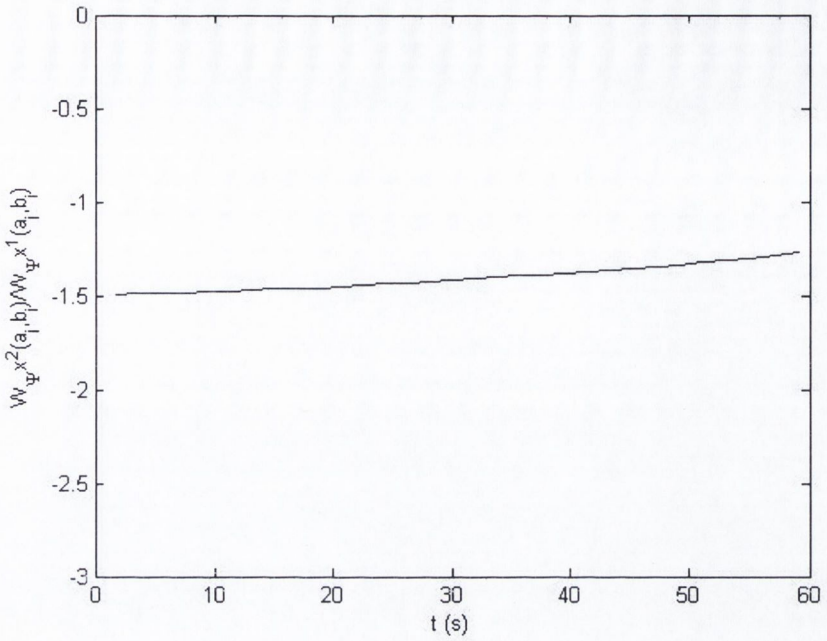


Figure 4.9: Ratio of the wavelet coefficients in the 2nd frequency band for $m = 5$

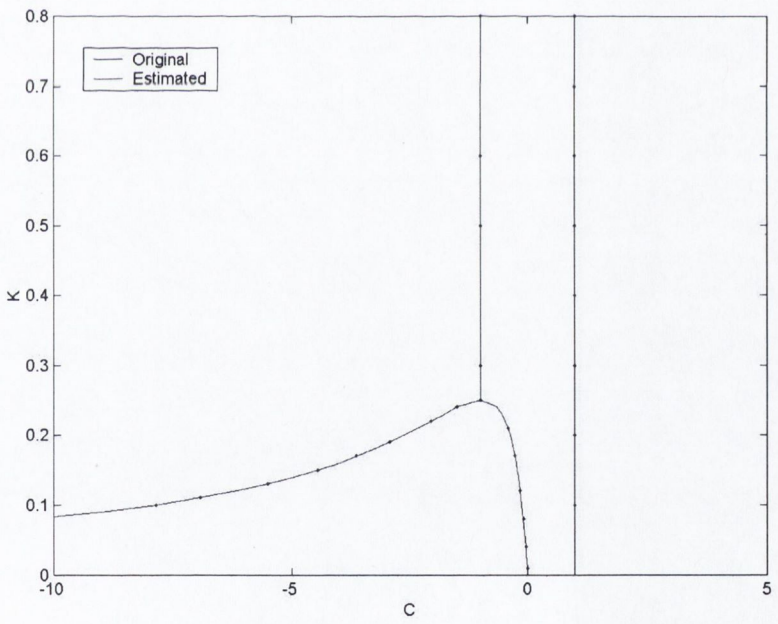


Figure 4.10: Estimated non-linear normal mode for $m = 3$ with different values of $K$ and $c$; '__' theoretical values and '.' Estimated values using wavelet analysis

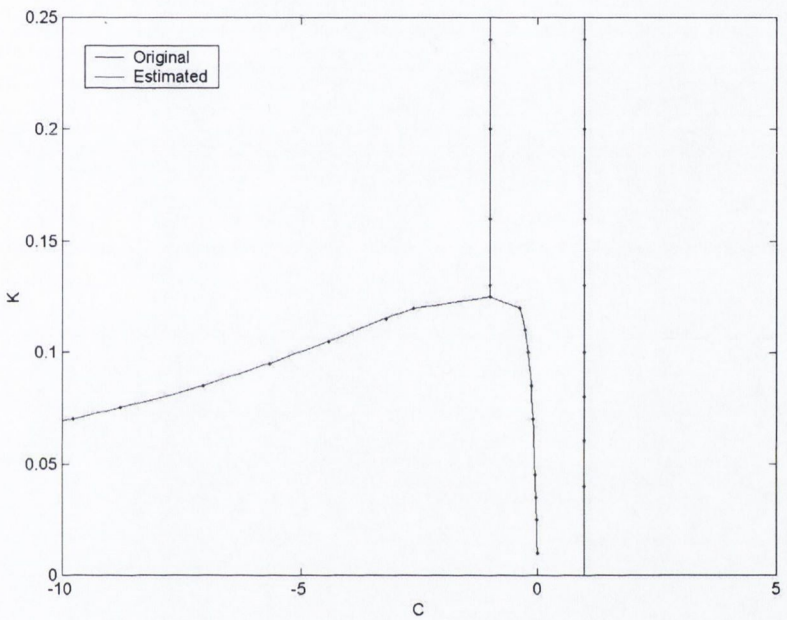


Figure 4.11: Estimated non-linear normal mode for $m = 5$ with different values of $K$ and $c$; '__' theoretical values and '.' Estimated values using wavelet analysis

| c | K(actual) | K(estimated) |
|---|---|---|
| -1.5 | 0.2400 | 0.2400 |
| -2.06 | 0.2200 | 0.2200 |
| -2.92 | 0.1900 | 0.1900 |
| -3.63 | 0.1700 | 0.1693 |
| -4.44 | 0.1500 | 0.1500 |
| -5.51 | 0.1300 | 0.1299 |
| -6.93 | 0.1100 | 0.1102 |
| -7.87 | 0.1000 | 0.1000 |
| -1.04 | 0.0800 | 0.0801 |
| -1.01 | 0.0100 | 0.0099 |
| -4.24 | 0.0400 | 0.0390 |
| -9.38 | 0.0800 | 0.0784 |
| -1.61 | 0.1200 | 0.1194 |
| -2.79 | 0.1700 | 0.1706 |
| -4.28 | 0.2100 | 0.2102 |

(a)

| c | K(actual) | K(estimated) |
|---|---|---|
| -9.7808 | 0.0700 | 0.0699 |
| -8.7881 | 0.0750 | 0.0749 |
| -7.0528 | 0.0850 | 0.0851 |
| -5.6609 | 0.0950 | 0.0950 |
| -4.4184 | 0.1050 | 0.1052 |
| -3.2082 | 0.1150 | 0.1155 |
| -2.6251 | 0.1200 | 0.1199 |
| -0.0103 | 0.0100 | 0.0098 |
| -0.0279 | 0.0250 | 0.0250 |
| -0.0410 | 0.0350 | 0.0349 |
| -0.0554 | 0.0450 | 0.0448 |
| -0.5671 | 0.0550 | 0.1243 |
| -0.1023 | 0.0700 | 0.0700 |
| -0.1415 | 0.0850 | 0.0850 |
| -0.1985 | 0.1000 | 0.0999 |
| -0.2590 | 0.1100 | 0.1100 |
| -0.3820 | 0.1200 | 0.1200 |
| -0.9998 | 0.1250 | 0.1250 |

(b)

Table 4.1: Estimated values of stiffness coefficients; (a) $m = 3$, (b) $m = 5$

## 4.4 Conclusions

In the present chapter a wavelet-based methodology is presented for the evaluation of normal modes of a non-linear system from the simulated samples of the response time histories. The success of the proposed methodology is due to the use of the LP wavelet basis in estimation of the response energy in non-overlapping frequency bands. The modified form of the L-P basis function possesses compact support in frequency domain and hence does not suffer problems of band overlapping in energy estimation. The numerical works show that the proposed method can effectively estimate the localized normal mode of a non-linear system accurately. The adopted basis function can evaluate the energy in non-overlapping frequency bands and hence can be used to evaluate the system parameters with desired level of accuracy when used in conjunction with the sub-band coding leading to wavelet packets. Once the localized modes are identified, the response of the non-linear system can be represented in terms of these NNM. Moreover, evaluation of stiffness parameter 'K' helps to evaluate the overall performance of the non-linear system and may be used to identify any change in the performance of the non-linear dynamical system from the point of view of structural health monitoring.

# Chapter 5: Characterization of Earthquake Ground Motions

## 5.1 Introduction

In the previous chapters, parameters of the dynamical systems have been identified using wavelet-based time-frequency analysis of the measured time history response. Once the system parameters are identified, these can be used to evaluate the response of the dynamical system when subjected to stochastic input. The problem of response calculation becomes more complex when the input contains time varying amplitude and frequency. Thus, a proper modelling of the input especially in the light of non-stationary frequency content is the preamble to the response analysis of the dynamical systems.

In the present chapter, a frequency dependent amplitude modulating function is proposed for the characterization of seismic ground motions. Using this proposed characterization, a generalized evolutionary model for earthquake ground motions is developed in the present study, which can take into account time varying stochastic nature of the ground motion in both intensity and frequency content. The earthquake ground motion process is modeled as a summation of amplitude modulated stochastic orthogonal processes in different frequency bands. A non-linear least square technique is adopted to minimize the error between the temporal energy growth of the recorded time history and that obtained from the proposed model in each frequency bands. For the purpose of minimizing the error in temporal energy, wavelet based time-frequency analysis is used to evaluate the time varying energy content in different frequency bands. A statistical simulation is then performed to validate the proposed model and to confirm its suitability for random vibration analysis of structures using the frequency dependent amplitude modulation function. Following the proposed model for single component

earthquake ground motion, a generalized wavelet based model for spatially varying earthquake is proposed. Structures whose spatial extent are large and are supported at multiple points are often subjected to these types of ground motions. The proposed wavelet based evolutionary stochastic differential support motions model can be used for spectral analysis of extended structures. The wavelet-based model is general in the sense that this can be used to characterize other spatially correlated non-stationary excitation such as winds and wave motions.

## 5.2 Frequency Dependent Temporal Energy Growth

Wavelet analysis is used in this section to represent the frequency dependent temporal energy growth of a non-stationary time signal. Wavelet transform is an integral transform that transforms a time signal into a two dimensional function, which enables to extract the local frequency variation. Let the ground acceleration signal $z(t)$ be a square integrable time function in Hilbert Space [i.e. $z(t) \in L^2(\boldsymbol{R})$], then wavelet transform of $z(t)$ is given by [Chan (1995), Rao (1998)]

$$W_\psi z(a,b) = \int_{-\infty}^{+\infty} z(t)\psi_{a,b}(t)dt \tag{5.1}$$

where, $W_\psi z(a,b)$ is the wavelet coefficients of the time function $z(t)$ and $\psi(t)$ is called the basis function or the mother wavelet. In equation 5.1, $\psi_{a,b}(t)$ is a family of scaled and dilated versions of the original mother wavelet (called the baby wavelets) that convolutes with $z(t)$ to provide the two dimensional sequence $W_\psi z(a,b)$.

In the present study, parameter '*a*' is discretized in a logarithmic scale [i.e. $a_j = \sigma^j$], which divides the frequency scale of the time function $z(t)$ into non-overlapping frequency bands and the time parameter 'b' is discretized uniformly [i.e. $b_i = (i-1)\Delta b$]. Using this discretization scheme, it can be shown that the instantaneous mean square energy of $z(t)$ is given by

$$E[\langle z,z\rangle] = E\left[\int z^2(t)dt\right] = K\sum_i\sum_j \frac{\Delta b}{a_j} E\left[W_\psi z^2(a_j,b_i)\right] \tag{5.2}$$

Thus the growth in temporal energy of $z(t)$ in the frequency band '*j*' is given by

$$E_j\left[\int z^2(t)dt\right]_{t=0}^{b_r} = K\sum_{i=0}^{r} \frac{E\left[W_\psi z^2(a_j,b_i)\right]}{a_j} \tag{5.3}$$

where, $K$ is a constant, which is given by $K = \frac{1}{4\pi C_\psi}\left(\sigma - \frac{1}{\sigma}\right)$.

## 5.3 Model for Earthquake Ground Motion: Non-stationary Process

Using the expression for growth in temporal energy in different frequency bands, present study proposes wavelet-based model for characterization of earthquake ground motion. The model is further extended to characterize spatially varying earthquake ground motions.

### 5.3.1 Single Component Model with Frequency Dependent Envelope Functions

Let $z(t)$ be an evolutionary random process, then $z(t)$ can be expressed as [Lin and Cai (1995)]

$$z(t) = \int_{-\infty}^{+\infty} A(t,\omega) e^{i\omega t} dG(\omega) \tag{5.4}$$

where, $A(t,\omega)$ is a deterministic envelope function in both time and frequency and $dG(\omega)$ is orthogonal increment process such that

$$E[dG(\omega)dG(\omega')] = S_{gg}(\omega)d\omega \qquad \omega = \omega' \tag{5.5}$$

$$= 0 \qquad \textit{otherwise}$$

In equation 5.4, $A(t,\omega)$ represents the local frequency variations and $dG(\omega)$ represents the stochastic nature of the time function $z(t)$. In the above equation, $S_{gg}(\omega)$ can be modeled as Kanai-Tajimi (1957, 1960) spectra, which is given by

$$S_{gg}(\omega)=\frac{1+4\eta_g^2(\omega/\omega_g)^2}{\left[1-(\omega/\omega_g)^2\right]^2+4\eta_g^2(\omega/\omega_g)^2} \tag{5.6}$$

where, $\omega_g$ and $\eta_g$ represent the natural frequency and damping of the soil layer at the site. In practice, evaluation of deterministic envelope function $A(t,\omega)$ often leads to complexity. For this purpose, a wavelet based time-frequency analysis is used in the present study to model the time varying stochastic nature of the function $z(t)$.

The objective of the present study is to develop a mathematical model of earthquake ground motions for the purpose of random vibration analysis, which is compatible with the recorded time history in stochastic sense. For this purpose, the evolutionary random process model that is given by equation 5.4 forms the basis of the present study. To characterize the local frequency contribution, a wavelet based time-frequency analysis is adopted here. Taking wavelet transform on both side of equation 5.4, it can be shown that the evolutionary random process can be expressed as [Spanos and Failla (2004)]

$$W_\psi z(a_j,b)=\int_{-\infty}^{+\infty}A(b,\omega)e^{i\omega b}dG_1(\omega) \tag{5.7}$$

where,

$$E[dG_1(\omega)dG_1(\omega')] = 2\pi a_j \left|\hat{\psi}(a_j\omega)\right|^2 S_{gg}(\omega) \quad \omega = \omega' \qquad (5.8)$$

$$= 0 \qquad \textit{otherwise}$$

It can be noticed that the left hand side of the equation 5.7 is also a random process that has the same property of $z(t)$. The wavelet coefficients in equation 5.7 give information about the local frequency content of the function $z(t)$ at a scale '$j$'. Therefore the deterministic envelope function $A(b,\omega)$ in equation 5.7 provides temporal variations of frequency signature at scale '$j$'. In the present study, it is assumed that within the $j^{th}$ frequency band, the envelope function has a constant frequency signature i.e. it is function of time only. Hence the wavelet coefficients in equation 5.7 at scale '$j$' can be modified as

$$W_\psi z(a_j,b) = A_j(b)\int_{-\infty}^{+\infty} e^{i\omega b}\, dG_1(\omega) \qquad (5.9)$$

The deterministic envelope function $A_j(b)$ represents the frequency signature of $z(t)$ at a scale '$j$'. Among the popular models of $A_j(b)$, the model proposed by Shinuzoka and Sato (1967) is widely used, which is given by

$$A_j(b) = \alpha_j \left[ e^{-\beta_j b} - e^{-\gamma_j b} \right] \tag{5.10}$$

where, $\alpha_j$, $\beta_j$ and $\gamma_j$ are the parameters of the envelope function for amplitude modulation in $r^{th}$ support and in $j^{th}$ frequency band. On multiplying both sides of equation 5.7 with its complex conjugate and taking expectation and integrating over '$b$', it can be shown that

$$K \int_{-\infty}^{+\infty} \frac{E\left[W_\psi z(a_j,b) W_\psi^* z(a_j,b)\right]}{a_j} db = K \int_{-\infty}^{+\infty} \frac{A_j(b) A_j^*(b) E\left[\int_{-\infty}^{+\infty} dG_1(\omega) dG_1(\omega)\right]}{a_j} db \tag{5.12}$$

Using the above equation and equation 5.3, it can be shown that the temporal energy growth of $z(t)$ at a scale '$j$' is given by

$$E_j\left[\int z^2(t)dt\right]_{t=0}^{b_r} = K \int_0^{b_r} \frac{2\pi a_j A_j^2(b) \int_{-\infty}^{+\infty} \left|\psi(a_j\omega)\right|^2 S_{gg}(\omega) d\omega}{a_j} db \tag{5.12}$$

On integrating both side of the above equation, the growth in temporal energy up to $t=b$ at a scale $a_j$ is given by

$$E_j\left[\int z^2(t)dt\right]_{t=0}^{b_r} = 2\pi K \sigma_{gg}^{j^2} \int_o^{b_r} A_j^2(b) db \tag{5.13}$$

where, $\sigma_{gg}^2$ is the variance at a scale $j$ and is given by

$$\sigma_{gg}^2 = \int_{-\infty}^{+\infty} \left|\psi(a_j\omega)\right|^2 S_{gg}(\omega)d\omega \tag{5.14}$$

Simplifying the right hand side of the equation 5.14, it can be shown that

$$E_j\left[\int z^2(t)dt\right]_{t=0}^{b_r} = 2\pi K\sigma_{gg}^{j^2}\alpha_j^2\left[\frac{1-e^{-2\beta_j t}}{2\beta_j} - 2\frac{1-e^{-(\beta_j+\gamma_j)t}}{\beta_j\gamma_j} + \frac{1-e^{-2\gamma_j t}}{2\gamma_j}\right] \tag{5.15}$$

Present study focuses on estimating the parameters on the right hand side of the above equation using non-linear least square technique. The error function representing the difference between the estimated energy growth and that proposed by the wavelet-based model is given by

$$\varepsilon_j = E\left[z^2(t)\right]_j - 2\pi K\sigma_{gg}^{j^2}\alpha_j^2\left[\frac{1-e^{-2\beta_j t}}{2\beta_j} - 2\frac{1-e^{-(\beta_j+\gamma_j)t}}{\beta_j\gamma_j} + \frac{1-e^{-2\gamma_j t}}{2\gamma_j}\right] \tag{5.16}$$

$$= E_j\left[z^2(t)\right] - C_j z(\beta_j,\gamma_j)$$

In the above equation $C_j$ defines the energy level of $z(t)$ at a scale '$j$'.

### 5.3.2 Spatially Varying Ground Motion Model in Wavelet Domain

Consider a simply supported multi-span bridge with $n$ supports, whose supports are subjected to non-stationary ground motions $\ddot{x}_{g_r}(t); r = 1,...,n$. The evolutionary random process representing the $r^{th}$ support motion is $\ddot{x}_{g_r}(t)$ and can be expressed as

$$\ddot{x}_{g_r}(t) = \int_{-\infty}^{+\infty} A^r(t,\omega) e^{i\omega t} dG_r(\omega) \tag{5.17}$$

In equation 5.17, $A^r(t,\omega)$ is a deterministic envelope function in both time '$t$' and frequency '$\omega$' represents the temporal frequency variations and $dG_r(\omega)$ is the orthogonal increment process associated with the $r^{th}$ support such that

$$E[dG_r(\omega) dG_r(\omega')] = S_{rr}(\omega) d\omega \qquad \omega = \omega' \tag{5.18}$$
$$= 0 \qquad \textit{otherwise}$$

In equation 5.18, $S_{rr}(\omega)$ represents the two sided power spectral density function of the stationary part of the random process and can be modeled as Kanai-Tajimi [Kanai (1957), Tajimi (1960)] spectra, which is given by equation 5.6. To characterize the local frequency contribution, a wavelet based time-frequency analysis as described in previous section is adopted here. On wavelet transforming of both sides of equation 5.17, it can be shown that the evolutionary random process can be expressed as

$$W_\psi \ddot{x}_{g_r}(a,b) = \int_{-\infty}^{+\infty} A_r(b,\omega) e^{i\omega b} d\tilde{G}_r(\omega) \tag{5.19}$$

where,

$$E\left[d\tilde{G}_r(\omega) d\tilde{G}_r(\omega')\right] = 2\pi a_j \left|\hat{\psi}(a_j\omega)\right|^2 S_{rr}(\omega) \quad \omega = \omega' \tag{5.20}$$

$$= 0 \qquad \textit{otherwise}$$

Equation 5.19 reveals that $W_\psi \ddot{x}_{g_r}(a,b)$ is also a random process, which has the similar random characteristic as of $\ddot{x}_{g_r}(t)$. The wavelet coefficients in equation 5.19 give information about the local frequency content of the function $\ddot{x}_{g_r}(t)$ at a scale '$a_j$'. Following this, it can be concluded that the deterministic envelope function $A^r(b,\omega)$ in equation 5.19 provides the envelope of the frequency signature at scale '$a_j$' and is constant for a particular scale. Hence the wavelet coefficients in equation 5.19 at scale '$a_j$' can be modified as

$$W_\psi \ddot{x}_{g_r}(a_j,b) = A_j^r(b) \int_{-\infty}^{+\infty} e^{i\omega b} dG_r(\omega) \tag{5.21}$$

In the above equation, the envelope function $A_j^r(b)$ represents the amplitude modulation for $\ddot{x}_{g_r}(t)$ at a scale '$a_j$'. In the present study, the model proposed by Shinuzoka and Shato (1967) is adopted for the amplitude modulation, which is given by

$$A_j^r(b) = \alpha_j^r \left[ e^{-\beta_j^r t} - e^{-\gamma_j^r t} \right] \tag{5.22}$$

where, $\alpha_j^r$ $\beta_j^r$ and $\gamma_j^r$ are the parameters of the amplitude modulation for the ground motion in the $j^{th}$ band and in the $r^{th}$ support. Multiplying both sides of equation 5.19 by its complex conjugate and taking expectation, it can be shown that the cross correlation of the wavelet coefficients of seismic ground motions at two different supports '$r$' and '$l$' and at a scale '$a_j$' is given by

$$E\left[W_\psi \ddot{x}_{g_r}(a_j, b) W_\psi \ddot{x}_{g_l}(a_j, b)\right] = A_j^r(b) A_j^l(b-\tau) \int_{-\infty}^{+\infty} E\left[dG_r(\omega) dG_l(\omega)\right] \tag{5.23}$$

where,

$$E\left[d\tilde{G}_r(\omega) d\tilde{G}_l(\omega')\right] = 2\pi a_j \left|\hat{\psi}(a_j\omega)\right|^2 S_{rl}(\omega) \quad \omega = \omega' \tag{5.24}$$

$$= 0 \qquad \textit{otherwise}$$

In equation 5.23, $\tau$ represents the delay in arrival of the $j^{th}$ frequency at $l^{th}$ support i.e. $\tau = L / v_j$, where L is the distance between the supports '$r$' and '$l$' and $v_j$ is the wave

velocity corresponding to scale '$a_j$'. It can be noticed in equation 5.24 that $E\left[d\widetilde{G}_r(\omega)d\widetilde{G}_l(\omega)\right]$ represents the cross power spectrum of the orthogonal processes between the supports *'r'* and *'l'*, which represents the spatial correlation of the ground motion due to incoherence and wave passage effects. In the present study, the cross-spectral density function $S_{rl}(\omega)$ between the ground accelerations at two supports *'r'* and *'l'* is modeled as

$$S_{rl}(\omega) = \gamma_{rl}(\omega)\sqrt{S_{rr}(\omega)S_{ll}(\omega)} \tag{5.25}$$

where, $\gamma_{rl}(\omega)$ is the coherency function that relates the spatial variation of the ground motion from one support to another. In the present thesis, five different coherence functions are used. The details of the coherence functions are given in Appendix A

## 5.4 Model Validation and Discussions

In the present study, two different models for single component earthquake ground motion and spatially varying ground motions respectively are presented.

### 5.4.1 Case I: Single Component Model

The proposed wavelet based non-stationary model for characterization of earthquake ground motions is developed and validated using the E-W component of the 1940 Imperial Valley earthquake ground motions measured at the El-centro site. From the energy spectrum using Fast Fourier Transform (FFT), it is observed that the mean energy lies around 9.89rad/s. The orthogonal increment stochastic process required for the characterization is modeled as a Kanai-Tajimi spectrum with the parameters $\omega_g = 10$ rad/s and $\eta_g = 5\%$.

Figure 5.1 shows the 3D PSD function of the recorded acceleration time history. For this purpose, wavelet based time-frequency analysis is used as proposed by Basu and Gupta (1998). From this figure, it can be observed that most of the input energy lies in frequency range 0 to 20rad/s. Hence to cover this frequency range; the lower cut-off frequency of the mother wavelet is assumed as 1.5 Hz and $\sigma$ is taken to be $2^{1/4}$. In the present study, 28 frequency bands are used to cover a frequency range of 0.4953rad/s to 60.4021rad/s. The band numbers increase with the increasing frequencies.

The error between the growth in temporal energy of the recorded accelerogram and that obtained from the proposed wavelet based model is minimized in a statistical sense using the non-linear least square technique described in section 3.0. For this purpose, the unknown parameters in equation 5.16 are evaluated using 'nonlincurvefit' function in MATLAB platform. Table 5.1 shows the optimized values of $\alpha_j$, $\beta_j$ and $\gamma_j$ in different frequency bands. Figure 5.2 shows the optimized envelope function for different frequency scales. It can be noticed that different envelope functions attain maxima at different time instants, which indicates the difference in arrival of different

frequencies. This is consistent with the non-stationary nature of earthquake ground motion explicitly representing the frequency non-stationarity.

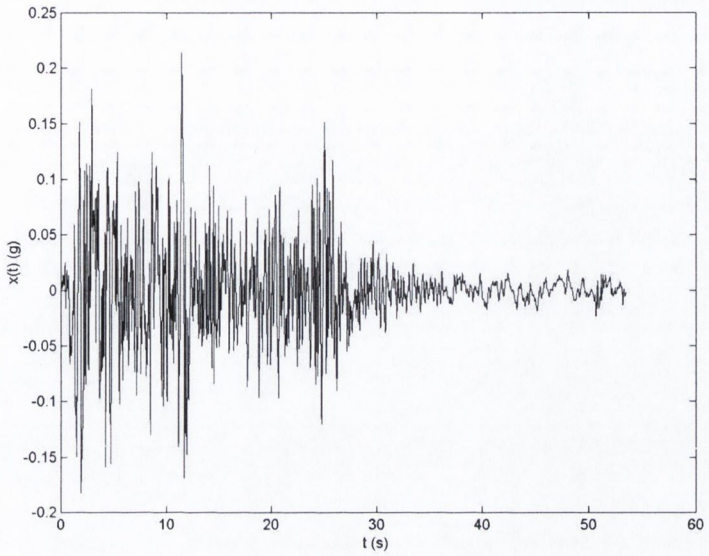


(a)

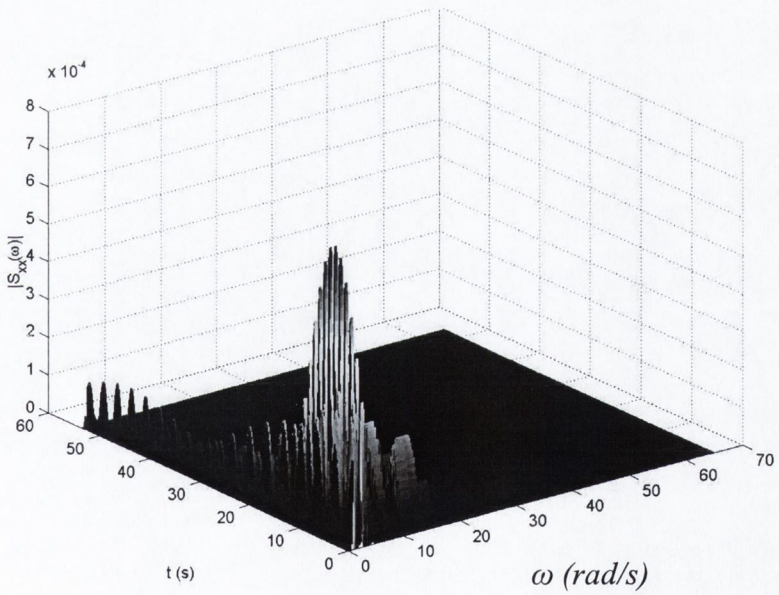


(b)

Figure 5.1: E-W component of El-centro ground motion; (a) time history and (b) PSD function

| Band Number | $\alpha$ | $\beta$ | $\gamma$ |
|---|---|---|---|
| 1 | 30.00164 | 0.0449 | 0.049121 |
| 2 | 29.84299 | 0.0824 | 0.090256 |
| 3 | 330.2238 | 0.1042 | 0.105069 |
| 4 | 16.9489 | 0.0916 | 0.107558 |
| 5 | 19.91785 | 0.0908 | 0.104127 |
| 6 | 35.31626 | 0.0746 | 0.080555 |
| 7 | 44.75151 | 0.0663 | 0.07044 |
| 8 | 39.51282 | 0.1001 | 0.107269 |
| 9 | 27.63662 | 0.2103 | 0.231993 |
| 10 | 67.13471 | 0.0843 | 0.087818 |
| 11 | 24.77418 | 0.1859 | 0.207441 |
| 12 | 122.3684 | 0.0598 | 0.06113 |
| 13 | 64.63215 | 0.1085 | 0.113203 |
| 14 | 53.86207 | 0.1517 | 0.159536 |
| 15 | 130.6111 | 0.1146 | 0.116974 |
| 16 | 80.4373 | 0.1882 | 0.194651 |
| 17 | 156.5035 | 0.0978 | 0.099483 |
| 18 | 92.96335 | 0.1346 | 0.138561 |
| 19 | 71.48464 | 0.2797 | 0.29051 |
| 20 | 72.47266 | 0.1316 | 0.136592 |
| 21 | 130.0072 | 0.0797 | 0.081399 |
| 22 | 101.9085 | 0.1170 | 0.120184 |
| 23 | 90.42829 | 0.0777 | 0.080038 |
| 24 | 75.27222 | 0.1819 | 0.188585 |
| 25 | 89.29339 | 0.1022 | 0.105359 |
| 26 | 81.59732 | 0.1761 | 0.182101 |
| 27 | 106.5307 | 0.1390 | 0.142596 |
| 28 | 163.8518 | 0.1659 | 0.168679 |

Table 5.1: Envelope function parameters in different frequency bands

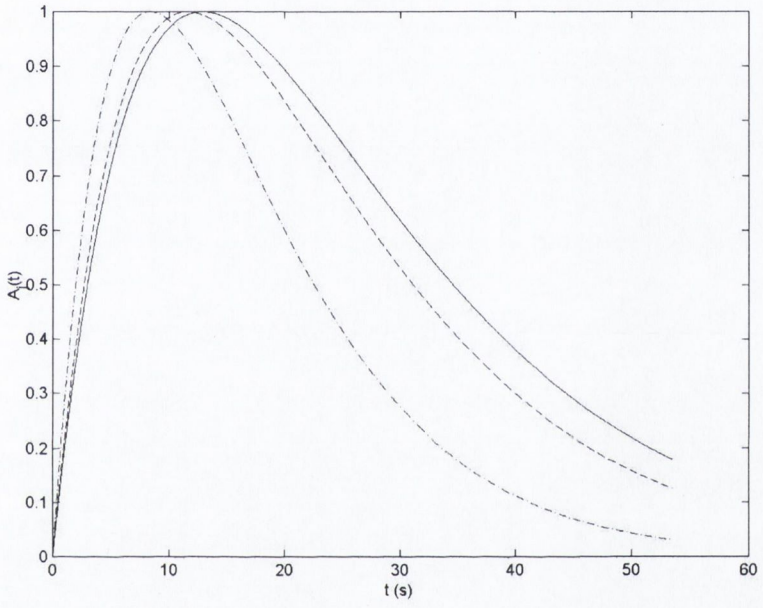


Figure 5.2: Scale dependent envelope functions; __ band 1 (0.50 to 0.59 rad/s), --- band 10 (2.36 to 2.80 rad/s) and --. Band 21 (15.85 to 18.85 rad/s).

Figures 5.3 to 5.5 show the growth in temporal energy of the recorded acceleration and from the proposed wavelet based model in frequency bands 2, 4, 6, 12, 14, 16, 24, 26 and 28 with frequency bands 0.59-0.70rad/s, 0.83-0.99rad/s, 1.98-1.40rad/s, 3.33-3.96rad/s, 4.71-5.60rad/s, 6.66-7.93rad/s, 26.66-3.96rad/s, 37.70-44.83rad/s and 53.31-63.40rad/s respectively. An excellent match is seen between them for all the bands. Using these frequency dependent envelope functions in different scales, 200 samples of ground motion are simulated. Figure 5.6 shows the E-W component of the El-centro ground motions and a single realization of the simulated sample. An exponentially decaying tail is observed in the simulated samples, which is due to the nature of the amplitude modulations assumed in different frequency bands. However, the non-stationary amplitude and frequency contents are clearly represented on the strong motion phase.

Since the objective of the present study is to a develop model for characterization of earthquake ground motions for the purpose of random vibration analysis, the simulation of the amplitude and frequency non-stationary features are vital, which has been successfully represented in the present research. To have a conclusive validation of this, a non-stationary random vibration analysis is performed using the wavelet-based model, the details of which is given by Basu and Gupta (1998). The results from the wavelet based analysis using frequency dependent modulating functions are compared from the statistical simulation results carried out using the 200 simulated samples. Figure 5.7 shows the expected pseudo spectral acceleration (PSA) estimated based on the proposed model along with their limits of exceedence corresponding to the probability of 5% and 95% respectively and comparison with simulation.

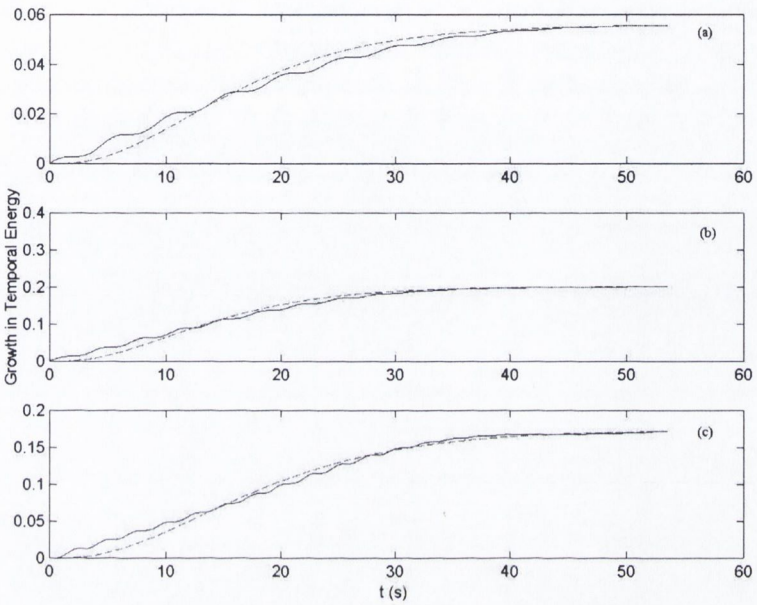


Figure 5.3: Growth in temporal energy in different frequency bands; (a) band 2 (0.59 to 0.70 rad/s), (b) band 4 (0.83 to 0.99 rad/s) and (c) band 6 (1.18 to 1.40 rad/s); ___ target, --- simulated

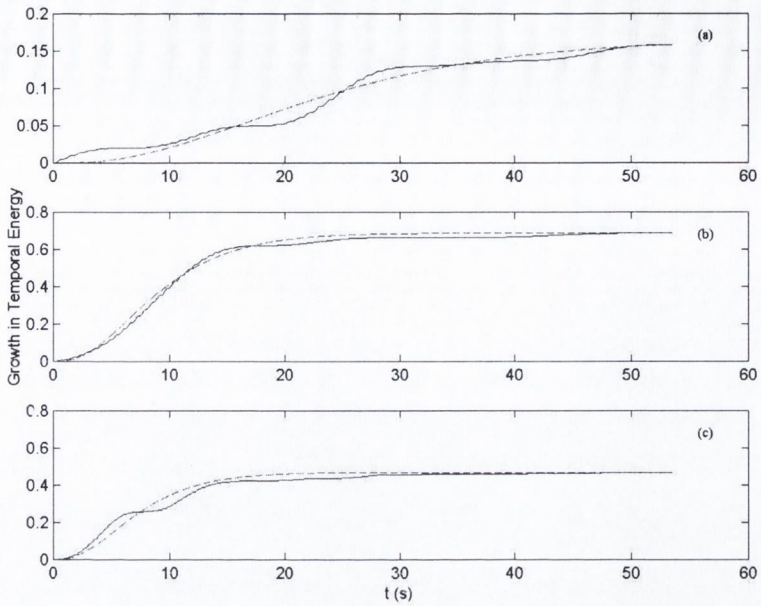


Figure 5.4: Growth in temporal energy in different frequency bands; (a) band 12 (3.33 to 3.96 rad/s), (b) band 14 (4.71 to 5.60 rad/s) and (c) band 16 (6.66 to 7.93 rad/s); ___ target, --- simulated

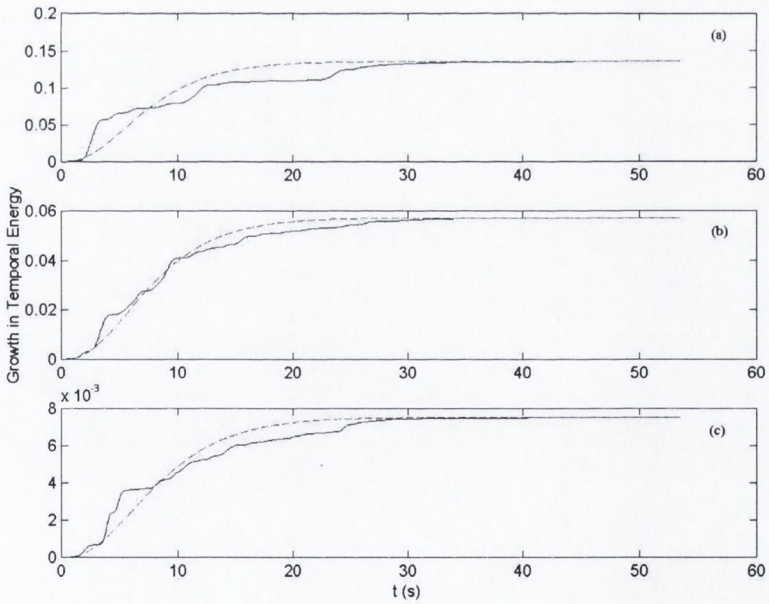


Figure 5.5: Growth in temporal energy in different frequency bands; (a) band 24 (26.66 to 31.70 rad/s), (b) band 26 (37.70 to 44.83 rad/s) and (c) band 28 (53.31 to 63.40 rad/s); ___ target, --- simulated

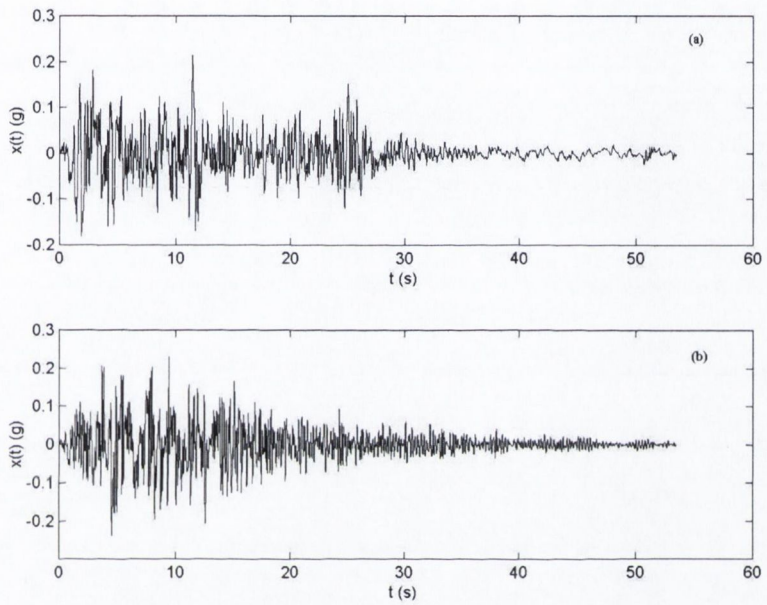


Figure 5.6: Time history of El-centro ground motion; (a) recorded and (b) simulated

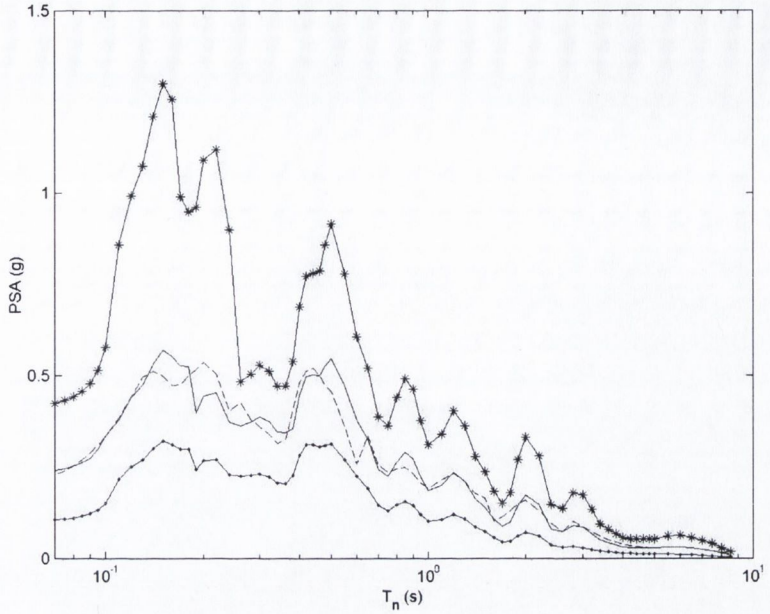


Figure 5.7: PSA obtained from the proposed wavelet-based model and simulated ground motions; '-*-' 95% exceedence limit, '-.-' 5% exceedence limit, '___' wavelet based model with 28 frequency bands and '---' using simulated time history records with frequency dependent amplitude modulation

It can be observed that the expected PSA of the simulated samples closely match the target in mean sense and remain well within the limit of exceedence, which proves the accuracy of the proposed model. It can be observed that the proposed wavelet based model has 84 unknown parameters for exact representation of recorded ground motion. An effort has been made to reduce the number of unknown parameters further by removing frequency bands, which has insignificant contribution on the overall energy content of the recorded time history. In this process, bands 9, 10, 11, 13, 14, 16, 17, 18, 19, 20, 21, 22, 23, 24, 25, 26, 27 and 28 (18 bands) are considered for PSA estimation neglecting the contribution of other bands. Figure 5.8 shows the estimated PSA obtained from exact wavelet-based model and reduced wavelet-based model with less number of

frequency bands. A close match has been observed between them, which ensure a further reduction of 30 parameters. From these results it can be concluded that the proposed

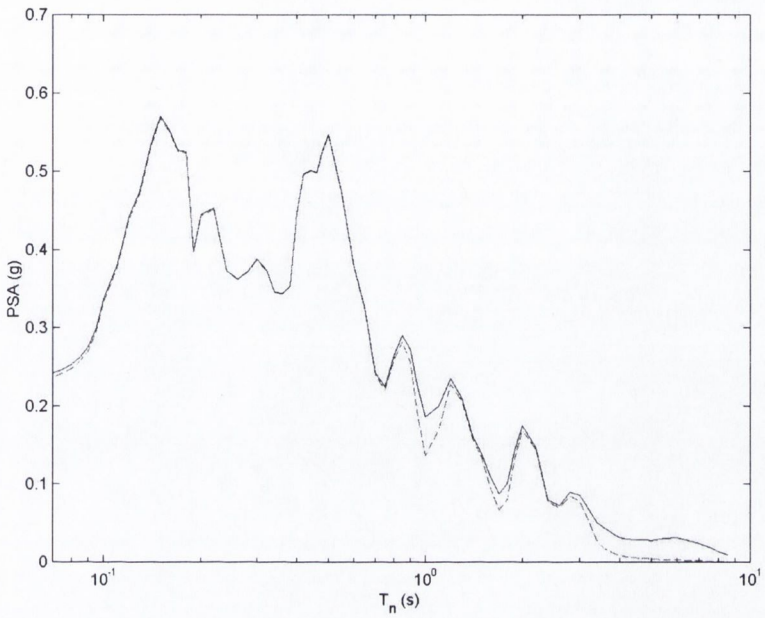


Figure 5.8: PSA obtained from the proposed wavelet-based model with all frequency bands and wavelet-based model with reduced number of frequency bands

wavelet based model is valid in stochastic sense and hence can be used for the purpose of random vibration analysis of dynamical systems. Moreover, it can be noticed that the parameter $\alpha_j^2$ in equation 5.16 is associated with the total energy of the respective band. Therefore, if the Fourier spectrum of the input is used in conjunction with the proposed model, a further reduction of 18 parameters is possible.

To justify the validity of the wavelet based model for earthquake ground motion in stochastic sense, energy growth of two different oscillators is estimated using wavelet based model with frequency dependent amplitude modulating functions and compared with that obtained from simulated samples. Figures 5.9 and 5.10 show the growth in

temporal energy for oscillators with time period 0.1s and 1s respectively. From these figures, it can be noticed that the temporal growth of the mean square energy of the response using simulated time histories matches well with the temporal growth of the response energy using the proposed model. This justifies the validity of the proposed wavelet based model for characterization of earthquake ground motions with frequency dependent amplitude modulation.

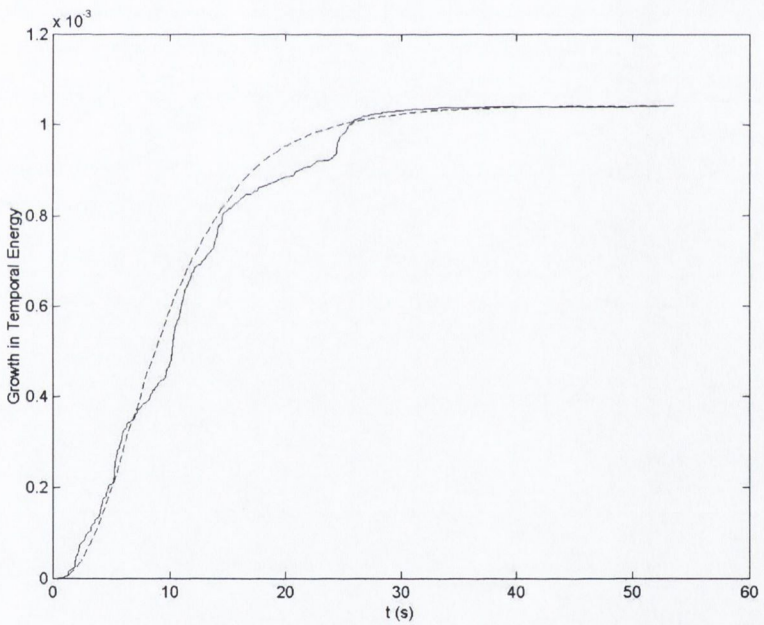


Figure 5.9: Growth in temporal energy of the response (T=0.1s); ___ random vibration based on the proposed wavelet-based model, --- simulated

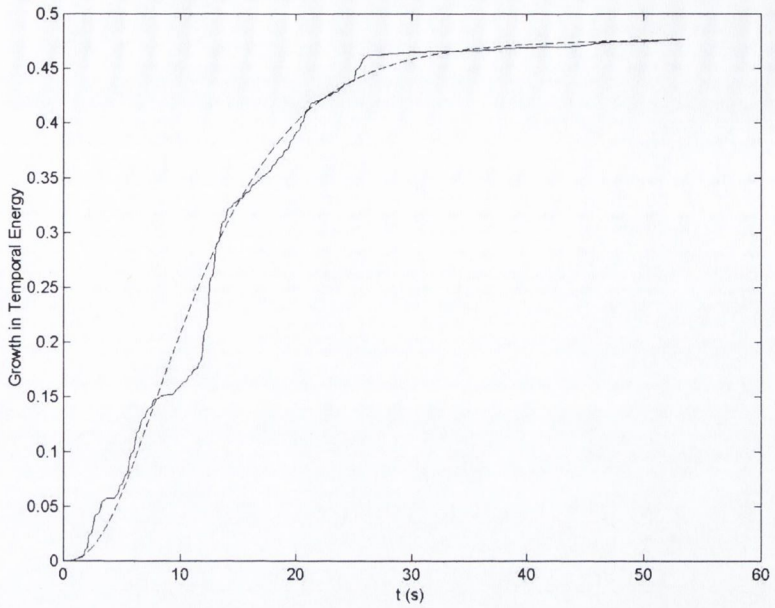


Figure 5.10: Growth in temporal energy of the response (T=1s); ___ random vibration based on the proposed wavelet-based model, --- simulated

## 5.4.2 Case II: Spatially Varying Ground Motions Model

Once the parameters are obtained for the envelope function to characterize the earthquake ground motion for a single support, the spatially varying ground motions can be generated from equations 5.25 [Shinuzoka and Jan (1972)] to account for frequency dependent attenuation and a time shift to account for arrival times of the waves. For this purpose, the values of $\alpha_j^r$, $\beta_j^r$ and $\gamma_j^r$ are assumed to be 4, 1/6.22 and 1/3.11 respectively for all '$j$'. The prerequisite of the digital simulation of earthquake time histories from the fully populated matrix of input PSD function is their decoupling using eigen analysis. For this purpose, an orthogonal decomposition is adopted based on the

eigen vector of the PSD matrix, which decouples the fully populated matrix into independent PSD functions. The digital simulation is then performed for each independent process as described in section 3.3.2. Finally, the joint time histories for each support is obtained form these independent time histories using the inverse transformation to their original coordinate.

For the purpose of simulation, a uniform amplitude modulation in two different supports is considered for all frequency bands. Figure 5.11 shows the auto PSD of the orthogonal increment processes, which are evaluated with $S_0$, $\eta_g$ and $\omega_g$ are $1\times10^{-2}$, 0.4% and 20rad/s for support one and $2.1\times10^{-2}$, 0.6% and 15rad/s for support two respectively. In the present study, simulation is performed for two extreme values of coherence i.e. 0 and 1. The coherence is assumed to be zero in the first case. Figures 5.12 and 5.13 show the PSD function of the orthogonal process for support one and two respectively and that obtained from inverse Fourier transform of the simulated time histories. A close match has been observed between the target PSD functions and the simulated PSD functions. Figures 5.14 and 5.15 show the cumulative distribution function at $t = 5s$ of simulated time histories for support one and two respectively, which proves the Gaussian nature of the simulated time histories. Figure 5.16 shows simulated sample time histories of earthquake ground motions after uniform amplitude modulation for support one and two respectively. Since the support motions are assumed independent, the simulation has been performed from their respective auto power spectrum, which does not demand for orthogonal transformation to decouple them.

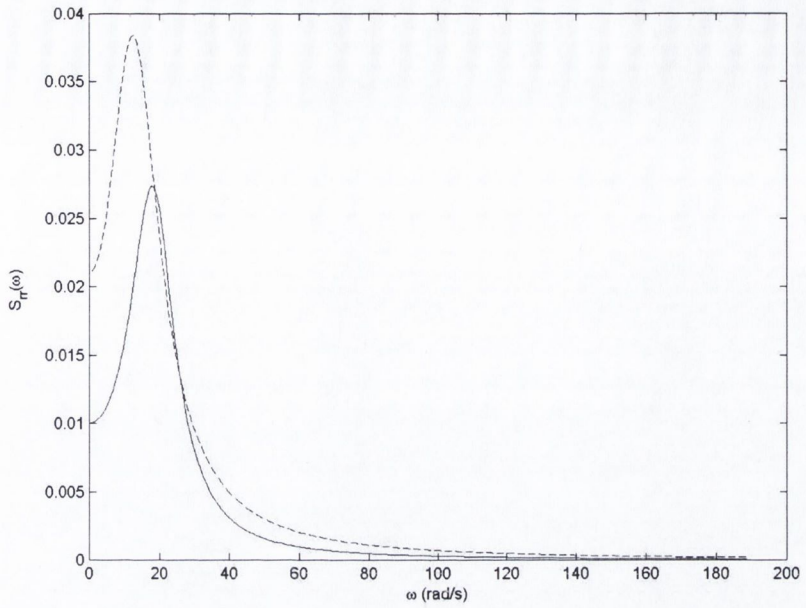


Figure 5.11: PSD of the orthogonal processes for supports one and two; ___ support one, ---- support two

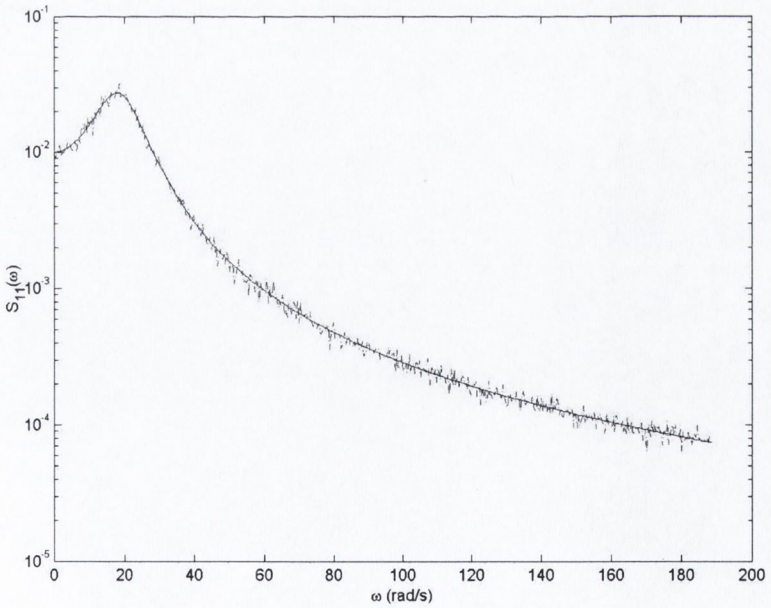


Figure 5.12: PSD of the stationary process for support one; ___ exact, ---- simulated

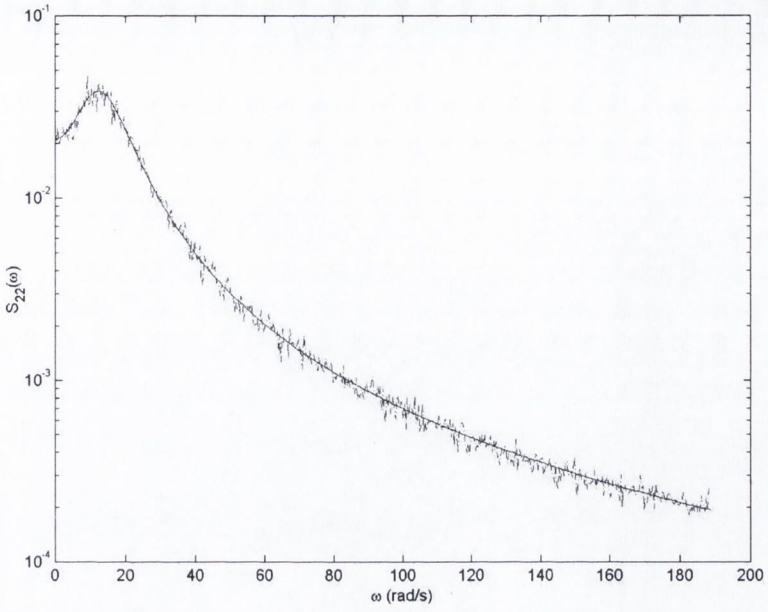


Figure 5.13: PSD of the stationary process for support two; ___ exact, ---- simulated

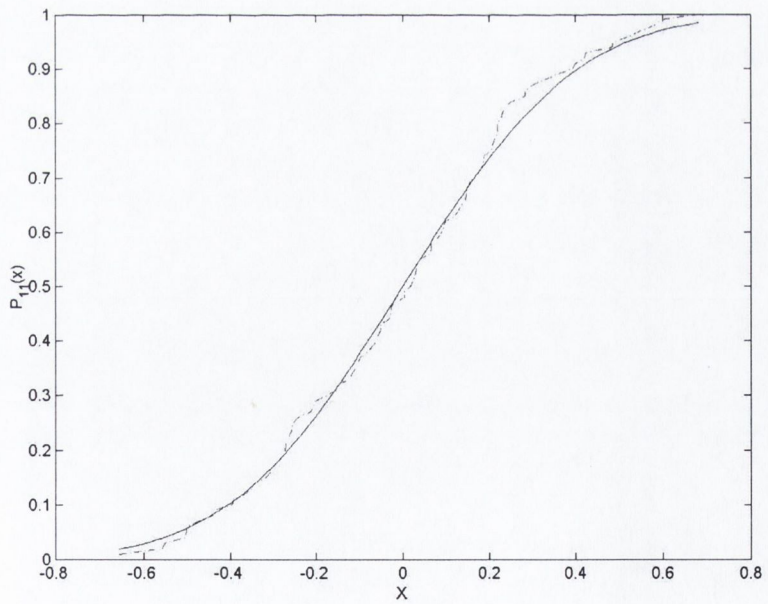


Figure 5.14: PDF of the simulated samples of the stationary process for support one at $t = 5s$ ; ___ exact, ---- simulated

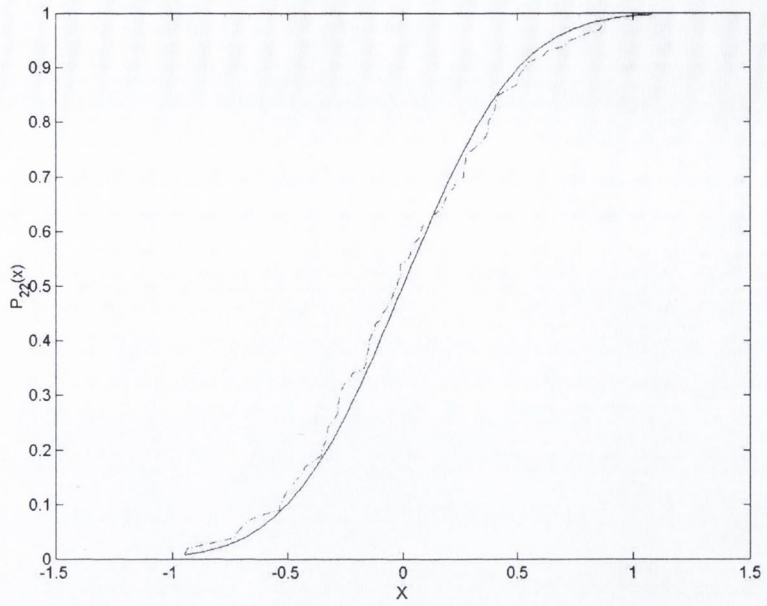


Figure 5.15: PDF of the simulated samples of the stationary process for support two at $t = 5s$ ; ___ exact, ---- simulated

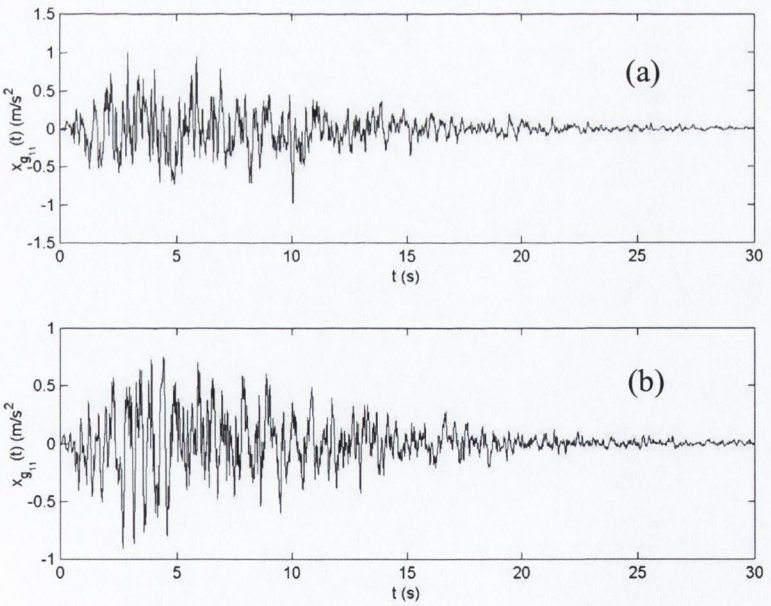


Figure 5.16: Simulated time history of random support motion; a) support one and b) support two

In the next case, the coherence is assumed to be 1. Figure 5.17 shows the PSD functions at the two supports and the independent PSD after orthogonal transformation using eigen analysis. Figures 5.18 and 5.19 show the PSD and cumulative distribution function (CDF) of the simulated time histories and their respective targets. It can be observed that both of them closely match with their target implying the accuracy of the simulation. Once the ensembles of time histories are generated from the independent PSD function, they are finally transformed to their original coordinate, which has a correlation of 1. Figures 5.20a and 5.20b show sample of time histories for support one and two respectively, which clearly show the initial build up phase followed by a strong motion part and finally a decaying phase that are typically observed in a strong motion earthquake ground motions.

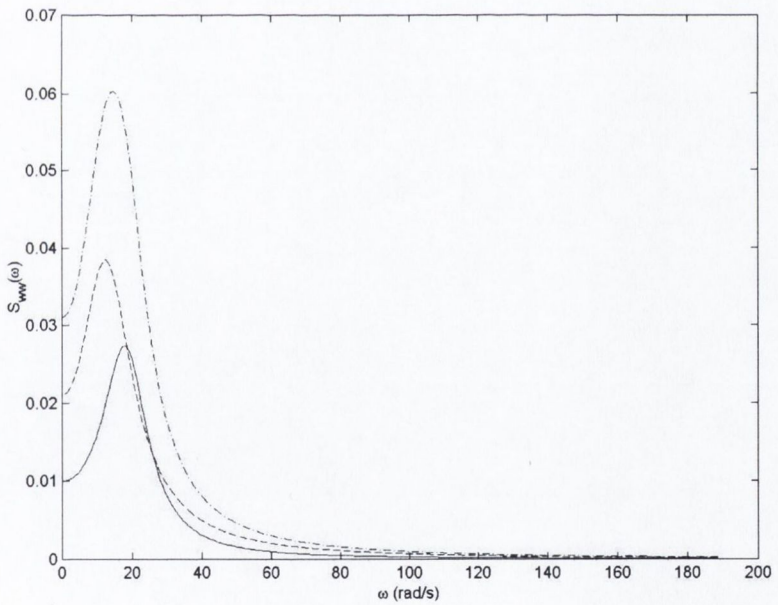


Figure 5.17: PSD of the orthogonal processes for supports one and two; ___ support one, ---- support two and -.- independent process obtained from orthogonal decomposition

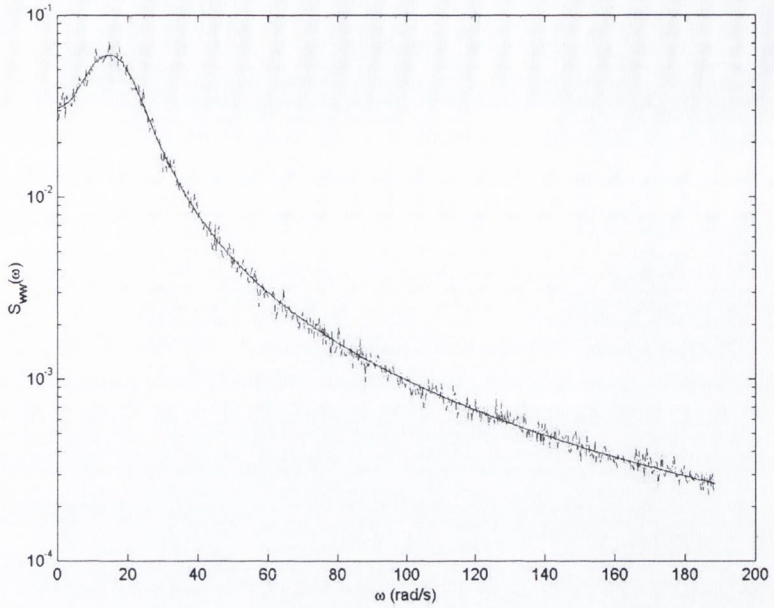


Figure 5.18: PSD of the independent orthogonal processes; ___ exact, ---- simulated

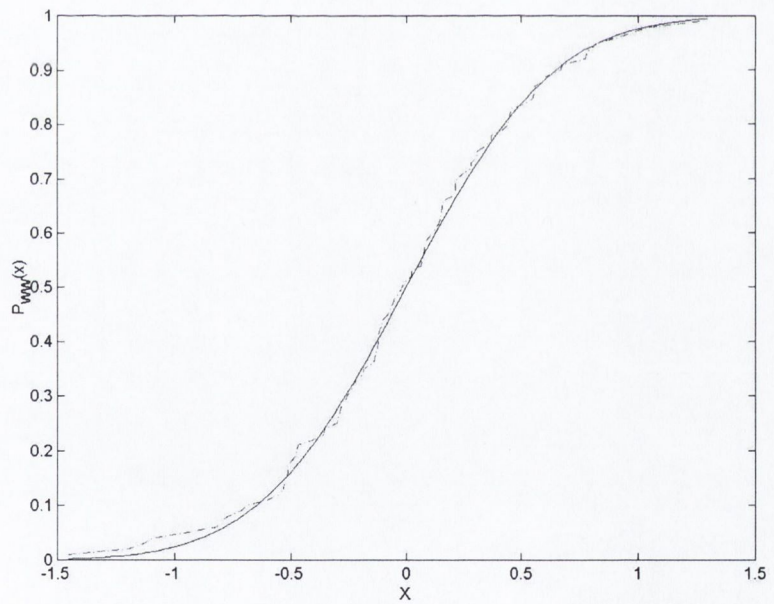


Figure 5.19: PDF of the simulated samples of the independent stationary process at $t = 5s$ ; ___ exact, ---- simulated

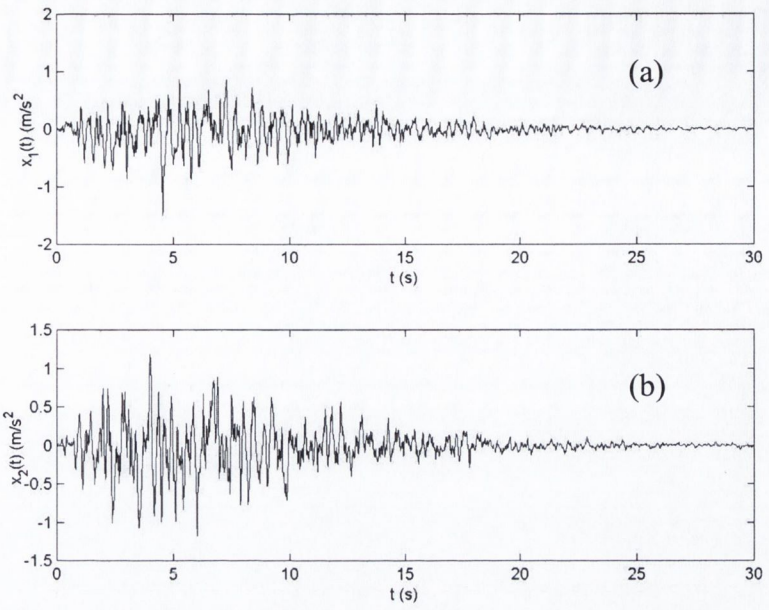


Figure 5.20: Simulated time history of random support motion; a) support one and b) support two

## 5.5 Conclusions

A robust wavelet based model for the characterization of non-stationary earthquake ground motion is presented here. The proposed model can efficiently represent earthquake ground motions with non-stationarity in both intensity and frequency content. For the purpose of representing the non-stationarity, wavelet based time-frequency analysis is adopted to evaluate the temporal energy growth in different frequency bands. A modified version of L-P wavelet basis function is used to evaluate the energy of the recorded ground motion. Using this basis function, the earthquake ground motion is

modelled as a summation of random process in different frequency bands. Each sub-process is then modelled as product of a deterministic envelope function and a stationary random process. The envelope functions are modelled as proposed by Shinozuka and Sato and the random sub-processes are modelled by Kanai-Tajimi spectra. The envelope functions in different frequency bands are different and hence this leads to frequency dependent amplitude modulating functions. The proposed wavelet based model using frequency dependent amplitude modulating functions can efficiently characterize an earthquake ground motion process with non-stationarity in both intensity and frequency content and hence can be used for random vibration analysis of linear and non-linear structures.

Finally, the proposed wavelet-based model is used to characterize the spatially varying ground motions. It can be observed from the simulation results that the frequency dependent amplitude modulation can be used to characterize SVEGM, which will be further used to solve a non-stationary response of a boundary value problem in the following chapter.

# Chapter 6: Non-stationary Response Analysis: Continuous Systems

## 6.1 Introduction

In Chapter 5, the modelling of the evolutionary random processes with amplitude and frequency non-stationary has been discussed. In this chapter, continuous wavelet transformation is used to evaluate the response of a short span bridge subjected to random differential support motions. An input-output relation is proposed using a modified form of L-P basis function, where the output is based on modal response as well as interaction between dynamic and pseudo static components. Further, a more generalized wavelet based evolutionary spectral analysis of simply supported beam subjected to stochastic differential support motions are presented. The non-stationary support motions at the ends of the beam are modelled using deterministic frequency dependent modulating functions and orthogonal stochastic processes. A wavelet based input-output relation is then developed for the time dependent power spectral density function of the total displacement response, which is composed of two parts (a) pseudo static and (b) dynamic. The proposed model can evaluate time dependent second order moment statistics of the output using different wavelet functions and hence is more general from the point of view of time-frequency analysis.

## 6.2 Wavelet-Based Analysis of Boundary Value Problem

In this section, attention is focused on wavelet-based evaluation of the non-stationary response of a linear boundary value problem subjected to evolutionary stochastic

processes as input. First, a simply supported short span bridge is considered, which is subjected to differential random support motions defined in terms of expected value of the square of wavelet coefficients. Next, a generalized formulation for boundary value problem is presented using the generalized model of the input processes that has been presented in chapter 5.

### 6.2.1 Short Span Bridges

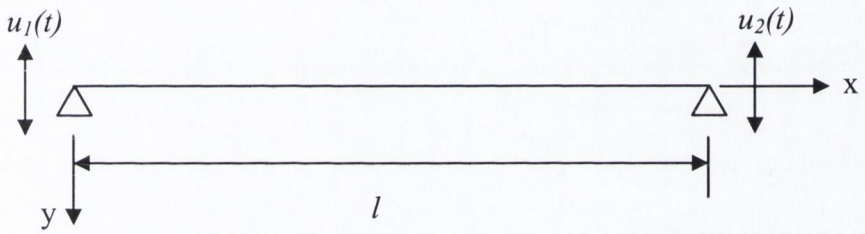


Figure 6.1: Simply supported beam with random differential support motions

In the present study, the bridge is modelled as a simply supported beam as shown in figure 6.1. The beam is subjected to differential support motions $u_1(t)$ and $u_2(t)$ respectively. The governing equation of the beam is given by

$$EI\frac{\partial^4 y(x,t)}{\partial x^4} + m_p\frac{\partial^2 y(x,t)}{\partial t^2} + c\frac{\partial y(x,t)}{\partial t} = 0 \tag{6.1}$$

In the above equation, $E$, $I$, $m_p$ and $c$ are Young's modulus, area moment of inertia of the section, mass per unit length, and viscous damping coefficient of the beam respectively. The boundary conditions associated with equation 6.1 are given by $y(0,t) = u_1(t)$, $y(l,t) = u_2(t)$, $y''(0,t) = 0$ and $y''(l,t) = 0$ while the initial conditions are $y(x,0) = 0$ and

$\dot{y}(x,0) = 0$, where prime and over-dot represent derivative with respect to space and time respectively. In the present study, Mindlin-Goodman (1950) transformation is used to transform equation 6.1 into a set of uncoupled modal differential equations with homogenous boundary conditions. Following this transformation, the total response $y(x,t)$ can be expressed in terms of pseudo static and dynamic components, which is given by

$$y(x,t) = \sum \phi_k(x) z_k(t) + h_1(x) u_1(t) + h_2(x) u_2(t) \tag{6.2}$$

where, $\phi_k(x)$ and $z_k(t)$ are the $k^{th}$ mode shape and $k^{th}$ modal response respectively while $h_1(x)$ and $h_2(x)$ are the shape functions associated with the pseudo static response. Based on the boundary conditions for simply supported beam, it can be shown that $h_1(x)$, $h_2(x)$ and $\phi_k(x)$ are given by $1-(x/l)$, $x/l$ and $\sin(k\pi x/l)$ respectively while the $k^{th}$ natural frequency is given by [Paz (1987)]

$$\omega_k = k^2\pi^2\sqrt{\frac{EI}{m_p l^4}},\ k = 1,2,3... \tag{6.3}$$

Using the transformation given by equation 6.2, it can be shown that the governing equation of motion of the total response can be expressed as a set of uncoupled modal responses with homogenous boundary conditions, which is given by

$$\ddot{z}_k(t) + (2\eta_k \omega_k)\dot{z}_k(t) + \omega_k^2 z_k(t) = f_k(t) \tag{6.4}$$

where, $\eta_k$ is the damping ratio in the $k^{th}$ mode. The $k^{th}$ modal load vector is given by

$$f_k(t) = \frac{\int_0^l f(x,t)\phi_k(x)dx}{\int_0^l m_p \phi_k^2(x)dx} \tag{6.5}$$

where, $f(x,t) = -\left(m_p h_1(x)\ddot{u}_1(t) + ch_1(x)\dot{u}_1(t)\right) - \left(m_p h_2(x)\ddot{u}_2(t) + ch_2(x)\dot{u}_2(t)\right)$.

First substituting the wavelet series expansion of the functions on both side of equation 6.4 and then taking the Fourier transform as proposed by Basu and Gupta (1998), it can be shown that

$$\sum_i \sum_j \frac{1}{a_j} W_\psi z_k(a_j, b_i)\psi_{a_j,b_i}(\omega) = \sum_i \sum_j \frac{1}{a_j} W_\psi f_k(a_j, b_i) H_k(\omega)\psi_{a_j,b_i}(\omega) \tag{6.6}$$

where, $H_k(\omega)$ is the frequency response function in the $k^{th}$ mode and is given by $1/\left(\left(\omega^2 - \omega_k^2\right) + i\left(2\eta_k \omega \omega_k\right)\right)$. On taking wavelet transform on both side of equation 6.2 and using equation 6.6, yields

$$\sum_i \sum_j \frac{1}{a_j} W_\psi y(x,a_j,b_i)\psi_{a_j,b_i}(\omega) = \sum_k \phi_k \sum_i \sum_j \frac{1}{a_j} W_\psi f_k(a_j,b_i) H_k(\omega)\psi_{a_j,b_i}(\omega) + h_1(x)\sum_i \sum_j \frac{1}{a_j} W_\psi u_1(a_j,b_i)\psi_{a_j,b_i}(\omega) + h_2(x)\sum_i \sum_j \frac{1}{a_j} W_\psi u_2(a_j,b_i)\psi_{a_j,b_i}(\omega) \tag{6.7}$$

Multiplying the above equation by its complex conjugate and integrating over $\omega$ and taking the ensemble average, the second order moment statistics of the total response $y(x,t)$ in the $j^{th}$ band can be expressed as [see Basu and Gupta (1998)]

$$\begin{aligned}
&\sum_i E\left[\left|W_\psi y(x,a_j,b_i)\right|^2\right] = \sum_k \phi_k^2 \sum_i E\left[\left|W_\psi f_k(a_j,b_i)\right|^2\right] \int_{-\infty}^{+\infty} \left|H_k(\omega)\right|^2 \left|\psi_{a_j,b_i}(\omega)\right|^2 d\omega \\
&+ \sum_k \sum_{m,m\neq k} \phi_k \phi_m \sum_i E\left[W_\psi f_k(a_j,b_i) W_\psi f_m(a_j,b_i)\right] \int_{-\infty}^{+\infty} H_k(\omega) H_m^*(\omega) \left|\psi_{a_j,b_i}(\omega)\right|^2 d\omega \\
&+ h_1^2(x)\sum_i E\left[\left|W_\psi u_1(a_j,b_i)\right|^2\right] \int_{-\infty}^{+\infty} \left|\psi_{a_j,b_i}(\omega)\right|^2 d\omega + h_2^2(x)\sum_i E\left[\left|W_\psi u_2(a_j,b_i)\right|^2\right] \\
&\int_{-\infty}^{+\infty} \left|\psi_{a_j,b_i}(\omega)\right|^2 d\omega + 2\sum_k \phi_k h_1(x) \sum_i E\left[W_\psi f_k(a_j,b_i) W_\psi u_1(a_j,b_i)\right] \int_{-\infty}^{+\infty} H_k(\omega) \left|\psi_{a_j,b_i}(\omega)\right|^2 d\omega \\
&+ 2\sum_k \phi_k h_2(x) \sum_i E\left[W_\psi f_k(a_j,b_i) W_\psi u_2(a_j,b_i)\right] \int_{-\infty}^{+\infty} H_k(\omega) \left|\psi_{a_j,b_i}(\omega)\right|^2 d\omega \\
&+ 2h_1(x)h_2(x) E\left[W_\psi u_1(a_j,b_i) W_\psi u_2(a_j,b_i)\right]
\end{aligned} \tag{6.8}$$

In the above equation, terms containing correlations of wavelet coefficients at two different instants of temporal parameter '*b*' become zero due to cancellation of oscillation during integration [see Basu and Gupta (1998)] and hence are neglected here. This is confirmed later in the following section for the numerical illustration. Moreover in the present study, support motions are assumed to be uncorrelated and hence the last term of

the above equation can be neglected. Using Perseval's theorem and the above equation, it can be shown that the energy of the total response $y(x,t)$ in the $j^{th}$ band can be expressed as [Basu and Gupta (1998)]

$$\int_{-\infty}^{+\infty} E\left[\left|Y^j(x,\omega)\right|^2\right] d\omega = \sum_k \phi_k^2 \sum_i \frac{K\Delta b}{a_j} E\left[\left|W_\psi f_k(a_j,b_i)\right|^2\right] \int_{-\infty}^{+\infty} \left|H_k(\omega)\right|^2 \left|\psi_{a_j,b_i}(\omega)\right|^2 d\omega$$

$$+ \sum_k \sum_{m,m\neq k} \phi_k \phi_m \sum_i \frac{K\Delta b}{a_j} E\left[W_\psi f_k(a_j,b_i) W_\psi f_m(a_j,b_i)\right] \int_{-\infty}^{+\infty} H_k(\omega) H_m^*(\omega) \left|\psi_{a_j,b_i}(\omega)\right|^2 d\omega$$

$$+ h_1^2(x) \sum_i \frac{K\Delta b}{a_j} E\left[\left|W_\psi u_1(a_j,b_i)\right|^2\right] \int_{-\infty}^{+\infty} \left|\psi_{a_j,b_i}(\omega)\right|^2 d\omega + h_2^2(x) \sum_i \frac{K\Delta b}{a_j} E\left[\left|W_\psi u_2(a_j,b_i)\right|^2\right] \quad (6.9)$$

$$\int_{-\infty}^{+\infty} \left|\psi_{a_j,b_i}(\omega)\right|^2 d\omega + 2\sum_k \phi_k h_1(x) \sum_i \frac{K\Delta b}{a_j} E\left[W_\psi f_k(a_j,b_i) W_\psi u_1(a_j,b_i)\right] \int_{-\infty}^{+\infty} H_k(\omega) \left|\psi_{a_j,b_i}(\omega)\right|^2 d\omega$$

$$+ 2\sum_k \phi_k h_2(x) \sum_i \frac{K\Delta b}{a_j} E\left[W_\psi f_k(a_j,b_i) W_\psi u_2(a_j,b_i)\right] \int_{-\infty}^{+\infty} H_k(\omega) \left|\psi_{a_j,b_i}(\omega)\right|^2 d\omega$$

The modified form of L-P basis function used in the present study divides the frequency scale into non-overlapping (and hence also orthogonal) bands in logarithmic scale. Furthermore the above integral equation can be considered true in point-wise for $\sigma$ close to 1 [Basu and Gupta (1998)]. Using the above expression point-wise, the evolutionary power spectral density (PSD) function of the total response $y(x,t)$ can be obtained as

$$S_{YY_i} = \sum_j \frac{E\left[\left|Y_i^j(x,\omega)\right|^2\right]}{\Delta b} = \sum_k \phi_k^2 \sum_j \frac{K}{a_j} E\left[\left|W_\psi f_k(a_j,b_i)\right|^2\right] \left|H_k(\omega)\right|^2 \left|\psi_{a_j,b_i}(\omega)\right|^2$$

$$+ \sum_k \sum_{m,m\neq k} \phi_k \phi_m \sum_j \frac{K}{a_j} E\left[W_\psi f_k(a_j,b_i) W_\psi f_m(a_j,b_i)\right] \mathrm{Re}\left[H_k(\omega) H_m^*(\omega)\right] \left|\psi_{a_j,b_i}(\omega)\right|^2$$

$$+ h_1^2(x) \sum_j \frac{K}{a_j} E\left[\left|W_\psi u_1(a_j,b_i)\right|^2\right] \left|\psi_{a_j,b_i}(\omega)\right|^2 + h_2^2(x) \sum_j \frac{K}{a_j} E\left[\left|W_\psi u_2(a_j,b_i)\right|^2\right] \left|\psi_{a_j,b_i}(\omega)\right|^2 \quad (6.10)$$

$$+ 2\sum_k \phi_k h_1(x) \sum_j \frac{K}{a_j} E\left[W_\psi f_k(a_j,b_i) W_\psi u_1(a_j,b_i)\right] \mathrm{Re}\left[H_k(\omega)\right] \left|\psi_{a_j,b_i}(\omega)\right|^2$$

$$+ 2\sum_k \phi_k h_2(x) \sum_j \frac{K}{a_j} E\left[W_\psi f_k(a_j,b_i) W_\psi u_2(a_j,b_i)\right] \mathrm{Re}\left[H_k(\omega)\right] \left|\psi_{a_j,b_i}(\omega)\right|^2$$

Equation 6.10 provides the output power spectral density of the displacement response, which is established using the expected value of the wavelet coefficients of the input processes. Next, a generalized formulation for boundary value problem is established using the proposed wavelet-based model of the input processes as discussed in section 5.3.2, which does not require the expected value of the wavelet coefficients of the excitation processes as input.

### 6.2.2 Generalized Formulation

A simply supported beam of length $l$ under random differential support motions $u_1(t)$ and $u_2(t)$ respectively at the two ends is considered. Figure 6.1 shows the simply supported beam, whose governing equation of motion is given by equation 6.1. The boundary conditions associated with equation 6.1 are given in section 6.2.1. In order to transform

equation 6.1 into a set of uncoupled modal differential equations with homogenous boundary conditions, the transformation proposed by Mindlin and Goodman (1950) is used here. Following this transformation, the total response $y(x,t)$ can be expressed as a sum of dynamic component $y_d(x,t)$ and pseudo static component $y_s(x,t)$, and is written as

$$y(x,t) = y_d(x,t) + y_s(x,t) = \sum \phi_k(x) z_k(t) + h_1(x) u_1(t) + h_2(x) u_2(t) \tag{6.11}$$

In equation 6.11, $\phi_k(x)$ and $z_k(t)$ are the $k^{th}$ mode shape and $k^{th}$ modal response respectively, and $h_1(x)$ and $h_2(x)$ are the shape functions associated with the pseudo static responses. Based on the initial and boundary conditions for the simply supported beam as given in section 6.2.1, it can be shown that the admissible shape functions for the simply supported beam are

$$h_1(x) = 1 - \frac{x}{l} \tag{6.12a}$$

$$h_2(x) = \frac{x}{l} \tag{6.12b}$$

and $$\phi_k(x) = \sin\left(\frac{k\pi x}{l}\right), \; k = 1,2,3...\infty \tag{6.12c}$$

Using the transformation given by equation 6.11, the governing equation of motion of the total response can be expressed as a set of uncoupled modal dynamic response as

$$\ddot{z}_k(t)+(2\eta_k\omega_k)\dot{z}_k(t)+\omega_k^2 z_k(t)=f_k(t),\ k=1,2,3...\infty \tag{6.13}$$

where, $\omega_K$ and $\eta_k$ are the natural frequency and the damping ratio associated with the $k^{th}$ mode respectively. It can be shown that the $k^{th}$ natural frequency of the simply supported beam is given by

$$\omega_k = k^2\pi^2\sqrt{\frac{EI}{m_p l^4}},\ k=1,2,3...\infty \tag{6.14}$$

Using Galarkin technique and normalizing the mass associated with the inertia term in equation 6.1, it can be shown that the $k^{th}$ modal load vector $f_K(t)$ in equation 6.13 is given by

$$f_k(t)=\frac{\int_0^l f(x,t)\phi_k(x)dx}{\int_0^l m_p\phi_k^2(x)dx} \tag{6.15}$$

where,

$$f(x,t)=-\left(m_p h_1(x)\ddot{u}_1(t)+ch_1(x)\dot{u}_1(t)\right)-\left(m_p h_2(x)\ddot{u}_2(t)+ch_2(x)\dot{u}_2(t)\right) \tag{6.16}$$

Neglecting the force due to damping, which decays faster than the other forcing terms, the $k^{th}$ modal load vector in equation 6.16 can be expressed as

$$f_k(t) = \frac{2}{k\pi}\left[-\ddot{u}_1(t) + (-1)^k \ddot{u}_2(t)\right] \tag{6.17}$$

In the present study, the differential support motions $\ddot{u}_1(t)$ and $\ddot{u}_2(t)$ are assumed to be non-stationary in both intensity and frequency content. Following the non-stationary representation of a random process as proposed by Priestley (1981), $\ddot{u}_1(t)$ and $\ddot{u}_2(t)$ can be represented as

$$\ddot{u}_1(t) = \int_{-\infty}^{+\infty} A_1(t,\omega) e^{i\omega t} dG_1(\omega) \tag{6.18a}$$

$$\ddot{u}_2(t) = \int_{-\infty}^{+\infty} A_2(t,\omega) e^{i\omega t} dG_2(\omega) \tag{6.18b}$$

where, $A_1(t,\omega)$ and $A_2(t,\omega)$ represent the deterministic envelope functions and $G_1(\omega)$ and $G_2(\omega)$ are the stationary orthogonal increment processes for $\ddot{u}_1(t)$ and $\ddot{u}_2(t)$, which are given by

$$E\left[dG_1(\omega) dG_1^*(\omega')\right] = S_{11}(\omega) \qquad \omega = \omega' \tag{6.19a}$$

$$= 0 \qquad \text{otherwise}$$

$$E\left[dG_2(\omega)dG_2^*(\omega')\right] = S_{22}(\omega) \qquad \omega = \omega' \qquad (6.19b)$$

$$= 0 \qquad \text{otherwise}$$

$S_{11}(\omega)$ and $S_{22}(\omega)$ in the equations 6.19a and 6.19b are the power spectral density function of the stationary processes represented by $G_1(\omega)$ and $G_2(\omega)$ respectively. On taking wavelet transformation of both sides of equations 6.18a and 6.18b, it can be shown that [Spanos and Failla (2004)]

$$W_\psi \ddot{u}_1(a_j, b) = \int_{-\infty}^{+\infty} A_1(b,\omega) e^{i\omega b} d\tilde{G}_1(\omega) \qquad (6.20a)$$

$$W_\psi \ddot{u}_2(a_j, b) = \int_{-\infty}^{+\infty} A_2(b,\omega) e^{i\omega b} d\tilde{G}_2(\omega) \qquad (6.20b)$$

In the above equations, $d\tilde{G}_1(\omega)$ and $d\tilde{G}_2(\omega)$ are the stationary processes in wavelet domain corresponding to the scale '$j$' and are given by

$$d\tilde{G}_1(\omega) = \sqrt{2\pi a_j}\,\hat{\psi}(a_j\omega)\,dG_1(\omega) \qquad (6.21a)$$

$$d\tilde{G}_2(\omega) = \sqrt{2\pi a_j}\,\hat{\psi}(a_j\omega)\,dG_2(\omega) \qquad (6.21b)$$

where, $\hat{\psi}(a_j\omega)$ is the Fourier transformation of $\psi_{a_j,b}(t)$. From equations 6.20a and 6.20b, it can be noticed that the time varying frequency content of the support motions $\ddot{u}_1(t)$ and $\ddot{u}_2(t)$ are governed by the deterministic envelope function $A_1(t,\omega)$ and $A_2(t,\omega)$

respectively. This is done by taking wavelet transform of the support accelerations $\ddot{u}_1(t)$ and $\ddot{u}_2(t)$, which gives localized frequency information around $t = b$ by dividing frequency into different scales '*j*'. Therefore it can be assumed that the deterministic envelope function in different scales '*j*' is a function of time only, whose frequency signature changes from one scale to another. Following this assumption, the wavelet representation of $\ddot{u}_1(t)$ and $\ddot{u}_2(t)$ as given by equations 6.20a and 6.20b respectively can be modified to

$$W_\psi \ddot{u}_1(a_j, b) = \int_{-\infty}^{+\infty} A_1^j(b) e^{i\omega b} d\tilde{G}_1(\omega) \tag{6.22a}$$

$$W_\psi \ddot{u}_2(a_j, b) = \int_{-\infty}^{+\infty} A_2^j(b) e^{i\omega b} d\tilde{G}_2(\omega) \tag{6.22b}$$

where, $A_1^j(b)$ and $A_2^j(b)$ are the band dependent envelope function in pseudo time domain '*b*'.

***Evolutionary Spectral Analysis of Beam***

On taking wavelet transform of both side of equation 6.13 and expressing the modal response in pseudo time domain 'b', the governing equation of motion can be expressed as [Basu and Gupta (2000)]

$$\frac{\partial^2}{\partial b^2} W_\psi z_k(a_j,b) + (2\eta_k\omega_k)\frac{\partial}{\partial b} W_\psi z_k(a_j,b) + \omega_k^2 W_\psi z_k(a_j,b) = W_\psi f_k(a_j,b) \quad (6.23)$$

where, $W_\psi z_k(a_j,b)$ represents the wavelet coefficient of the $k^{th}$ modal response $z_k(t)$ at a scale '$j$' and $W_\psi f_k(a_j,b)$ is the wavelet coefficient of the $k^{th}$ modal load vector $f_k(t)$ and is given by

$$W_\psi f_k(a_j,b) = \frac{2}{k\pi}\left[-W_\psi \ddot{u}_1(a_j,b) + (-1)^k W_\psi \ddot{u}_2(a_j,b)\right] = l_1 W_\psi \ddot{u}_1(a_j,b) + l_2 W_\psi \ddot{u}_2(a_j,b) \quad (6.24)$$

In the above equation, $l_1$ and $l_2$ are given by $-2/(k\pi)$ and $(-1)^k 2/(k\pi)$ respectively. Assuming zero initial conditions, $k^{th}$ modal response $z_k(t)$ can be evaluated using Duhamel's integral, which is given by

$$W_\psi z_k(a_j,b) = l_1 \int_0^b h_k(b-\tau) W_\psi \ddot{u}_1(a_j,\tau) d\tau + l_2 \int_0^b h_k(b-\tau) W_\psi \ddot{u}_2(a_j,\tau) d\tau \quad (6.25)$$

where, $h_k(b)$ is the response of a linear single degree of freedom system due to an unit impulse [Paz (1987)]. Using expressions for $\ddot{u}_1(t)$ and $\ddot{u}_2(t)$ in wavelet domain as given in equation 6.20a and 6.20b respectively in equation 6.25, the wavelet coefficient of the $k^{th}$ modal response $z_k(t)$ is given by

$$W_\psi z_k(a_j,b) = \int_{-\infty}^{+\infty} M_1(b,\omega) e^{i\omega b} d\tilde{G}_1(\omega) + \int_{-\infty}^{+\infty} M_2(b,\omega) e^{i\omega b} d\tilde{G}_2(\omega) \tag{6.26}$$

where,

$$M_1^j(b,\omega) = l_1 \int_0^b h_k(b-\tau) A_1^j(\tau) e^{i\omega(\tau-b)} d\tau \tag{6.27a}$$

$$M_2^j(b,\omega) = l_2 \int_0^b h_k(b-\tau) A_2^j(\tau) e^{i\omega(\tau-b)} d\tau \tag{6.27b}$$

From equation 6.27a and 6.27b, it can be noticed that the frequency dependent amplitude modulation is performed in each band using an exponentially decaying function as given by equation 5.10, which decays slowly over time. The unit impulse response function $h_k(\tau)$ used in the equations 6.27a and 6.27b decays at a faster rate as compared to deterministic envelope functions $A_1^j(\tau)$ and $A_2^j(\tau)$. Moreover, wavelet transformation provides localized frequency information of a time function around $t = b$. Using this time localization property of the wavelet transformation along with less oscillatory nature of the band dependent envelope functions, equation 6.27a and 6.27b can be approximated as

$$M_1^j(b,\omega) \approx l_1 A_1^j(b) \int_0^b h_k(b-\tau) e^{-i\omega(b-\tau)} d\tau \approx l_1 A_1^j(b) H_k(\omega) \tag{6.28a}$$

$$M_2^j(b,\omega) \approx l_2 A_2^j(b) \int_0^b h_k(b-\tau) e^{-i\omega(b-\tau)} d\tau \approx l_1 A_2^j(b) H_k(\omega) \tag{6.28b}$$

Using equations 6.28a and 6.28b into equation 6.26, wavelet coefficient of the $k^{th}$ modal response $z_k(t)$ can be expressed as

$$W_\psi z_k(a_j,b)=\sum_{p=1}^{2}\int_{-\infty}^{+\infty} l_p A_p^j(b) H_k(\omega) e^{i\omega b} d\tilde{G}_p(\omega) \tag{6.29}$$

Therefore, taking wavelet transform of equation 6.11 and using equation 6.29, wavelet coefficient of the dynamic response of the beam can be expressed as

$$W_\psi y_d(x,a_j,b)=\sum_{k=1}^{N}\phi_k(x)\sum_{p=1}^{2}\int_{-\infty}^{+\infty} l_p A_p^j(b) H_k(\omega) e^{i\omega b} d\tilde{G}_p(\omega) \tag{6.30}$$

where, $W_\psi y_d(x,a_j,b)$ is the wavelet coefficient of the dynamic component $y_d(x,t)$ of the total response of the beam. Similarly, wavelet coefficient of the total response $W_\psi y(x,a_j,b)$ can be expressed as

$$W_\psi y(x,a_j,b)=\sum_{k=1}^{N}\phi_k(x)\sum_{p=1}^{2}\int_{-\infty}^{+\infty} l_p A_p^j(b) H_k(\omega) e^{i\omega b} d\tilde{G}_p(\omega)+\sum_{p=1}^{2} h_p(x) W_\psi u_p(a_j,b) \tag{6.31}$$

Multiplying both of equation 6.31 by its complex conjugate and taking expectation subsequently and using the relation of the derivative of an evolutionary random process in the Appendix B, it can be shown that the second order moment of the wavelet coefficient of the dynamic response is

$$E\left[W_\psi y^2(x,a_j,b)\right] = E\left[W_\psi y_d^2(x,a_j,b)\right] + E\left[W_\psi y_s^2(x,a_j,b)\right] + E_{sd} \tag{6.32a}$$

where,

$$E\left[W_\psi y_d^2(x,a_j,b)\right] = \sum_{k=1}^{N} 4\pi a_j \phi_k^2(x) \sum_{p=1}^{2}\sum_{q=1}^{2} l_p l_q A_p^j(b) A_q^j(b) \int_{-\infty}^{+\infty} |H_k(\omega)|^2 |\psi(a_j\omega)|^2 S_{pq}(\omega) d\omega \tag{6.32b}$$

$$E\left[W_\psi y_s^2(x,a_j,b)\right] = \sum_{k=1}^{N} 4\pi a_j \sum_{p=1}^{2}\sum_{q=1}^{2} h_p(x) h_q(x) A_p^j(b) A_q^j(b) \int_{-\infty}^{+\infty} |\psi(a_j\omega)|^2 \frac{S_{pq}(\omega)}{\omega^4} d\omega \tag{6.32c}$$

and

$$E_{sd} = \sum_{k=1}^{N} 4\pi a_j \phi_k(x) \sum_{p=1}^{2}\sum_{q=1}^{2} l_p h_q(x) A_p^j(b) A_q^j(b) \int_{-\infty}^{+\infty} \frac{e^{iwb} H_k(\omega) |\psi(a_j\omega)|^2 S_{pq}(\omega)}{\omega^2} d\omega \tag{6.32d}$$

In equation 6.32c, $E_{sd}$ represents the expected value of the square of the wavelet coefficient of the interaction between pseudo static and dynamic component of the total response. Once the second order moment of the wavelet coefficients of the total response $y(x,t)$ is found out, evolutionary power spectral density function $S_{yy}(b,w)$ can be estimated as [Spanos and Failla (2004)]

$$S_{yy}(b,\omega) = \sum_{j=1}^{n_b} C_j(b) \left|\hat{\psi}(a_j\omega)\right|^2 \tag{6.33}$$

where, $n_b$ is the number of frequency scales used in wavelet calculation and $C_j(b)$ is a time dependent coefficient, which can be evaluated by solving the following set of algebraic equations.

$$\begin{bmatrix} Q_{1,1} & Q_{1,2} & \cdots & Q_{1,n_b} \\ Q_{2,1} & Q_{2,2} & \cdots & Q_{2,n_b} \\ \cdots & \cdots & \cdots & \cdots \\ Q_{n_b,1} & Q_{n_b,2} & \cdots & Q_{n_b,n_b} \end{bmatrix} \begin{bmatrix} C_1(b) \\ C_2(b) \\ \vdots \\ C_{n_b}(b) \end{bmatrix} = \begin{bmatrix} E\left[W_\psi y_d^2(x,a_1,b)\right] \\ E\left[W_\psi y_d^2(x,a_2,b)\right] \\ \vdots \\ E\left[W_\psi y_d^2(x,a_{n_b},b)\right] \end{bmatrix} \tag{6.34}$$

In the above equation, elements of the square matrix $Q$ is defined as

$$Q_{r,s} = \int_{-\infty}^{+\infty} \left|\hat{\psi}(a_r\omega)\right|^2 \left|\hat{\psi}(a_s\omega)\right|^2 d\omega \tag{6.35}$$

It may be emphasized that the wavelet transformation of time function *f(t)* presented by equation 6.24 is independent of the choice of the basis function provided it satisfies the admissibility criteria given by equation 1.2.

***Characterization of Input Processes***

It can be observed from equations 6.25 to 6.30 that the input to the simply supported beam at each support is modelled as the product of a stochastic process with appropriate band dependent amplitude modulating function. In the present study, the input motions at the two supports correspond to the stochastic processes with the auto-PSDs $S_{11}$ and $S_{22}$

respectively, each assumed to be equal to $\overline{S}$, which is given by [Spanos and Failla (2004)]

$$\overline{S} = S_{11} = S_{22} = \frac{S_0 \left( \frac{2\eta_g \omega}{\omega_g} \right)^2}{\left[ 1 - \left( \frac{\omega}{\omega_g} \right)^2 \right]^2 + \left( \frac{2\eta_g \omega}{\omega_g} \right)^2} \tag{6.36}$$

where, $\eta_g$ and $\omega_g$ are the natural frequency and damping ratio of the soil at the site and $S_0$ is the intensity of the white noise. The cross PSD function for the joint process between support *1* and *2*, $S_{12}$, is given by

$$S_{12} = \gamma(\omega)\overline{S} = \gamma(\omega)\sqrt{S_{11}(\omega)S_{22}(\omega)} \tag{6.37}$$

where, $\gamma(\omega)$ is the frequency dependent coherence function.

The processes $\ddot{u}_1(t)$ and $\ddot{u}_2(t)$at the two supports can be generated [see Nigam and Narayana (1994)] by using orthogonal decomposition of the PSD matrix and then applying the frequency dependent amplitude modulating function on the generated orthogonal stochastic processes. In this chapter, the following amplitude modulating functions $A_1(t)$ and $A_2(t)$ are used for all frequency bands to modulate the orthogonal stationary processes, which are defined as

$$A_1(t) = A_1^j(t) = \alpha_1[\exp(-t/\beta_1) - \exp(-t/\gamma_1)] \tag{6.38a}$$

$$A_2(t) = A_2^j(t) = \alpha_2[\exp(-t/\beta_2) - \exp(-t/\gamma_2)] \tag{6.38b}$$

## 6.3 Numerical Results and Discussions

The numerical simulation results using the proposed wavelet-based model for non-stationary response analysis are discussed in this section. Even though the formulation is independent of the wavelet basis used, the characteristics of wavelet basis largely affect the end results and hence different wavelet basis functions have been proposed in literature for specific end uses. In the present study two different types of wavelet basis functions are used to evaluate the time dependent stochastic response of the beam, which are – (a) a modified form of LittleWood-Paley (L-P) basis function (section 1.5.2) and (b) Morlet wavelet basis function (section 1.5.3).

### 6.3.1 Short Span Bridge

The wavelet based evolutionary spectral analysis of a simply supported beam as discussed in the previous sections, has been illustrated numerically. The fundamental frequency of the short span bridge is assumed to be *7.5rad/s* while the damping is assumed to be 5% uniformly in all modes. The effects of first two modes are considered in the time-frequency analysis here. An ensemble of *24* ground motions is generated

using SYNACC program based on the parameters of Loma-Prieta earthquake measured at Dumberton bridge site [Trifunac (1990) and Wong and Trifunac (1979)]. Using these ground acceleration, velocity and displacement, evolutionary power spectrum of the total displacement is obtained using equation 6.10. For this purpose, the wavelet coefficients are evaluated for $j = -17$ to 4 and $\sigma = 2^{1/4}$. The parameter '$b$' varies continuously at an interval of 0.2s. Figure 6.2 shows the normalized instantaneous second order moment statistics (i.e. $E\left[y_i^2(x)\right] / \sum E\left[y_i^2(x)\right]$) of the total displacement at the quarter span from the left end support.

A good agreement has been observed between wavelet based result and simulation, which shows the accuracy of the proposed model. Although the variance of the total displacement matches more closely with simulation, when the cross terms (as discussed in equation 6.8) are included, the difference between the approximate wavelet based model (ignoring the cross term) and the exact wavelet based model with cross terms is marginal and is hardly noticeable. Figure 6.3 shows the evolutionary PSD function of the dynamic response at the quarter span of the beam. From this figure, it can be noticed that the proposed wavelet based algorithm effectively accounts for both amplitude and frequency non-stationarity.

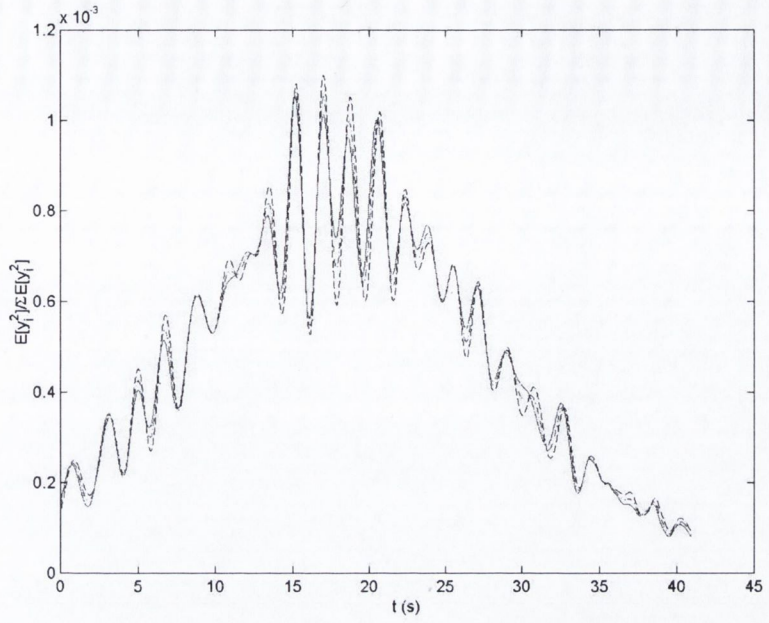


Figure 6.2: Normalized variance of the total response at the quarter span from the left end support: – wavelet, -. wavelet with cross term, -- simulation

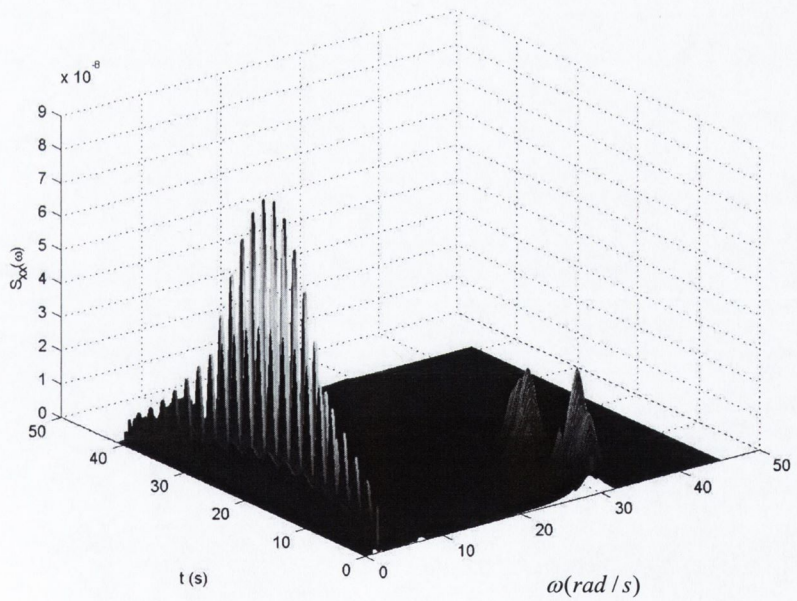


Figure 6.3: PSD of the dynamic response at the quarter span from the left end support

### 6.3.2 Generalized Formulation

The wavelet based model for evolutionary spectral analysis of beam under random differential support motions as discussed in the previous sections, is used for the numerical illustration. For this purpose, two different wavelet basis functions are used. The fundamental frequency of the bridge is assumed to be *3.5rad/s* and the damping ratio is assumed to be 5% in all modes. Effects of first two modes are considered in the time-frequency analysis. Two different cases of vector random processes are used in present study to illustrate the effect of non-stationarity in both intensity and frequency content. In the first case, single amplitude modulated zero mean stationary Gaussian random process is used as discussed in the previous section. An ensemble of 200 ground motion time histories is simulated using equations 6.36 to 6.38 [see Shinozuka and Jan (1972)]. The values of $S_0, \alpha_1, \alpha_2, \beta_1, \beta_2$, $\gamma_1$ and $\gamma_2$ are taken to be 1.0 $cm^2s^{-3}$, 4, 4, 0.25, 0.15, 0.5 and 0.3 respectively. Envelope functions $A_1(t)$ and $A_2(t)$ has maximum value of 1 at 2.5s and *5s* respectively.

Instantaneous root mean square (RMS) value of the total displacement at quarter span from the left support is obtained using equations 6.32a – 6.32b, where the wavelet coefficients are evaluated for $j = -5$ to 14 for modified L-P basis function and $j = 1$ to 3 for Morlet basis function respectively. To ensure the accuracy of the proposed formulation, normalized instantaneous RMS response is compared with Monte-Carlo simulation results. In this context, the normalized RMS response is obtained by dividing

instantaneous RMS value by the maximum RMS response over time (i.e. $\sqrt{E\left[y^2(x,t)\right]}/\max\sqrt{E\left[y^2(x,t)\right]}$). Figure 6.4 shows the normalized RMS value at a

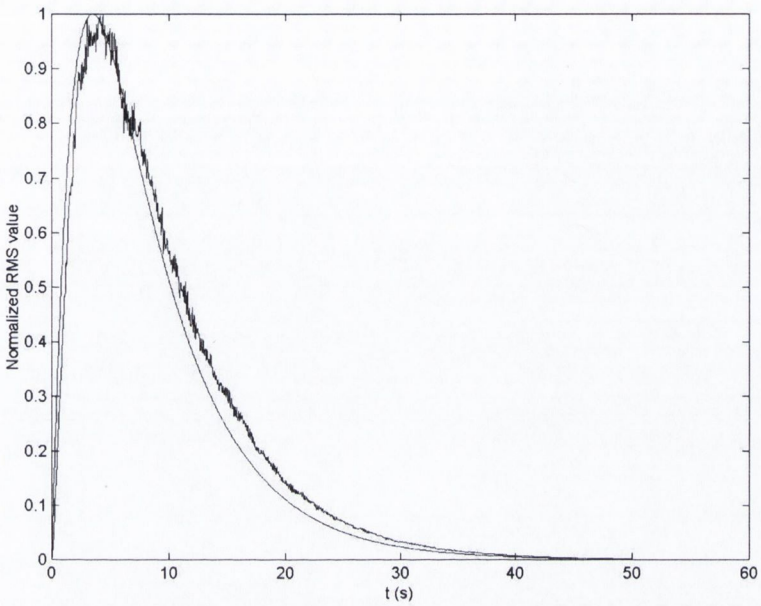


Figure 6.4: Normalized RMS value of the total displacement at l/4 from the left end support; ___ MLP basis, --. Morlet basis and ---- Simulation

distance of l/4 from left end obtained from the proposed wavelet based model and from simulation results obtained by direct time integration. Since the theoretical normalized RMS value corresponds to the average of the amplitude modulations used to model the input processes, an exact match has been observed between two different basis functions. A good agreement between wavelet model and simulation results is observed, which prove the accuracy of the proposed algorithm. The little difference between the wavelet results and the simulation results may be due to the initial transient effect present in the simulation results. Figure 6.5 shows the instantaneous RMS value of the dynamic

response at quarter span for two extreme values of the coherency function $\gamma(\omega)$ i.e. 0 and 1 respectively. It can be noticed that fully correlated support motion has significant effect on the dynamic response as compared to uncorrelated motions. Figures 6.6 and 6.7 show instantaneous PSD of the total response at $t = 4s$ respectively using modified L-P basis function and Morlet basis

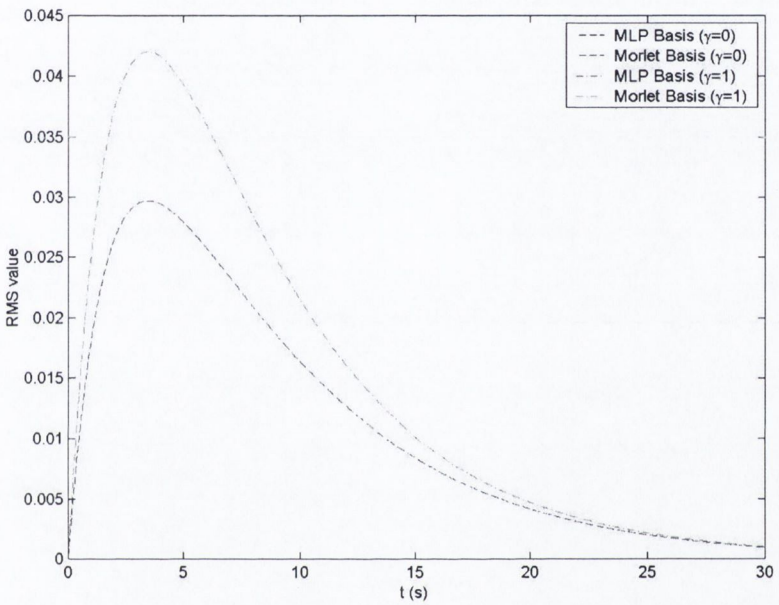


Figure 6.5: RMS value of the total displacement at l/4 from the left end support (Instantaneous RMS values for $\gamma = 0$ and 1 obtained by using ML-P basis function and Morlet basis function exactly match with each other)

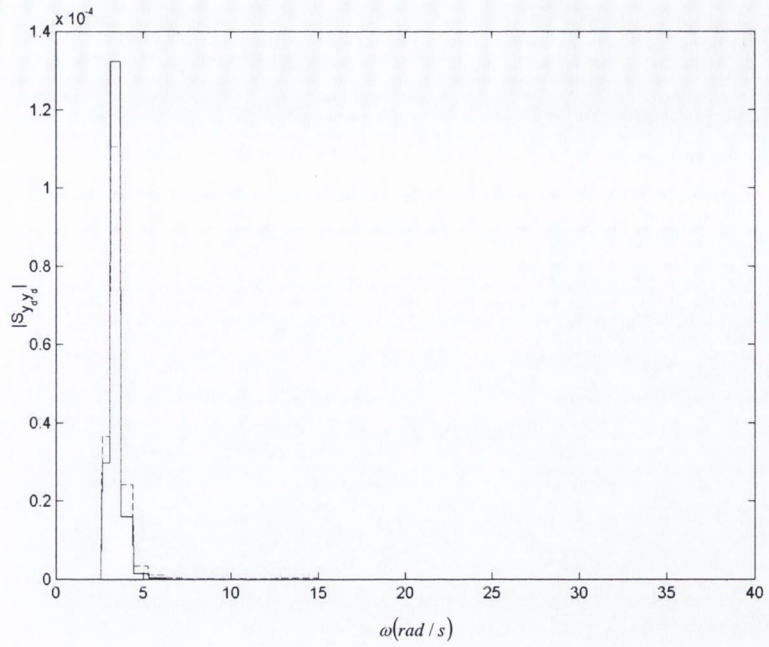


Figure 6.6: Power Spectral Density function of the dynamic response at L/4 from the left end support at $t = 4s$ ($\gamma = 1$); ____ MLP basis and ----Simulation

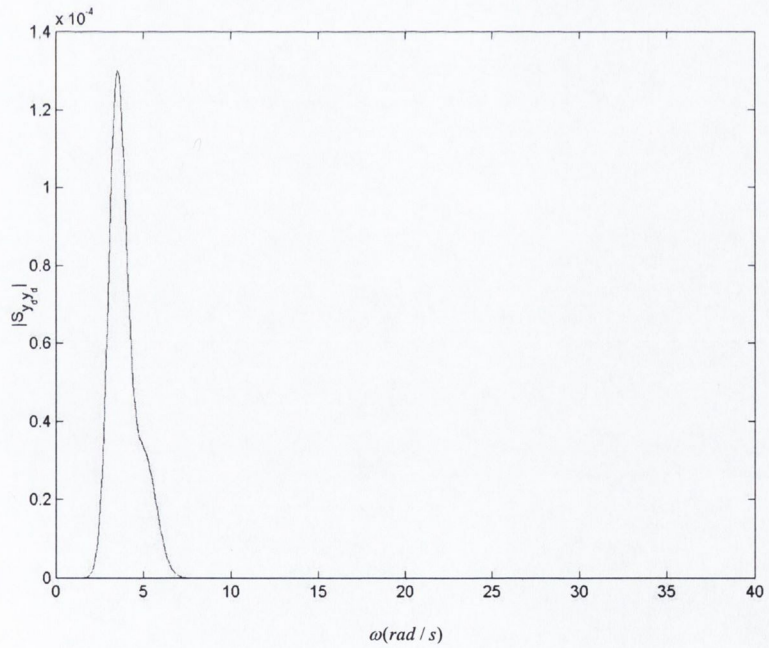


Figure 6.7: Power Spectral Density function of the dynamic response at L/4 from the left end support at $t = 4s$ ($\gamma = 1$); ____ Morlet basis and ----Simulation

function in the proposed model and simulation for $\gamma = 0$. It can be observed that the energy is concentrated around the first natural frequency as expected. Figures 6.8 to 6.11 show PSD of the different displacement responses at the quarter span. From this figure it can be observed that the proposed algorithm can estimate evolutionary spectral response of the dynamical system under non-stationary input. Moreover figures 6.10 and 6.11 show that interaction between dynamic and pseudo static components contribute much in the total response and hence must be considered for the purpose of safe design of the structure.

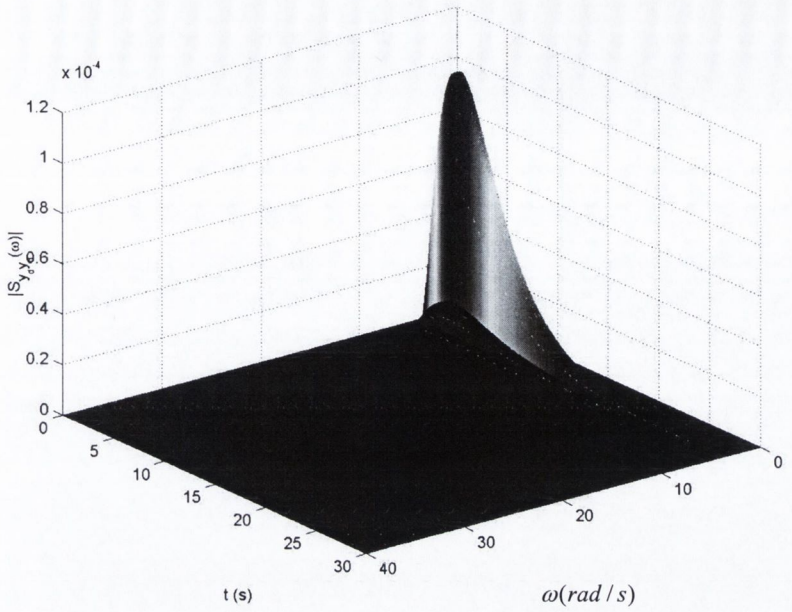


(a)

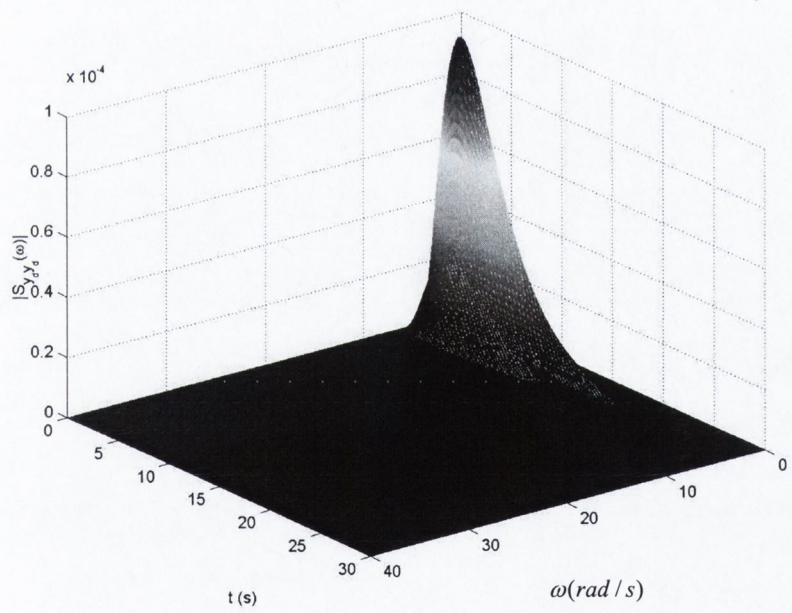


(b)

Figure 6.8: PSDF of the dynamic response at L/4 from the left end support for $\gamma = 1$; (a) ML-P basis and (b) Morlet basis

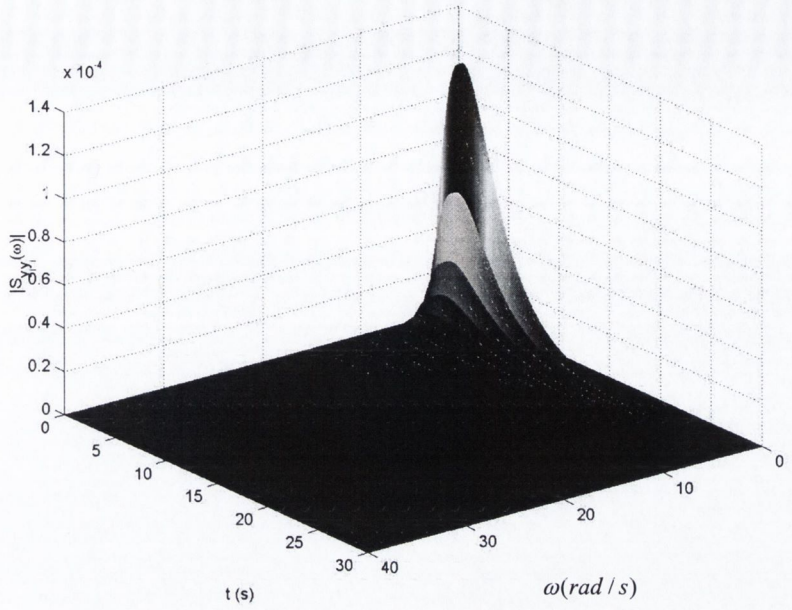


(a)

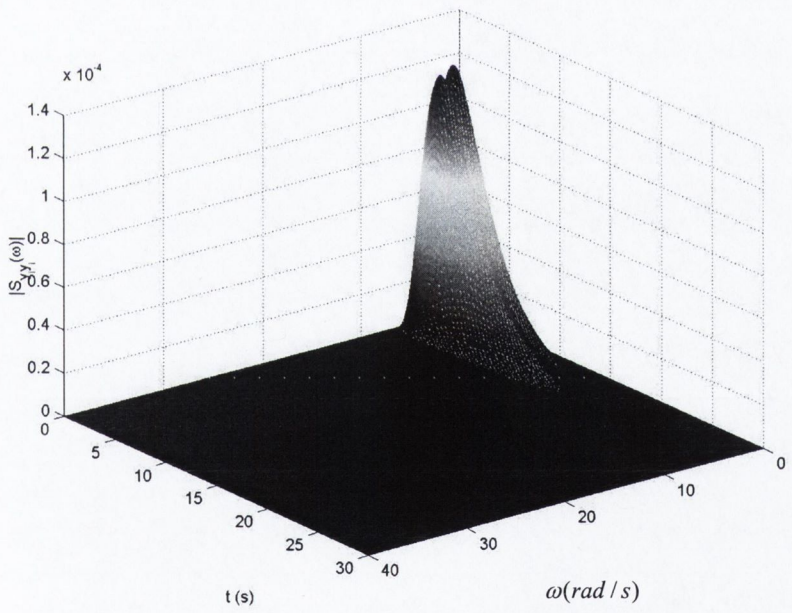


(b)

Figure 6.9: PSDF of the interaction between dynamic and pseudo static responses at L/4 from the left end support for $\gamma = 1$; (a) ML-P basis and (b) Morlet basis

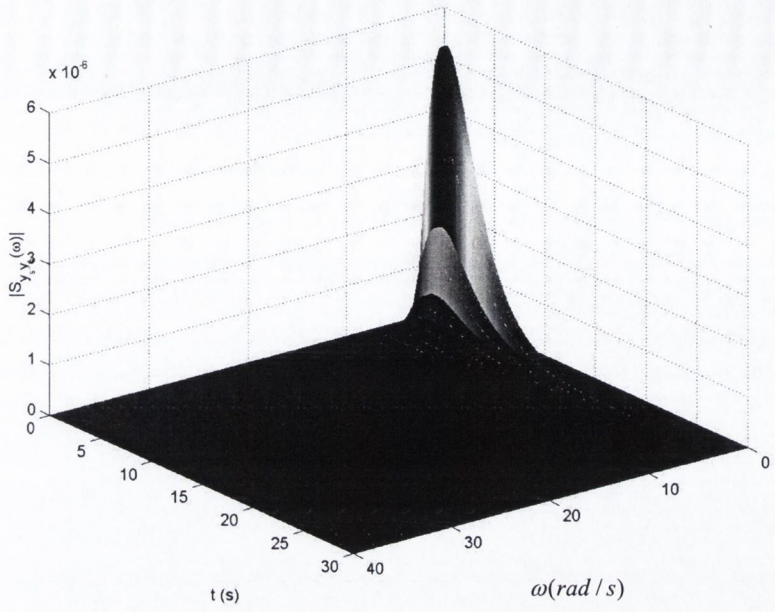


(a)

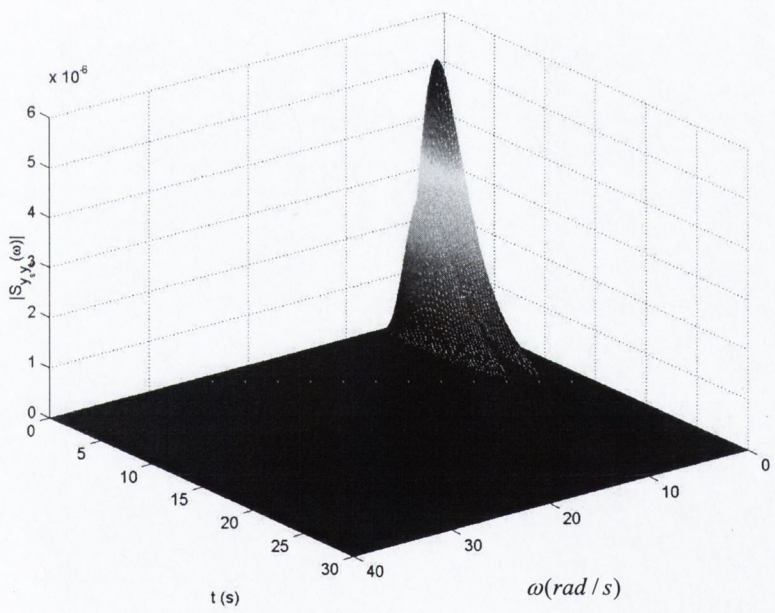


(b)

Figure 6.10: PSDF of the pseudo static response at L/4 from the left end support for $\gamma = 1$; (a) ML-P basis and (b) Morlet basis

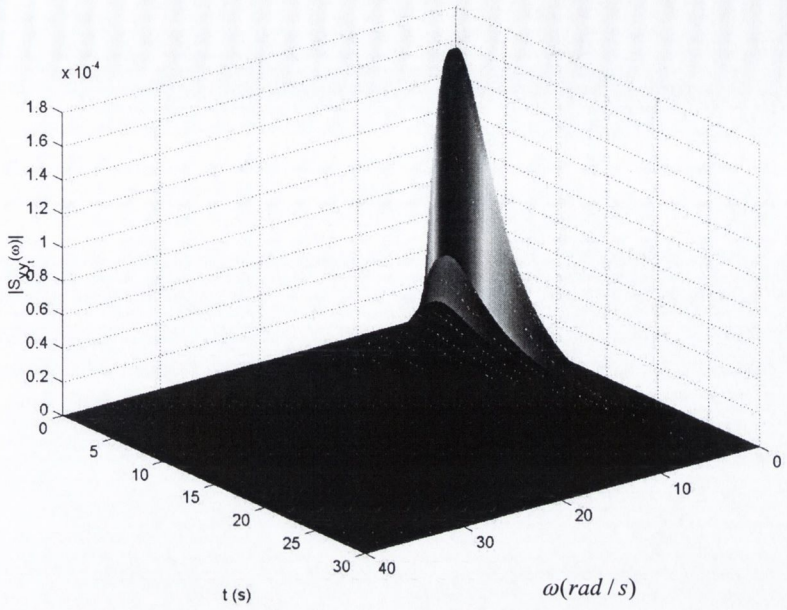


(a)

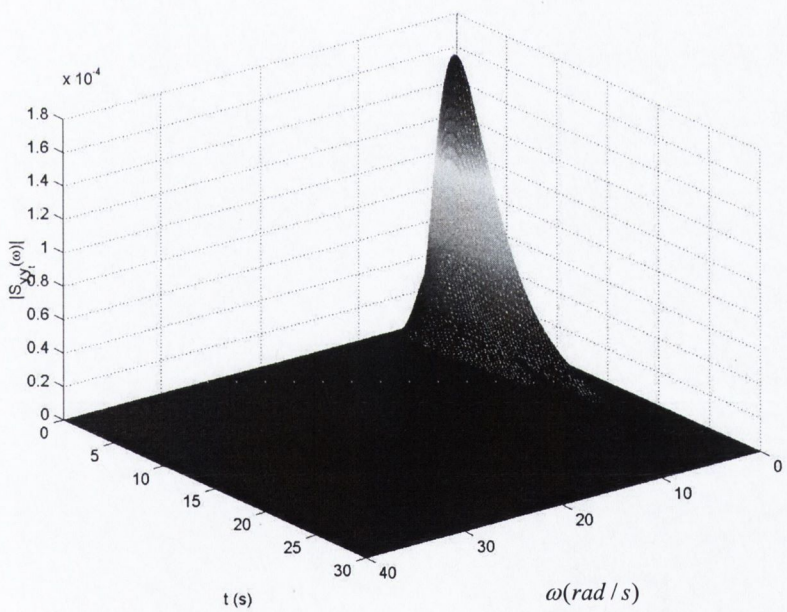


(b)

Figure 6.11: PSDF of the total response at L/4 from the left end support for $\gamma = 1$; (a) ML-P basis and (b) Morlet basis

To illustrate the effect of frequency non-stationary, two independent processes (i.e. $N = 2$) are added together for each support, where the first process is kept same as in case one and the second process is simulated by shifting the peak of the amplitude modulation by *5s*. Figure 6.12 shows the normalized RMS value obtained from wavelet-based model using two different basis functions, which exactly match with each other as has been noticed in the previous case. A good agreement is observed between the proposed model and simulation. Moreover it can be noticed that peaks of two different independent processes arrives at two different time instants, which is typically observed in earthquake ground motions. Figure 6.13 shows the envelopes of RMS value for coherence function varying from 0 to 1. Figures 6.14 to 6.17 show evolutionary PSD function of different response components. From these figures, one can notice that the proposed wavelet based model can evaluate non-stationary response with non-stationarity in both intensity and frequency content and hence can be used for the purpose of evolutionary spectral response analysis of the dynamical systems.

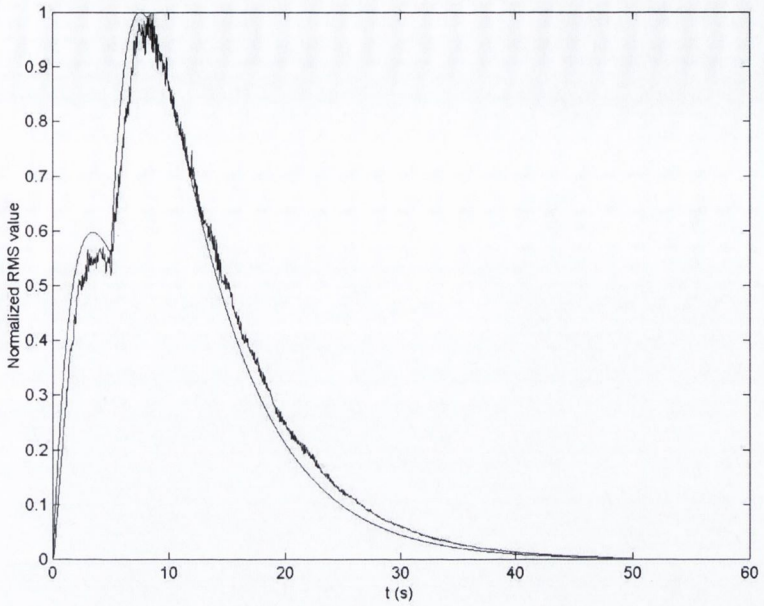


Figure 6.12: Normalized RMS value of the total displacement at l/4 from the left end support; ___ MLP basis, --. Morlet basis and ---- Simulation

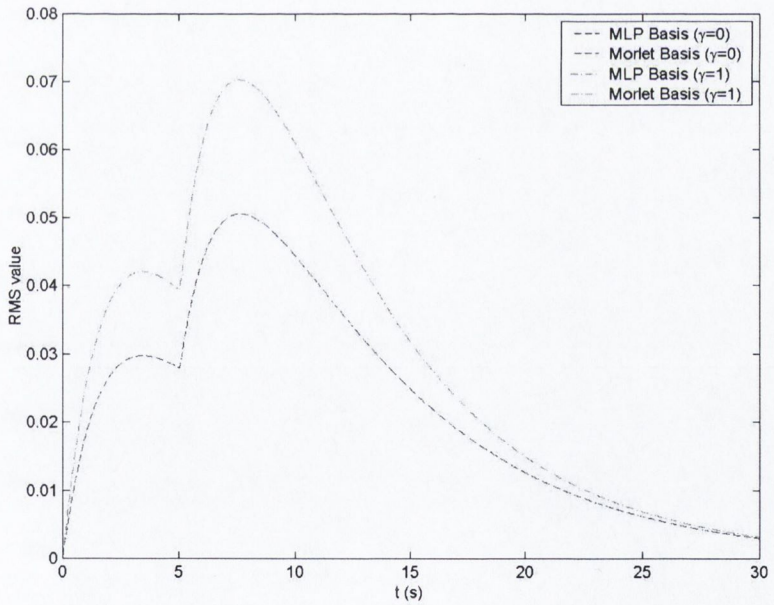


Figure 6.13: RMS value of the total displacement at l/4 from the left end support (Instantaneous RMS values for $\gamma = 0$ and 1 obtained by using ML-P basis function and Morlet basis function exactly match with each other)

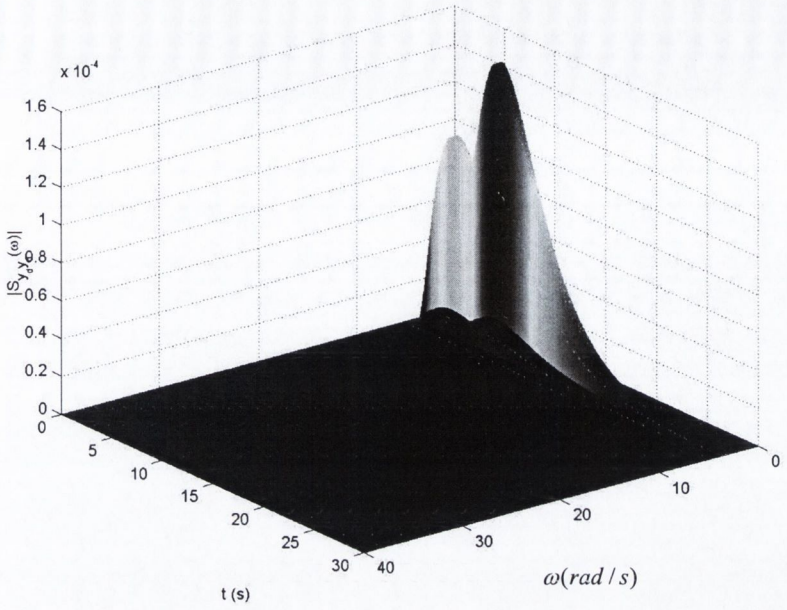


(a)

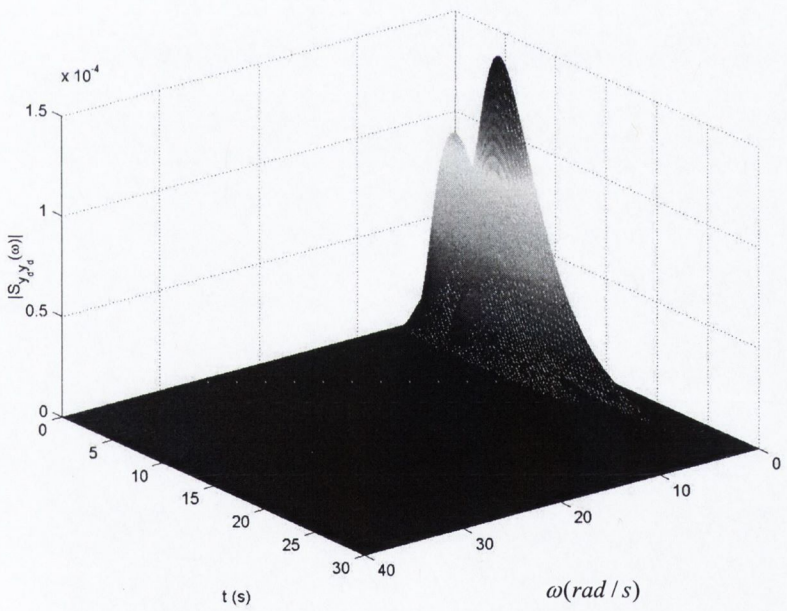


(b)

Figure 6.14: PSDF of the dynamic response at L/4 from the left end support for $\gamma = 1$; (a) ML-P basis and (b) Morlet basis

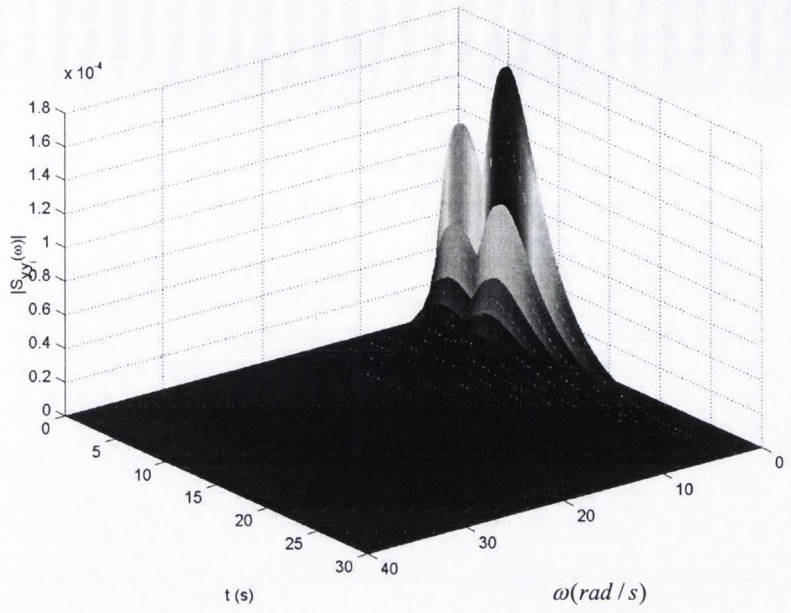


(a)

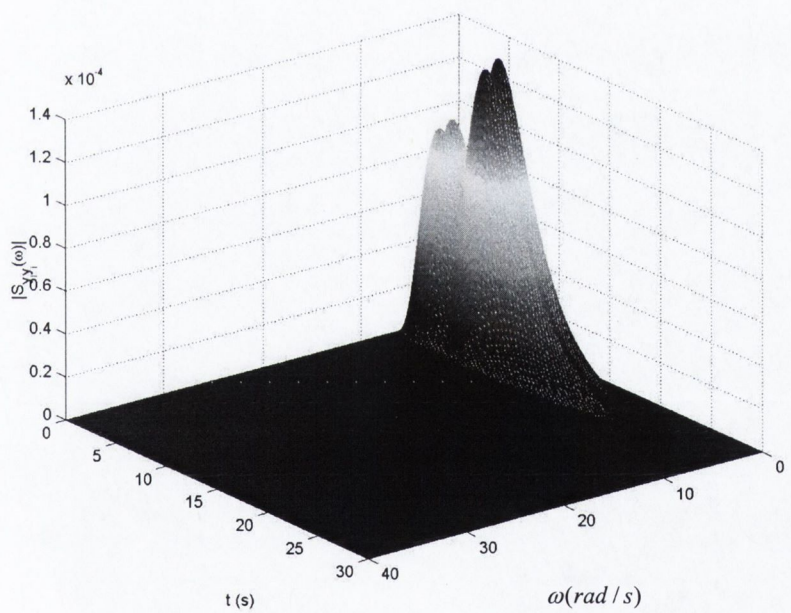


(b)

Figure 6.15: PSDF of the interaction between dynamic and pseudo static responses at L/4 from the left end support for $\gamma = 1$; (a) ML-P basis and (b) Morlet basis

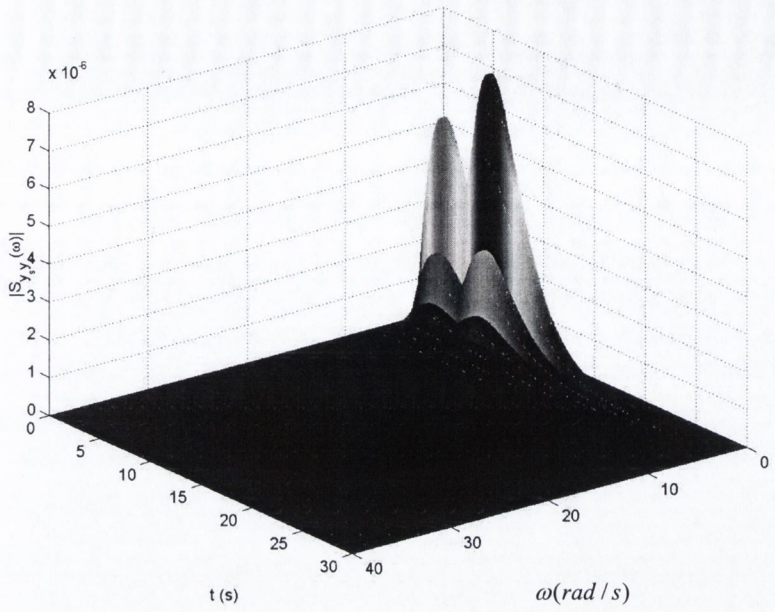


(a)

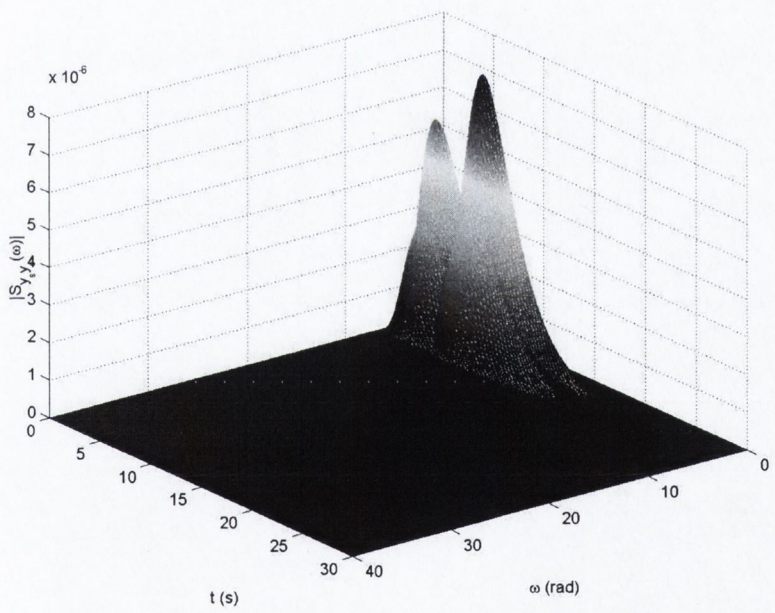


(b)

Figure 6.16: PSDF of the pseudo static response at L/4 from the left end support for $\gamma = 1$; (a) ML-P basis and (b) Morlet basis

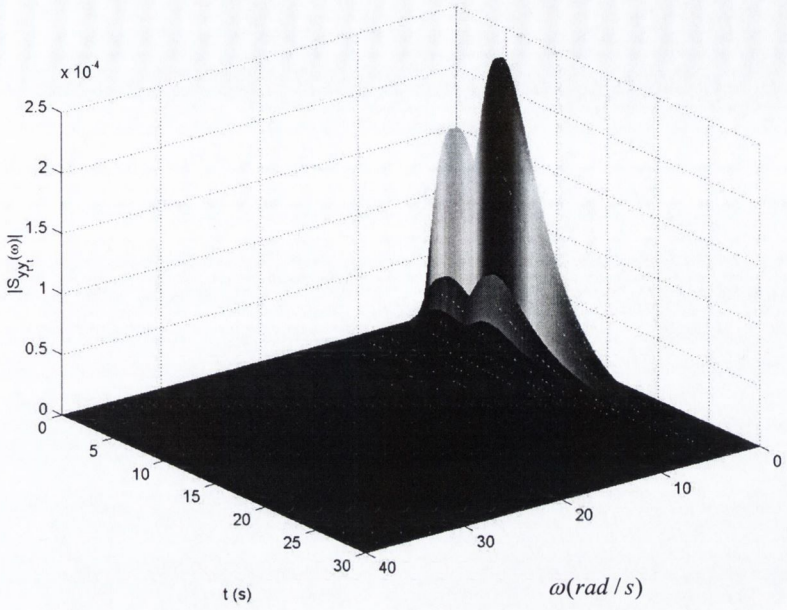


(a)

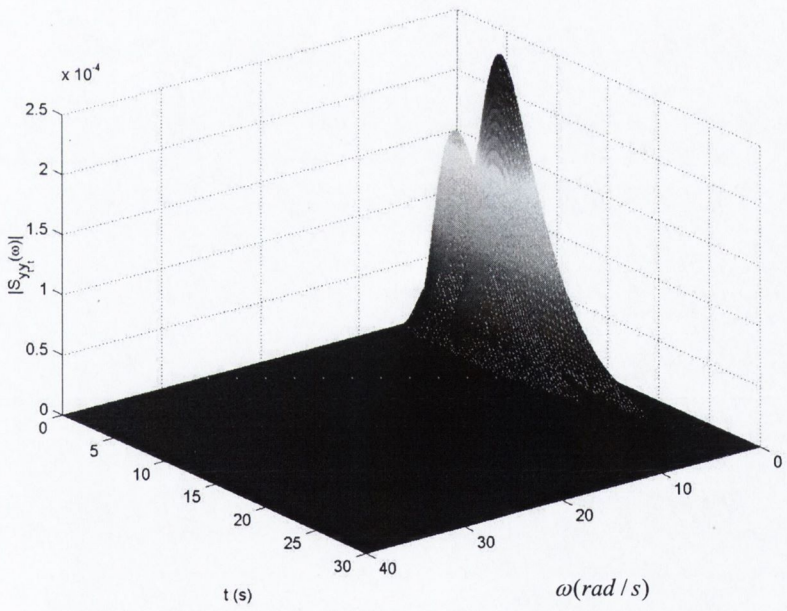


(b)

Figure 6.17: PSDF of the total response at L/4 from the left end support for $\gamma = 1$; (a) ML-P basis and (b) Morlet basis

## 6.4 Conclusions

A wavelet based method for non-stationary response analysis of short span bridge has been presented here. Time dependent stochastic response is evaluated based on the interaction between response in different modes as well as dynamic and pseudo static components. The numerical results presented here show the efficiency and accuracy of the proposed algorithm. The modified form of L-P basis function used in the present study is completely localized in frequency and thus can evaluate stochastic response in non-overlapping frequency bands. The proposed wavelet based methodology is more effective than conventional non-stationary response analysis as it can account frequency non-stationarity more efficiently.

Next, a generalised wavelet based method for non-stationary response analysis of simply supported beam subjected to random differential support motions is presented here. The proposed methodology is easier to implement than conventional evolutionary spectral analysis using Fourier-Stieltz integral as it estimates time variant stochastic response from the input stochastic process using conventional frequency response function and deterministic envelope functions at different scales in wavelet domain. In this context, the ease of the proposed method lies in construction of wavelet coefficients of the response directly from the stochastic description of the input process without evaluating the wavelet coefficients of the input time signal, and hence computationally more efficient. Moreover, there is no assumption is made on the choice of the wavelet basis function to evaluate the time dependent stochastic response. The proposed wavelet based methodology can evaluate time dependent frequency content of the response and

hence is more generalized than conventional technique for non-stationary response analysis. The numerical results presented show the efficiency and accuracy of the proposed algorithm. Furthermore the present methodology can be extended to the non-stationary response analysis of multi degree of freedom system as well as non-linear systems via equivalent linearization.

# Chapter 7: Non-stationary Response Analysis of Discrete Systems

## 7.1 Introduction

An evolutionary spectral analysis of boundary value problem is presented in Chapter 6 with the input-output relation established using continuous system model coupled with wavelet transform. In this chapter, discrete systems in finite element framework are considered.

First of all, an input-output relation for the response of a long span bridge subjected to random differential support motions is proposed in the present chapter. The bridge has been modelled as a multi-span simply supported beam in the finite element (FE) framework to obtain the dynamic properties. The non-stationary spatially varying earthquake ground motions (SVEGM) at different supports are characterized following a generalized wavelet-based formulation as proposed in Chapter 5.

Next, a wavelet-based non-stationary response analysis of a typical primary-secondary (P-S) system is proposed in this chapter, where the secondary piping network is housed inside the secondary structure. The examples of these structures are mechanical instruments installed inside buildings, piping network in industry or in nuclear power plants. The stiffness and damping characteristics of the two sub-systems vary considerably and hence give rise to a system with non-classical damping. The P-S system is modelled as MDOF system and the primary structure is subjected to random support motions with non-stationarity in both amplitude and frequency content.

## 7.2 Wavelet-Based Representation of the Response

The wavelet-based response analysis of multi-supported structural systems such as large span bridges, primary-secondary systems is discussed in the following sections.

### 7.2.1 Structures Subjected to SVEGM

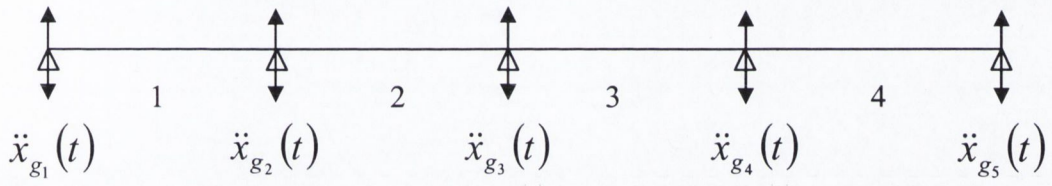


Figure 7.1: Simply supported bridge with four spans subjected to spatially varying ground motion

A simply supported bridge as shown in figure 7.1 is considered in the present study, which is subjected to differential support motions. The bridge is modeled in the Finite Element (FE) framework using 2D beam elements (for details, see Appendix C). The governing equation of motion is given by

$$[M]\{\ddot{X}\}+[C]\{\dot{X}\}+[K]\{X\}=-[M][I]\{\ddot{x}_{g_r}\} \tag{7.1}$$

where, $\{X(t)\}$ represents the vertical displacement vector relative to the vertical support motions, which are represented by $\{\ddot{x}_{g_r}\}, r = 1,2,...n$ . In equation 7.1, $[M]$, $[C]$ and $[K]$ are the $N \times N$ mass, damping and stiffness matrices and $I$ is the $N \times n$ influence matrix for the differential support motions. In the present study, the formulation is proposed in a generalized framework such that the proposed model can be applicable for systems with either classical or non-classical damping. For this purpose, the governing equation is expressed in state-space, which is given by

$$[A]\{\dot{y}\} + [B]\{y\} = \{Q(t)\} \tag{7.2}$$

where, $A = \begin{bmatrix} [0] & [M] \\ [M] & [C] \end{bmatrix}$, $B = \begin{bmatrix} -[M] & [0] \\ [0] & [K] \end{bmatrix}$, $\{y\} = \begin{Bmatrix} \{\dot{X}\} \\ \{X\} \end{Bmatrix}$ and $\{Q(t)\} = \begin{Bmatrix} \{0\} \\ -[M]\{I\}\{\ddot{x}_g(t)\} \end{Bmatrix}$

are the $2N \times 2N$ matrices. Equation 7.2 has $2N$ complex eigen values and it can be decoupled using the $2N \times 2N$ complex eigen vector $\Phi$. Using this complex eigen vector, equation 7.2 can be decoupled by the following transformation, which is given by

$$\{y\} = [\Phi]\{z\} \tag{7.3}$$

Using this transformation, governing equation of motion can be expressed into a set of uncoupled first order differential equations as

$$\dot{z}_k + \gamma_k z_k = f_k = \sum_{r=1}^{n} \chi_k^r \ddot{x}_{g_r}(t) \; k = 1,..., N \tag{7.4}$$

On taking wavelet transform of both sides of equation 7.4, the $k^{th}$ modal response $z_k$ in the wavelet domain can be expressed as [see Basu and Gupta (2000)]

$$\frac{\partial}{\partial b} W_\psi z_k(a_j,b) + \gamma_k W_\psi z_k(a_j,b) = \sum_{r=1}^{n} \chi_k^r W_\psi \ddot{x}_{g_k}(a_j,b) \tag{7.5}$$

In the present study, the wavelet-based model for SVEGM as proposed in section 5.3.2 is used for ground motion characterization. The solution of equation 7.5 can be evaluated using Duhamel's integral, which is given by

$$W_\psi z_k(a_j,b) = \sum_{r=1}^{n} \chi_k^r \int_{-\infty}^{+\infty} M_{r_j}^k(\omega,b) e^{i\omega b} d\tilde{G}_r(\omega) \tag{7.6}$$

where,

$$M_{r_j}^k(b,\omega) = \int_0^b h_k(b-\tau) A_j^r(\tau) e^{i\omega(\tau-b)} d\tau \tag{7.7}$$

From the above equation, it may be noticed that the unit impulse response function $h_k(\tau)$ oscillates at a faster rate as compared to the deterministic envelope functions $A_j^r(\tau)$. Furthermore, wavelet transformation provides localized frequency information of a time function around $t = b$. Using this time localization property of the wavelet

transformation along with less oscillatory nature of the band dependent envelope functions, equation 7.7 can be approximated as

$$M_{r_j}^{k}(b,\omega) \approx A_j^k(b)\int_0^b h_k(b-\tau)e^{-i\omega(b-\tau)}d\tau \approx A_j^k(b)H_k(\omega) \tag{7.8}$$

where, $H_k(\omega)$ is the conventional frequency response function in $k^{th}$ mode and is given by

$$H_k(\omega) = \frac{1}{\omega + i\gamma_k} \tag{7.9}$$

On taking wavelet transform of both sides of equation 7.3, it can be shown that

$$W_\psi x_p(a_j,b) = \sum_{k=1}^{N_d} \Phi_{p,k} W_\psi z_k(a_j,b) \tag{7.10}$$

where, $W_\psi x_p(a_j,b)$ is the wavelet coefficient of relative displacement at $p^{th}$ degree of freedom. It can be shown that the auto-correlation of the relative displacement of the $p^{th}$ degrees of freedom in wavelet domain is given by

$$E\left[W_\psi^2 x_p(a_j,b)\right] = \sum_{k=1}^{N_d}\sum_{m=1}^{N_d} \Phi_{p,k}\Phi_{p,l} E\left[W_\psi z_k(a_j,b) W_\psi z_m(a_j,b)\right] \tag{7.11}$$

On using the expressions of $W_\psi z_k(a_j,b)$ and $W_\psi z_m(a_j,b)$ as given in equations 7.6 and 7.8 respectively and simplifying it can be shown that the second order moment of the relative displacement along $p^{th}$ degrees of freedom is given by

$$E\left[W_\psi^2 x_p(a_j,b)\right] = \sum_{k=1}^{N_d}\sum_{m=1}^{N_d} 2\Phi_{p,k}\Phi_{p,l}\sum_{r=1}^{N_i}\sum_{l=1}^{N_i}\chi_k^r\chi_k^l A_r^j(b)A_l^j(b-\tau)\int_0^\infty f_j(\omega)d\omega \qquad (7.12)$$

where,

$$f_j(\omega) = 2\pi a_j\left|H_k(\omega)\right|^2 S_{rl}(\omega)\left|\psi(a_j\omega)\right|^2 \qquad (7.13)$$

In the above equation, $S_{rl}(\omega)$ represents cross-power spectrum between the supports '*r*' and '*l*', as discussed in equation 5.25.

***Systems with Classical Damping: Special Case***

The proposed model for non-stationary response analysis can be used in classical damping framework. In this case, damping matrix $C$ is expressed as a summation of scaled mass and stiffness matrices $M$ and $K$ respectively. i.e.

$$C = \alpha M + \beta K \qquad (7.14)$$

Using the above expression for $C$ in the governing equation of motion, equation 7.1 can be decoupled by following transformation

$$X = \widetilde{\Phi} Z \tag{7.15}$$

where, $\widetilde{\Phi}$ is the real $N \times N$ eigenvector obtained from eigen analysis of mass and stiffness matrices without considering damping. Using equation 7.15, the governing equation of motion can be expressed as

$$\ddot{z}_k + 2\eta_k \omega_k \dot{z}_k + \omega_k^2 z_k = \sum_{r=1}^{n} \chi_k^r \ddot{x}_g(t) \tag{7.16}$$

On taking wavelet transformation of both sides of equation 7.16, the dynamic equilibrium in $k^{th}$ mode can be expressed as

$$\frac{\partial^2}{\partial b^2} W_\psi z_k(a_j, b) + 2\eta_k \omega_k \frac{\partial}{\partial b} W_\psi z_k(a_j, b) + \omega_k^2 W_\psi z_k(a_j, b) = \sum_{r=1}^{n} \chi_k^r W_\psi \ddot{x}_{g_k}(a_j, b) \tag{7.17}$$

The solution of the equation in kth mode can be obtained using Duhamel's integral, which is given by equation 7.6 to 7.8, with only difference lies evaluation of frequency response function $H_k(\omega)$, which is given by

$$H_k(\omega) = \frac{1}{\omega_k^2 - \omega^2 + 2\eta_k \omega_k i\omega} \tag{7.18}$$

***Evaluation of Response Power Spectrum***

Using the second order moment of the wavelet coefficients of the relative displacement $x_p(t)$, evolutionary power spectral density function $S_{pp}(b,w)$ can be estimated as [see Spanos and Failla (2004)]

$$S_{pp}(b,\omega)=\sum_{j=1}^{n_b} C_j(b)\left|\hat{\psi}(a_j\omega)\right|^2 \tag{7.19}$$

where, $n_b$ is the number of frequency scales used in wavelet calculation and $C_j(b)$ is a time dependent coefficient, which can be evaluated by solving the following set of algebraic equations.

$$\begin{bmatrix} Q_{1,1} & Q_{1,2} & \cdots & Q_{1,N_d} \\ Q_{2,1} & Q_{2,2} & \cdots & Q_{2,N_d} \\ \cdots & \cdots & \cdots & \cdots \\ Q_{N_d,1} & Q_{N_d,2} & \cdots & Q_{N_d,N_d} \end{bmatrix} \begin{bmatrix} C_1(b) \\ C_2(b) \\ \vdots \\ C_{N_d}(b) \end{bmatrix} = \begin{bmatrix} E\left[W_\psi x_1^2(x,a_1,b)\right] \\ E\left[W_\psi x_2^2(x,a_2,b)\right] \\ \vdots \\ E\left[W_\psi x_{N_d}^2(x,a_{n_b},b)\right] \end{bmatrix} \tag{7.20}$$

In the above equation, elements of the square matrix $Q$ is defined as

$$Q_{r,s}=\int_{-\infty}^{+\infty}\left|\hat{\psi}(a_r\omega)\right|^2\left|\hat{\psi}(a_s\omega)\right|^2 d\omega \tag{7.21}$$

### 7.2.2 Numerical Results and Discussions

The wavelet-based model of the long span bridge as discussed in the previous section is used for numerical illustration. The bridge has four spans as shown in figure 7.1. Each span is assumed to 100m long. The first five natural frequency of the bridge are 0.34, 0.40, 0.53, 0.69 and 1.50 *rad/s*. Although, the proposed model can evaluate non-stationary response of a system for both classical and non-classical damping, present numerical illustration is performed using modal damping only, which is assumed to be constant in all modes and is taken to be 5%. The ground motion is modelled as summation of random processes in different frequency bands.

In each frequency band, the random process is modelled as a product of a deterministic envelope function and a stochastic orthogonal process. An exponential envelope function as proposed by Shinozuka and Sato (1967) is considered here. Table 5.1 shows the value of the parameters of the envelope function for left end support. In the present study, 28 different frequency bands ranging from 0.045rad/s to 30rad/s is used to model the support motions. A logarithmic discretization as proposed by Basu and Gupta (1998) is introduced in the present study. For this purpose, the parameter $\sigma$ in equation 7.12 is taken to be $2^{1/4}$. Figure 7.2 shows the envelope function for left end support corresponding to the frequency band 5, 15 and 28 corresponding to the frequency ranges 0.9907-1.1781rad/s, 5.6040-6.6643rad/s and 53.3146-63.4021rad/s respectively. A wave velocity of 1000m/s is assumed in the present study. Based on the distance of the other supports from the left end, a time shift has been introduced in these envelope functions such that different waves with different frequency arrives at the other supports

accordingly. Besides deterministic frequency dependent amplitude modulation, present model for earthquake ground motions require characterization of stochastic orthogonal processes for different supports and their spatial coherence functions. For this purpose, the orthogonal stochastic process is modelled by Kanai-Tajimi spectra as discussed in section 5.3. Table 7.1 shows the values of $S_0$, $\omega_g$ and $\eta_g$ to evaluate the Kanai-Tajimi spectra as described in equation 6 for different supports. Figure 7.3 shows the orthogonal spectra used for different supports. Using these envelope functions and orthogonal processes in different frequency bands, earthquake ground motion is simulated for the left end support, a sample of which is shown in figure 7.4. It can be observed that the simulated time history shows an initial build up phase, intermediate strong motion phase and finally an exponentially decaying phase, which is typically observed in strong motion accelerograms. In the present study, five different spatial coherence functions are used as given in Appendix A. Figure 7.5 shows

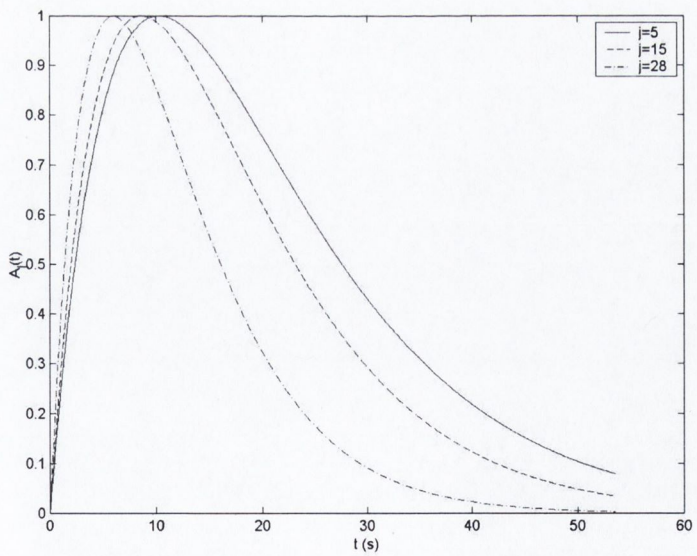


Figure 7.2: Envelope functions in ifferent frequency bands for left end support

| Support Number | $S_0$ | $\eta_g$ (%) | $\omega_g$ (rad/s) |
|---|---|---|---|
| 1 | 1.00E-04 | 0.4 | 10 |
| 2 | 1.20E-04 | 0.5 | 20 |
| 3 | 5.00E-05 | 0.4 | 5 |
| 4 | 7.00E-05 | 0.6 | 12 |
| 5 | 1.40E-04 | 0.4 | 15 |

Table 7.1: Parameters for orthogonal stochastic processes in different supports

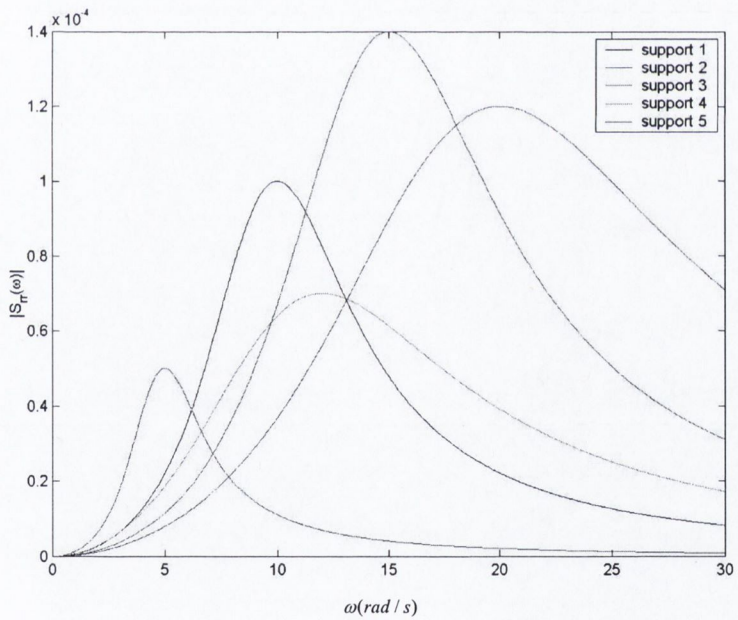


Figure 7.3: Orthogonal processes used for different supports

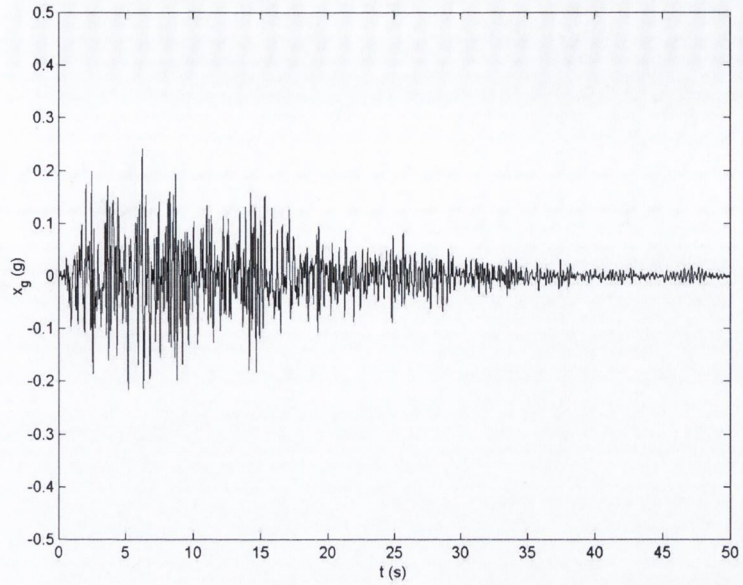


Figure 7.4: Simulated time history of the ground motion for left end support

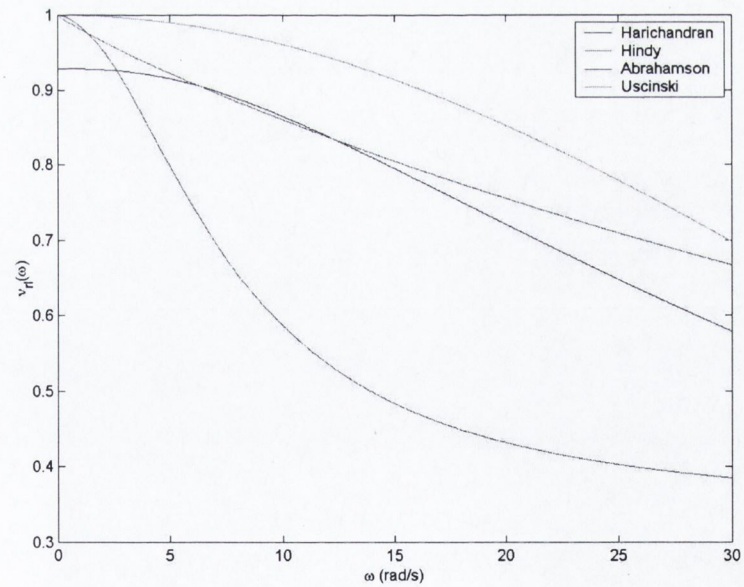


Figure 7.5: Coherency function used for spatial correlation; ___ Abrahamson model, ___ Hindy model, ___ Hao model, ___ Harichandran model and ___ Uscinski model.

different coherence functions used for numerical analysis. It can be noticed that the model proposed by Abrahamson decays much faster as compared to the other models.

Using these models for ground motions as input, non-stationary response analysis is performed as discussed in the section 7.2.1. The beam is modelled in FE framework using 2D beam element, which has four degrees of freedom (DOF) per element. The details of element mass and stiffness matrices are given in Appendix C. First a sensitivity analysis is performed to identify the optimum number of elements to be used in the FE analysis. For this purpose, displacement at the mid point of the left end span is considered. Figure 7.8 shows the root mean square value (RMS) of the displacement obtained using 2, 4, 8 and 10 elements per span respectively. It can be noticed that the solution converges after 8 elements. Using this optimum number of

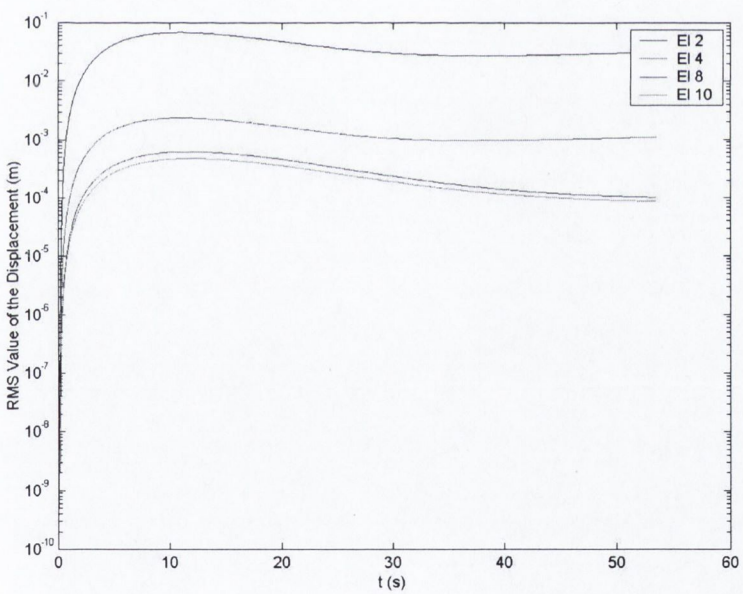


Figure 7.6: RMS value of the displacement at mid point of the left end span for various numbers of elements per span

elements per span, a non-stationary response analysis is performed. Two different locations on span 1 and span 2 are considered for numerical illustration. These are quarter point and the mid point from the left end of the respective spans. Figures 7.7 and 7.8 shows the time varying power spectral density of the displacement at quarter point and mid point in span 1, while figures 7.9 and 7.10 show the same for span 2. It can be noticed that most of the response energy is concentrated in a frequency range of 0 to 5 rad/s, which contains the first five natural frequencies. Furthermore, these figures reveal that the response is non-stationary with peaks of different frequencies arriving at different time instants, which depicts the necessity of proper mathematical model to realise the behaviour of the structures subjected to input with time varying frequency content.

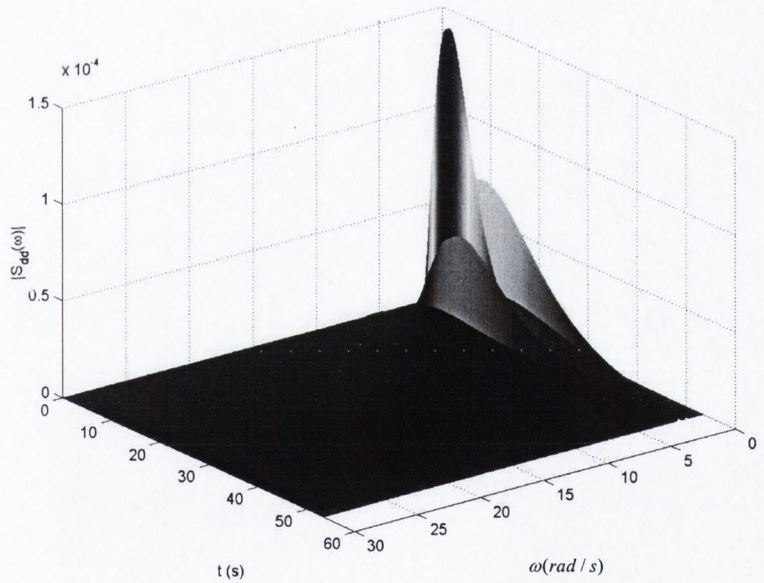


Figure 7.7: PSD of relative displacement at quarter point from left end support of span 1

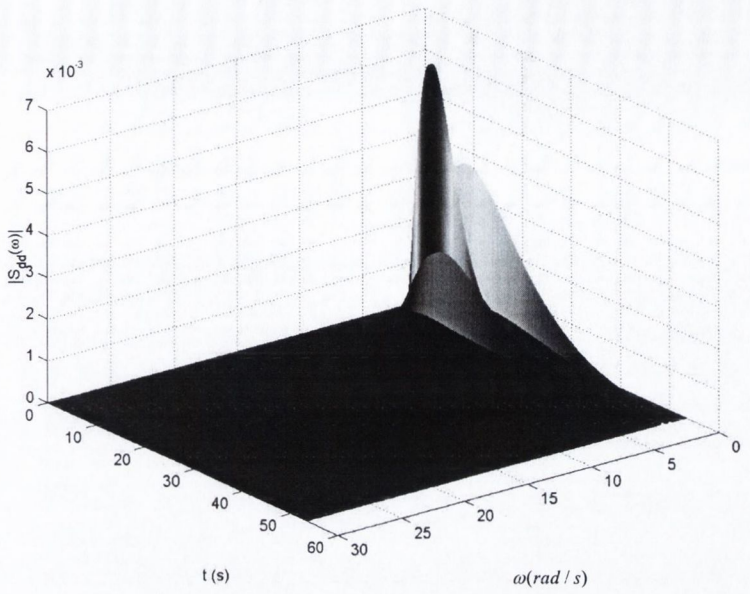


Figure 7.8: PSD of relative displacement at mid point from left end support of span 1

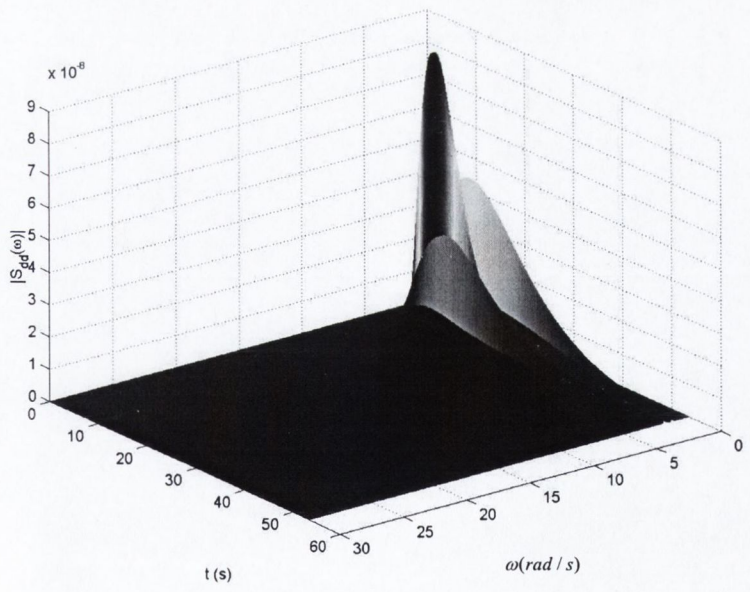


Figure 7.9: PSD of relative displacement at quarter point from left end support of span 2

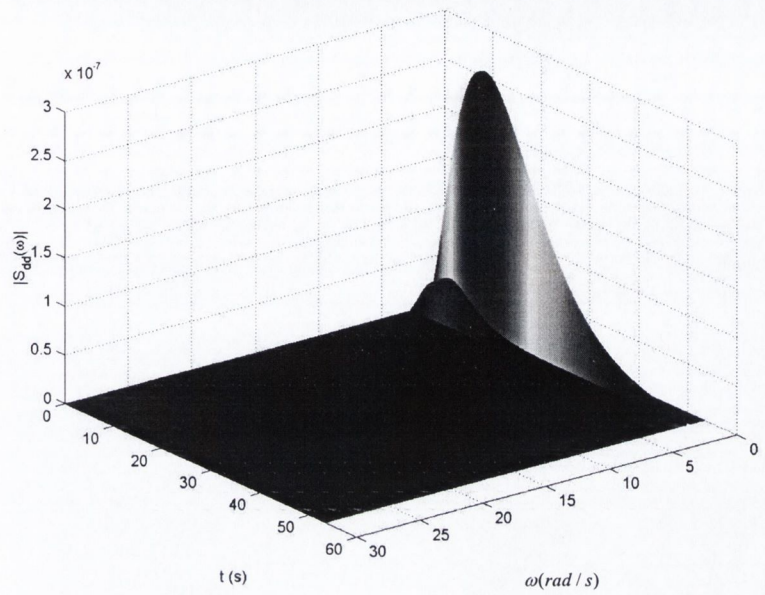


Figure 7.10: PSD of relative displacement at mid point from left end support of span 2

Since, the structural response attains maximum value at different time instants and in different vibration modes, the present observation reveals that the design based on the peak response in the fundamental mode or ignoring the effect of frequency non-stationarity might lead to non-conservative design for extended structures.

Figures 7.11 to 7.14 show the RMS value of the displacement at mid point of the left end span for span length of 50m, 100m, 150m and 200m respectively. The RMS value is obtained using five different spatial coherence models as discussed in Appendix A. A close match has been noticed between the responses obtained from different coherence models for a span length of 50m except for the model proposed by Hao. As the span length increases, the response obtained from Harichandran and Vanmarcke model estimates less than other models while the response obtained using the model proposed

by Hao provide conservative results. Therefore, from these figures, it can be noticed that the proposed wavelet based model can evaluate non-stationary response with non-stationarity in both intensity and frequency content and hence can be used for the purpose of evolutionary spectral response analysis of the extended structures subjected to spatially varying ground motion.

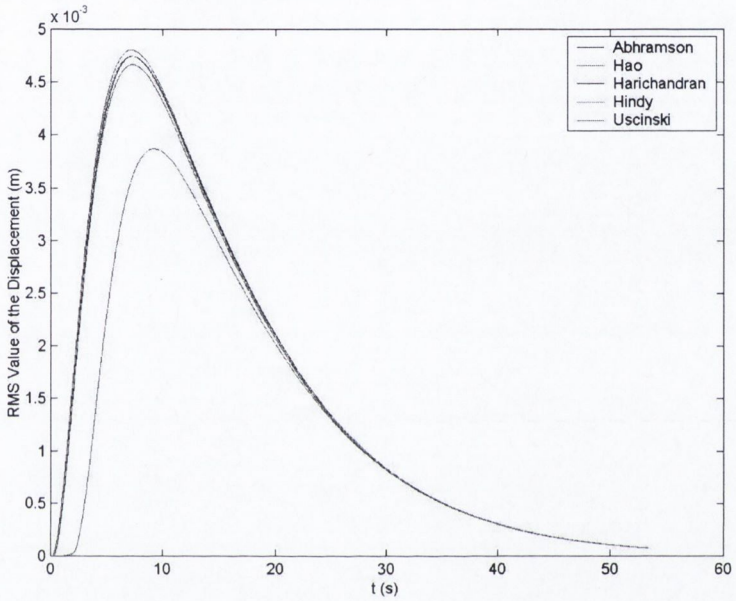


Figure 7.11: RMS value of the displacement at mid point of the left end span for span length of 50m

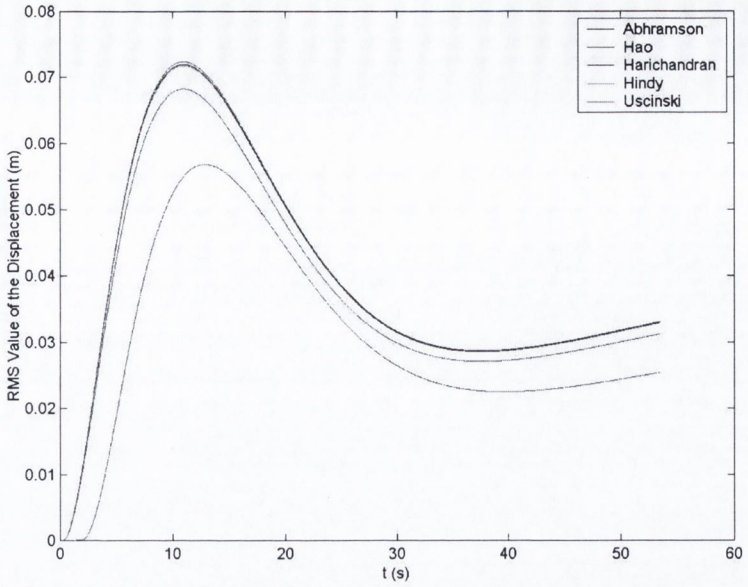


Figure 7.12: RMS value of the displacement at mid point of the left end span for span length of 100m

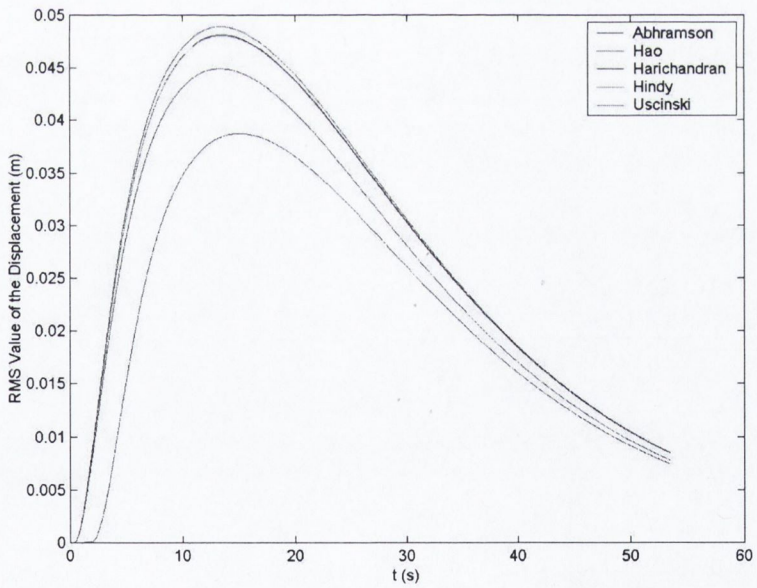


Figure 7.13: RMS value of the displacement at mid point of the left end span for span length of 150m

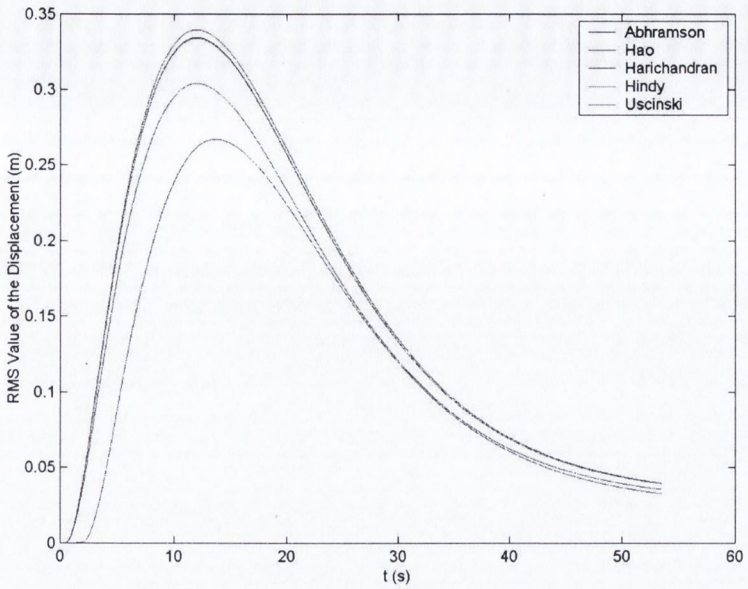


Figure 7.14: RMS value of the displacement at mid point of the left end span for span length of 200m

## 7.3 P-S Systems Subjected to Evolutionary Support Motion

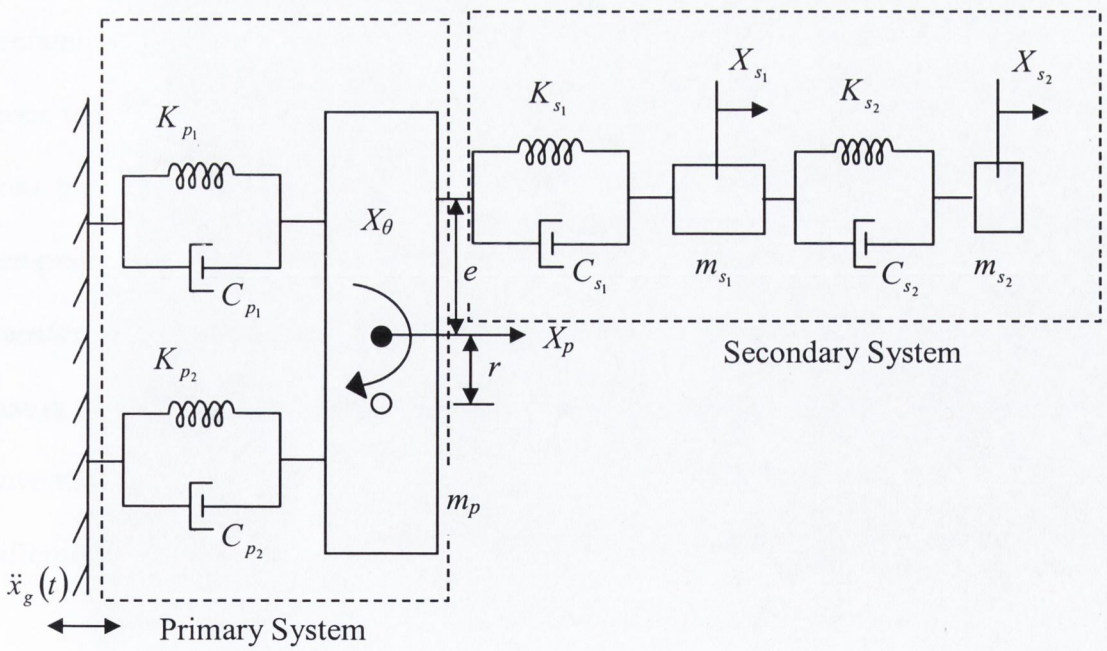


Figure 7.2: Torsionally coupled P-S system; ● CG and ○ Center of rotation

Figure 7.15 shows a P-S system that has been considered in the present study. The combined system is subjected to a support motion of $\ddot{x}_g(t)$ as shown in figure 7.15. The governing equation of motion of the combined system is given by

$$[M]\{\ddot{X}\}+[C]\{\dot{X}\}+[K]\{X\}=-[M]\{I\}\ddot{x}_g(t) \tag{7.22}$$

where, $[M]$, $[C]$ and $[K]$ represent mass, damping and stiffness matrices respectively and $\{I\}$ is the influence vector of the support motion. The details of $[M]$, $[C]$ and $[K]$ and $\{I\}$ can be found in Appendix D. Over dot in equation 7.22 represents differentiation with respect to time. $\{X\}$ $(=\{X_p, X_\theta, X_{s_1}, X_{s_2}\}^t)$ is the displacement vector of the P-S system relative to the support motion $x_g(t)$. Due to wide variation of material properties and damping characteristics between the primary and secondary systems, classical modal decoupling based on real eigen values does not exist. To overcome this problem, a state-space representation of equation 7.22 is proposed in the literature where the decoupling is done based on the complex modal matrix obtained from the eigen-analysis considering damping matrix, as given by equation 7.2, which can be decoupled using the transformation given by equation 7.3. In the equation 7.3, $\Phi$ is the complex modal matrix obtained from eigen-analysis of the matrices $A$ and $B$. Using this transformation, governing equation of motion can be expressed into a set of uncoupled first order differential equations as

$$\dot{z}_k+\gamma_k z_k=f_k=\alpha_k\ddot{x}_g(t) \quad k=1,2,....n \tag{7.24}$$

### 7.3.1 Wavelet Based Evolutionary Response Analysis of P-S System

On taking wavelet transform of both sides of equation 7.24, the $k^{th}$ modal response $z_k$ in the wavelet domain can be expressed as [see Basu and Gupta (2000)]

$$\sum_i \sum_j \frac{1}{a_j} W_\psi z_k(a_j, b_i)\left\{\dot{\psi}_{a_j,b_i}(t) + \gamma_k \psi_{a_j,b_i}(t)\right\} = \alpha_k \sum_i \sum_j \frac{1}{a_j} W_\psi \ddot{x}_g(a_j, b_i)\psi_{a_j,b_i}(t) \quad (7.25)$$

where,

$$\alpha_k = \left[\Phi^t A \Phi\right]^{-1} \Phi^t Q \quad (7.26)$$

It may be noticed that on taking wavelet transform of equation 7.24, differentiation of the $k^{th}$ modal response $z_k$ with respect to time '$t$' is shifted over the known wavelet basis function $\psi_{a_j,b_i}(t)$ and the dynamic equilibrium equation is established through the wavelet coefficients. On taking Fourier transform of both sides of equation 7.25, it can be shown that

$$\sum_i \sum_j \frac{1}{a_j} W_\psi z_k(a_j, b_i)\hat{\psi}_{a_j,b_i}(\omega) = \alpha_k \sum_i \sum_j \frac{1}{a_j} W_\psi \ddot{x}_g(a_j, b_i) H_k(\omega)\hat{\psi}_{a_j,b_i}(\omega) \quad (7.27)$$

where, $H_k(\omega)$ is the $k^{th}$ modal response function [$H_k(\omega) = 1/(\omega + i\gamma_k)$] and $\hat{\psi}_{a_j,b_i}(\omega)$ is the Fourier transform of the basis function $\psi_{a_j,b_i}(t)$. Multiplying both sides of equation

7.27 by its complex conjugate and taking expectation, it can be shown that the cross correlation at a scale '$j$' between the wavelet coefficients of the responses in $k^{th}$ and $l^{th}$ mode is given by

$$\sum_i E\left[W_\psi z_k(a_j,b_i) W_\psi z_l(a_j,b_i)\right] = \sum_i \alpha_k \alpha_l E\left[W_\psi^2 \ddot{x}_g(a_j,b_i)\right] \int_{-\infty}^{+\infty} H_k(\omega) H_l^*(\omega) \left|\hat{\psi}_{a_j,b_i}(\omega)\right|^2 d\omega \quad (7.28)$$

On taking wavelet transform of both sides of equation 7.24 and multiplying by its complex conjugate and using equation 7.28, it can be shown that the total expected energy of the relative displacement along $R^{th}$ degree of freedom in $j^{th}$ frequency band is given by [for details, see Basu and Gupta (1998)]

$$\int_{-\infty}^{+\infty} E\left[\left|X_R^j(\omega)\right|^2\right] d\omega = \int_{-\infty}^{+\infty} \sum_i \frac{\overline{K}\Delta b}{a_j} E\left[W_\psi^2 \ddot{x}_g(a_j,b_i)\right] \sum_m \sum_n \phi_R^m \phi_R^n \alpha_m \alpha_n H_m(\omega) H_n^*(\omega) \left|\hat{\psi}_{a_j,b_i}(\omega)\right|^2 d\omega \quad (7.29)$$

In the above expression, $\phi_R^m$ represents the $R^{th}$ element of the $m^{th}$ mode shape. Using Parseval's identity and equation 7.29, the instantaneous mean square energy of the relative displacement along the $R^{th}$ degree of freedom can be expressed as

$$E\left[X_R^2(t)\right]_{t=b_i} = \sum_j \frac{\overline{K}}{a_j} E\left[W_\psi^2 \ddot{x}_g(a_j,b_i)\right] \int_{-\infty}^{+\infty} \sum_m \sum_n \phi_R^m \phi_R^n \alpha_m \alpha_n H_m(\omega) H_n^*(\omega) \left|\hat{\psi}_{a_j,b_i}(\omega)\right|^2 d\omega \quad (7.30)$$

It can be noticed that, as the value of $\sigma$ tends to unity in the expression for $\hat{\psi}_{a_j,b_i}(\omega)$, the above integral equation can be assumed to be valid point-wise. Thus, using the relation given by equation 7.30 in point wise sense, the instantaneous power spectral density of the relative displacement along $R^{th}$ degrees of freedom can be expressed as

$$S^i_{x_R x_R}(\omega) = \sum_j \frac{E\left[\left|X^j_R(\omega)\right|^2\right]}{\Delta b}$$

$$= \sum_j \frac{\overline{K}}{a_j} E\left[W^2_\psi \ddot{x}_g(a_j,b_i)\right] \sum_m \sum_n \phi^m_R \phi^n_R \alpha_m \alpha_n H_m(\omega) H^*_n(\omega) \left|\hat{\psi}_{a_j,b_i}(\omega)\right|^2 \qquad (7.31)$$

### 7.3.2 Numerical Results and Discussions

Using the proposed wavelet-based input-output relation for P-S systems, numerical analysis is performed to establish the efficiency and accuracy of the proposed model, especially in the light of non-stationary amplitude and frequency content. Figure 7.2 shows the P-S system considered in the present study. It can be seen that the secondary structure is modelled as a 2DOF system with masses $m_{s_1}$ and $m_{s_2}$, linear springs $K_{s_1}$ and $K_{s_2}$ and dampers $c_{s_1}$ and $c_{s_2}$, which are mounted over a torsionally coupled primary system. The primary system consists of a mass ($m_p$) supported by two linear springs ($K_{p_1}$ and $K_{p_2}$) and dampers ($C_{p_1}$ and $C_{p_2}$) respectively, allowing it to turn around its centre of rotation, which is situated at a distance '$r$' from the centre of gravity. The

details of the mass, stiffness and damping properties are given in Table 7.3. The damping is assumed to be 5% and 20% for primary and secondary system respectively. The natural frequencies of the P-S system are 0.9980, 8.3475, 10.6201 and 33.9064rad/s respectively.

| | |
|---|---|
| $m_p$ | 10 kg |
| $m_{s1}$ | 0.5 kg |
| $m_{s2}$ | 0.5 kg |
| $K_{p1}=K_{p2}$ | 1000 N/m |
| $K_{s1}$ | 500 N/m |
| $K_{s2}$ | 45 N/m |
| $e$ | 0.6 m |
| $r$ | 3 m |

Table 7.2: Structural properties of the P-S system

The combined damping matrix is obtained from inverse analysis of the individual modal damping. From the values of these parameters, it can be shown that the secondary system is tuned at the fundamental frequency of the primary system. It can be observed from equation 7.32 that the input-output relation of the P-S system is established through the second order moment statistics. In the present study, numerically simulated samples of the Loma-Prieta earthquake using SYNACC program [Trifunac (1990), Wong and Trifunac(1979)] based on the parameters measured at the Dumbarton Bridge site is used. Figure 7.16a shows a sample time history of the Loma-Prieta earthquake. From this figure, it can be observed that the input has non-stationary amplitude as well as frequency content. Using an ensemble of 20 time histories, expected value of the wavelet coefficients of the ground motion is evaluated, which is the basis of the proposed input-output relation as established in equation 7.32. For this purpose, a modified form of LP

basis function as proposed by Basu and Gupta (1997) is used to calculate the wavelet coefficients. Besides having temporal decaying characteristics similar to dynamical system, this basis is completely localized in frequency. Hence it does not suffer from problems due to band overlapping. This frequency localization characteristic of the LP basis function simplifies the evaluation of the energy in equation 7.30 as compared to other basis function [for details see Basu and Gupta (1998)]. The input wavelet coefficients are evaluated for $j = -17$ to 4 and $\sigma = 2^{1/4}$ while parameter '$b$' varies continuously at an interval of 0.02s. Figure 7.16b shows a typical displacement time history of the secondary response $X_{s_1}$ relative to support due to the support motion, which is shown in figure 7.16a. For the design of P-S systems, the assumption of cascading approximation is common in the engineering practise. It is generally assumed that the output of the primary system acts as an input of the secondary system, where the interaction between primary and secondary system is ignored. Figures 7.17 and 7.18 show the secondary system response $X_{s_1}$ obtained from exact time history integration with interaction between P-S system and using cascading approximation, when the secondary system is tuned and de-tuned at the first natural frequency of the primary system respectively. It can be noticed that although during de-tuning, the initial response of the secondary system obtained using cascading approximation and exact simulation are similar in their absolute values, the frequency signature of the responses are completely different when the cascading approximation is made. From this observation, it can be concluded that cascading approximation lead to erroneous results especially when the input has evolutionary frequency content. Figures 7.19(a), 7.19(b), 7.19(c), 7.20(a),

7.20(b), 7.21(a) and 7.21(b) show the time history of the secondary response $X_{s_1}$ obtained from time history simulations with interaction between P-S system for different ratios of the mass of the secondary system $m_{s_1}$ to the primary mass $m_p$ and the energy of these time histories in different frequency bands. From these figures, it may be noticed that the response has time dependent frequency content at low mass ratio with significant energy contribution in different frequency bands. Besides ratio of the primary and secondary masses, rotational inertia also plays vital role on the evolutionary nature of the frequency content of the response of the P-S systems. Figures 7.22(a) and 7.22(b) show the response of the secondary $X_{s_1}$ for different values of '*r*' and figures 7.23(a) and 7.23(b) show their respective time varying frequency content of the energy spectrum.

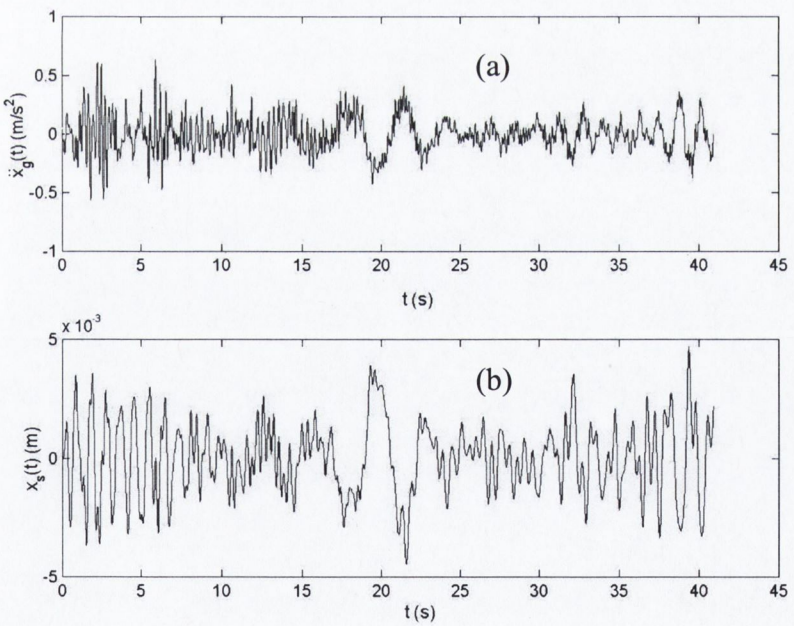


Figure 7.16: Time history at input and output; (a) input and (b) displacement response ($X_{s_1}$) of the secondary system

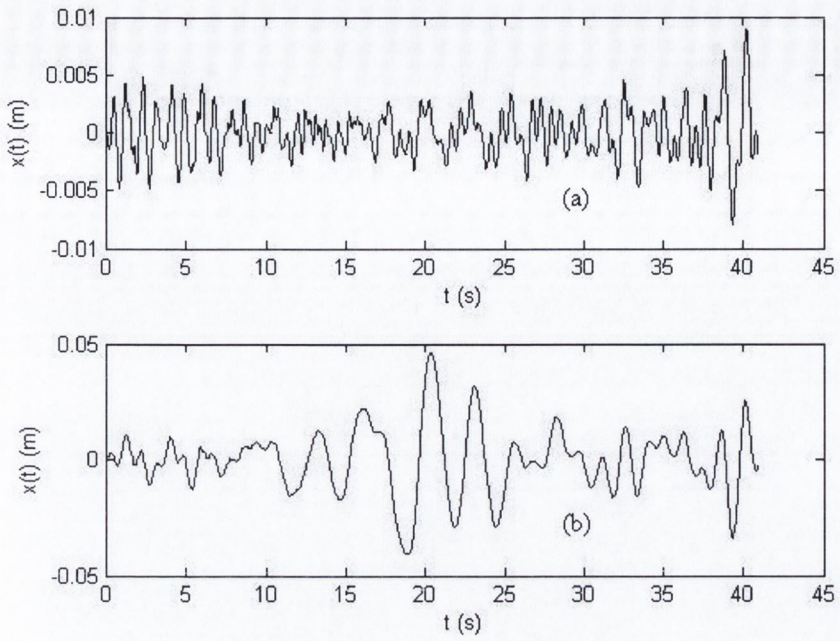


Figure 7.17: Time history of the secondary response $X_{s_1}$ when the secondary system is tuned with primary system; (a) interaction between the P-S system and (b) cascading approximation between the P-S systems

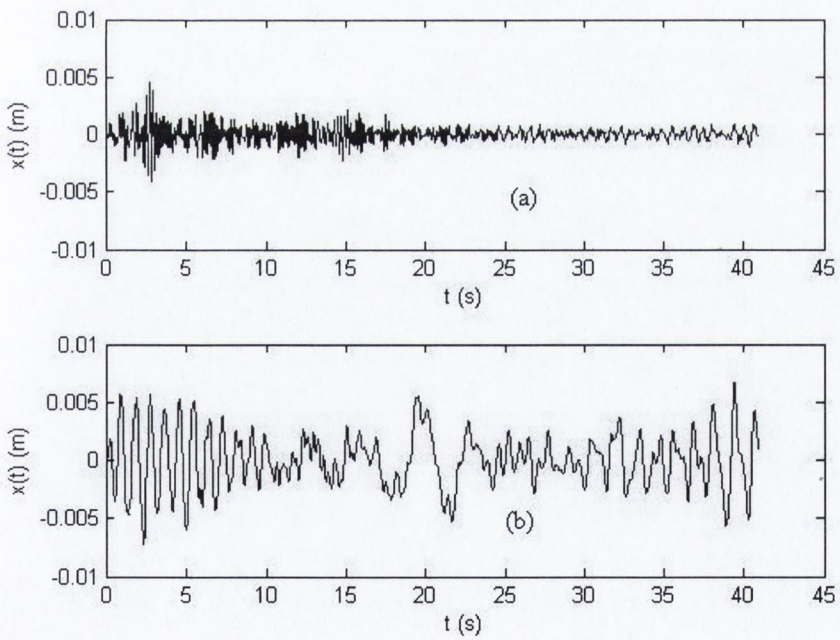


Figure 7.18: Time history of the secondary response $X_{s_1}$ when the secondary system is de-tuned with primary system; (a) interaction between the P-S system and (b) cascading approximation between the P-S systems

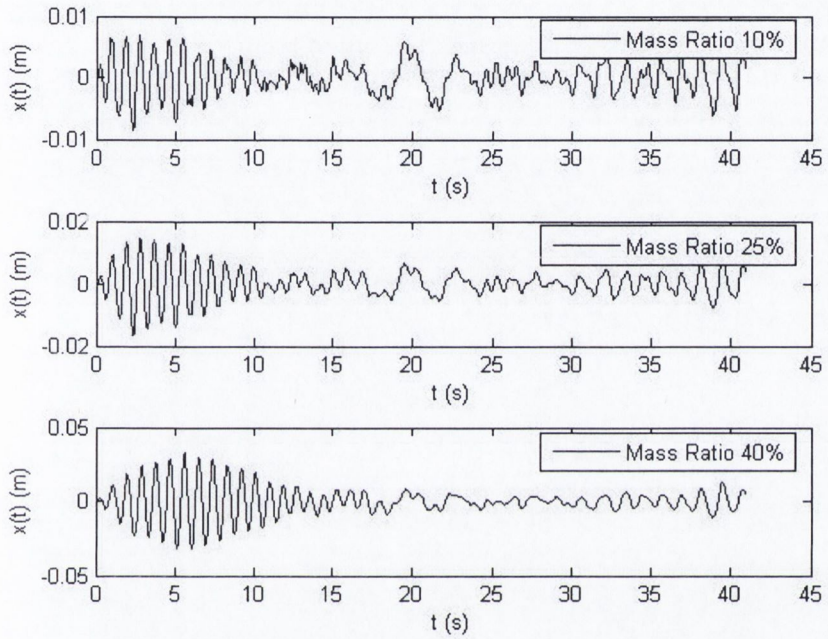


Figure 7.19: Time history of the secondary response $X_{s_1}$ for different mass ratios of the P-S system

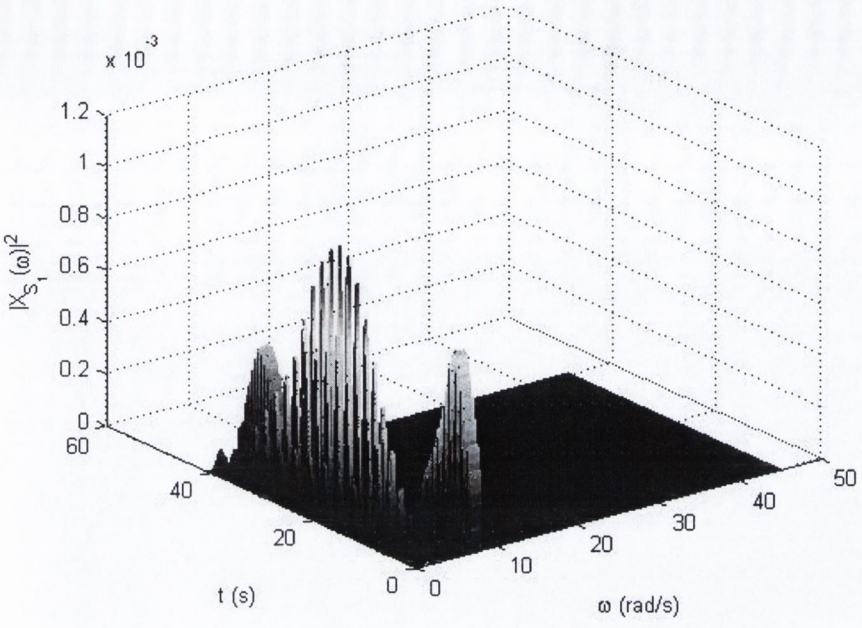


(a)

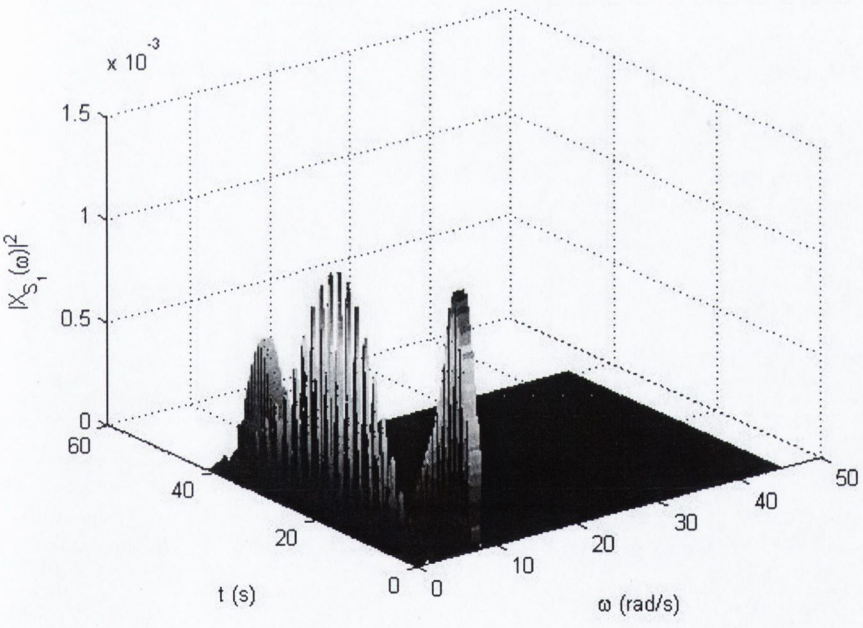


(b)

Figure 7.20: Time varying energy spectrum of the secondary response $X_{s_1}$ for different mass ratios of the P-S system; (a) 5% mass ratio and (b) 10% mass ratio

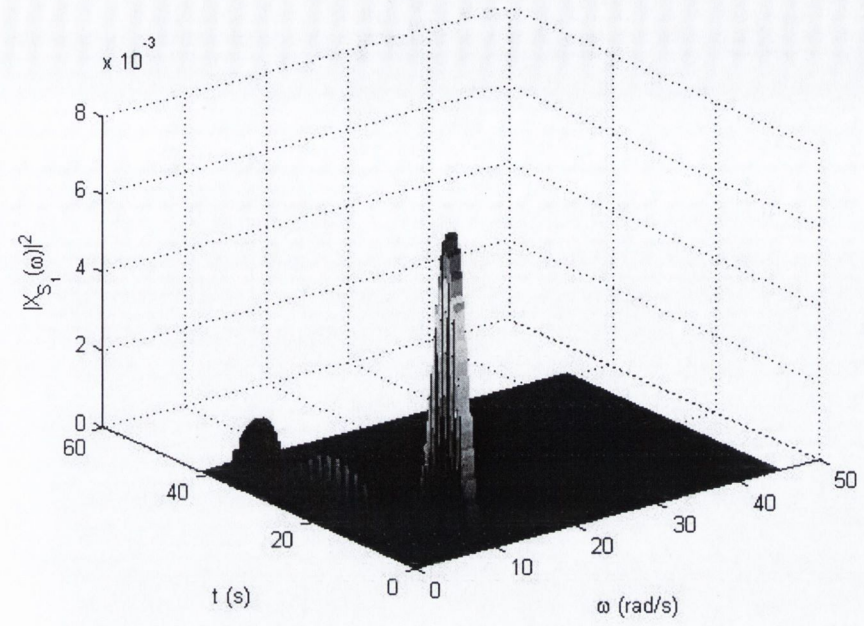


(a)

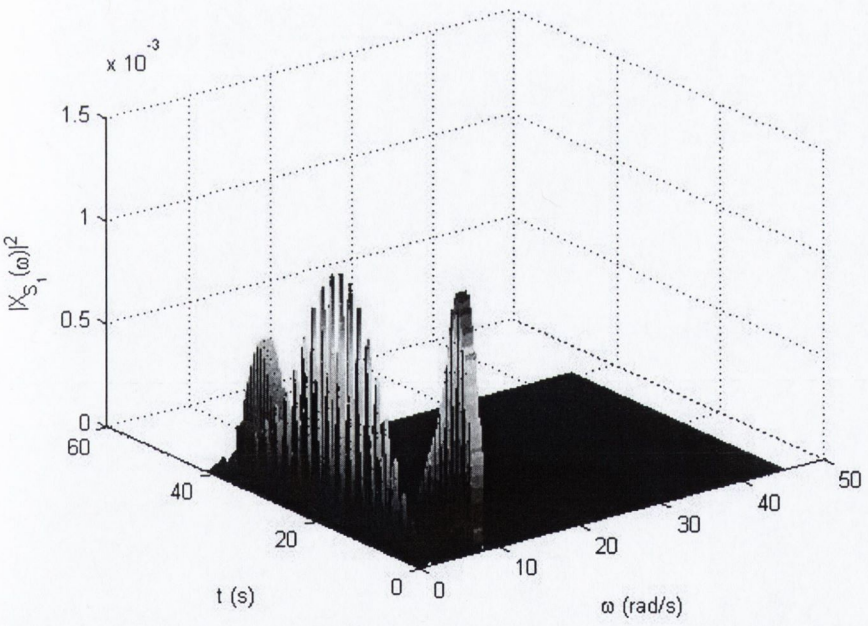


(b)

Figure 7.21: Time varying energy spectrum of the secondary response $X_{s_1}$ for different mass ratios of the P-S system; (a) 25% mass ratio and (b) 40% mass ratio

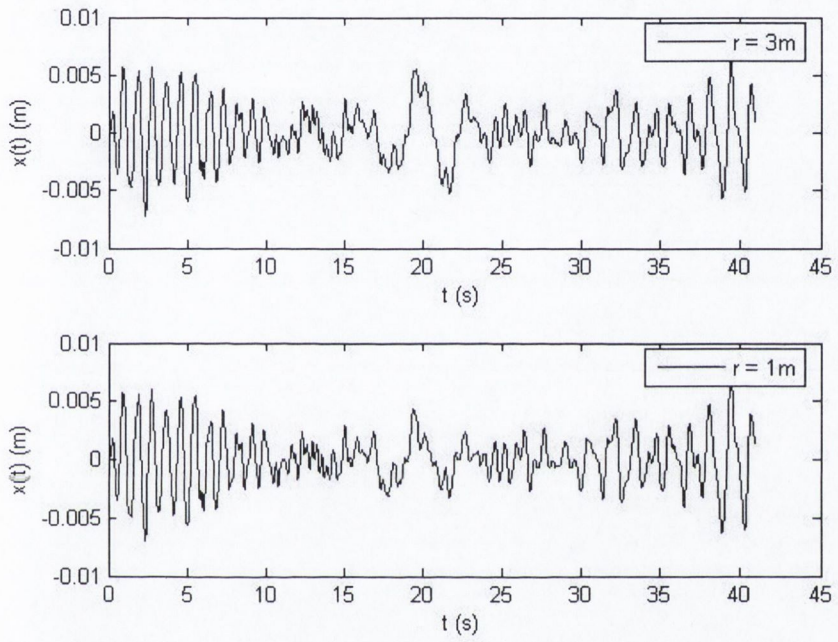


Figure 7.22: Time history of the secondary response $X_{s_1}$ when the secondary system for different torsional coupling

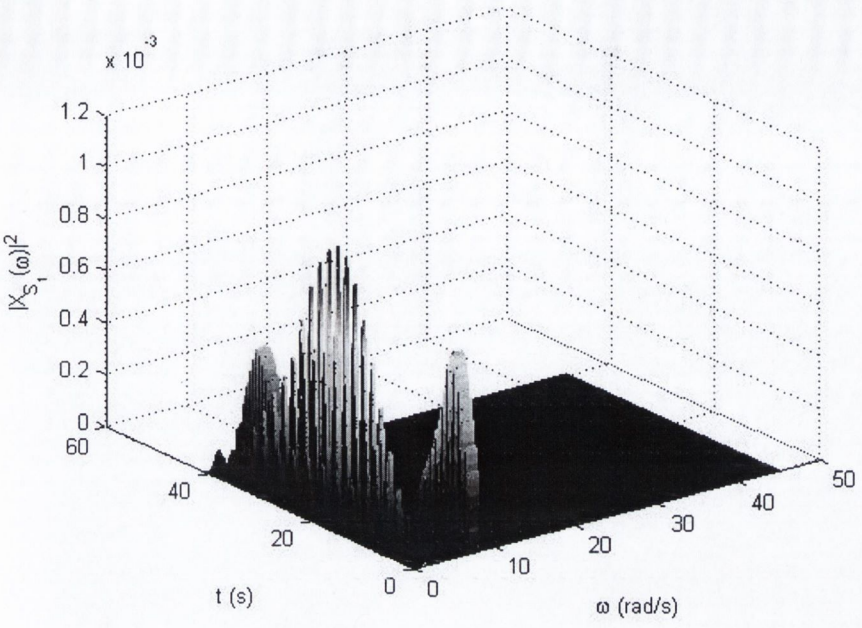


(a)

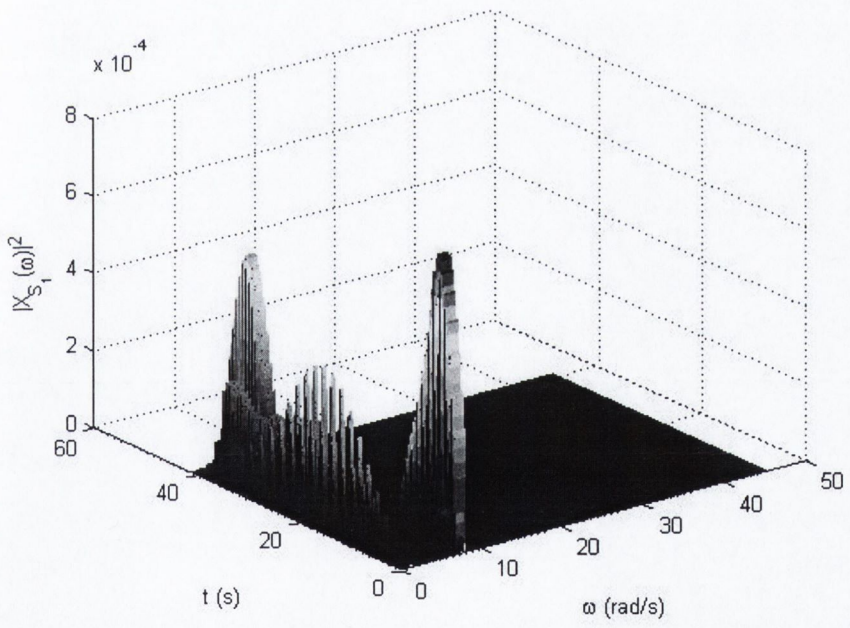


(b)

Figure 7.23: Time varying energy spectrum of the secondary response $X_{s_1}$ for different degrees of torsional coupling; (a) R = 3m and (b) R = 1m

It can be noticed that the evolutionary frequency content is largely affected by the rotational inertia, which is clearly visible in the range of 10s to 25s of the response time histories. Moreover, with the decrease in the values of '*r*', energy in frequency bands 2 to 7 (between frequencies 0.99rad/s to 5rad/s) decreases, which leads to insignificant energy contribution in those bands. From these figures, it can be noticed that the output of a torsionally coupled P-S system contains non-stationarity in both intensity and frequency content, which justifies the requirement of more rigorous model to tackle these issues.

In the present study, mean square value of the relative displacement $X_{s_1}$ and the growth in temporal energy obtained using proposed wavelet based model is compared with statistical simulation. Figure 7.24 shows the normalized instantaneous second order moment of $X_{s_1}$ (i.e. $E\left[X_{s_i}^2\right]/\sum E\left[X_{s_i}^2\right]$). A close match in mean sense has been observed from 5s to 7s and from 15s to 35s between the results from the proposed wavelet based model and simulations except initially, which may be due to the effect of the initial transients that are present in direct integration based simulation results. Moreover, due to lack of data, a relatively low sample size is used in direct simulation, which is reflected in the fluctuation of the simulation results. Figure 7.25 shows the growth in the temporal energy obtained from cumulative summation of the instantaneous energy as described in equation 7.31. It may be noticed that the wavelet based model matches closely with simulation depicting the efficiency of the proposed model. Figure 7.26 shows the evolutionary spectral density function of the relative displacement $X_{s_1}$. This figure shows that the proposed methodology can effectively evaluate non-stationarity in both intensity and frequency content. Hence the proposed model can be used for evolutionary stochastic response analysis of P-S systems with non-classical damping.

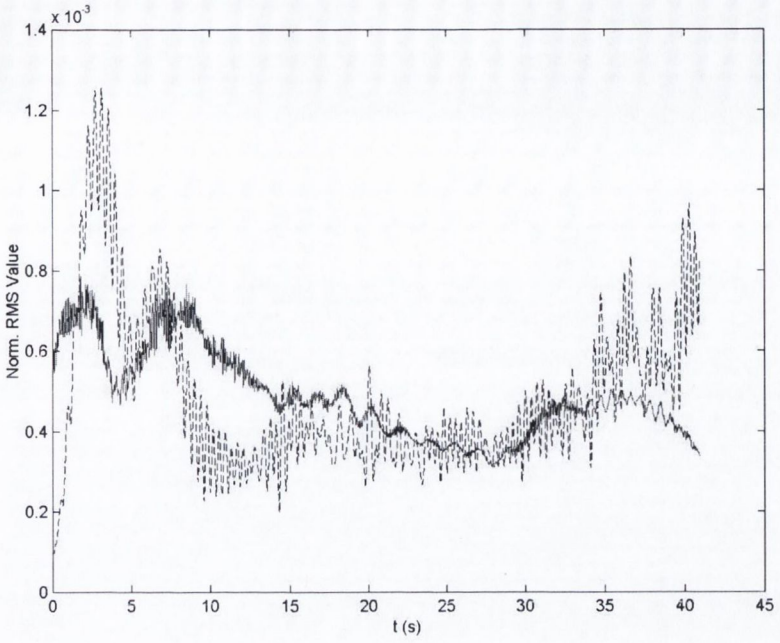


Figure 7.24: Normalized RMS value of the secondary response $X_{s_1}$ ; __ wavelet formulation; _ _ simulation

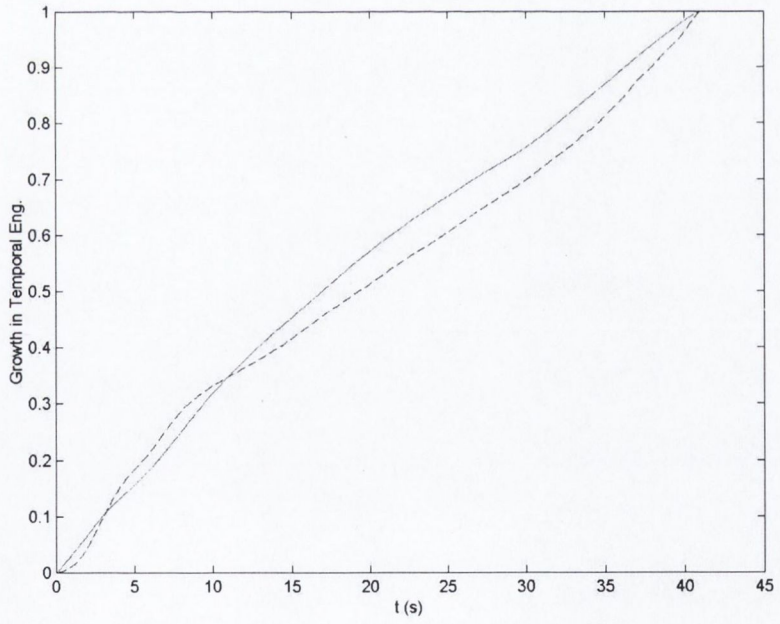


Figure 7.25: Growth in temporal energy of the secondary response $X_{s_1}$ ; __ wavelet formulation; _ _ simulation

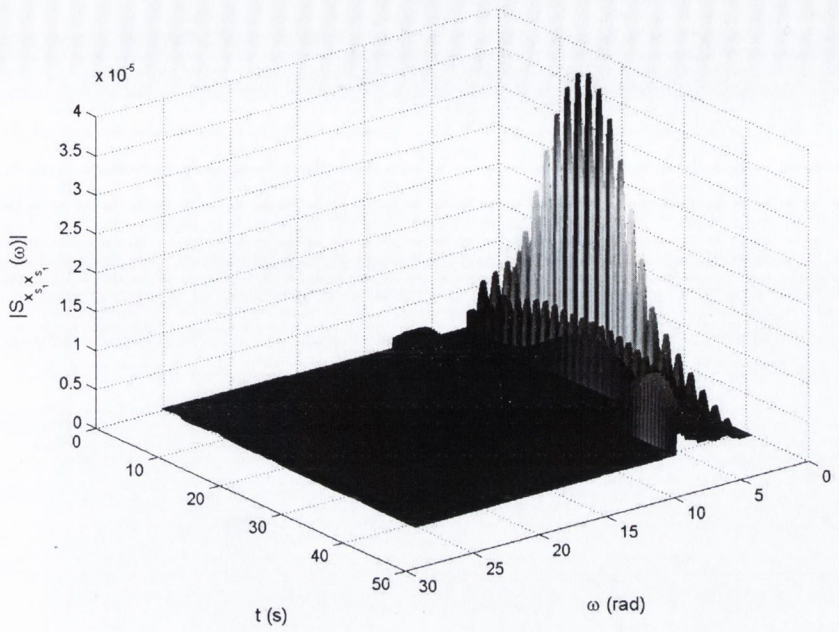


Figure 7.26: Time varying power Spectral Density function of the displacement response $X_{s_1}$ of the secondary system

## 7.4 Conclusions

In this chapter, first a generalised wavelet based method for evolutionary spectral response analysis of extended structures subjected to spatially varying differential support motions has been proposed. The input-output relation of non-stationary response is established in wavelet domain. The multi-supported bridge is modelled in finite-element framework and response is evaluated directly from the wavelet-based characterization of the evolutionary stochastic processes at the input. The proposed method the modelling of the non-stationary random processes is achieved by the summation of random processes

in different frequency bands in wavelet domain, where each sub-process is expressed as product of scale dependent deterministic envelope function and orthogonal stochastic process. For this purpose, a modified form of the LP basis function is used, which has compact support in frequency domain and hence can evaluate wavelet coefficients in non-overlapping frequency bands. For the process of response evaluation, conventional frequency response function coupled with deterministic envelope functions at different frequency scales in wavelet domain is used, which makes it easier to implement than conventional evolutionary spectral analysis using Fourier-Stieltz integral. The proposed wavelet based methodology can evaluate non-stationarity in both amplitude and frequency content of the response, which is shown in the numerical results presented.

Next, a non-stationary input-output relation of P-S systems is presented. Attention is mainly focused on the stochastic response of the secondary systems. The response is obtained using second order moment statistics of the input processes in wavelet domain. An ensemble of simulated time histories of Loma-Prieta earthquake based on the recorded parameters at Dumbarton Bridge site, which has characteristic temporal variations in the frequency content, is used as an input to the primary structure. The wavelet-based evaluations of the response statistics are obtained using a modified L-P basis function. From the temporal variation in the energy spectrum, it is clear that the response of the secondary system contains strong frequency non-stationarity, which is significantly affected by the rotational inertia and the eccentricity in the location of the secondary system. In addition, the cascading approximation even though acceptable for design of P-S systems in detuned cases from the peak displacement response point of

consideration, is unable to capture the time varying frequency content in the response particularly when the input is non-stationary.

# Chapter 8: Summary and Conclusions

## 8.1 General Summary and Conclusions

The study in this thesis mainly focuses on the application of wavelet-based time-frequency analysis for parameters estimation of linear and non-linear dynamical systems from measured time history responses, modelling of evolutionary stochastic processes and evolutionary spectral analysis of multi-supported multi degree and continuous structures with classical and non-classical damping. The thesis is concerned with three major topics – (a) system identification, (b) random process modelling and (c) random vibration analysis of dynamical systems.

### 8.1.1 System Identification

A methodology is proposed for identification of the modal frequencies and mode shapes of a structure by using the wavelet transformation with the modified L-P wavelet for time-frequency analysis. The technique presented is used for extracting the modal parameters of a linear multi degree of freedom (MDOF) system by decomposition of the original signal into frequency bands via wavelet transform, and time dependent analysis of each band using the basic properties of eigenvalues of vibration modes. First of all, two example cases of a three degree of freedom (3DOF) and a five degree of freedom (5DOF) linear viscously damped systems have been considered here. The response time histories of the damped MDOF systems are generated using free vibration conditions. The response signals are used to identify the modal parameters, namely natural frequency, mode shape and modal damping. The numerical study reveals that the

proposed wavelet-based system identification can estimate the modal parameters with desired level of accuracy. In this context, the strength and uniqueness of the proposed technique depends on the choice of the wavelet basis function. The modified form of the L-P basis function works better being close to vibrating signals. Further, this can be used to develop a sub-band coding leading to the wavelet packets for better accuracy as desired. The basis is also localized in frequency and hence does not suffer from the problem of band overlapping.

Following the estimation of system parameters of the discrete systems from the measured ambient vibration response, the proposed time-frequency analysis is further applied for identification of system parameters from the noise-contaminated measurement when the system is subjected to unknown input. For this purpose, a bridge-vehicle problem is first simulated coupled with Gaussian white noise as measurement errors. Using this simulated noise contaminated measurement, the fundamental frequency and mode shape of the bridge are identified. A laboratory experiment is then performed using simply supported reinforced concrete beam, which is excited by impulsive load at the middle. Axial strains are measured at a few locations along the bottom fiber of the beam using strain gauges. The proposed time-frequency analysis is then performed and the modal parameters are identified. Next, a discrete system is considered, which is excited by random amplitude modulated stochastic input. The measured response of the dynamical system is then analyzed to identify the modal parameters. In all the cases, the wavelet-based identification algorithm is seen to perform satisfactorily to the desired level of accuracy and with greater ease, which proves the usefullness of the proposed algorithm.

Besides off-line identification of structural parameters, on-line identification is the preamble for real time vibration control. For this purpose, a wavelet based on-line identification of stiffness of structural system has been proposed. Formulations for a SDOF system and a MDOF system have been presented. The developed theory can identify on-line variation in natural frequency of a SDOF system and the natural frequencies and mode shapes of a MDOF system arising out of change in stiffness (es). The modified L-P wavelet basis function has been used and has the advantage of adapting for wavelet packets for desired accuracy in estimation. The analytical results confirm the ability of the technique to track in several cases of stiffness variation considered here. The proposed method is simple and easy to implement for on-line identification and vibration control of stiffness varying structural systems. Illustrations have been used to show the efficiency of the proposed tracking algorithm.

The proposed wavelet-based algorithm for identification of parameters of the dynamical systems has been extended further to identify the localized modes (NNMs) of the non-linear dynamical systems. Besides other methods for response analysis like perturbation techniques and method of averaging, the application of non-linear normal modes is also very popular among the scientists and engineers. Although, modal decoupling using eigen analysis is not possible for non-linear systems, a synchronous motion is observed among the degrees of freedom, where all of them vibrates in phase or out of phase or pass though zero simultaneously. Since this localized phenomenon is observed surrounding the equilibrium points, the wavelet-based identification algorithm is further utilized for the estimation of NNM of non-linear systems. For this purpose, the advantage of using the modified form L-P basis function is that it can evaluate response

energy in non-overlapping frequency bands and is capable further division into sub-bands. For this purpose, a 2DOF system is considered with non-linear springs. The spring stiffness is assumed to vary with the odd power of the displacement. The numerical results suggest that the wavelet-based time-frequency analysis is capable of evaluating NNMs.

### 8.1.2 Random Process Modelling

The estimated structural parameters of the dynamical system help to access the overall performance from the point of view of structural health. To evaluate the remaining service life and to decide the measures that are required to maintain the designed serviceability criteria throughout the remaining service life, a detailed response analysis due to the action of the service loads are required. This needs modelling of the excitation processes.

Thus, a wavelet-based non-stationary model is proposed for the characterization of earthquake ground motions for the purpose of random vibration analysis, which accounts for time varying amplitude as well as frequency contents. The fundamental basis of the proposed algorithm lies in expressing the evolutionary process as sum of random processes in different frequency scales. For this purpose, a modified form of L-P basis function is used to calculate the wavelet coefficients of the recorded time history in different frequency bands. The evolutionary sub-processes are then expressed as the product of the band dependent envelope functions and stationary random processes at each frequency bands/scales. The parameters of the band dependent envelope function

are evaluated by minimizing the error between the growth in the temporal energy of the recorded accelerogram and the simulated time histories in each band using non-linear least square technique. The different amplitude modulations in different frequency bands, thus, represent the arrival of different frequencies at different instant of time. Moreover each modulation function of time corresponding to their scales represents the signature of the dominant frequencies in that scale. Together, these represent the non-stationarity associated with intensity and the frequency content of the earthquake ground motions. The proposed model is validated using statistical simulation based on the recorded acceleration time history of the 1940 Imperial Valley earthquake at the El-Centro site. The numerical results reveal that the proposed wavelet-based model for earthquake ground motion can capture non-stationary in amplitude as well as frequency content and hence, can be used for the purpose of evolutionary spectral analysis of the randomly excited dynamical systems.

The proposed model for single component earthquake ground motion has been used further to model multi-variate stochastic processes. A special case of multi-variate stochastic processes in earthquake engineering is the spatially varying earthquake ground motions. Seismic waves travel at different speeds and through different soil layers. In this process, the seismic waves suffer reflection and refraction in different soil strata. The proposed wavelet-based single component earthquake ground motion is used in this study to model the spatially varying ground motions. This single component wavelet-based model can be extended for differential support motions, where each support excitation is modeled as a single component excitation and the correlation between the support motions are modeled using conventional exponential correlation in the amplitude

modulating functions (coherence) associated with the stationary processes at each frequency scale and a time shift due to the different arrival times. The proposed time-frequency model for spatially varying earthquake enables to study the behaviour of the extended structures subjected differential support motions, especially in the light of frequency non-stationarity, which has not been focused properly by researchers so far.

### 8.1.3 Evolutionary Response Analysis

Finally, an evolutionary response analysis of the dynamical systems is presented, where the input is modelled as discussed the previous sub-section. For this purpose, both continuous parameter models as well as discrete parameter models are studied separately. The input-output relation is obtained using wavelet-based time-frequency analysis of the dynamical systems.

At first, wavelet transformation is used to evaluate the response of a short span bridge subjected to random differential support motions using continuous parameters model. An input-output relation is proposed using a modified form of L-P basis function, where the output is based on modal response as well as interaction between dynamic and pseudo static components. Since the spatial extent of the structure is small, seismic motions do not suffer attenuation. The response of the structural systems has been obtained using second order moment statistics of the input processes. Then, a wavelet based evolutionary spectral analysis of simply supported beam subjected to stochastic differential support motions is presented. The non-stationary support motions at the ends of the beam are modelled using deterministic frequency dependent modulating functions

and orthogonal stochastic processes. A wavelet based input-output relation is then developed for the time dependent power spectral density function of the total displacement response, which is composed of two parts (a) pseudo static and (b) dynamic. The proposed model is easy to implement than conventional evolutionary spectral analysis as it utilizes the conventional modal frequency response function coupled with continuous wavelet transformation to evaluate the square of the expected value of wavelet coefficients of the total displacement response at the output. The proposed model can evaluate time dependent second order moment statistics of the output for different wavelet basis functions (both orthogonal and non-orthogonal) and hence is general from the point of view of time-frequency analysis. The advantage of the proposed wavelet-based response analysis of systems with random boundary conditions is that it can be used for evolutionary spectral analysis of any boundary value problem relating plates and shells, which has not received much attention by the researchers till date.

Although, the continuous system dynamical model provides input-output relation in a closed form in some cases, their implementation in real life structures becomes increasingly difficult with complexity involve in the geometry of the structural system. An alternate solution to this is the use of finite element (FE) analysis. Thus, a wavelet based evolutionary spectral analysis of a multi-span simply supported large bridge subjected to stochastic differential support motions are presented in a FE framework. The non-stationary motions at each support are modeled as summation of orthogonal stochastic processes modulated by deterministic frequency dependent modulating functions at different frequency scales in wavelet domain. An envelope function proposed in literature (for uniform modulation) is used in this study for frequency dependent

amplitude modulation, whose parameters at different frequency scales are evaluated by non-linear least square technique. The spatial variability of the support motions is obtained through the coherency functions. A wavelet based input-output relation is then developed for the time dependent power spectral density function of the total displacement response at different locations. Using this model of earthquake ground motion, the response of the extended structures has been evaluated. A modified form of Littlewood-Paley (L-P) wavelet basis function has been used, which offers certain advantages such as non-overlapping frequency bands for wavelet bases at different scale. Using the generalized definition of non-stationary random processes, which is valid for any wavelet basis function (orthogonal or non-orthogonal), a generalized model for input-output relation of extended structures under spatially varying non-stationary earthquake ground motions is proposed in the present thesis. An interesting observation from the numerical works reveals that the higher modes of the dynamical systems might be excited through an input process with non-stationary amplitude as well as frequency content. Hence, proper modeling for both input processes as well as the response of the dynamical systems are required from the point of view of safe design of the structure as often design is based on the assumption of the response being contributed by the fundamental mode. The excitation of higher modes would not be revealed in stochastic analysis unless frequency non-stationarity is considered in the analysis.

Since the proposed model utilizes the FE analysis, it can also be used for any structure modeled in a discrete parameter framework. A special case of this is a structure whose components have wide variations in material and damping characteristics (e.g. primary-secondary systems). The proposed evolutionary model for response analysis is

further used for evaluating the response of the primary-secondary systems, which is subjected to evolutionary stochastic input. Although, cascading approximation works better for detuned systems, the analysis in this study reveals that it is unable to capture the frequency non-stationarity in the system response. Moreover, the results show that the rotational inertia affects the dynamic behaviour of the secondary system significantly. The effects of detuning and rotational inertia together give rise to the frequency non-stationarity in the response of the secondary systems and hence a time-frequency analysis is advocated for proper response modeling. The advantage of the proposed evolutionary models are that it is easy to implement as it utilizes the conventional modal frequency response functions together with continuous wavelet transformation are used to evaluate the second order moment statistics of the response. The proposed methodology can evaluate time dependent second order moment statistics of the response using wavelet transform and can be used in conjunction with any available finite-element software.

## 8.2 Recommendations for Further Work

The aim in the present thesis has been study application of the contemporary signal processing tools using wavelet transform for different applications in the field of dynamics and random vibrations; namely parameter estimation, process simulation and stochastic response analysis. A few areas have been outlined here, which offers further scope of research.

*System Identification*: Although wavelet-based model have successfully implemented for parameter estimation of the linear systems, great difficulties are associated in identifying of parameters of non-linear systems. Although a class of conservative system has been studied in the present thesis, a generalized framework is required for both conservative as well as non-conservative system. In this context, it may be noticed that the number of NNMs for non-linear system may be more than the degrees of freedom especially during bifurcation and depends the degree of non-linearity. The present identification technique is applicable, when prior information is available about the nature and type of the non-linear systems. Thus, a more general formulation is required, which may be applicable without prior knowledge of the non-linearity if the parameters are required to be estimated from the measured time history response.

*Random Process Modeling*: The proposed model for single component earthquake ground motion has been further used in this thesis for spatially varying earthquake ground motions. But their validation using measured time history record has not been performed due to the lack of availability of the spatially varying earthquake records. Although the analytical response of the structural system obtained by using the proposed model for multi point earthquake ground motions has shown to perform satisfactorily with numerical simulation, characterization and simulation of spatially varying earthquake requires further research based on the observed/recorded phenomena.

*Evolutionary Response Analysis*: In the present study, evolutionary response of linear dynamical systems is obtained using wavelet-based time-frequency analysis in both continuous model as well as in FE framework. But a fresh kind of problem arises if the

non-linearity associated with the dynamical system is considered. Although the concept of equivalent linearization is well studied for different types of non-linearity, the problems of equivalent linearization offers several challenges when the non-stationarity associated with the frequency content of the input processes are considered, particularly for the continuous or FE models. Besides response analysis via equivalent linearization, wavelet-based time-frequency analysis can be used for evolutionary response of the non-linear systems coupled with conventional techniques such as perturbation technique, harmonic balance technique etc.

# References

[1] Abrahamson N. A. (1993) 'Spatial variation of multiple support inputs', Proceedings of 1st US Seminar on Seismic Evaluation and Retrofit of Steel Bridges, California.

[2] Agarwal A. K. (2000) 'Response of light equipment on torsional building with passive tuned mass damper', Computers and Structures, 78, 591-602.

[3] Amin M. and Ang A. H. S. (1968) 'Non-stationary stochastic model of earthquake motions', Journal of Engineering Mechanics ASCE, 94(2), 559-583.

[4] ASME boiler and pressure vessel code, (July 1981) 'ANSI/ASME BPV-III-1-A, Rules of construction of nuclear power plant components, Div. 1, App. N, July 1981.

[5] Barnoski R. L. and Maurer J. R. (1969) 'Mean-square response of mechanical systems to non-stationary random excitation', Journal of Applied Mechanics ASME, 221-227.

[6] Basu B. and Gupta V. K. (1997) 'Non-stationary seismic response of MDOF systems by wavelet transform', Earthquake Engineering and Structural Dynamics, 26, 1243-1258.

[7] Basu B. and Gupta V. K. (1998) 'Seismic response of SDOF system by wavelet modeling of non-stationary processes', Journal of Engineering Mechanics ASCE, 124(10), 1142-1150.

[8] Basu B. and Gupta V. K. (2000) 'Stochastic seismic response of SDOF systems through wavelets', Engineering Structures, 22, 1714-1722.

[9] Basu B. (2003) 'Wavelet analysis for identification of stiffness degradation', Proceedings of Concrete research in Ireland, Belfast.

[10] Basu B. (2004) 'Wavelet analysis for identification of stiffness degradation', 7th International Conference Railway Engineering, London.

[11] Basu B. (2005) 'Identification of stiffness degradation in structures using wavelet analysis', Journal of Construction and Building Materials, 19, 713-721.

[12] Bathe K. J. (1997) 'Finite Element Procedures', Prentice Hall, USA.

[13] Beck J. L. (1980) 'Structural identification using linear models and earthquake records', Earthquake Engineering and Structural Dynamics, 8, 145-160.

[14] Berrah M. and Kausel E. (1992) 'Response spectrum analysis of structures subjected to spatially varying motions', Earthquake Engineering Structural Dynamics, 21, 461-470.

[15] Boivin N., Pierre C. and Shaw S. W. (1995) 'Non-linear normal modes, invariance, and modal dynamics approximations of non-linear systems', Nonlinear Dynamics, 8, 315–346.

[16] Borino G., Di Paola M. and Muscolino G. (1988) 'Non-stationary spectral moments of base excited MDOF systems', Earthquake Engineering Structural Dynamics, 16, 745-756.

[17] Caughey T. K. and Stumph H. J. (1961) 'Transient response of a dynamic system under random excitation', Journal of Applied Mechanics ASME, 28, 563-566.

[18] Chan Y. T. (1995) 'Wavelet Basics', Kluwer Academic Publishers, Boston.

[19] Chatterjee P. and Basu B. (2004) 'Wavelet based non-stationary seismic rocking response of flexibly supported tanks', Earthquake Engineering and Structural Dynamics, 33, 157-181.

[20] Chen M. T and Harichandran R. S. (2001) 'Response of an earth dam to spatially varying earthquake ground motion', Journal of Engineering Mechanics ASCE, 127(9), 932-939.

[21] Chui C. K. (1992) 'An Introduction to Wavelets', Academic Press, New York.

[22] Chusilp P. (1999) 'Application of Digital Filtering to Investigate Higher Mode Effects on Nonlinear Seismic Responses in Wall type Building', Masters Dissertation, Asian Institute of Technology, Bangkok, Thailand.

[23] Clough R. W. and Penzien J. (1993) 'Dynamics of Structures', New York, McGraw-Hill Inc.

[24] Cohen L. (1989) 'Time-frequency distributions – A review', Proceedings of the IEEE, 77(7), 941-981.

[25] Conte J. P. and Peng B. F. (1997) 'Fully non-stationary analytical earthquake ground motion model', Journal of Engineering Mechanics ASCE, 123(1), 15-24.

[26] Daubechies I. (1992) 'Ten Lectures on Wavelets', SIAM Publication, Pennslyvania, USA.

[27] Der Kiureghian A., Sackman J. L. and Nour-Omid B. (1983b) 'Dynamic analysis of light equipment in structures – response to stochastic input', Journal of Engineering Mechanics ASCE, 109(1), 90-110.

[28] Der Kiureghian A. and Crempien J. (1989) 'An evolutionary model for earthquake ground motion', Structural Safety, 6(2-4), 235-246.

[29] Der Kiureghian A. and Hofer A. N. (1992) 'Response spectrum method for multi-support seismic excitation', Earthquake Engineering Structural Dynamics, 21, 713-740.

[30] Ewins D. J. (2001) 'Modal Testing: Theory, Practice and Application', Taylor & Francis Group.

[31] Failla G., Spanos P. D. and Di Poala M. (2003) 'Response power spectrum of multi degree of freedom nonlinear systems by a Galerkin technique', Journal of Applied Mechanics ASME, 70, 708-714.

[32] Foss K. A. (1958) 'Coordinates which uncouple the equations of motion of damped linear systems', Journal of Applied Mechanics, ASME, 25, 361-364.

[33] Gasprini D. (1979) 'Response of MDOF systems to non-stationary random excitation', Journal of Engineering Mechanics, ASCE, 105(1), 13-27.

[34] Gasprini D. and DebChaudhury A. (1980) 'Dynamic response to non-stationary non-white excitation', Journal of Engineering Mechanics ASCE, 106(6), 85-102.

[35] Ghanem R. and Shinozuka M. (1995) 'Structural system identification. I, Theory', Journal of Engineering Mechanics, ASCE, 121(2), 255-264.

[36] Ghanem R. and Romeo F. (2000) 'A wavelet based approach for the identification of linear time-varying dynamical systems', Journal of Sound and Vibration, 234(4), 555-576.

[37] Ghanem R. and Romeo F. (2001) 'A wavelet based approach for model and parameter identification of non-linear systems', Non-linear Mechanics, 36, 835-859.

[38] Hao H., Olivera C.S. and Penzien J. (1989) 'Multiple-station ground motion processing and simulation based on SMART-I array data', Nuclear Engineering and Design, 111, 293-310.

[39] Harichandran, R. S., and Wang, W. (1988). 'Response of simple beam to spatially varying earthquake excitation', Journal of Engineering Mechanics, ASCE, 114(9), 1526-1541.

[40] Harichandran R. S. and Vanmarcke E. (1986) 'Stochastic variation of earthquake motion in space and time', Journal of Engineering Mechanics ASCE, 112, 154-174.

[41] Harichandran, R. S., Hawwari, A., and Sweidan, B. N. (1996). 'Response of long-span bridges to spatially varying ground motion', Journal of Structural Engineering, ASCE, 122(5), 476-484.

[42] Hart G. C. and Yao J. T. P. (1977) 'System identification in structural dynamics', Journal of Engineering Mechanics, ASCE, 103(6), 1089-1104.

[43] Hind A. and Novak M. (1980) 'Earthquake response of buried insulated pipes', Journal of Engineering Mechanics, ASCE, 1106(6), 1135-1149.

[44] Hoshiya M. and Saito E. (1984) 'Structural identification by extended Kalman filtering', Journal of Engineering Mechanics, ASCE, 110, 1757-1770.

[45] Housner G. W. and Jennings P. C. (1964) 'Generations of artificial earthquakes', Journal of Engineering Mechanics ASCE, 90(1), 113-150.

[46] Jezequel L. and Lamarque C. H. (1991) 'Analysis of nonlinear dynamical systems by normal form theory', Journal of Sound and Vibration, 149(3), 429–448.

[47] Kanai K. (1957) 'Semi-empirical formula for the seismic characteristics of the ground', Tokyo Bulletin of Earthquake Research Institute, 35, 309-325.

[48] King M. E. and Vakakis A. F. (1994) 'An energy-based formulation for computing nonlinear normal modes in un-damped continuous systems', Journal of Vibration and Acoustics, 116, 332–340.

[49] Kitada Y. (1998) 'Identification of nonlinear structural dynamic system using wavelet', Journal of Engineering Mechanics, ASCE, 124(10), 1059-1066.

[50] Kozin F. and Natke H. G. (1986) 'System identification technique', Structural Safety, 3, 269-316.

[51] Lardies J. and Gouttebroze S. (2002) 'Identification of modal parameters using the wavelet transforms', International Journal of Mechanical Science, 44, 2263-2283.

[52] Lin C. W. and Loceff F. A. (1980) 'A new approach to compute system response with multiple support response spectra input', Nuclear Engineering and Design, 60, 347-352.

[53] Lin C. C., Soong T. T. and Natke H. G. (1990) 'Real time system identification of degrading structures', Journal of Engineering Mechanics, ASCE, 116(10), 2258-2274.

[54] Lin Y. K. and Cai G. Q. (1995) 'Probabilistic Structural Dynamics', McGraw-Hill Inc., Singapore.

[55] Loh C. H. (1985) 'Analysis of the spatial variation of seismic waves and ground movements from SMART-1 array data', Earthquake Engineering Structural Dynamics, 14, 561-581.

[56] Loh C. H. and Ku B. D. (1995) 'An efficient analysis of structural response for multiple-support seismic excitations', Engineering Structures, 17(1), 15-26.

[57] Mallat S. (1989) 'A theory for multi-resolution signal decomposition: The wavelet representation', IEEE Transactions and Pattern Analysis and Machine Intelligence, 11, 674-693.

[58] Meirovitch L. (1993) 'Dynamics and Control of Structures', John Wiley, New York.

[59] Micaletti R. C., Cakmak A. S., Nielsen S. R. K. and Kirkegaard P. H. (1999) 'Construction of time-dependent spectra using wavelet analysis for determination of global damage', Proceedings of 21st International Symposium on Modal Analysis, 993-1003.

[60] Mindlin R. D. and Goodman L. E. (1950) 'Beam with time dependent boundary conditions', Journal of Applied Mechanics ASME, 377-380.

[61] Mukherjee S. and Gupta V. K. (2002a) 'Wavelet based characterization of design ground motions', Earthquake Engineering and Structural Dynamics, 31, 1173-1190.

[62] Mukherjee S. and Gupta V. K. (2002b) 'Wavelet-based generation of spectrum-compatible time-histories', Soil Dynamics and Earthquake Engineering, 22(12), 817-822.

[63] Nayfeh A. H. and Mook D. T. (1984) 'Nonlinear Oscillations', Wiley, New York, USA.

[64] Nayfeh A. H. (2000) 'Perturbation methods', Wiley, New York, USA.

[65] Nayfeh A. H., Chin C. and Nayfeh S. A. (1996) 'On nonlinear normal modes of systems with internal resonance', Journal of Vibrations and Acoustics, 118, 340–345.

[66] Newland D. E. (1983) 'An Introduction to Random Vibration, Spectral and Wavelet Analysis', Longman Scientific and Technical, Essex.

[67] Newland D. E. (1993) 'Harmonic wavelet analysis', Proceedings of the Royal Society of London (A), 443, 203-225.

[68] Newland D. E. (1994a) 'Wavelet analysis of vibration, Part I: Theory', Journal of Vibration and Acoustics, Transactions of ASME, 116, 409-416.

[69] Newland D. E. (1994b) 'Wavelet analysis of vibration, Part II: Wavelet maps', Journal of Vibration and Acoustics, Transactions of ASME, 116, 417-425.

[70] Paz M. (1987) 'Structural Dynamics', CBS Publishers & Distributors, Delhi.

[71] Perotti F. (1990) 'Structural response to non-stationary multiple-support random excitation', Earthquake Engineering Structural Dynamics, 19, 513-527.

[72] Pesheck E., Shaw S. W. and Pierre C. (2002) 'A new Galerkin-based approach for accurate nonlinear normal modes through invariant manifolds', Journal of Sound and Vibration, 249(5), 971–993.

[73] Piombo B. A. D., Fasana A., Marchesiello S. and Ruzzene M. (2000) 'Modeling and identification of the dynamic response of a supported bridge', Mechanical Systems and Signal Processing, 14(1), 75-89.

[74] Priestley M. B. (1981) 'Spectral Analysis and Time Series', Academic Press Inc., New York.

[75] Prochazka A., Uhlir J. and Rayner P. J. W. (1998) 'Signal Analysis and Prediction', Birkhauser, Switzerland.

[76] Qian S and Chen D. (1996) 'Joint Time-Frequency Analysis: Method and Application', Prentice-Hall, USA.

[77] Rao R. M. and Bopardikar A. S. (1998) 'Wavelet Transforms, Introduction to Theory and Applications', Addison Wesley Longman, Inc. Massachusetts, USA.

[78] Rofooei F. R., Aghababaii M. and Ahmadi G. (2001) 'Generation of artificial earthquake records with a non-stationary Kanai-Tajimi model', Engineering Structures, 23, 827-837.

[79] Rosenberg R. M. (1966) 'On nonlinear vibrations of systems with many degree of freedom', Advances in Applied Mechanics, 242(9), 155–242.

[80] Sackman J. L., Der Kiureghian A. and Nour-Omid B. (1983a) 'Dynamic analysis of light equipment in structures - Modal properties of the combined system', Journal of Engineering Mechanics ASCE, 109(1), 73-89.

[81] Saragoni G. R and Hart G. C. (1974) 'Simulation of artificial earthquakes', Journal of Earthquake Engineering Structural Dynamics, 2, 249-267.

[82] Segawa R., Yamamoto S., Sone A. and Masuda A. (2000) 'Cumulative damage estimation using wavelet transform of structural response', Proceedings of 12th World Conference on Earthquake Engineering, 1212-1220.

[83] Seneviratna G. D. P. K. and Krawinkler H. (1996) 'Modifications of seismic demands for MDOF systems', Proceedings of 11th World Congress on Earthquake Engineering, 570-590.

[84] Shaw S. W. and Pierre C. (1991) 'Non-linear normal modes and invariant manifolds', Journal of Sound and Vibration 150, 170–173.

[85] Shaw S. W. and Pierre C. (1993a) 'Normal modes for non-linear vibratory systems', Journal of Sound and Vibration, 164(1), 85–124.

[86] Shaw S. W. and Pierre C. (1993b) 'Normal modes of vibration for non-linear continuous systems', Journal of Sound and Vibration 169, 319–347.

[87] Shaw S. W., Pierre C. and Pesheck E. (1999) 'Modal analysis-based reduced-order models for nonlinear structures—an invariant manifold approach', The Shock and Vibration Digest, 31, 3–16.

[88] Shinozuka M. and Sato Y (1967) 'Simulation of non-stationary random processes', Journal of Engineering Mechanics ASCE, 93(1), 11-40.

[89] Shinozuka M. and Jan C. M. (1972) 'Digital simulation of random process and its applications', Journal of Sound and Vibration, 25(1), 111-128.

[90] Shinozuka M. and Deodatis G. (1988) 'Stochastic process model for earthquake ground motion', Probabilistic Engineering Mechanics, 3(3), 114-123.

[91] Shinozuka M. and Ghanem R. (1994) 'Structural system identification. II, Experimental Verification', Journal of Engineering Mechanics, ASCE, 121(2), 265-273.

[92] Singh M. P. (1975) 'Generation of seismic floor spectra', Journal of Engineering Mechanics ASCE, 101, 593-607.

[93] Sinha R. and Igusa T. (1995) 'Response of primary-secondary systems to short duration, wide-band input', Journal of Sound and Vibration, 185(1), 119-137.

[94] Smyth A. W., Masri S. F., Chassiakos A. G. and Caughey T. K. (1999) 'On-line parametric identification of MDOF non-linear hysteretic systems', Journal of Engineering Mechanics, ASCE 125(2), 133-142.

[95] Sone A., Yamamoto S. and Masuda A. (2000) 'Detection of inelastic excursions in hysteretic systems for cumulative damage estimation using wavelet transform of response time histories', Proceedings of 12th World Conference in Earthquake Engineering, 1220-1228.

[96] Soong T. T. (1990) 'Active structural control: Theory and practice', Longman, New York.

[97] Spanos P. D and Failla G. (2004) 'Evolutionary Spectra Estimation Using Wavelets', Journal of Engineering Mechanics ASCE, 130(8), 952-960.

[98] Spencer B. and Nagarajaiah S. (2003) 'State of the art of Structural Control', Journal of Engineering Mechanics, ASCE, 129(7), 845-856.

[99] Spina D., Valente C. and Tomlinson G. R. (1996) 'A new procedure for detecting non-linearity from transient data using the Gabor transform', Nonlinear Dynamics, 11, 235-254.

[100] Staszewski W. J. (1997) 'Identification of damping in MDOF system using time-scale decomposition', Journal of Sound and Vibration, 203(2), 283-305.

[101] Staszewski W. J. (1998) 'Identification of non-linear systems using multi scale ridges and skeleton of wavelet transform', Journal of Sound and Vibration, 214(4), 639-658.

[102] Tajimi T. (1960) 'A statistical method for determining the maximum response of a building structure during an earthquake', Proceedings of the 2nd World Conference on Earthquake Engineering, 781-797.

[103] Tratskas P. and Spanos P. (2003) 'Linear multi-degree of freedom system stochastic response by using harmonic wavelet transform', Journal of Applied Mechanics ASME, 70, 724-731.

[104] Trifunac M. D. (1990) 'Curvograms of strong motion', Journal of Engineering Mechanics ASCE, 1990, 116(6), 1426-1432.

[105] Uscinski B. J. (1977) 'The elements of wave propagation in random media', McGraw-Hill, New York.

[106] U.S. Nuclear regulatory commission, Subsystem response review, NUREG/CR-1700, Jan 1981.

[107] Vakakis A. F. (1997) 'Nonlinear normal modes (NNMs) and their applications in vibration theory: an overview', Mechanical Systems and Signal Processing, 11(1), 3–22.

[108] Vakakis A. F., Manevitch L. I., Mikhlin Y. V., Pilipchuk V. N. and Zevin A. A. (1996) 'Normal Modes and Localization in Nonlinear Systems', Wiley, New York, USA.

[109] Varadarajan N. and Nagarajaiah S. (2004) 'Wind response control of building with variable stiffness tuned mass damper using empirical model decomposition/Hilbert transform', Journal of Engineering Mechanics, ASCE, 130(4), 451-458.

[110] Villaverde R. (1988) 'Rosenblueth's modal combination rule for systems with non-classical damping', Earthquake Engineering and Structural Dynamics, 16, 315-328.

[111] Wong H. L. and Trifunac M. D. (1979) 'Generation of artificial strong motion accelerograms', Earthquake Engineering and Structural Dynamics, 7, 506-527.

[112] Yang J. N., Agarwal A., Samali B. and Wu J. C. (2004) 'Benchmark problem for response control of wind-excited tall buildings', Journal of Engineering Mechanics ASCE, 130(4), 437-446.

# Appendix A: Coherence Functions for SVEGM

In the present thesis, five different coherence functions are used to evaluate the stochastic response of the bridge.

**a)** Harichandran and Vanmarcke (1986) model:

$$\gamma_{rl}(\omega) = A\exp\left[-\frac{2v}{\alpha\theta(\omega)}(1-A+\alpha A)\right] + (1-A)\exp\left[-\frac{2v}{\theta(\omega)}(1-A+\alpha A)\right] \quad \text{(A.a)}$$

$$\theta(\omega) = k\left[1+(\omega/\omega_0)^b\right]^{-1/2} \quad \text{(A.b)}$$

where, '$v$' is the distance between the two supports '$r$' and '$l$', $\alpha$ and $A$ are constants and $\theta(\omega)$ represents frequency dependent spatial scale fluctuation. In the equations 14a and 14b $A = 0.636$, $\alpha = 0.0186$, $k = 31200\text{m}$, $\omega_0 = 9.49$ rad/s, and $b = 2.95$.

**b)** Hao *et al* (1989) model:

$$\gamma_{rl}(\omega) = \exp(-\beta_1 v^L - \beta_2 v^T).\exp\left(-\left(\alpha_1\sqrt{v^L} + \alpha_2\sqrt{v^T}\right)\left(\frac{\omega}{2\pi}\right)^2\right) \quad \text{(A.1)}$$

$$\alpha_1 = \frac{2\pi a}{\omega} + \frac{\omega b}{2\pi} + c\,;\ \alpha_2 = \frac{2\pi d}{\omega} + \frac{e\omega}{2\pi} + g\,;\ 0.314 \le \omega \le 62.83\ rad/s \quad \text{(A.2)}$$

where, $\beta_1 = 1.109$, $\beta_2 = 0.673$, $a = 35.83$, $b = -0.181$, $c = 1.177$, $d = 51.63$, $e = -0.076$ and $g = -1.905$.

**c)** Hindy and Novak (1980) model:

$$|\gamma_{rl}(\omega)| = \exp\left(-\alpha(\omega v)^{\beta}\right) \tag{A.3}$$

where, $\alpha = 3.007E-4$ and $\beta = 0.9$.

**d)** Abrahamson (1993) model:

$$|\gamma_{rl}(f)| = |\gamma_1(f,v)|h(f,v) \tag{A.4}$$

$$|\gamma_1(f,v)| = \tanh\left(\frac{c_3(v)}{1+c_4(v)f+c_7(v)f^2} + (4.8-c_3(v))\exp(c_6(v)f) + 0.35\right) \tag{A.5}$$

$$c_3(v) = \frac{3.95}{1+0.0077v+0.000023v^2} + 0.85\exp(-0.00013v) \tag{A.6}$$

$$c_4(v) = \frac{0.4\left[1-\dfrac{1}{1+(v/5)^3}\right]}{\left[1+(v/190)^8\right]\left[1+(v/180)^3\right]} \tag{A.7}$$

$$c_6(v) = 3(\exp(-v/20)-1) - 0.0018v \tag{A.8}$$

$$c_7(v) = -0.598 + 0.106\ln(v+325) - 0.0151\exp(-0.6v) \tag{A.9}$$

$$h(f,v) = \frac{1}{1+[f/c_8(v)]^6} \tag{A.10}$$

$$c_8(v) = \exp(8.54 - 1.07\ln(v+200)) + 100\exp(-v) \tag{A.11}$$

**e)** Uscinski (1977) model:

$$|\gamma_{rl}(\omega)| = \exp\left(-\alpha^2\omega^2v^2\right) \tag{A.12}$$

where, $\alpha = 2E-4$ s/m.

# Appendix B: Derivative of the Evolutionary Process

Let $f(t)$ be a random vector process, which is represented by

$$f(t) = \int_{-\infty}^{+\infty} A(\omega,t) e^{i\omega t} dG(\omega) \tag{B.1}$$

Derivative of $f(t)$ with respect to time $t$ is given by

$$\frac{d}{dt} f(t) = \int_{-\infty}^{+\infty} \left\{ \dot{A}(\omega,t) e^{i\omega t} + A(\omega,t) i\omega e^{i\omega t} \right\} dG(\omega) \tag{B.2}$$

Since $A(\omega,t)$ is slowly varying envelope function as compared to $e^{i\omega t}$, and thus, its derivative with respect to time $t$ can be neglected. Hence

$$\frac{d}{dt} f(t) \approx \int_{-\infty}^{+\infty} A(\omega,t) i\omega e^{i\omega t} dG(\omega) \tag{B.3}$$

Similarly, it can also be shown that

$$\frac{d^2}{dt^2} f(t) \approx -\int_{-\infty}^{+\infty} A(\omega,t) \omega^2 e^{i\omega t} dG(\omega) \tag{B.4}$$

# Appendix C: 2D Beam Element

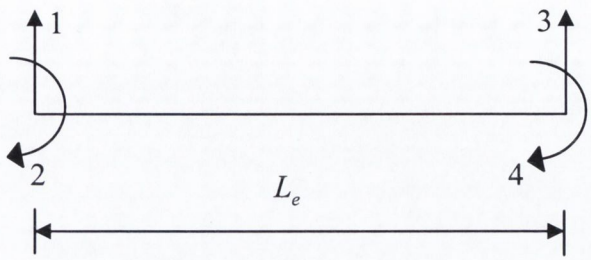


Figure B.1: 2D Beam element

Figure B.1 shows a 2D beam element of length $L_e$. It has 4 degrees of freedom (2 rotations and 2 translations). The element mass matrix $M_e$ and element stiffness matrix $K_e$ are given by

$$M_e = \frac{\overline{m}L}{420}\begin{bmatrix} 156 & 22L_e & 54 & -13L_e \\ 22L_e & 4L_e^2 & 13L_e & -3L_e^2 \\ 54 & 13L_e & 156 & -22L_e \\ -13L_e & -3L_e^2 & -22L_e & 4L_e^2 \end{bmatrix} \tag{C.1}$$

$$K_e = \frac{2EI}{L^3}\begin{bmatrix} 6 & 3L_e & -6 & 3L_e \\ 3L_e & 2L_e^2 & -3L_e & L_e^2 \\ -6 & -3L_e & 6 & -3L_e \\ 3L_e & L_e^2 & -3L_e & 2L_e^2 \end{bmatrix} \tag{C.2}$$

# Appendix D: Torsionally Coupled P-S System

The torsionallly coupled P-S that is considered in the present study is shown in the figure 7.2. It is subjected to random support motion $\ddot{x}_g(t)$ and the governing equation of motion is given by

$$[M]\{\ddot{X}\}+[C]\{\dot{X}\}+[K]\{X\}=-[M]\{I\}\ddot{x}_g(t) \tag{D.1}$$

where, $M$, $C$ and $K$ are the mass, damping and stiffness matrices respectively and I is the influence vector. Over dot represents differentiation with respect to time. The displacement vector $X$ is given by $\{X_p, X_\theta, X_{s_1}, X_{s_2}\}$ and the influence vector is given by $\{1,0,1,1\}^T$. The mass and stiffness matrices are given by [Agarwal (2000)]

$$[M]=diag[m_p \quad m_p r^2 \quad m_{s_1} \quad m_{s_2}] \tag{D.2}$$

and

$$[K]=\begin{bmatrix} K_p+K_{s_1} & K_p r+K_{s_1} e & -K_{s_1} & 0 \\ K_p r+K_{s_1} e & K_\theta+K_s e^2 & -K_{s_1} & 0 \\ -K_{s_1} & -K_{s_1} & K_{s_1}+K_{s_2} & -K_{s_2} \\ 0 & 0 & -K_{s_2} & K_{s_2} \end{bmatrix} \tag{D.3}$$

where, $K_p = K_{p_1} + K_{p_2}$.